# THE JOURNAL OF PHYSICAL CHEMISTRY

(Registered in U. S. Patent Office)

# DETONATION PROPERTIES AND REACTION KINETICS OF 2,4-DINITROTOLUENE[1]

By Melvin A. Cook and William S. Partridge

*Explosives Research Group, University of Utah, Salt Lake City, Utah*

*Received August 2, 1954*

The experimental detonation velocity–diameter and wave shape–diameter curves for 2,4-dinitrotoluene of particle size −65 + 100 mesh and density 0.95 g./cc. are presented. The velocity–diameter curves are interpreted by means of the nozzle and curved front theories, which predict (best fit) reaction zone lengths of 2.9 cm. (total reaction time about 7 μsec.) and 1.5 cm. (total reaction time about 4 μsec.), respectively. Within the accuracy of the measurements the detonation wave fronts seemed to be spherical throughout, and the observed steady state radius of curvature/diameter $R_m/d$ increased uniformly from 0.57 near the critical diameter to 1.65 (still increasing) at the maximum diameter studied (25 cm.). The critical diameter $d_c$ was between 3.8 and 5 cm.

DNT has long been known to be explosive; in fact, 4500 pounds of DNT exploded accidentally in 1943.[2] However, no data are recorded in available literature on the detonation properties or reaction kinetics of DNT, owing perhaps to the lack of interest in DNT as a practical explosive by itself. DNT is, however, used extensively in numerous commercial and some military explosives including various liquid explosives (*e.g.*, the commercial nitroglycerine–DNT mixture EL 389) and solid explosives (*e.g.*, "Nitramon," dynamites, and many others).

For studies of the kinetics of chemical reactions in detonation, DNT offers several interesting advantages. Owing to its relatively low detonation temperature, one would expect DNT to react relatively slowly in detonation reactions. As a pure explosive compound DNT offers, moreover, a well defined and readily tractable reaction rate problem. By selecting a single isomer (2,4-DNT in this case) one can obtain DNT in solid form in uniform particle size. DNT is, of course, similar chemically to TNT which has been studied extensively and for which reaction rate studies have also been carried out.[3] Whereas one requires specially prepared TNT of large particle sizes to obtain suitable velocity diameter data for theoretical study, even the

regular fine-grained DNT is suitable for this purpose. Indeed −65 + 100 mesh (2,4)-DNT exhibits a diameter effect on velocity over a much broader range even than −4 + 6 mesh TNT.

This article presents measured velocity–diameter and wave shape $(R_m/d)$–diameter curves for solid 2,4-DNT, together with the theoretical "best fit" velocity–diameter curves of the nozzle,[4] and curved front[5] theories. Ideal detonation properties of DNT computed for densities of 1.04 and 1.59 g./cc. (log $F$ values[6] of 3.0 and 6.0) by methods reported previously[6,7] are also presented (Table I).

## Experimental

The DNT used in this investigation was technical grade 2,4-DNT obtained from the du Pont Company. This product was carefully screened, and the portion through 65 on 100 mesh standard Tyler mesh screens was used in this study. Containers were manila paper tubes of about 1 mm. wall thickness. One end of each tube observed in wave shape studies was cut on a lathe exactly perpendicular to the longitudinal axis. A glass plate was placed over this end of the tube to improve photographic definition of the emerging detonation wave. Pin inserts were placed in the tubes at accurately measured positions for velocity measurement in all except the smallest diameter tubes. In small diameters windows were cut and lined with scotch tape along the side of the charge for velocity measurements by a streak camera. The charges were all vibrator-packed to obtain

(1) This study was supported by Office of Naval Research (Contract Number N7-onr-45107, Project Number 357 239).

(2) C. S. Robinson, "Explosives, Their Anatomy and Destructiveness," McGraw-Hill Book Co., New York, N. Y., 1944.

(3) M. A. Cook, G. S. Horsley, W. S. Partridge, and W. O. Ursenbach (submitted for publication).

(4) H. Jones, *Proc. Roy. Soc. (London)*, **A189**, 415 (1947).

(5) H. Eyring, R. E. Powell, G. H. Duffey and R. B. Parlin, *Chem. Revs.*, **45**, 70 (1949); R. B. Parlin and D. W. Robinson, Technical Report No. VII, ERG, Utah University, October 3, 1952.

(6) M. A. Cook, G. S. Horsley, A. S. Filler and R. T. Keyes, This Journal, **58**, 1114 (1954).

(7) M. A. Cook, *J. Chem. Phys.*, **15**, 518 (1947).
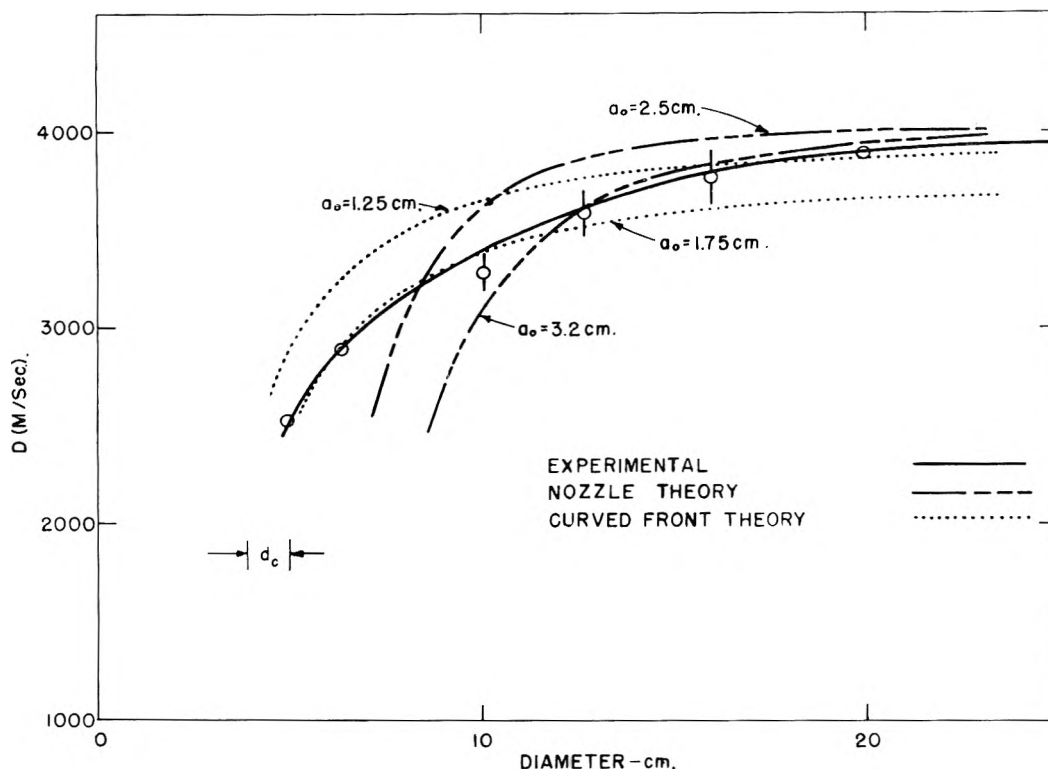
Fig. 1.—Experimental and theoretical (curved front and nozzle) velocity–diameter curves for 2,4-DNT.

uniform density, and the open end was sealed with masking tape. The average density of each charge was measured by total volume and weight determinations. All charges except those at 25 cm. were made at a length/diameter ($L/d$) ratio of six, and those at 25 cm. had an $L/d$ of 4.5.

TABLE I

DETONATION PROPERTIES OF DNT

| log F | 3.00 | 6.00 |
|---|---|---|
| ($H_2$) moles/kg. | 0.54 | 0.00 |
| ($N_2$) moles/kg. | 4.51 | 5.07 |
| (CO) moles/kg. | 5.36 | 0.23 |
| ($CO_2$) moles/kg. | 4.87 | 6.85 |
| (H) moles/kg. | 0.00 | 0.00 |
| ($CH_4$) moles/kg. | 2.24 | 0.11 |
| ($CH_3OH$) | 2.54 | 6.95 |
| (HCN) moles/kg. | 1.00 | 0.13 |
| ($H_2O$) moles/kg. | 4.42 | 1.20 |
| ($NH_3$) moles/kg. | 0.97 | 0.73 |
| (C) moles/kg. | 22.4 | 24.2 |
| $n$ moles/kg. | 26.5 | 21.3 |
| Q (kcal./kg.) | 956 | 1020 |
| $C_v$ (kcal./kg./°K.) | 0.404 | 0.428 |
| $\rho_1$ (g./cc.) | 1.04 | 1.59 |
| $T \times 10^{-3}$ (°K.) | 3.00 | 3.17 |
| $D \times 10^{-3}$ (m./sec.) | 4.21 | 5.47 |
| $p_2 \times 10^{-4}$ (atm.) | 4.49 | 10.9 |

The charges were all fired with cast 50/50 Pentolite boosters. Velocity was measured in all except the smallest diameter charges by an accurate "pin-oscillograph" designed and constructed in this Laboratory. For diameters near the critical diameter $d_c$, velocity measurements were made by means of a rotating mirror "streak" camera having a maximum film speed of 5 mm./$\mu$sec. Velocities were corrected to an average density $\rho_1$ of 0.95 g./cc. by use of the theoretical velocity–density slope $\Delta D/\Delta\rho_1 = 2270$ m./sec. However, only a small density correction was required in any case.

For wave shape measurements, the rotating mirror camera was used throughout. Owing to the low luminosity associated with the detonation wave of DNT, a thin, approximately 1 mm. thick, layer of tetryl was placed between the glass plate and the DNT across the field of view of the camera slit. This procedure was used also in velocity measurements made by the "streak" camera method and gave very satisfactory photographic traces. Wave shapes were photographed placing the charge so that the image of the camera slit coincided with a diameter of the charge. The trace of the emerging detonation wave was converted to actual wave shape by use of the experimental velocity, the appropriate magnification factor determined by photographing a "static image" on the film, and the speed of the camera.

### Results and Interpretations

The critical diameter of 2,4-DNT (−65 + 100 mesh) was found to be between 3.8 and 5.04 cm., consistent failures resulting at 3.8 cm. and consistent detonations at 5.04 cm. Figure 1 shows the experimental and theoretical detonation velocity–diameter plots for this explosive. The theoretical $D^*(\rho_1)$ (ideal velocity vs. density) relation computed by means of the $\alpha(v)$ equation of state and the empirical $\alpha(v)$ curve[5,6] is given by the equation

$$D^* = 4125 + 2270(\rho_1 - 1.0)$$

While it is uncertain from the experimental results that the experimental $D$–$d$ curve of Fig. 1 should level off at the velocity predicted from this equation, the use of this equation in theoretical calculations appears to give as satisfactory agreement as possible for each of the theories. At $d = 25$ cm. the measured velocity, in fact, was only 100 m./sec. lower than $D^*$ computed from this equation. An experimental evaluation of $D^*$ would have required a prohibitive amount of explosive due to the large diameters required to obtain ideal detonation, namely, about 35–40 cm.
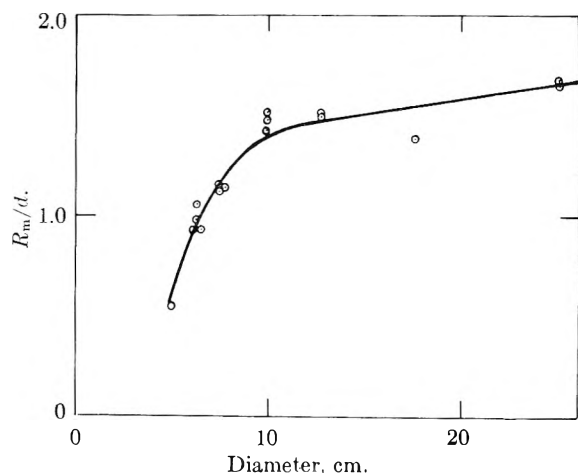
Fig. 2.—Steady state radius of curvature/diameter $(R_m/d)$ vs. diameter $(d)$ curves for 2,4-DNT.

of 2.5 and 3.2 cm. Those of the curved front theory were computed for $a_0 = 1.25$ and 1.75 cm. From the evidence of best fit, the best total reaction time according to the nozzle theory was about 7 $\mu$sec. while that for the curved front theory was about 4 $\mu$sec.

The curve front theory requires that the radius of curvature in the detonation wave in ideal explosives $(D = D^*)$ should always be equal to the length of propagation $L$. However, studies at this Laboratory show that $R/d$ increases with $L$ only over the first three to four charge diameters after which it attains a steady state or constant value $R_m$. In non-ideal explosives $(D < D^*)R/d$ increases with $L$ over even shorter distances than in ideal explosives and reaches a lower steady state $(R_m/d)$ value than in ideal explosives. Figure 2 shows the $R_m/d$ curve obtained for 2,4-DNT, showing a value of 0.57 at $d = 5$ cm. (just above $d_c$) and a maximum value (still increasing with diameter) of 1.6 at the



| $d = 7.54$ cm. | $d = 12.72$ cm. | $d = 25.2$ cm. |
| $R_m/d = 1.15$ cm. | $R_m/d = 1.48$ cm. | $R_m/d = 1.63$ cm. |
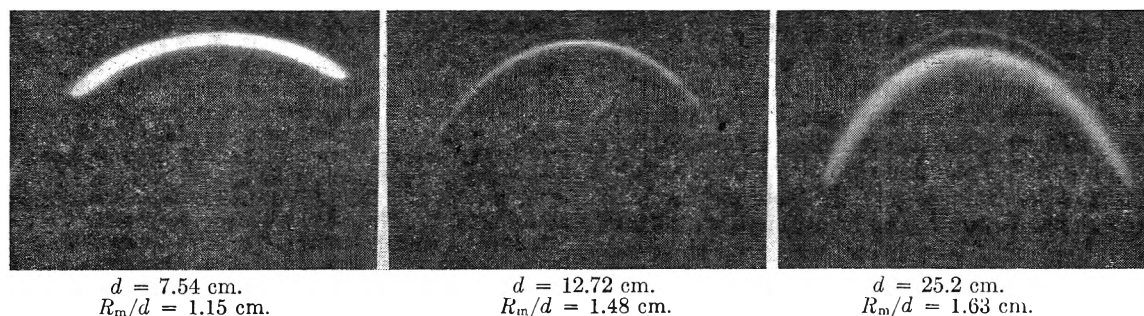
Fig. 3.—Typical rotating minor "streak" camera traces of the wave shape of 2,4-DNT ($-65 + 100$ mesh.)

The theoretical curves of the nozzle theory shown in Fig. 1 were computed for reaction zone lengths $a_0$

largest diameter studied, 25 cm. Typical wave shape traces for DNT are shown in Fig. 3.

# REACTION RATES OF AMMONIUM NITRATE IN DETONATION[1]

MELVIN A. COOK, EARLE B. MAYFIELD AND WILLIAM S. PARTRIDGE

*Explosives Research Group, University of Utah, Salt Lake City, Utah*

Detonation velocity and wave shape were measured as a function of charge diameter over wide diameter ranges in the explosives (1) cast 70.7/29.3 composition B-ammonium nitrate (AN), (2) cast 50/50 amatol (TNT–AN), (3) a loose-packed mechanical mixture of 50/50 TNT–AN, and (4) pure AN. The velocity-diameter curves were interpreted by the existing theories ("nozzle," "curved front") of reaction rates in detonation. Comparisons of the computed reaction rates of AN in low and high density 50/50 TNT–AN showed that the specific rate constant was two to three times as great at a density $\rho_l$ of 1.53 g./cc. as at $\rho_l = 1.0$ g./cc. This seems to show that the detonation temperature is about 300 to 600° higher at $\rho_l = 1.53$ than at $\rho_l = 1.0$ which bears out the approximate validity of the covolume $\alpha(v)$ equation of state for this explosive. Wave shape measurements showed consistently spherical wave fronts of steady state radius of curvature/diameter $(R_m/d)$ ratios between 0.5 and 3.8 depending on the explosive and its diameter and density. The $R_m/d$ ratio in pure AN was near unity in all cases and showed no definite diameter dependence. In loose-packed 50/50 TNT–AN, $R_m/d$ was 0.51 at the critical diameter and 2.1 at the maximum diameter studied (25 cm.). In 50/50 cast amatol $R_m/d$ increased from below unity near the critical diameter to 2.3 (still increasing) at the maximum diameter studied (20 cm.) and in cast composition B–AN, $R_m/d$ increased from below unity at the critical diameter to a maximum value of 3.8 which maintained for all diameters greater than 3.8 cm.

## Introduction

In a previous article[2] the rate of reaction of TNT in detonation was studied by analyzing the velocity $(D)$ vs. diameter $(d)$ curves obtained for pure TNT of various particle sizes. The existing theories on the influence of chemical reaction rate on the nature

of the $D(d)$ relations were used in this analysis, namely, the "nozzle,"[3] and the "curved front"[4] theories. By fitting all the curves in each case by the use of one empirical constant and the calculated theoretical hydrodynamic velocity $D^*$, the

(3) H. Jones, *Proc. Roy. Soc.* (*London*), **189A**, 415 (1947).

(4) (a) H. Eyring, R. E. Powell, G. H. Duffey and R. B. Parlin, *Chem. Revs.*, **45**, 16 (1949); (b) R. B. Parlin and D. W. Robinson, Technical Report No. VII, October 3, 1952, Explosives Research Group, University of Utah.

theoretical curves of the nozzle theory were found to be in excellent agreement with the experimental ones, but those of the curved front theory were in rather poor agreement. The experimental results of the influence of particle size were in agreement with the Eyring surface erosion model in which the flame front is assumed to penetrate the grain under constant gas phase temperature at constant radial rate with the total reaction time $\tau$ given by

$$\tau = \bar{R}_g/\lambda k' \qquad (1)$$

where $\bar{R}_g$ is the average or effective particle radius, $\lambda$ is the diameter of a molecule, and $k'$ is the specific rate constant given by

$$k' = \frac{kT}{h} e^{\Delta H^*/R} e^{-\Delta S^*/RT} \qquad (2)$$

in which the symbols have their usual significance.

A further evaluation of the curved front theory was obtained in the coarse TNT studies of reference 2 by comparing the observed shapes of the detonation wave fronts with those described by the theory. The wave shapes were found to be quite different from those described by the curved front theory.

Another explosive (or explosive ingredient) particularly desirable for theoretical study of reaction rate and in which reaction rate plays an important part in the determination of the "blasting action" of explosives based on it is ammonium nitrate (AN). Copp and Ubbelohde[5] measured the detonation velocities of cast 60/40 amatol (TNT–AN) in cyclindrical charges of diameters between 2.5 and 7.7 cm. using AN grists having surface areas ($A$) of 195 and 310 cm.$^2$/g. From their data together with data obtained by Payman, *et al.*, and Parisot and Laffitte for 60/40 and 50/50 amatol and pure AN, Copp and Ubbelohde arrived, by use of the nozzle theory, at average total reaction times $\bar{t}$ for the amatols given by the equations

$$\bar{t} = 3.7 \times 10^{-4}/A + 9 \times 10^{-7} \text{ (sec.) (60/40 amatol)}$$
$$\bar{t} = 3.3 \times 10^{-4}/A + 7 \times 10^{-7} \text{ (sec.) (50/50 amatol)}$$

These investigators concluded from their experimental studies that the reaction of AN in detonation has a low activation energy and the slow step may thus involve a physical rather than chemical rate process. This conclusion appears, however, to be based on an insufficiently broad range of experimental conditions and is not borne out by the more extensive experimental studies presented in this article.

This investigation was undertaken to provide data required for a thorough analysis of the reaction kinetics of AN in detonation by application of the existing theories. It includes the measurement over broad ranges in diameter of detonation velocities in the explosives 70.7/29.3 composition B–AN, 50/50 loose-packed and cast TNT–AN, and pure AN. Also included are numerous wave shape–diameter measurements on these explosives. The data are analyzed by means of the above theories of reaction rates. These results are then compared with those obtained by extrapolation of isothermal decomposition data for AN in accord with the requirements of the Eyring surface burning concept. Finally the evidence of the experimental data on

the determination of detonation temperature and the validity of the cov volume $\alpha(v)$ equation of state[6,7]

$$pv = nRT + \alpha(v)p \qquad (3)$$

is discussed.

## Experimental Methods and Results

All cast charges used in this investigation were poured in approximately one millimeter thick manila paper tubes at length/diameter ($L/d$) ratios greater than six. Except in the smallest diameters (near the critical diameter $d_c$), the tubes contained pin inserts for measurement of detonation velocity by a "pin-oscillograph" constructed in this Laboratory capable of measuring velocity with an accuracy of $\pm 0.1\%$. The AN used in the 70.7/29.3 composition B–AN casts and sample II of the 50/50 amatol cast series was a spherically grained product ("spray dried"). It was carefully screened through 20 and on 30 mesh standard U. S. gage screens. The AN used in sample I of the cast 50/50 amatol charges was likewise spherically grained but was not screened. An average screen analysis is given in Table I.

The loose-packed 50/50 TNT–AN charges were vibrator-packed into approximately one-millimeter thick manila paper tubes containing for the large diameters accurately spaced and measured pin inserts for velocity measurements by the "pin-oscillograph" method. (The tubes used in small diameters in both the cast and loose-packed charges did not contain pin inserts, but rather had plastic tape-lined windows for measurement of velocity by means of a rotating mirror "streak" camera constructed in this Laboratory having a maximum writing speed of 5 mm./$\mu$sec. and excellent photographic definition.)

All low density TNT–AN as well as the cast charges had an $L/d \geq 6.0$. The AN used in the low density TNT–AN series was a coarse unscreened product of spherical grains (spray dried). The screen analysis of this product is given in Table I along with that for the TNT and AN used in the other charges.

The pure AN charges were loose-packed by hand-tamping into tubes varying in wall thickness from 2 mm. in the smallest diameters (10–12.5 cm.) to 5 mm. in the largest sizes (40–46 cm.). Velocity measurements in this series were made by means of the pin-oscillograph methods in all cases. In order to use no more AN than necessary in the large sizes, finished charges were fired at an $L/d$ of 4.5 instead of six. For wave shape measurements the tubes were all accurately cut with the ends perpendicular to the longitudinal axis of the charge, and the slit of the "streak" camera was focussed across a diameter. Bare ends were used in some of the cast charges, and in the others a glass plate was placed over the end. In pure AN and the low density TNT–AN mixture, it was necessary to use a thin, approximately one millimeter thick, layer of tetryl between the glass plate and the explosive in order to obtain sufficient luminosity to record the emerging wave by means of the streak camera. All wave shape measurements were obtained in the steady state region which maintains beyond four charge diameters from the point of initiation in ideal explosives ($D = D^*$) to as low as one charge diameter in non-ideal ($D < D^*$) explosives. Since all charges used in this study had an $L/d$ of six or greater (except some of the largest AN charges where $L/d$ was 4.5) the values of the radius of curvature $R$ were thus the maximum or steady state values $R_m$.

Samples of the cast charges were sectioned to determine radial and axial density variations. Maximum density variations along the charge axis were found to be about 1% with a slight tendency for increased density toward the bottom of the charge. Radial variations in density were random but somewhat greater with maximum values no greater in any case than 2%. (Densities were measured in each shot both in the cast and loose-packed charges by carefully weighing and measuring the entire charge; densities obtained were thus average values.) The velocity data given in Fig. 1 and Table II were all corrected to given average densities by use of the appropriate $D(\rho_1)$ equation of the form

$$D = D_{1.0} + M(\rho_1 - 1.0) \qquad (4)$$

Corrections in all cases were small (corresponding to $\Delta \rho_1'$ of

(5) J. L. Copp and A. R. Ubbelohde, *Trans. Faraday Soc.*, **44**, 646 (1948).

(6) M. A. Cook, *J. Chem. Phys.*, **15**, 518 (1947).

(7) M. A. Cook, R. T. Keyes, G. S. Horsley and A. S. Filler, This Journal, **58**, 1114 (1954).

### Table I

#### Screen Analysis of AN and TNT[a]

| U. S. standard sieve | A, % | | B, % | C, % | D, % |
|---|---|---|---|---|---|
| − 12 + 16 | ... | ... | 8.9 | | ... |
| − 16 + 20 | ... | ... | 44.8 | 17.0 | ... |
| − 20 + 30 | ... | ... | 35.6 | 42.1 | ... |
| − 30 + 40 | 5.5 | 0.4 | 8.6 | 20.9 | 3.3 |
| − 40 + 50 | 48.7 | 73.4 | 2.1 | 10.4 | 35.7 |
| − 50 + 100 | 39.7 | 16.6 | ... | 9.6 | 43.9 |
| − 100 + 150 | 5.0 | 6.6 | ... | ... | 17.1 |
| − 150 | 3.4 | 3.4 | ... | ... | ... |

[a] A = Pure AN series. B = Loose-packed 50/50 TNT–AN series; C = Series I of 50/50 cast amatol series; D = TNT used in loose-packed 50/50 TNT–AN series.

ess than 0.1 g./cc.), and possible inaccuracies in the constants of equation 4 used were thus relatively unimportant. Values of $M$ used were 3500 m./sec./g./cc. in the cast charges and 3000 m./sec./g./cc. in the low density TNT–AN. No corrections were needed in the AN series, the density variations being negligible from one charge to the next with a given lot of AN. The limiting factor in velocity determinations was in all cases that imposed by density fluctuations and the experimental error in density determinations ($\lesssim \pm 2\%$).
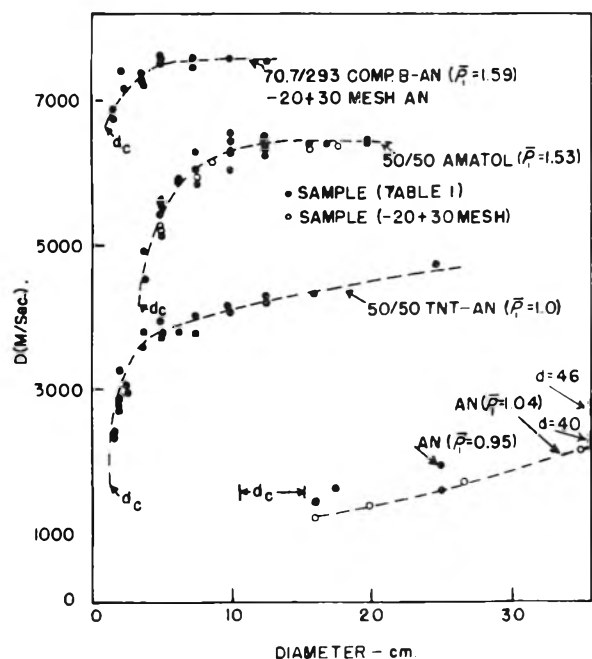


Fig. 1.—Velocity–diameter curves.

All cast charges as well as pure AN were shot with cast 50/50 pentolite boosters. The loose-packed TNT–AN charges were fired directly with No. 8 E.B. caps. For synchronization purposes most of the charges were fired by the discharge of a one-microfarad condenser charged at about 5000 volts. By this means the caps detonate within about 1 to 3 $\mu$sec. from the instant of discharge with a "jitter" of less than $\pm 2$ $\mu$sec.

The experimental velocity ($D$) vs. diameter ($d$) curves for the four AN explosives determined in this study are shown in Fig. 1 and Table II. In cast 70.7/29.3 composition B-AN the critical or minimum propagation diameter $d_c$ was about 1.3 cm., and the minimum diameter $d_m*$ for ideal ($D = D*$) detonation was about 5–8 cm. For 50/50 cast amatol $d_c$ was 3.5 cm. for both series of products, $d_m*$ was about 12–16 cm., and the measured $D*$ was about 6400 m./sec. In the loose-packed 50/50 amatol $d_c < 1.2$ cm., $d_m* < 25$ and $D* < 4700$ (theoretical velocity—4900 m./sec. computed from $\alpha(v)$ equation of state).

The velocity in pure AN as expected increased quite slowly with diameter and was still considerably below the theoretical velocity of 4300 m./sec. ($\rho_1 = 1.04$) computed from the $\alpha(v)$ equation of state at the maximum diameter fired (46 cm.).

Measurements of the shape of the wave front when converted to actual shape from the camera speed and magnification data showed that the wave front was spherical in shape in all cases. $R_m/d$ was reproducible within about 10% except in pure AN; results for pure AN while showing excellent spherical wave shape were less reproducible. The observed steady state radius of curvature/diameter ratios ($R_m/d$) are plotted against diameter in Fig. 2. These results show that $R_m/d$ fell between 0.5 and 1.0 at $d_c$. For 70.7/29.3 composition B-AN the $R_m/d$ vs. diameter curve appeared to level off at a value $R_m/d$ of 3.8 at $d \geq 5$ cm., but for the cast 50/50 amatol the $R_m/d$ curve was apparently still increasing at $d = 20$ cm. at which diameter $R_m/d$ was about 2.3. $R_m/d$ was obtained only at $d_c$ and at 24.6 cm. for the loose-packed 50/50 TNT–AN giving values of 0.51 at $d_c$ and 2.1 at 24.6 cm. In pure AN no definite diameter variation of $R_m/d$ was established, values all falling in the range $0.78 < R_m/d < 1.15$. The failure to observe a definite diameter dependence of $R_m/d$ was probably associated not with the fact that $R_m/d$ does not increase with $d$ in this case, but exhibits a very small $R_m/d$ vs. $d$ slope and poor experimental reproducibility.
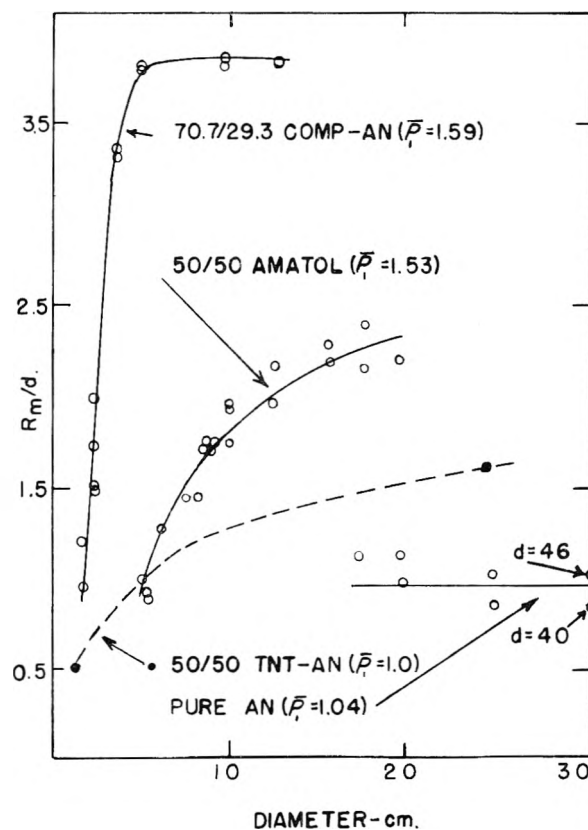


Fig. 2.—Steady state wave shape vs. diameter curves (wave fronts in general spherical with radius of curvature $R_m$).

### Discussion of Results

The nozzle theory equations and methods of analysis were outlined by Copp and Ubbelohde[5] and were also applied in reference 2. One requires the evaluation of one empirical constant ($a_0$—reaction zone length) and the calculated $D*$ or the observed maximum velocity which was accomplished by use of the values giving the best fit of the experimental curves. Actually no thermo-hydrodynamic data are required to apply the nozzle theory since the observed asymptotic velocity may be used for $D*$.

TABLE II

EXPERIMENTAL DETONATION VELOCITY-DIAMETER DATA

| a. 50/50 Amatol, cor. to $\rho_1 = 1.53$ g./cm.³ | | | | b. 55/50 TNT-ammonium nitrate granular mix, (cor. to $\rho_1 = 1.00$ g./cm.³ | | c. 70.7/29.3 composition B ammonium nitrate, cor. to $\rho_1 = 1.59$ g./cm.³ | | d. Pure ammonium Nitrate | |
| A. Sample I | | B. Sample II | | | | | | | |
| Dia., cm. | D, m./sec. | Dia., cm. | D, m./sec. | Dia.,[a] cm. | D, m./sec. | Dia.,[b] cm. | D, m./sec. | Dia., cm. | D, m./sec. |
|---|---|---|---|---|---|---|---|---|---|
| 3.50 | Failed | 3.40 | Failed | 1.25 | Failed | 1.37 | 6700 | 12.72 | Failed |
|  |  |  |  | 1.28 | 1766 |  | Failed |  |  |
| 3.81 | 4888 | 3.81 | 4765 |  | 1866 |  | 6700 | 16.0 | 1455 |
|  | 4509 |  | Failed |  | 1825 |  | Failed |  | 1150 |
|  |  |  |  |  | 1819 |  | Failed |  |  |
| 5.04 | 5397 | 5.04 | 5405 |  |  |  |  | 17.4 | 1545 |
|  | 5541 |  | 5190 | 1.60 | 2315 | 1.71 | 6868 |  | 1350 |
|  | 5456 |  | 5199 |  | 2406 |  | 6784 |  |  |
|  | 5411 |  | 5207 |  |  |  | 6769 | 19.89 | 1630 |
|  | 5199 |  | 5195 | 1.90 | 2825 |  | 6862 |  | 1665 |
|  | 5217 | 6.30 | 5847 |  | 3269 |  | 6862 |  | 1360 |
|  | 5590 |  | 5847 |  | 2727 |  |  |  |  |
|  | 5094 | 7.62 | 6067 |  | 2681 | 2.48 | 7051 | 25.4 | 1890 |
|  | 5602 |  | 6090 | 2.53 | 2945 |  | 7051 |  | 1600 |
|  |  |  |  |  | 3053 |  | 6997 |  | 1610 |
| 7.62 | 6270 | 8.89 | 6135 | 3.83 | 3789 |  | 7133 |  |  |
|  | 6116 |  | 6163 |  | 3583 |  | 7135 | 35.7 | 2150 |
|  | 5953 | 10.16 | 6250 | 5.04 | 3720 |  | 7138 |  |  |
|  | 5812 |  | 6237 |  | 3890 | 3.82 | 7270 | 40.4 | 2420 |
|  | 6023 | 12.70 | 6303 |  | 3750 |  | 7355 |  | 2300 |
|  |  |  |  | 6.30 | 3815 |  | 7277 |  |  |
| 10.16 | 6459 |  | 6350 |  | 3750 |  | 7381 | 46.0 | 2820 |
|  | 6005 | 15.80 | 6284 |  | 3855 |  | 7209 |  | 2705 |
|  | 6428 |  | 6320 | 7.54 | 3745 | 5.08 | 7545 |  |  |
|  | 6540 | 17.78 | 6316 |  | 3990 |  | 7762 |  |  |
|  | 5999 | 19.90 | 6368 |  | 3970 |  | 7608 |  |  |
|  | 6221 |  | 6370 | 8.82 | 3875 |  | 7488 |  |  |
|  |  |  |  |  | 3905 |  | 7533 |  |  |
| 12.70 | 6280 |  |  |  | 4000 | 7.56 | 7425 |  |  |
|  | 6478 |  |  | 9.94 | 4150 |  | 7571 |  |  |
|  | 6299 |  |  |  | 4025 |  | 7514 |  |  |
|  | 6263 |  |  |  | 4045 | 10.10 | 7540 |  |  |
|  | 6230 |  |  | 12.72 | 4177 |  | 7510 |  |  |
| 17.78 | 6351 |  |  |  | 4267 | 12.80 | 7510 |  |  |
|  |  |  |  |  | 4297 |  | 7525 |  |  |
|  |  |  |  | 16.00 | 4313 |  |  |  |  |
|  |  |  |  | 24.6 | 4705 |  |  |  |  |

[a] 12.7 cm. diameter with very fine AN used for hydrodynamic velocity $D^*_{1.00} = 5100$ m./sec. [b] for $d = 1.00$ cm., five out of five shots failed.

Equations applicable in the curved front theory are given in reference 2. Again one requires the evaluation of the empirical constant $(a_0)$ and $D^*$, and in addition thermohydrodynamic data are required to evaluate the parameters of the curved front theory. In other theories applied the detailed mechanism of grain burning is necessary in a pure explosive compound, and in mixtures thermohydrodynamic data are also needed. In order properly to carry out this investigation, therefore, detailed thermohydrodynamic calculations were made using the $\alpha(v)$ equation of state (equation 3). The results of these calculations are summarized in Table III. These data are applied whenever needed in the remaining discussion using interpolations where necessary.

For convenience the equations of the theories applicable in this study are repeated here. For the nozzle theory

$$(D^*/D)^2 = 1 + 9/4 \left[ \varphi^4 \left( \frac{a_0}{y} \right) - 1 \right] \quad (5)$$

$$\varphi \left( \frac{a_0}{y} \right) = 37/20 \left[ 1 - \left( \frac{a_0}{y} \right) \cot \theta \right] \quad (6)$$

$$a_0/y = 34/37 \left[ \sin \theta / (1 + \cos \sqrt{2}\theta) \right] \quad (7)$$

($y$ is the charge radius). For the curved front theory

$$y/a_0 = (M + N)K_c - N \quad (8)$$

$$K_c = \frac{2}{\delta(1 - \delta^2)^{1/2}} \tan^{-1} \left( \frac{1 + \delta}{1 - \delta} \right)^{1/2} = \frac{\pi}{2\delta} \quad (9)$$

where $\delta = D/D^*$, $M = 0.7/(1 + L)$, $N = 0.7/(2 \cdot (L' - 1) - L)$, $L = (v_1 - v_2)/v_2$ and $L' = 1 +$

TABLE III

THERMOHYDRODYNAMIC DATA[a] CALCULATED BY USE OF THE $\alpha(v)$ EQUATION OF STATE AND EMPIRICAL $\alpha(v)$ CURVE

| | Composition B | 70.7/29.3 Comp. B-AN | AN | | 50/50 Amatol | | | | TNT | |
|---|---|---|---|---|---|---|---|---|---|---|
| $\rho_1$ | 1.56 | 1.65 | 0.82 | 1.30 | 0.86 | 1.13 | 1.41 | 1.55 | 0.95 | 1.47 |
| $v_2$ | 0.508 | 0.480 | 0.91 | 0.58 | 0.875 | 0.682 | 0.550 | 0.508 | 0.76 | 0.52 |
| $Q$ (kcal./kg.) | 1140 | 1127 | 352 | 350 | 865 | 933 | 974 | 961 | 870 | 1125 |
| $n$ (moles/kg.) | 31.4 | 30.3 | 43.7 | 43.7 | 39.5 | 35.6 | 32.6 | 31.1 | 31.8 | 34.2 |
| $\bar{C}_{v*}$ (kcal./kg./deg.) | 0.348 | 0.374 | 0.307 | 0.315 | 0.336 | 0.353 | 0.366 | 0.370 | 0.334 | 0.375 |
| $T_2$ (°K.) | 4425 | 4160 | 1730 | 1830 | 3310 | 3430 | 3495 | 3555 | 3580 | 4050 |
| $D^*$ (m./sec.) | 7475 | 7630 | 3490 | 5270 | 4610 | 5330 | 6100 | 6500 | 4850 | 6480 |
| $p_2$ (atm.) $\times 10^{-3}$ | 188 | 200 | 25 | 67 | 45 | 74 | 114 | 139 | 60 | 135 |

[a] $\rho_1$, density of original explosive; $v_2$, specific volume at Chapman-Jouguet plane; $Q$, heat of explosion; $n$, moles of gas/kg.; $\bar{C}_{v*}$, average (ideal) heat capacity between 300°K. and $T_2$; $T_2$, detonation temperature; $D^*$, ideal detonation velocity; $p_2$, detonation pressure.

$\bar{C}_v(v_2 - \alpha)/nRv_2$ (see Table III for other definitions).

The calculated $D(d)$ curves from the theories (including the detonation head model which will not be discussed here) are compared with each other and with the experimental curves in Fig. 3. Values of the reaction time $\tau$, $a_0$ and $D^*$ are shown also in Fig. 3. In 50/50 amatol the nozzle theory gave excellent agreement but was less attractive in the other three explosives. As with coarse TNT the curved front theory was again not applicable. An experimental study of the absolute values of the reaction rate of AN found by the various methods employing the direct rate-of-pressure-development method will be presented separately as mentioned above.

Detailed discussion of the observed wave shape data will not be presented in this paper owing to several involved factors which must first be considered. One need simply remark that the results were not in accord with the basic postulates and predictions of the curved front theory. The approximations introduced in the application of the equation of continuity to this problem have been re-examined in this Laboratory in light of the experimental observations of spherical wave fronts in both ideal and non-ideal explosives, and the results showed that the curved front theory will require drastic change in order to treat properly wave shape and reaction rates in detonation.

The total reaction times obtained in this study by means of the two theories are compared in Table IV with values computed by equations 1 and 2 using the values $ke^{\Delta S^*/R}/h = 4 \times 10^9$ sec.$^{-1}$/°K. and $\Delta H^* = 38{,}300$ cal./mole measured in this Laboratory in isothermal decomposition studies of pure AN, and temperatures computed by the $\alpha(v)$ equation of state. The nozzle theory gives reaction times consistently between 0.1 and 0.04 as large as those extrapolated from isothermal decomposition data and the curved front theory between 0.05 and 0.02 times those computed by extrapolation of isothermal decomposition data. Results of the unpublished detonation head model are also included without discussion, as a matter of interest, since this theory has received wide circulation in classified literature.

Finally the experimental studies presented here for 50/50 cast amatol and loose-packed 50/50 TNT-AN provide evidence regarding the actual form of the equation of state applicable in detonation. It has been shown in reference 7 that, if one adopts the equation of state in the form

$$pv = nRT\varphi, \quad \varphi = e^z, \quad x = f(v)T^c \qquad (10)$$

where $c$ is a constant and $f(v)$ is a function of $v$ chosen for convenience in the form $g(v)v^{-1}$, the calculated detonation temperature obtained in the inverse method (use of the experimental $D(\rho_1)$ data)
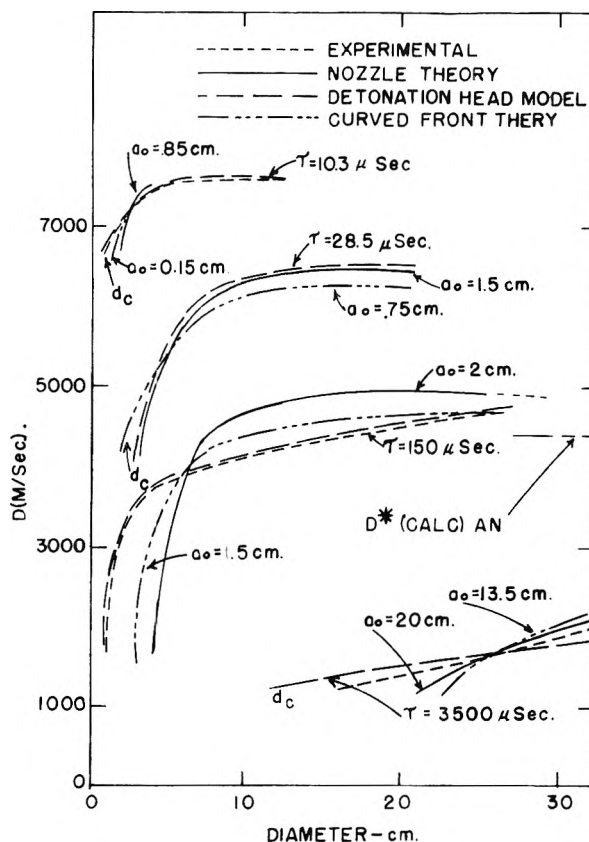


Fig. 3.—Comparisons of theoretical and experimental $D(d)$ curves.

depends critically on the value chosen for $c$. If $c$ is chosen to be zero corresponding to the $\alpha(v)$ equation of state, $T_2$ in general increases with $\rho_1$ between 200 and 600° in changing $\rho_1$ from about 1.0 to 1.6 g./cc. depending on the nature of the explosive, i.e., the nature of the products of decomposition and their variation with density. If $c$ is chosen to be

TABLE IV

COMPARISON OF CALCULATED TOTAL REACTION TIMES FOR AN

| Explosive | $T_2{}^a$ | $\tau^b$ (det. head) ($\mu$sec.) | $\tau_2$ (nozzle) ($\mu$sec.) | $\tau_2$ (curved front) ($\mu$sec.) | $\tau_2{}^c$ (isothermal) ($\mu$sec.) |
|---|---|---|---|---|---|
| 70.7/29.3 comp. B–AN | 4150 | 10.3 | 1.5 | 0.26 | 15 |
| 50/50 cast Amatol | 3510 | 20 | 3.4 | 1.7 | 39 |
| 50/50 TNT–AN ($\bar{p} \sim 1$) | 3300 | 150 | 7.4 | 5.4 | 110 |
| Pure AN | 1720 | 3500 | 130 | 100 | 5000 |

$^a$ Computed from $\alpha(v)$ equation of state. $^b$ From the approximation $\tau \cong 4\, a_0/3\bar{D}$. $^c$ Computed from equations $\tau = \bar{R}_g/\lambda k'$ and $k' = 4 \times 10^9\, Te^{-38,300/RT}$ (isothermal decomposition).

$-0.25$ corresponding approximately to the Kistiakowsky–Wilson–Brinkley equation of state

$$pv = nRT(1 + xe^x); \quad x = kT^c/v \qquad (11)$$

in general $T_2$ decreases about 200 to 400°K. over the same increase in density. If, on the other hand, $c$ is chosen to be positive (an unlikely value), $T_2$ increases with density even more rapidly than in the $\alpha(v)$ equation of state. It may also be noted that while $T_2$ depends rather critically on the form of the equation of state chosen, or on $c$, all other thermohydrodynamic quantities computed by the hydrodynamic theory are relatively insensitive to the form of the equation of state.

These considerations suggest that comparisons of reaction rates for explosives of constant composition but different densities, by means of the absolute reaction rate theory equation

$$k'(\rho_1')/k'(\rho_1'') = \frac{T_2'}{T_2''}e^{-\frac{\Delta H^*}{R}\left(\frac{1}{T_2'} - \frac{1}{T_2''}\right)} \qquad (12)$$

should give important information on the nature of the equation of state. Thus if the $\alpha(v)$ equation of state were correct using $\Delta H^* = 38.3$ kcal./mole, one would expect $k'(1.53)/k'(1.0)$ for 50/50 TNT–AN to be somewhat greater than unity. For $T_2\cdot(1.53) - T_2(1.0) = 200$ to 500°K., $k(1.53)/k'(1.0)$ should be about 1.4 to 2.5. With the K–W–B equation of state in which $T_2(1.53) - T_2(1.0) = -(200$ to 400); however, $k'(1.53)/k'(1.0)$ should be about 0.7 to 0.35. The experimental results obtained in this study show that the ratio $\tau_2(1.0)/\tau_2(1.53)$ varied between 7.5 and 2.2 depending on which theory one assumes to be correct. Part of the ratio $\tau_2(1.0)/\tau_2(1.53)$ is associated with the larger particle size of the AN used in the low density compared with that used in the cast amatol series. The calculated value of $\bar{R}_g(1.0)/\bar{R}_g(1.53)$ is roughly two. Hence $k'(1.53)/k'(1.0)$ is between 1.2 and 3.5, the most probable value being about 2.0. This would require $T_2(1.53) - T_2(1.0)$ to be about 300 to 400°K. which is only slightly higher in this case than that computed by the $\alpha(v)$ equation of state. It is clear, moreover, that $k'(1.53)/k'(1.0)$ is greater than unity showing that the K–W–B equation is inapplicable in this case. In later papers similar evidence will be presented for other explosives and ingredients also lending strong support to the validity of the equation of state(3).

---

# THE STRUCTURE OF ICE[1]

## By R. E. Rundle

*Contribution No. 384, Institute for Atomic Research, and Department of Chemistry, Iowa State College, Ames, Iowa*

Problems connected with the structure of ice are reviewed, particularly the problem connected with residual entropy and polar vs. non-polar structures. It is shown that if, at low temperature, ice is truly hexagonal, then there is a good reason to believe it is polar. A polar structure is attractive in explaining some of the physical properties of ice, but it leaves the residual entropy problem unsolved (though not hopeless), while the non-polar structure leaves some physical properties unexplained, but accounts for the entropy.

There have been many proposals for the structure of ice, the most successful of which has been the random structure of Pauling.[2] This structure accounts in a natural way for the residual entropy of ice,[3] and is compatible with the neutron diffraction study,[4] but it leaves unexplained other perplexing problems, such as why ice is hexagonal, certain electrical phenomena, and disorder-streaking of X-ray diagrams.

Various crystallographic studies have indicated that ice is polar, which is incompatible with the Pauling structure. These have included many reports of bullet-shaped snow crystals,[5] pitting of artificial ice single crystals on a single end of the crystals during sublimation,[6] and various electrical effects,[7] the most striking of which is the report that under proper conditions ice crystals show a strong piezoelectric effect.[8] Several investigations have failed to confirm the latter effect,[9] however, and the other support for the polar ice has been objected to on several grounds and is not definitive. On the theoretical side, arguments such as Bjerrum's[10] on

(1) Work was performed in the Ames Laboratory of the Atomic Energy Commission.

(2) L. Pauling, *J. Am. Chem. Soc.*, **57**, 2580 (1935).

(3) W. F. Giauque and J. W. Stout, *ibid.*, **58**, 1144 (1936).

(4) E. O. Wollan, W. L. Davidson and H. G. Shull, *Phys. Rev.*, **75**, 1348 (1949).

(5) U. Nakaya, "Snow Crystals, Natural and Artificial," Harvard University Press, Cambridge, Mass., 1954.

(6) J. M. Adams, *Proc. Roy. Soc. (London)*, **A128**, 588 (1930).

(7) See E. S. Cambell, *J. Chem. Phys.*, **20**, 1413 (1952) for a review of these reports.

(8) F. Rossmann, *Experientia*, **6**, 182 (1950).

(9) S. Steinemann, *ibid.*, **9**, 135 (1953); J. Mason and P. G. Owston *Phil. Mag.*, **43**, 911 (1952).

(10) N. Bjerrum, *Science*, **115**, 385 (1952).

the nature of dipolar interactions in ice are strong, and lead to an expectation of polar ice. So far, the most compelling reason for believing that ice is non-polar is that no polar model has yet been found which will explain the residual entropy of ice in the natural manner of the Pauling structure.

If one considers that, at least at very low temperatures, ice is truly rather than statistically hexagonal, then there is another reason for believing that ice is polar. Let us, for example, require that the true symmetry at each oxygen position be three-fold, as is required if ice is hexagonal. Let us also require $H_2O$ molecules. Now looking at one puckered net in the ice structure (Fig. 1) we see that there are two *kinds* of oxygens; oxygens of the *first kind* lie slightly above the average plane and have a ligand along the $C$-axis directed upward, while oxygens of the *second kind* lie slightly below the average plane and have a ligand along the $C$-axis but directed downward.
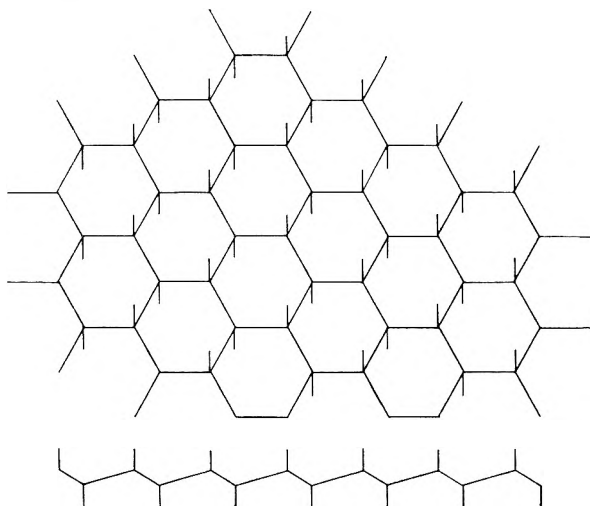


Fig. 1.—Hexagonal net of oxygens from the ice structure. The hexagonal axis is normal to the net, and the net is puckered with oxygens lying alternately at $\pm \ ^1/_{16} \ C$ above and below the plane. All oxygens at $+ \ ^1/_{16} \ C$ are linked to an oxygen in the plane above, those at $- \ ^1/_{16} \ C$ to an oxygen in the plane below, as noted in the bottom of this figure.

Directing attention to one oxygen of the *first kind*, Fig. 2, we see that there are six ways of putting two hydrogens on the four tetrahedral lines joining the oxygen to its neighbors. These six configurations fall into two classes, three with a hydrogen on the $C$-axis and three with no hydrogen along this direction.

We could describe the first three configurations in terms of a hydrogen in a parabolic well at positions 1, 2 or 3 which would result in the usual harmonic oscillator wave functions centered at positions 1, 2 or 3. (Let us call these $U_1$, $U_2$ and $U_3$.) These would not, however, be the proper wave functions for describing the system in a symmetrical field. Instead, the correct linear combinations are

$$U_{\rm s} = \frac{1}{\sqrt{3}} (U_1 + U_2 + U_3)$$

Type I $\quad U_{\rm A} = \frac{1}{\sqrt{3}} (U_1 + U_2 e^{2\pi i/3} + U_3 e^{4\pi i/3})$

$$U_{\rm A}' = \frac{1}{\sqrt{3}} (U_1 e^{4\pi i/3} + U_2 + U_3 e^{2\pi i/3})$$
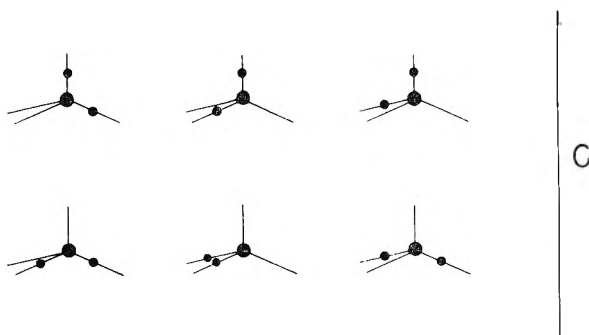


Fig. 2.—Possible hydrogen positions about an oxygen in the ice structure. There is one set of three equivalent structures (above) with a hydrogen on the $C$ axis, and one set of three (below) with no hydrogen on the $C$ axis.

where $U_{\rm S}$ is totally symmetric and is, in general, of different energy, than the functions $U_{\rm A}$ and $U_{\rm A}'$, which will be degenerate.

A similar set of three functions would describe the other three configurations of Fig. 2, with two hydrogens in the three symmetrical positions. Again, the correct description would involve a totally symmetric linear combination plus two other degenerate combinations differing in phase angle. We shall call these wave functions Type II.

The point of interest is that all wave functions of Type I result in a proton density of $^1/_3$ at each of the three sites 1, 2 and 3, while those of Type II result in a density of $^2/_3$ at each site. Choice of one type of wave function for one oxygen in the plane determines the choice at every set if we require that there be one hydrogen per O–H–O bond. This can be seen in Fig. 3, where one circle represents Type
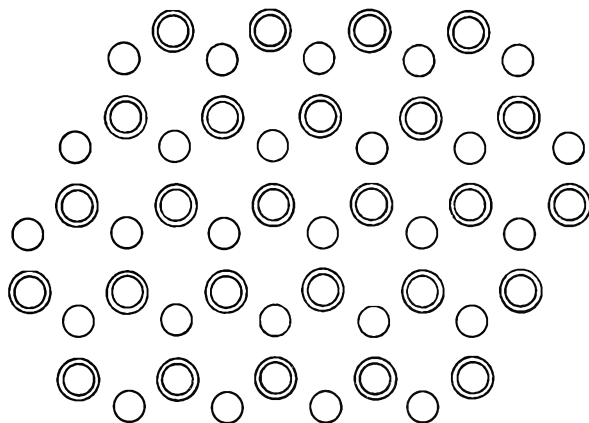


Fig. 3.—Arrangement of hydrogen distributions in wells about oxygen in the hexagonal net of the ice structure. A single circle represents a distribution of Type I, with $^1/_3$ hydrogen in each of the three wells about oxygen, a double circle represents a Type II distribution with $^2/_3$ hydrogen in each well about oxygen. To achieve one hydrogen on each O---O link, distributions must alternate.

I, and two circles represents Type II at each point, and it is noted that nearest neighbors must alternate between Type I and Type II. Furthermore all oxygens with Type I distribution are of the same *kind*, thus, their O–H bonds point in the same direction along $C$. Moreover, it is required that the oxygen directly above in the next plane be of the opposite kind, etc., which determines the entire arrangement. Furthermore, all Type I atoms in all

planes are of the same *kind* with their O–H bands pointing in the same sense along the $C$-axis, so that the structure is polar.

The question of the residual entropy of such a structure, using this non-classical count, is harder to settle. The three wave functions at each site are not all degenerate, even if no interaction among sites is assumed, and if the totally symmetrical state is the lowest in each case, as seems likely, there would be no residual entropy. If, however, the difference in energy is very low, as it would be for a high barrier for rotation about the threefold axis at each hydrogen site, then the three wave functions would become substantially degenerate leading to a residual entropy of $R \ln 3$. Furthermore, interactions among sites will undoubtedly alter the simple picture given here, lowering the degeneracy, and all that I feel prepared to say is that the residual entropy for this structure will lie between zero and $R \ln 3$.

It should be noted that one does not know the real symmetry at an oxygen site at low temperatures. At temperatures not far below the freezing point of ice, ice shows remarkable disorder scattering, and this is probably best explained if ice has only statistical rather than true hexagonal symmetry. However, this disorder scattering gradually fades as the temperature is lowered, and has substantially disappeared at a temperature above 90°K.[11]

The residual entropy, as obtained from calorimetric work, persists at least to 15°K., the lowest temperature involved in the heat capacity studies.[3] Hence, the disorder causing the diffuse scattering appears to be different from that leading to the residual entropy.

The structure above has substantially the same hydrogen positions as one I suggested some time ago.[12] It has only partial hydrogens at all sites except those along the $C$-axis, which are fully ordered, and the neutron diffraction data reported by Wollan, Davidson and Shull[4] do not distinguish between it and the Pauling structure. Data extending to reflections with larger values of $l$, the hexagonal index, could, however, distinguish between this polar structure and the Pauling structure, and further work on ice is reportedly in progress at both Oak Ridge and Brookhaven. Because of the disorder scattering at higher temperatures, and large thermal effects, such work will be most definitive if carried out at very low temperatures. (Indeed, neutron diffraction work at high and low temperatures may lead to an understanding of the disorder scattering.)

It should be noted that another polar structure has been found by Owston[13] which satisfies Bjerrum's arguments. It has monoclinic symmetry, and is a fully ordered structure, requiring that the reported

residual entropy be in error. Because of the close agreement between the residual entropy of $D_2O$[14] and $H_2O$[3] I have supposed that the residual entropy has been verified, and is an important feature which any correct structure must explain.

Owston's work does emphasize anew that the disordered, non-polar structure of Pauling does not seem to be the structure of lowest energy. Moreover, the relaxation time in ice is low enough to make it difficult to see how the full disorder required by Pauling's structure can be frozen in if there are appreciable differences in the energies of various hydrogen configurations. Troubles of this sort do not arise with the polar, hexagonal structure.

A tendency for ice to become polar might conceivably help in understanding both the disorder scattering and the slickness of ice. It has long been noted that one can skate on ice, not because the pressure melts the ice, but because even down to fairly low temperatures the surface of ice seems wet, that is, the surface energy of ice in air must be lowered by a surface film. If ice were strongly polar, the surface energy would be high due to surface charge unless disorder at the surface led to neutralization. Moreover, a highly polar ice would probably lead to twinning in which there is alternation of the direction of the polar axis, much as in the domains of a ferromagnetic single crystal. Such twinning should arise since a parallel arrangement of dipoles is fine when they are placed end to end, but very unfavorable when they are placed side by side. Submicroscopic twinning of this type would leave the $C$-axis parallel, or anti-parallel in all twins, and would be difficult to detect optically or crystallographically. Moreover, one might expect somewhat altered oxygen distances at the boundary between twins, leading to disorder scattering. The volume in the boundary layer should decrease with decreasing temperature due to the decrease in importance of the entropy factor which aids the stability of the disordered region. (It is possible that near the melting point the largest part of an ice crystal consists of the disordered regions.) These points are, at least qualitatively, in accord with observations of the disorder scattering, and are quite possibly amenable to experimental check.

Finally, it should be stated that the evidence for polar ice seems far from conclusive, and that unless a proper explanation for the residual entropy for polar ice can be given, the Pauling structure must be considered more probable. However, it has seemed worth noting that the evidence for the Pauling structure is also subject to challenge, and, indeed, some points seem easier to understand in terms of a polar structure. It is hoped that this discussion, if it does nothing else, at least makes it clear that there are still problems in the ice structure which deserve further study.

(11) P. G. Owston and K. Lonsdale, *J. Glaciology*, 1, 118 (1951).

(12) R. E. Rundle, *J. Chem. Phys.*, 21, 1311 (1953).

(13) P. G. Owston, *J. chim. phys.*, 50, C13 (1953).

(14) E. A. Long and J. D. Kemp, *J. Am. Chem. Soc.*, 58, 1829 (1936).

# THE KINETICS OF THE THERMAL DECOMPOSITION OF NITRIC ACID IN THE LIQUID PHASE

By Glenn D. Robertson, Jr., David M. Mason and William H. Corcoran

*Chemical Engineering Laboratory, California Institute of Technology, Pasadena, California*

*Received December 27, 1954*

The kinetics of the liquid phase decomposition of $HNO_3$ in the temperature range 54 to 88° suggests that the unimolecular decomposition of $N_2O_5$ which is known to exist in fuming nitric acid solutions plays a significant role in the rate-determining step. A rate mechanism experimentally indistinguishable from that of the $N_2O_5$ hypothesis involves the product $(NO_2^+)$-$(NO_3^-)$. The effect of several inorganic additives, namely, $H_2O$, $N_2O_4$, $N_2O_5$, $KNO_3$, $KHSO_4$, $NOHSO_4$, $H_2SO_4$ and $HClO_4$, on the rate of decomposition was in agreement with these postulated rate mechanisms. The inhibition of the decomposition rate by various additives tested was found to be insufficient to prevent the eventual attainment of high equilibrium pressures resulting from the decomposition of fuming nitric acid when stored in closed containers for periods of about a month in the temperature range 54 to 88°. Of all the additives tested on both a molal and a weight basis, $H_2O$ gave the most pronounced inhibiting effect on $HNO_3$ decomposition.

## Introduction

The thermal decomposition of fuming nitric acid[1] introduces many problems in storage and handling of this important material which is used as an oxidant for rocket fuels and as a nitrating agent in chemical syntheses. Some of the factors involved in the kinetics of its thermal decomposition are discussed here.[2]

The work of other investigators[3-6] has established the over-all stoichiometry of the decomposition to be

$$4HNO_3 \rightleftharpoons 4NO_2 + 2H_2O + O_2 \qquad (1)$$
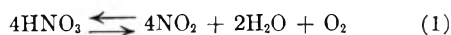
for both the liquid and gas phase reactions. Available equilibrium data[7] show that with an increase in temperature the products of decomposition are favored. These products have been observed over a temperature range from room temperature to 80° for the liquid phase reaction[3,6] and to 475° for the gas phase reaction.[4,5] At the temperatures encountered in the present investigation, *i.e.*, 54 to 88°, the formation of NO by the decomposition of $NO_2$ from the equation

$$2NO_2 \rightleftharpoons 2NO + O_2 \qquad (2)$$
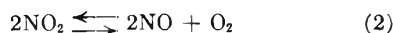
is negligible.[8]

Investigations[4,5] have shown that the rate of decomposition of $HNO_3$ in the vapor phase is not sufficiently high to account for the rates of pressure rise observed under actual storage conditions when both liquid and gas phases are present. Therefore a more detailed study of the kinetics of the liquid phase decomposition was undertaken, and measurements of pressure as a function of time under isochoric conditions were used to follow the rate of formation of $O_2$ and correspondingly the rate of decomposition of $HNO_3$.

## Description of Methods and Equipment

**Apparatus for Determining Decomposition Rate by Measurement of Pressure as a Function of Time.**—The usual method of following the rate of a chemical reaction is to observe the change with time of the concentration of one of the products or reactants. It is frequently more convenient, although not always feasible, to observe some physical property of the system which is related to the concentration of one of the species. In the present system, either electrolytic conductance[9] or optical absorbance[10] could have been observed since these properties have been shown to vary measurably with composition of the acid. Their use as analytical tools, however, would have required lengthy calibration procedures, and for this reason they were not utilized.

The increase in pressure resulting from the formation of oxygen offers an easily interpreted measure of the rate at which $HNO_3$ is decomposing. A sample of $HNO_3$ was confined in a precision-bore, glass capillary-tube (3 mm. i.d.) by Fluorolube[11] which has a greater density than the liquid acid. The liquid and gas phase volumes of the sample were determined to within ±0.0004 cc. by locating the gas–liquid and liquid–liquid interfaces with a cathetometer. Concentric with the capillary tube was another tube which was vacuum jacketed. Mineral oil, the temperature of which could be controlled to within ±0.05° of any desired value between 35 and 90°, flowed rapidly along the capillary tube in the annular space between it and the surrounding tube. To ensure constant physical equilibrium between phases, an iron pellet encased in glass was driven back and forth through the gas and liquid phase of the acid sample once per second by means of a pair of intermittently actuated electromagnets.

The pressure within the capillary tube was transmitted from the confining fluid through the mercury U-tube to an oil-filled pressure balance which was capable of measuring pressure with a precision of ±0.005 atmosphere up to a total pressure of 22 atmospheres. This balance had been calibrated against a standard balance which was periodically checked against the vapor pressure of $CO_2$ at the ice point.

While rate measurements were being made, the system containing about 1 ml. of liquid sample was maintained constant at approximately 25% ullage[12] by making small adjustments on a plunger in the hydraulic system, and the

(1) The term fuming nitric acid represents the ternary system $HNO_3$-$NO_2$-$H_2O$ for concentrations of $HNO_3$ greater than about 0.75 weight fraction. For the sake of brevity, $NO_2$ is used throughout this paper to designate equilibrium mixtures of $NO_2$ and $N_2O_4$ unless otherwise specified. Compositions are expressed in weight fractions on a formal basis. Also $HNO_3$ designates equilibrium mixtures with associated species such as $(HNO_3)_2$. See R. Dalmon and R. Freymann, *Compt. rend.*, **211**, 472 (1940).

(2) The material reported here is based largely on a thesis presented at the California Institute of Technology in 1953 by Glenn D. Robertson, Jr., in partial fulfillment of the requirements for the degree of Chemical Engineer. The work was part of a program sponsored by the Jet Propulsion Laboratory at the California Institute under Contract No. Da-04-495 ORD-18 for the U. S. Army Ordnance Corps.

(3) H. H. Franck and W. Schirmer, *Z. Elektrochem.*, **54**, 254 (1950).

(4) H. S. Johnston, L. Foering, Y. Tao and G. H. Messerly, *J. Am. Chem. Soc.*, **73**, 2319 (1951).

(5) H. S. Johnston, L. Foering and R. J. Thompson, THIS JOURNAL, **57**, 390 (1953).

(6) D. M. Mason, L. L. Taylor and H. F. Keller, Jet Propulsion Laboratory Report No. 20-72, Pasadena, California, 1953.

(7) W. R. Forsythe and W. F. Giauque, *J. Am. Chem. Soc.*, **64**, 48 (1942).

(8) D. M. Yost and H. Russell, Jr., "Systematic Inorganic Chemistry," Prentice–Hall, Inc., New York, N. Y., 1944.

(9) G. D. Robertson, Jr., D. M. Mason and B. H. Sage, *Ind. Eng. Chem.*, **44**, 2928 (1952).

(10) S. Lynn, D. M. Mason and B. H. Sage, *ibid.*, **46**, 1953 (1954).

(11) An inert, fluorinated hydrocarbon liquid manufactured by Hooker Electrochemical Co., Niagara Falls, N. Y.

(12) Ullage is a term used to describe the percentage of the gas phase volume relative to the total volume of the system.

pressure was recorded with time. The rate of increase of pressure with time can be related to the rate at which nitric acid decomposes as described in the section which follows.

Fluorolube S was observed to be quite inert with respect to $HNO_3$ at elevated temperatures, and $H_2O$ and $HNO_3$ are immiscible with this liquid. $NO_2$ appears, however, to be soluble in all proportions. This solubility could vitiate experiments made over extended periods of time. However, since only the initial rate of the forward reaction of equation 1 was of primary interest in this investigation, experiments did not exceed 1 hour in duration. In this time the loss of $NO_2$ from the system by diffusion into Fluorolube S was insignificant. The method used is capable of reproducing rates to within ±1%.

For convenience and to prevent contamination by moisture in the air, liquids were transferred by means of glass syringes fitted with long stainless steel hypodermic needles. The presence of dissolved air in the samples was not precluded.

**Calculation of Decomposition Rate from Pressure–Time Measurements.**—It was assumed that while the experiments were being conducted the gas phase was in continuous equilibrium with the liquid phase and contained $O_2$, $HNO_3$, $NO_2$, $H_2O$ and traces of inert gas (primarily $N_2$) from air initially dissolved in the liquid phase. Under isochoric, isothermal conditions the pressure was measured as a function of time. Decomposition in the gas phase was assumed to be negligible. It was assumed that the gas phase obeyed the perfect gas law and Dalton's law. From the stoichiometry of equation 1, it is evident that, for each mole of $O_2$ formed, 4 moles of $HNO_3$ decomposed and that

$$\frac{-d \text{ (moles } HNO_3)}{dt} = 4 \frac{d \text{ (moles } O_2)}{dt} \quad (3)$$

Some of the $O_2$ formed passed into the gas phase, and the remainder was dissolved in the liquid phase. The solubility of $O_2$ in fuming nitric acid is summarized in Fig. 1.[13] $O_2$
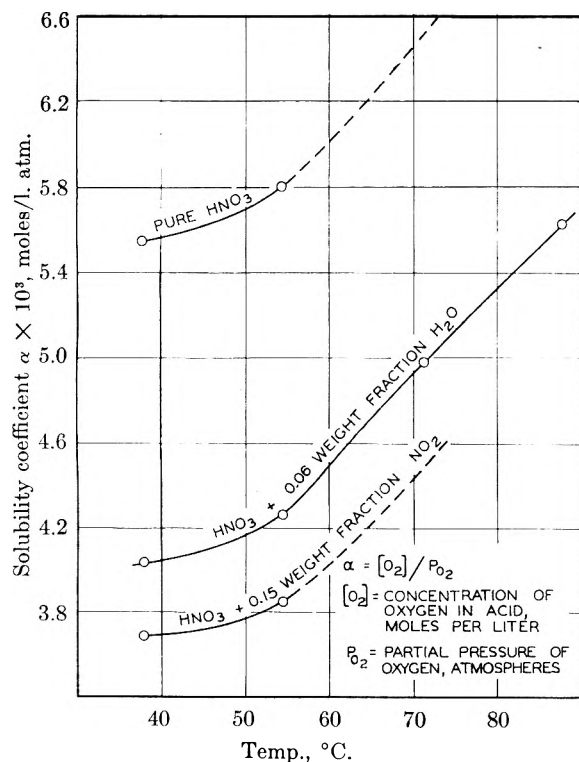


Fig. 1.—The solubility of oxygen in fuming nitric acid.

obeys Henry's law under the conditions encountered here. It was assumed that during the initial stages of decomposition of $HMO_3$ the ullage and Henry's law coefficients were constant. It was also assumed that the vapor pressures of

(13) G. D. Robertson, Jr., D. M. Mason and W. H. Corcoran, to be published in *Ind. Eng. Chem.*

the condensable components, as obtained from Fig. 2,[14-17] were constant during the measurements. By use of the stated assumptions the following expression relating the rate of decomposition of $HNO_3$, $-d [HNO_3]/dt$, to the observed pressure rise, $dP/dt$, was obtained. For a given value of ullage $U$, and Henry's law coefficient $\alpha$

$$\frac{-d [HNO_3]}{dt} = 4 \left[ \frac{U}{(100 - U)RT} + \alpha \right] \frac{dP}{dt} \quad (4)$$

Pressure–time data in the figures and initial-rate-of-pressure-rise data in the tables were converted from the experimental value of ullage to an ullage of 25% so that they are on a comparable basis. It was assumed that the volume of liquid was independent of ullage in the range of ullages studied from the experimental ullage to the 25% ullage.
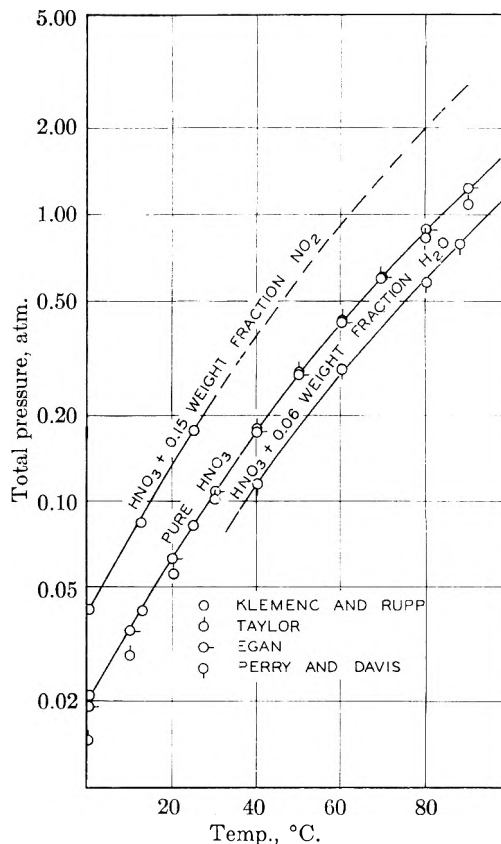


Fig. 2.—The effect of temperature on the total pressure of vapor above fuming nitric acid.

## Nomenclature

$d$    differential operator
$E_p$    experimental apparent activation energy in kcal./mole obtained from the variation of experimental rate with temp.
$k$    specific rate constant
$K$    thermodynamic equilibrium constant
$\ln$    natural logarithm
$P$    pressure (atm.)
$R$    universal gas constant
$t$    time (sec.)
$T$    temperature (°K., unless otherwise specified)
$U$    ullage, defined as $V_G/(V_G + V_L) \times 100$ (%)
$\alpha$    Henry's law coefficient (moles/l. atm.)

## Materials

$HNO_3$ was prepared by vacuum distillation at 40° from a mixture of $KNO_3$ and $H_2SO_4$.[7] The product was condensed at −79° and subsequently stored under refrigeration at

(14) A. Klemenc and J. Rupp, Z. anorg. allgem. Chem., **194**, 51 (1930).

(15) G. B. Taylor, Ind. Eng. Chem., **17**, 663 (1925).

(16) E. P. Egan, Jr., ibid., **37**, 303 (1945).

(17) J. H. Perry and D. S. Davis, Chem. Met. Eng., **41**, 188 (1934).

−30°. The acid thus prepared was analyzed for $H_2O$ by acidimetric titration with NaOH and was always found to contain less than 0.001 weight fraction $H_2O$. Previous experience with optical absorbance[10] has shown that quantities of the species $NO_2$ too minute to be determined easily by chemical analysis were sufficient to impart a definite yellow color to $HNO_3$, which itself is water-white at 0°. Therefore no specific test for $NO_2$ was made, but the acid was considered to be free of this species if, before a test, the sample lacked any trace of yellow. Commercial $NO_2$ was fractionated and dried over $P_2O_5$. Distilled $H_2O$ was obtained from the available laboratory supply.

Materials used in the studies of the effects of additives on the liquid phase decomposition of $HNO_3$ were obtained from various sources. Anhydrous $NH_4NO_3$, $KNO_3$ and $KHSO_4$ of reagent-grade quality were carefully dried under vacuum to remove any traces of adsorbed moisture. NOHSO$_4$ was prepared from $NO_2$ and concentrated $H_2SO_4$ in accordance with a method tested by Elliott, et al.,[18] $N_2O_5$ containing about 0.05 weight fraction of a mixture of $HNO_3$ and $NO_2$, was obtained by distilling $HNO_3$ to which an excess of $P_2O_5$ had been added.[8]

Anhydrous $H_2SO_4$ was prepared by mixing concentrated $H_2SO_4$ and $SO_3$ until an acidimetric titration indicated that an excess of 0.005 weight fraction $SO_3$ existed. Commercial concentrated $HClO_4$ containing 0.30 weight fraction $H_2O$ was mixed with an excess of $H_2SO_4$ and distilled to yield a product which contained less than 0.006 weight fraction $H_2O$ as indicated by titration with a standard solution of NaOH.

## Results

### Experimental Verification of Phase Equilibrium.

—Original experimental measurements of pressure as a function of time for 25 tests are available elsewhere.[19] From these tests rates of pressure rise with time at zero time were calculated from the slope of the pressure–time curves corrected to 25% ullage at 71.1°. The results are summarized in Table I. In Table II the initial rates of decomposition in terms of moles $HNO_3$/liter sec. are shown and were calculated from the corresponding initial rates of pressure rise obtained from pressure–time curves adjusted to 25% ullage. Examples of pressure–time curves at 87.8° from which initial rates of pressure rise were obtained are shown corrected to 25% ullage in Fig. 3. The increased pressures obtained with $NH_4NO_3$ were attributed to the formation of $N_2$ and $N_2O$ as a result of decomposition of $NH_4NO_3$ in $HNO_3$. The linearity of the initial portion of the curves in Fig. 3 indicates that the reverse of the reaction of equation 1 was not taking place to any appreciable extent during the period in which the initial rates were being determined. As the reverse reaction becomes more prominent, curvature is observable, as is evident in the curves of Fig. 3 at high values of time. Eventually as equilibrium with respect to equation 1 is attained, the rate of change of pressure approaches zero.

To determine the practicability and limits of the method chosen to follow the course of the reaction, several preliminary experiments were performed. For example, since $O_2$ bubbles visibly formed within the liquid phase, it was necessary to know if under

(18) G. A. Elliott, L. L. Kleist, F. J. Wilkins and H. W. Webb, *J. Chem. Soc.*, 1219 (1926).

(19) Material supplementary to this article has been deposited as Document number 4550 with the ADI Auxiliary Publications Project, Photoduplication Service, Library of Congress, Washington 25, D. C. A copy may be secured by citing the Document number and by remitting $1.25 for photoprints, or $1.25 for 35 mm. microfilm in advance by check or money order payable to: Chief, Photoduplication Service, Library of Congress.
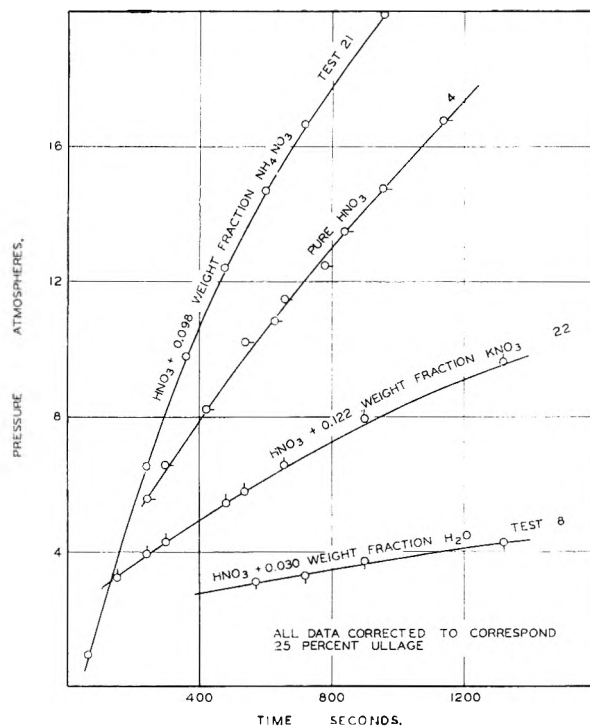


Fig. 3.—The effect of various additives on the initial pressure rise due to decomposition of nitric acid at 87.8°.

the experimental conditions supersaturation of $O_2$ occurred in that phase. The pressure–time data without agitation were irregular, and, in most instances at a given time the pressure without agitation had a value less than that with agitation, indicating that where agitation was not present supersaturation of $O_2$ in the liquid phase occurred. Kinetic data were thus obtained with agitation, and the rate of agitation was assumed to be sufficient to maintain physical equilibrium between the gas and liquid phases.

**Homogeneity of Liquid Phase Reaction.**—To show whether or not the liquid phase reaction was heterogeneous, the liquid–glass interfacial area was increased tenfold by adding glass wool to the liquid phase. The presence of the glass wool prevented agitation and thus permitted supersaturation of the liquid phase by $O_2$. This effect was

TABLE I

Summary of the Effect of Various Additives on the Initial Rate of Pressure Rise in Liquid Nitric Acid Mixtures at 71.1°

| Test no. | Additive | Amount, mole frac. | Initial rate of pressure rise,[a] atm./ 24 hr. day |
|---|---|---|---|
| 21 | $NH_4NO_3$[b] | 0.0982 | 2080 |
| 14 | $N_2O_5$ | .103 | 1570 |
| 3 | None | . . . | 194 |
| 12 | $N_2O_4$ | .111 | 90 |
| 15 | $KNO_3$ | .105 | 57 |
| 16 | $KHSO_4$ | .109 | 44 |
| 18 | $H_2SO_4$ | .108 | 25 |
| 17 | NOHSO$_4$ | .100 | 20 |
| 19 | $HClO_4$ | .090 | 16 |
| 7 | $H_2O$ | .099 | 10 |

[a] The initial rate of rise is given per 24-hr. day for acid stored at 25% ullage.   [b] Measurements made at 87.8°.

TABLE II

SUMMARY OF INITIAL RATE OF DECOMPOSITION OF NITRIC ACID IN THE LIQUID PHASE

| Test no. | Compn.[a] of the system, wt. frac. | Concn. of additive,[b] additive, moles/l. | mole frac. | Temp., °C. | $-\dfrac{d[HNO_3]}{dt} \times 10^5$, moles/l. sec. |
|---|---|---|---|---|---|
| 1 | 1.00 HNO₃ | 0 | 0 | 54.4 | 1.49 |
| 2 | 1.00 HNO₃ | 0 | 0 | 62.8 | 5.06 |
| 3 | 1.00 HNO₃ | 0 | 0 | 71.1 | 16.1 |
| 4 | 1.00 HNO₃ | 0 | 0 | 87.8 | 140 |
| 5 | 0.0088 H₂O | 0.69 | 0.030 | 71.1 | 3.34 |
| 6 | .0088 H₂O | 0.68 | .030 | 87.8 | 33.4 |
| 7 | .0304 H₂O | 2.39 | .099 | 71.1 | 0.85 |
| 8 | .0304 H₂O | 2.34 | .099 | 87.8 | 10.5 |
| 9 | .0600 H₂O | 4.59 | .183 | 87.8 | 1.84 |
| 10 | .0509 NO₂ | 0.80 | .035 | 71.1 | 11.1 |
| 11 | .0971 NO₂ | 1.56 | .069 | 71.1 | 8.60 |
| 12 | .1536 NO₂ | 2.50 | .111 | 71.1 | 6.30 |
| 13 | .0089 H₂O ⎱ .0866 NO₂ ⎰ | 0.73 ⎱ 1.38 ⎰ | .031 ⎱ .060 ⎰ | 71.1 | 2.51 |
| 14 | .165 N₂O₅ | 2.5 | .103 | 71.1 | 131 |
| 15 | .1586 KNO₃ | 2.6 | .105 | 71.1 | 4.78 |
| 16 | .2085 KHSO₄ | 2.7 | .109 | 71.1 | 3.85 |
| 17 | .1836 NOHSO₄ | 2.5 | .100 | 71.1 | 1.60 |
| 18 | .1584 H₂SO₄ | 2.4 | .108 | 71.1 | 2.03 |
| 19 | .1363 HClO₄ | 2.0 | .090 | 71.1 | 1.31 |
| 20 | .1363 HClO₄ | 2.0 | .090 | 87.8 | 13.3 |

[a] When not expressed, the remainder of the sample consists of HNO₃. [b] These values of concentration and mole fraction for the additives are given on a formal basis for the molecular species indicated.

minimized, however, by conducting the experiment at 87.8° where the lack of external agitation was shown to have a small effect. The data obtained when the glass wool was present agreed very closely with those which were obtained in the absence of glass wool. This agreement indicates that the reaction which occurred in the liquid phase was homogeneous with respect to a glass surface.

**Predominance of Liquid Phase Reaction.**—The visual evidence that bubbles of $O_2$ originated throughout the liquid phase as decomposition proceeded supports qualitatively the fact that in the range of temperatures investigated, 54 to 88°, the liquid phase reaction was controlling. Also there is evidence that the initial rate of pressure rise in pure $HNO_3$ increased with a decrease in ullage. This fact further supports a liquid phase controlling reaction because the concentration and consequently the rate of thermal decomposition of $HNO_3$ in the vapor phas aree not a function of ullage. It is known, however, that $HNO_3$ vapor can decompose thermally[4,5] and under the influence of light.[20] Reynolds and Taylor[20] showed that photochemical action is effective only for the decomposition of $HNO_3$ in the gas phase and that the corresponding rate is of a much lower order of magnitude than that of the liquid phase thermal decomposition being studied. To demonstrate that the rate of the photochemical gas phase reaction was negligible under the conditions encountered in the present work, $HNO_3$ vapor at about 35 mm. of mercury in a 250-cc. spherical flask was subjected to

artificial light of the same intensity as that which existed in the studies using the high pressure capillary tube. The constancy of pressure with time for this system at 80° indicated that no appreciable decomposition occurred.

Data obtained by Johnston, et al.,[4,5] for the gas phase thermal reaction indicate that it is heterogeneous in nature below 300° and slow compared with the liquid phase reaction at the temperatures investigated in the present study. The lowest temperature investigated by Johnston, et al., was about 130°. An extrapolation of the reported rate constants to the highest temperature of the present investigation, i.e., 87.8°, yields the value of $2 \times 10^{-5}$ mole/l. sec. for the rate of disappearance of $HNO_3$ caused by gas phase decomposition. Thus at 25% ullage and assuming gas phase decomposition Johnston's data give an upper limit on the rate of $HNO_3$ decomposing in the gas phase in contact with 1 liter of pure liquid $HNO_3$ as $0.7 \times 10^{-5}$ mole/sec. In the present investigation a rate of $140 \times 10^{-5}$ mole/sec. (cf. test 4 in Table II) was observed under these conditions. Thus it may be inferred that liquid phase decomposition is controlling. In the heterogeneous gas phase reaction the energy of activation is about 5 kcal./mole, whereas in the liquid phase decomposition, as is discussed subsequently, the experimental energy of activation lies in the range 32 to 37 kcal./mole. A consideration of the latter energy shows the large temperature dependence of the liquid phase decomposition and indicates again that the gas phase reaction is not controlling. It has thus been assumed that the rate of decomposition in the gas phase is negligible in the results that are presented.

**General Effect of Additives on the Rate of Thermal Decomposition.**—Table II gives a summary of the initial rates of decomposition of $HNO_3$ in the liquid phase at the temperature specified in the range 54.4 to 87.8°. In this table compositions are expressed both in mole fraction and in moles per liter. Density data for the $HNO_3$–$NO_2$–$H_2O$ system used to convert composition from weight fraction to mole fraction were obtained from the work of Klemenc and Rupp[14] and that of Berl.[21] The rate data were derived from the pressure–time data[19] by the method previously described. Included in the data are the effects of various additives ($H_2O$, $NO_2$, $N_2O_5$, $KNO_3$, $KHSO_4$, $NOHSO_4$, $H_2SO_4$ and $HClO_4$) on the rate of decomposition. It is seen from Tables I and II that, whereas it was possible to inhibit the reaction with some of the additives, this inhibition is insufficient to prevent extensive decomposition for prolonged storage periods.

$H_2O$ is most effective as an inhibitor. Figure 4 depicts the effects of $H_2O$ concentration on the initial rate of decomposition of $HNO_3$ at temperatures of 71.1 and 87.8°. As the mole fraction of $H_2O$ is changed from 0 to 0.183, corresponding to 0 to 4.59 moles/liter, there is an 18-fold decrease in the initial rate of decomposition of the $HNO_3$.

Where solid salts were added, the partial molar volumes were assumed to be negligible, and additive volumes were used where $H_2SO_4$ and $HClO_4$ were

(20) W. G. Reynolds and W. H. Taylor, J. Chem. Soc., 101, 131 (1912).

(21) E. Berl, Chem. Met. Eng., 46, 234 (1939).
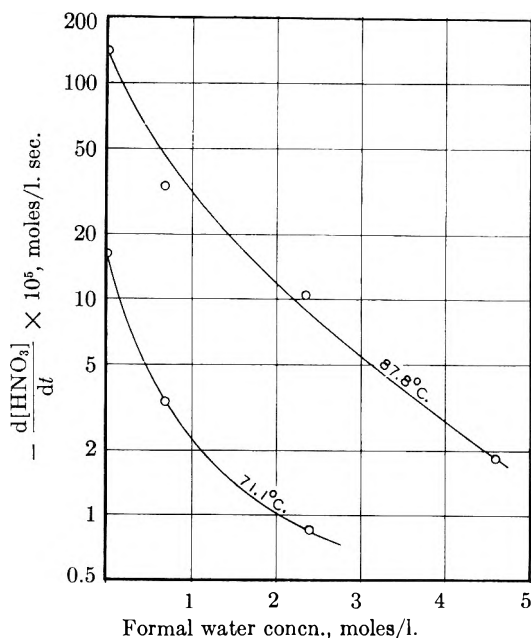
Fig. 4.—The effect of water on the initial rate of decomposition of nitric acid.

introduced. For the kinetics studies most of the data on initial rates were obtained at 71.1°, since at 87.8° the rates with pure $HNO_3$ were too great to allow accurate determination.

**Effect of Temperature on Rate of Thermal Decomposition.**—To determine the effect of temperature upon the rate of thermal decomposition, rate measurements with pure $HNO_3$ were made at 54.4° (test 1), 62.8° (test 2), 71.1° (test 3) and 87.8° (test 4). The pressure–time curves for these tests are shown in Fig. 5. The rate of decomposition of $HNO_3$ at 87.8° was so great that the resulting data are not considered reliable for obtaining quantitative values of initial rates. By the method described previously, the initial slopes of the curves in Fig. 5 are expressed in terms of the initial rate of decomposition of $HNO_3$. If the variation of specific rate constants with temperature were known, the Arrhenius equation could be used to determine the energy of activation of the rate-determining step in the decomposition. In this investigation the actual concentration of the reacting species was not determinable because of the unknown extent of various equilibria existing in $HNO_3$ solutions, as is discussed in a subsequent section. Consequently no specific rate constants could be calculated. An apparent energy of activation $E_p$ was obtained, however, by employing a relationship of the form of the Arrhenius equation[22]

$$\frac{d \ln \text{rate}}{d (1/T)} = - \frac{E_p}{R} \quad (5)$$

where

$$\text{rate} = - \frac{d [HNO_3]}{dt} \quad (6)$$

in moles per liter per second.

Figure 6 shows the results of a plot of the log of initial rate of decomposition *versus* $1000/T$ at three

(22) For the sake of brevity, the term rate is used throughout this report to designate the rate of decomposition of $HNO_3$. Since the liquid phase reaction is controlling, the rate is expressed in terms of moles of $HNO_3$ decomposed per liter of liquid $HNO_3$.
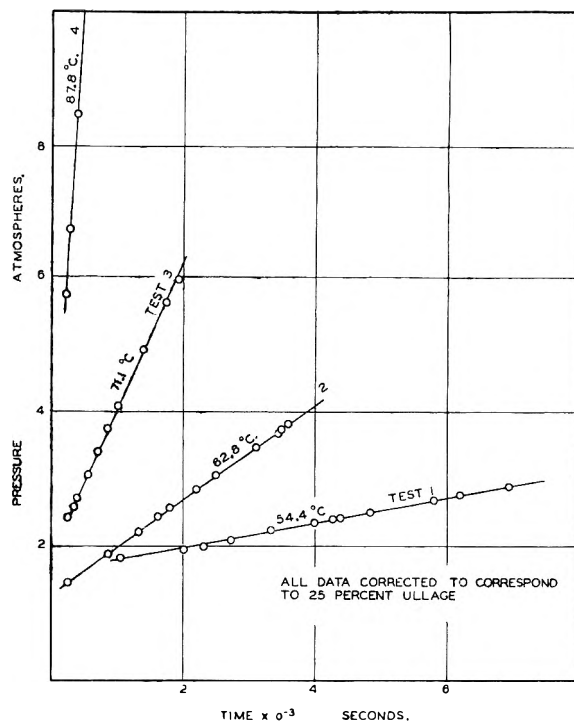


Fig. 5.—The effect of temperature on the initial pressure rise due to decomposition of pure nitric acid.

different temperatures for pure $HNO_3$ (tests 1 to 3). Curves are also shown for mixtures of $HNO_3$ with $H_2O$ (tests 7 and 8) and with $HClO_4$ (tests 19 and 20). The values of $E_p$ calculated from the slopes of the straight lines for these three systems are presented in Table III.
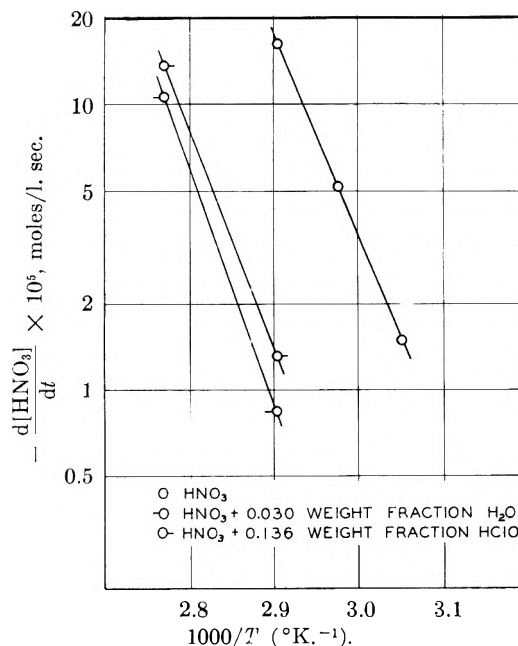


Fig. 6.—The variation with temperature of the rate of decomposition of nitric acid mixtures.

## Analysis of Results

**Possible Role in the Reaction Mechanism of Various Equilibria in $HNO_3$ Solutions.**—The work of Franck and Schirmer[3] where they proposed

TABLE III

APPARENT ENERGY OF ACTIVATION OF FUMING NITRIC ACID

| Test no. | System | $E_p$ kcal./mole |
|---|---|---|
| 1 to 3 | Pure $HNO_3$ | 32 |
| 19 and 20 | $HNO_3$ + 0.136 wt. frac. $HClO_4$ | 34 |
| 7 and 8 | $HNO_3$ + 0.030 wt. frac. $H_2O$ | 37 |

that the decomposition of $HNO_3$ proceeds by the first-order decomposition of $N_2O_5$ was done before the recent evidence for the self-ionization[23-27] of pure $HNO_3$ and other equilibria in $HNO_3$ solutions was available. The newer data should be examined to see what bearing they may have on the mechanism of decomposition.

It has been shown that the following ionic equilibrium exists in $HNO_3$ containing less than about 5% $H_2O$

$$2HNO_3 \rightleftharpoons NO_2^+ + NO_3^- + H_2O \qquad (7)$$
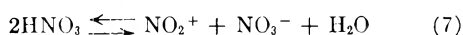
The fractional ionization of pure $HNO_3$ at $0°$ has been determined[28] from optical absorbance measurements to be about 0.05. This ionization may occur in two steps.[25] The first step is a proton shift resulting in the formation of the nitricacidium ion $H_2NO_3^+$ and $NO_3^-$, that is

$$2HNO_3 \rightleftharpoons H_2NO_3^+ + NO_3^- \qquad (8)$$
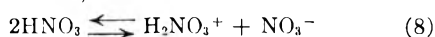
Subsequently $H_2NO_3^+$ almost completely dissociates into the nitronium ion $NO_2^+$ and $H_2O$ as

$$H_2NO_3^+ \rightleftharpoons NO_2^+ + H_2O \qquad (9)$$
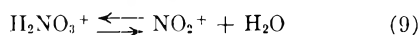
and the net result is given by equation 7.

$NO_2$[27] ionizes in $HNO_3$ solution in accordance with the equation

$$2NO_2 \rightleftharpoons N_2O_4 \rightleftharpoons NO^+ + NO_3^- \qquad (10)$$

The fractional ionization of $NO_2$ in $HNO_3$ solutions is quite large, being about 0.7 according to optical absorbance measurements.[28] $N_2O_5$ also ionizes to a large extent in $HNO_3$ solutions[26,27] in the following manner

$$N_2O_5 \rightleftharpoons NO_2^+ + NO_3^- \qquad (11)$$
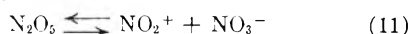
The equilibrium position of equation 11 has been shown[26] to lie far to the right, even at $N_2O_5$ concentrations as high as 0.6 molar. $HNO_3$ also is known to undergo a solvation reaction with $NO_3^-$ from compounds such as $KNO_3$[29,30]

$$2HNO_3 + NO_3^- \rightleftharpoons (HNO_3)_2NO_3^- \qquad (12)$$
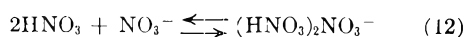
It is likely that $NO_3^-$ formed by the ionization of $NO_2$ (cf. eq.10) reacts with $HNO_3$ in accordance with equation 12.

Raman spectral and thermal studies[30] have shown that the following solvation of $HNO_3$ and $H_2O$ occurs in concentrated $HNO_3$ solutions

(23) C. K. Ingold and D. J. Millen, J. Chem. Soc., 2612 (1950).

(24) W. J. Dunning and C. W. Nutt, Trans. Faraday Soc., 47, 15 (1951).

(25) E. G. Taylor, L. M. Lyne and A. G. Follows, Can. J. Chem., 29, 439 (1951).

(26) R. J. Gillespie, E. D. Hughes and C. K. Ingold, J. Chem. Soc., 2552 (1950).

(27) J. D. S. Goulden and D. J. Millen, ibid., 2620 (1950).

(28) S. Lynn, D. M. Mason and W. H. Corcoran, THIS JOURNAL, 59, 238 (1955).

(29) J. Chédin and S. Fénéant, Compt. rend., 228, 242 (1949).

(30) D. M. Mason, L. L. Taylor and S. P. Vango, Anal. Chem., in press.

$$nHNO_3 + H_2O \rightleftharpoons (HNO_3)_nH_2O \qquad (13)$$
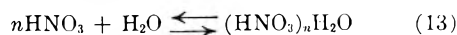
The existence of the foregoing equilibria which affect the actual concentration of $N_2O_5$ existing in solution prevents Franck and Schirmer's[3] first-order rate expression from being confirmed without knowing the actual concentration of $N_2O_5$. Consistent with their data and assumptions is the possibility that the rate-determining species may not be $N_2O_5$ but instead may be one or both of the products of its ionic dissociation such as $NO_3^-$ or $NO_2^+$. In ensuing discussions the equilibria in reactions (7) through (13) are assumed to be attained very rapidly as compared with the rate of decomposition of $HNO_3$.

**Inhibiting Effect of $H_2O$ and Accelerating Effect of $N_2O_5$ on Reaction Rate.**—It was experimentally observed (cf. Fig. 4) that a marked decrease in rate resulted from the addition of a relatively small amount of $H_2O$ to $HNO_3$, the effect decreasing with increase in water added. By the reaction of equation 7 an increase in $H_2O$ tends to increase the concentration of $HNO_3$ and correspondingly of $H_2NO_3^+$ (cf. eq. 8) whereas by the reaction of equation 13 an increase in $H_2O$ reduces the $HNO_3$ and $H_2NO_3^+$ concentration. The marked change in rate of decomposition of $HNO_3$ for such a relatively small added amount of $H_2O$ appears to eliminate $HNO_3$ in the rate-determining step since the concentration of $HNO_3$ is little affected by such small additions of water. Although the quantitative effect of $H_2O$ on the concentration of $H_2NO_3^+$ depends upon the interdependent equilibria of equations 7 through 13, the net qualitative effect is that of increasing the amount of $H_2NO_3^+$, as is expressed by equation 9. Such behavior eliminates $H_2NO_3^+$ as the rate-determining species. The effect of $H_2O$ in decreasing the rate is in keeping with the corresponding reduction of $NO_2^+$ by equation 7 or $N_2O_5$ by the reaction

$$2HNO_3 \rightleftharpoons N_2O_5 + H_2O \qquad (14)$$
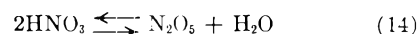
That either $N_2O_5$ or $NO_2^+$ may be the rate-determining species is also qualitatively supported by the marked increase in decomposition rate observed with the addition of $N_2O_5$ (test 14 in Table II) which ionizes to give $NO_2^+$ and $NO_3^-$ by equation 11. Thus a mechanism involving either $N_2O_5$ or $NO_2^+$ as the rate-determining species is in keeping with the experimentally observed effect of $H_2O$ reducing and of $N_2O_5$ increasing the rate of decomposition of $HNO_3$, as is shown in Table II. The mechanism involving the first-order decomposition of $N_2O_5$ is ambiguous since the expression

$$- \frac{d [HNO_3]}{dt} = k_{15} [NO_2^+][NO_3^-] \qquad (15)$$

is indistinguishable from the equation

$$- \frac{d [HNO_3]}{dt} = k_{16} [N_2O_5] \qquad (16)$$

because of the interdependence of $NO_2^+$, $NO_3^-$ and $N_2O_5$ in the rapid equilibrium of equation 11.

**Inhibition of Reaction Rate by $H_2SO_4$ and $HClO_4$.**—One means of differentiating between the mechanism involving $N_2O_5$ or $NO_2^+$ alone is to add components to the system so that $NO_2^+$ is increased and $N_2O_5$ is decreased in concentration; $H_2SO_4$

and $HClO_4$ are such additives. It has been shown from Raman spectra that acids which are stronger than $HNO_3$ can donate a proton to $HNO_3$ to form $H_2NO_3^+$ which dissociates, as is shown in equation 9. The effect of adding $H_2SO_4$ to $HNO_3$ is represented by

$$HNO_3 + H_2SO_4 \rightleftharpoons NO_2^+ + H_2O + HSO_4^- \quad (17)$$
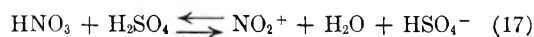
and this equation combined with equation 14 gives

$$N_2O_5 + H_2SO_4 \rightleftharpoons NO_2^+ + HSO_4^- + HNO_3 \quad (18)$$
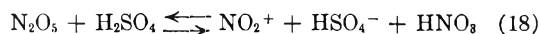
The effect of adding $HClO_4$ to $HNO_3$ is represented by

$$HNO_3 + HClO_4 \rightleftharpoons NO_2^+ + H_2O + ClO_4^- \quad (19)$$

and equation 19 combined with equation 14 gives

$$N_2O_5 + HClO_4 \rightleftharpoons NO_2^+ + ClO_4^- + HNO_3 \quad (20)$$
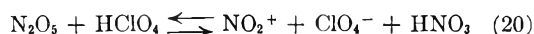
From the high concentration of $NO_2^+$ detected by Raman spectra,[31] the position of the equilibria in equations 18 and 20 lies very far to the right. It is seen from Table II that both $H_2SO_4$ and $HClO_4$ markedly decrease the rate of decomposition of $HNO_3$. This behavior is in keeping with the hypothesis that $N_2O_5$, and not $NO_2^+$ alone, is the rate-determining species since both $H_2SO_4$ and $HClO_4$ reduce the amount of $N_2O_5$ and increase the amount of $NO_2^+$.

**Effect of Several Salts Including Nitrates on Reaction Rate.**—Both neutral salts and nitrates (to a lesser extent) are found to decrease rate. Since the equilibria in equations 17 and 19 lie far to the right, $KHSO_4$ and $KClO_4$ can be considered neutral salts in $HNO_3$, and they would exert little mass action effect on ionic equilibria such as those represented by equations 7 through 13. Of these two salts only $KHSO_4$ was sufficiently soluble (0.1 mole fraction) to permit its use for evaluating the salt effect in this investigation. The reduction of the decomposition rate by the salt effect which is caused by the addition of $KHSO_4$ to $HNO_3$ is shown in Table II, where it can be compared with other additives. The normal result of an increase in ionic strength is to decrease the rate of a reaction occurring in solution between two ions of unlike charge. Thus the observed decrease in rate caused by the inert salt $KHSO_4$ is to be expected from a rate expression (*cf.* eq. 15) containing unlike ions. However, theories valid only at low ionic strength are not strictly applicable to $HNO_3$ solutions since at $70°$ the self-ionization of $HNO_3$ alone is sufficient to give an ionic strength probably greater than 0.3 mole/liter.[26]

It is evident from Table II that, for amounts of either $NO_2$ or $KNO_3$ which are equivalent to the neutral salt $KHSO_4$, less inhibiting effect occurs with the $NO_2$ and $KNO_3$. Thus a net catalytic effect which over-shadows the neutral salt effect is evidenced by these compounds which give $NO_3^-$. Such behavior would be expected if $N_2O_5$ and not $NO_2^+$ were the rate-determining species since equation 11 shows that $NO_3^-$ increases $N_2O_5$ and decreases $NO_2^+$. The increase in $N_2O_5$ by $NO_3^-$ according to equation 11 is not as pronounced as might be due to the competing reaction equation 12 in-

(31) C. K. Ingold, D. J. Millen and H. G. Poole, *J. Chem. Soc.*, 2676 (1950).

volving association of $NO_3^-$ with $HNO_3$. At very low concentrations of $NO_3^-$ it is expected that the inhibition of the reaction due to the salt effect would be reduced and that a net increase in rate of decomposition of $HNO_3$ would occur.

The marked decrease in rate caused by $NOHSO_4$ (*cf.* Table II) indicates not only the salt effect shown by $KHSO_4$ but in addition a greater inhibiting effect, probably because $NO^+$ reacts with $NO_3^-$ to form the species $NO_2$ and $N_2O_4$ in accordance with equation 10. This decrease in $NO_3^-$ requires a shift to the right in the equilibrium of equation 11 which lowers the concentration of $N_2O_5$ and, at the same time, increases $NO_2^+$. Thus in agreement with the hypothesis that $N_2O_5$ and not $NO_2^+$ is the rate-determining species, $NOHSO_4$ should cause more of a reduction in rate than $KHSO_4$.

**Apparent Energy of Activation of Reaction.**— If the actual concentration of the molecular species $N_2O_5$ were known, a specific rate constant $k_{16}$ could be calculated from the observed rate of decomposition, and the energy of activation $E$ could then be obtained from the Arrhenius equation. However, since the actual concentration of $N_2O_5$ is not known, the apparent activation energy defined by equation 5 is used.

The experimental apparent energies of activation obtained from the slopes in Fig. 6 are shown in Table III to vary between 32 and 37 kcal./mole. These data were obtained for pure $HNO_3$, for an $HNO_3$ solution containing 0.136 weight fraction $HClO_4$, and for a solution containing 0.030 weight fraction $H_2O$. Within experimental precision the apparent energies of activation for these different $HNO_3$ solutions are in close agreement, and it can therefore be implied that $HNO_3$ is decomposing in a similar fashion in these different solutions. A value for the energy of activation of about 24 kcal./mole for the decomposition of $HNO_3$ was reported by Franck and Schirmer.[3]

### Conclusions

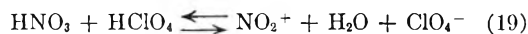This investigation presents the effects of several additives on the rate of the thermal decomposition of $HNO_3$ in the liquid phase. It has been shown that the presence of any of these additives in quantities up to 0.1 mole fraction does not inhibit the rate of decomposition sufficiently to prevent the eventual approach to equilibrium for storage periods of the order of months at elevated ambient temperatures. On both a molal and weight basis $H_2O$ was the most effective inhibitor tested.

The kinetic studies suggest that the rate-determining step in the decomposition reaction involves the first-order decomposition of the molecular species $N_2O_5$ or the interaction of its products of ionization, $NO_2^+$ and $NO_3^-$. Which of these mechanisms prevails is indeterminable by the present methods of measurement. It might be speculated that $N_2O_5$ decomposes to $NO_2$ and $NO_3$ molecules and that $NO_3$ in turn yields $NO_2$ and $O$. Extensive investigation, however, is necessary to establish a definite mechanism. An experimental energy of activation has been determined for the decomposition of pure $HNO_3$ and for the $HNO_3$–$H_2O$ and $HNO_3$–$HClO_4$ systems. To determine the actual energy of activation and to substantiate $N_2O_5$ as the rate-de-

termining species, it is suggested that a physico-chemical technique such as measurement of optical absorbance in the ultraviolet range[32] might be employed to determine the concentration of $N_2O_5$ and perhaps $NO_3^-$ present in $HNO_3$.

The effects of the various additives used in this investigation were emphasized by introducing them at relatively high concentrations of about 0.1 mole

(32) R. N. Jones and G. D. Thorn, *Can. J. Res.*, **27B**, 580 (1949).

fraction. If further studies in this field are undertaken, it is suggested that more dilute solutions be investigated. Such a procedure permits the use of additives such as $KClO_4$ which, by virtue of their low solubility in $HNO_3$, could not be investigated in the present work. Moreover, in dilute solutions the neutral salt effect of nitrates may be diminished to the extent that the expected acceleration of the rate of decomposition by $NO_3^-$ could be observed.

---

# AN IMPROVED METHOD FOR OPERATING ION-EXCHANGE RESIN COLUMNS IN SEPARATING THE RARE-EARTH ELEMENTS[1]

By Walter E. Nervik

*University of California, Radiation Laboratory Livermore Site, Livermore, Cal.*

A "gradient elution" method has been adapted for operating an ion-exchange resin column using an eluting agent in which the pH is changed continuously. The method shortens the column operating time required for separation of the rare earth elements without adversely affecting their purity.

## I. Introduction

Procedures for separating individual members of the rare-earth group of elements through the application of synthetic cation exchange resins have been described by many investigators.[2-5] The exact experimental conditions in each case depended on the number of elements to be separated and the degree of separation desired. In general, the rare earth elements were first adsorbed on the top portion of a long narrow column of cation-exchange resin, then selectively eluted by passing a solution containing a suitable complexing agent through the resin column and collecting portions of the eluent. The degree of separation for a given experimental arrangement depends on variables such as temperature, type of cation-exchange resin, size of the resin particles, dimensions of the column, eluting agent used, concentration and pH of the eluting agent, flow rate of the eluting agent, etc., but for a given eluting agent the relative position of the various rare earths remains approximately constant.[3] An experimental consequence of this phenomenon is the fact that if operating conditions are adjusted to effect separation of the heavy rare earths, the light rare earths require excessively long column operating times before being eluted. If conditions are adjusted to give separation of the light rare earths in reasonable operating times, the heavy rare earths are usually eluted too quickly to give high purity. Ordinarily the chemist has to make some compromise between purity of individual rare earths and column operating time. This series of experiments has been undertaken to determine whether introduction of an additional variable, *i.e.*, continuous change in pH of the eluting solution, could be used to effect complete separation of all of

the individual rare earths in relatively short column operating times.

Although the author was not aware of it at the time, the elution technique which was finally developed was quite similar to the "gradient elution" chromatographic method originally described by Alm, Williams and Tiselius.[6] In addition, the physical arrangement of the various reservoirs and column equipment components was similar to that used by Busch, Hurlbert and Potter.[7]

## Experimental

**Materials.**—Commercial 12% cross-linked Dowex-50 cation-exchange resin of "minus 400" mesh size was graded to obtain that portion which settled between 1.0 and 1.5 cm./min. in distilled water. The resin was washed with 6 $M$ ammonium thiocyanate until the red ferric thiocyanate color was no longer visible, then washed in turn with distilled water, 6 $N$ hydrochloric acid and distilled water again. Finally, the resin was converted to the ammonium form with 1 $M$ ammonium lactate and stored in distilled water until loaded on the column.

The eluting agents were prepared from conductivity water, Baker and Adamson reagent grade 85% lactic acid, and concentrated ammonium hydroxide. All solutions were 1 $M$ in total lactate concentration with the pH adjusted with concentrated ammonium hydroxide and measured on a Beckman Model G pH meter. The solutions were also made approximately 0.01 $M$ in phenol to prevent deterioration of the lactate.

Rare earth activities were obtained by bombarding a target consisting of alternate layers of pure uranium and tantalum metal foil with 340 Mev. protons in the 184-inch Berkeley synchrocyclotron. The target foils were dissolved in a solution of concentrated hydrofluoric acid and nitric acid to which 5 mg. of lanthanum carrier and 1 mg. each of strontium, zirconium, niobium, molybdenum, ruthenium, rhodium, palladium, tin, antimony, tellurium and barium carriers had been added. The mixed rare earth activities were then purified as a group by fairly well-known chemical steps which included a fluoride precipitation in the presence of dichromate, a barium sulfate "scavenge" in dilute acid solution, precipitation of the rare earth hydroxides with ammonium hydroxide, passage of the rare earth group through a small Dowex A-1 anion-exchange resin column in concentrated hydrochloric acid (to remove those elements

(1) This work was performed under the auspices of the U. S. Atomic Energy Commission.

(2) B. H. Ketelle and G. E. Boyd, *J. Am. Chem. Soc.*, **69**, 2800 (1947).

(3) S. W. Mayer and E. C. Freiling, *ibid.*, **75**, 5647 (1953).

(4) F. H. Spedding, J. E. Powell and E. J. Wheelwright, *ibid.*, **76**, 612 (1954).

(5) E. C. Freiling and L. R. Bunney, *ibid.*, **76**, 1021 (1954).

(6) R. S. Alm, R. J. P. Williams and A. Tiselius, *Acta Chem. Scand.*, **6**, 826 (1952).

(7) H. Busch, R. B. Hurlbert and V. R. Potter, *J. Biol. Chem.*, **196**, 717 (1952).

which form anionic chloride complexes under these conditions), and a zirconium phosphate "scavenge" in 4 $N$ hydrochloric acid. Each of these steps was performed at least twice before the rare earth group was considered pure enough to be used on the column. Previous experience had shown that activities of all of the rare earths were formed in this type of bombardment in sufficient quantities for easy detection and that no measurable amounts of fission product activities other than the rare earths were present after the initial chemical purification.

**Apparatus.**—Preliminary experiments indicated that "gravity feed" of the eluting agent, *i.e.*, controlling the flow rate of the eluting agent through the resin by adjusting the height of the reservoir containing the eluting agent, did not give sufficiently high flow rates for the long column dimensions and fine resin particles that were to be used in the current experiments. Therefore, an apparatus (a schematic diagram of which is shown in Fig. 1) was designed which would permit a wide range of accurate external pressures to be applied to the solution passing through the resin bed and which, in addition, would be relatively simple in operation and maintenance. The ion-exchange resin bed dimensions were 7 mm. i.d. × 60 cm.; this column was surrounded by a 7 cm. o.d. reservoir filled with water, and around the reservoir was wound a 3 inch by 60 inch "Electrothermal" heating tape. The temperature in this entire apparatus was controlled by a "Variac" variable transformer connected to the heating tape and measured by means of a thermometer in a well immersed in the water reservoir. Since normal operating temperatures were above 90°, a small water-cooled condenser was installed above the water level in the reservoir to minimize losses due to evaporation. Elution characteristics of rare earths on columns using this type of heating arrangement were found not to differ in any way from those which used the conventional heating systems with either trichloroethylene or steam vapor jacketing.

The eluting agent reservoir system consisted of two 2,000-ml. flasks arranged in such a manner that the solution in the upper flask could be made to drop into the lower flask at any desired rate by means of a stopcock control. Both of these units were connected to a "Nullmatic" pressure regulator which was found to maintain the desired pressures to ±1 inch of water. This regulator was then connected to the laboratory air pressure system through a small air filtering unit.

**Procedure.**—When preparing for a run, the equipment was assembled and the column unit brought up to a stable temperature of approximately 90°. The resin was boiled in distilled water to remove dissolved gases and transferred to the column unit while hot. The new resin bed was preconditioned by passing through at least 100 ml. of the eluting agent which was to be used in the run. The rare earth activities were adsorbed on a small amount of resin by equilibrating in a hot solution of low ionic strength for several minutes. The resin was then washed twice with boiling distilled water and transferred while still hot to the top of the resin bed. Since the purpose of the experiments was to determine the effect of various continuous rates of change of $pH$ on the elution characteristics of the rare earths, an attempt was made to keep all experimental conditions other than the rate of change of $pH$ constant. A single resin bed was used throughout, the resin being reconditioned between runs by passing suitable quantities of $pH$ 7, 1 $M$ lactate and $pH$ 3.19, 1 $M$ lactate solutions through the column. A pressure of 5 p.s.i., which gave a flow rate of approximately 0.4 ml./cm.²/min., was used on all runs. The initial $pH$ of the eluting agent in the lower reservoir was 3.19. The upper reservoir contained a solution of the same total lactate concentration at a $pH$ of 7.0, and the flow rate of this solution into the lower reservoir was adjusted during each run to give the desired rate of change of $pH$. In most cases the initial volume of $pH$ 3.19 solution in the lower reservoir was adjusted so that the flow rate of the $pH$ 7 solution was approximately the same as the flow rate of the solution through the column. In order to ensure complete and continuous mixing of the solution in the lower reservoir, a small magnetic stirring device was kept in operation during each run.

After a run had begun, samples of the eluent were collected in the collecting tubes over three-minute intervals by means of an automatic sampling turntable. For the activity assay, a drop of the eluent was obtained on an aluminum plate, evaporated to dryness under a heat lamp, and the activity in each sample counted in a proportional
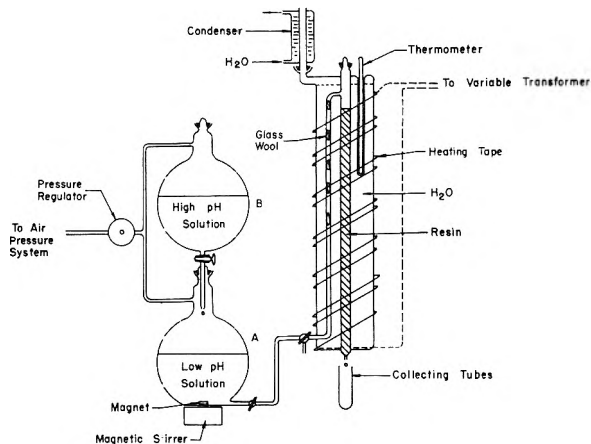


Fig. 1.—A schematic diagram of an ion-exchange column apparatus in which the $pH$ of the eluting agent may be changed continuously.

counter. Unequivocal identification of the individual peaks could be made through the known decay characteristics of the active nuclides present in each element. Determination of the $pH$ of the eluting agent was made by direct measurement with the Beckman $pH$ meter on the solution in the collecting tubes.

## III.  Results and Discussion

An initial $pH$ of 3.19 was used since it was found to effect satisfactory separation of the three heaviest rare earths in a reasonable column operating time under these experimental conditions. A "standard" elution curve which was obtained by passage of $pH$ 3.19 solution through the column without any change in $pH$ is shown in Fig. 2. While the curve shows some evidence of excessive "tailing" on several of the peaks, it has the general characteristics of a "normal" elution curve. The heavy elements (lutetium, ytterbium and thulium) are quite closely spaced but reasonably pure with a column operating time of two hours and thirty-five minutes for lutetium. The lighter elements are also separated but the column operation time rapidly becomes excessive, samarium requiring more than 38 hours for elution.

Figure 3 shows the elution curve which was obtained with an initial $pH$ of 3.19 and an average rate of change of $pH$ ($dpH/dt$) of 0.107 $pH$ unit/ hour. Actually, this run was made before that shown in Fig. 2, so that the short-lived activities of erbium and holmium could still be seen. Comparison of the curves of Fig. 2 and Fig. 3 shows several striking differences. The heavy elements are eluted slightly sooner with the changing $pH$ (1 hour and 55 minutes *versus* 2 hours and 35 minutes for lutetium) but the separation between adjacent elements is still satisfactory. However, lighter rare earths are eluted much more rapidly in the second case than in the first without any adverse effect on their purity. Thus, with this rate of change of $pH$, samarium was eluted in 4 hours and 58 minutes as against 38 hours and 25 minutes for the constant $pH$ elution. Lanthanum was eluted in 8 hours and 20 minutes while, with no change in $pH$, it may reasonably have been expected to take more than 100 hours to elute.

Additional elution curves similar to that shown in Fig. 3 have been obtained with average $dpH/dt$
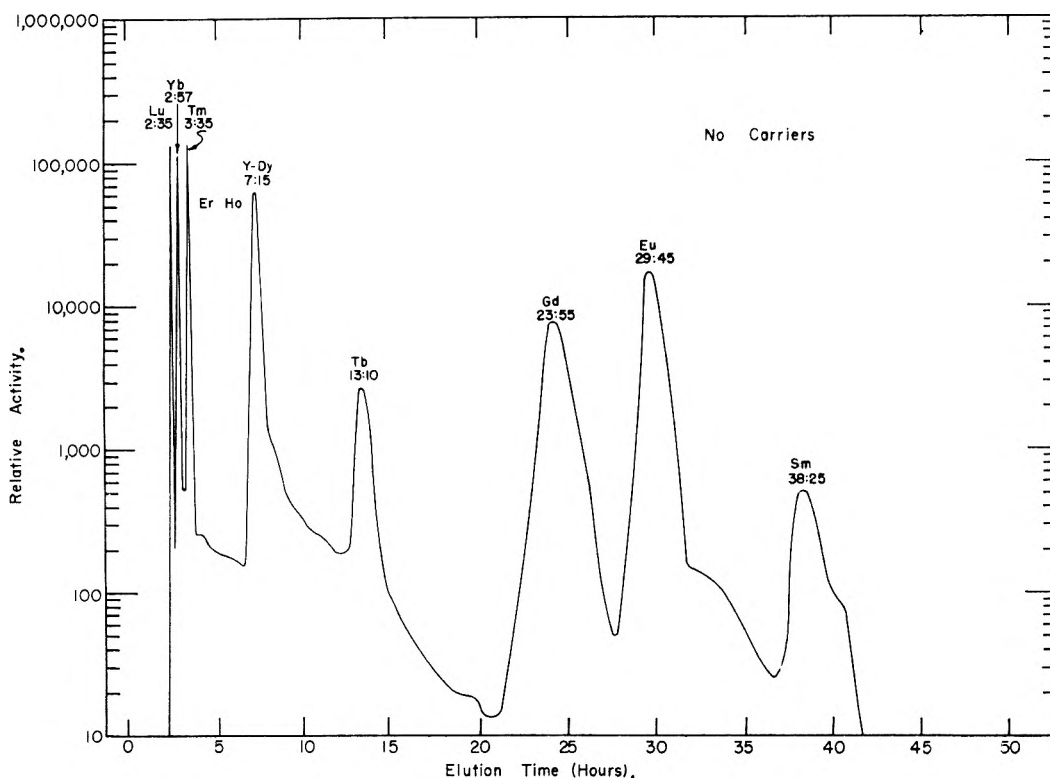
Fig. 2.—Elution curve of carrier-free rare earth tracer activities at a constant pH of 3.19.
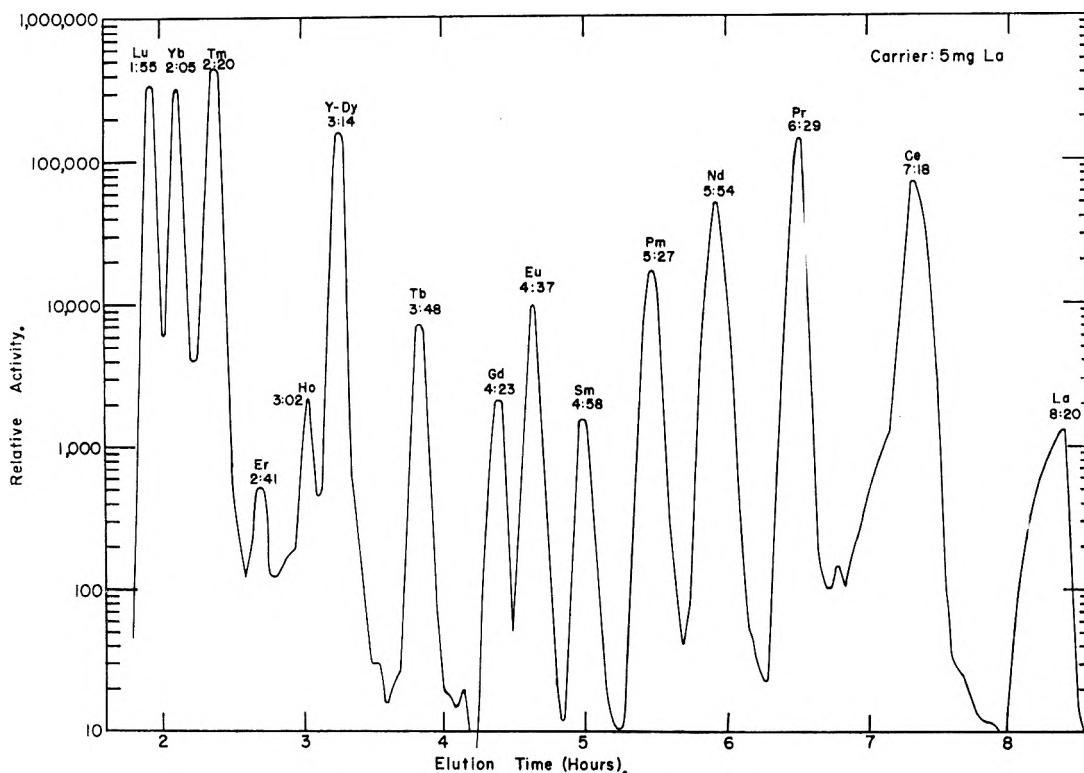


Fig. 3.—Elution curve of rare earth tracer activities plus 5 mg. of lanthanum; initial pH 3.19; pH changed continuously at 0.107 pH unit/hour.

rates of 0.007, 0.015, 0.031 and 0.067 pH unit/ hour. Since the elution times for the light rare earths under constant pH condition are extremely sensitive to the experimental conditions, several elution curves were run at a constant pH of 3.19.

Data for all runs are summarized in Fig. 4, where the column operation time required for elution of a given element is plotted *versus* $(\mathrm{d}pH/\mathrm{d}t)$. From Fig. 4 it may be seen that the elution time for heavier rare earths, the so called "yttrium" group, is

not affected greatly by any of the $dpH/dt$ values used. However, elution of the lighter rare earths is affected markedly even by a slowly changing $pH$. Thus the elution time for neodymium is halved for a $dpH/dt$ of 0.01 $pH$ unit/hour. It may be noted also that the speed of elution is not increased very much for any of the rare earths when the $pH$ is changed faster than approximately 0.07 $pH$ unit/hour.

The elution curve shown in Fig. 3 represents separation of a mixture of rare earth activities in which the only carrier present was 5 mg. of lanthanum. It is well known that the presence of weighable amounts of carrier may easily distort the shape of an elution peak and affect the separation of adjacent elements. In order to determine the kind and extent of such distortions with a changing $pH$ elution, a series of runs were made in which known amounts of various rare earths were added to the mixed tracer activities. Two elution curves which show the typical effects of massive amounts of carrier are reproduced in Figs. 5 and 6. Figure 5 shows the curve which was obtained when a mixture of 9 mg. of yttrium, 3 mg. of neodymium, 2 mg. of praseodymium and 5 mg. of lanthanum, with tracers of all of the rare earths, was run with an average $dpH/dt$ of approximately 0.1 $pH$ unit/hour. Peaks for those elements of which only tracers were present (lutetium, ytterbium, thulium, gadolinium, europium, samarium, promethium and cerium) show the same symmetrical shape as those in Fig. 3. However, the peaks for neodymium, praseodymium and lanthanum are definitely wider than in Fig. 3, although there is still satisfactory separation between the neodymium and praseodymium peaks. The yttrium peak, with 9 mg. of carrier present, shows approximately a fivefold increase in width over the carrier-free yttrium peak in Fig. 3. The shape of the yttrium peak is also quite different from that of a carrier-free element, the activity rising slowly on the leading edge and falling abruptly after all of the yttrium had been eluted. This effect could be noticed most strikingly on the plates which were counted. As the yttrium came off the column, deposits of yttrium carrier could be seen on the plates after the lactate solution had been evaporated. These deposits became increasingly large up to the point where the column had been operating for 6 hours and 19 minutes, after which no additional yttrium deposit was seen. The plate for 6:19 had the heaviest of the visible carrier deposits and a considerable amount of activity while the plate for 6:22 had no visible deposit but approximately four times the activity of the 6:19 plate. From the curve of Fig. 5, it may be seen that the yttrium peak was so wide that it completely displaced the terbium activity. The terbium was probably eluted in a very narrow band after all of the yttrium had come off the column. If there had been only a small amount of terbium activity present, it would have been completely hidden under the yttrium peak instead of appearing as the sharp "spike" shown in Fig. 5.

Figure 6 shows the elution curve which was obtained when a mixture of 8 mg. of yttrium, 10 mg. of europium, 8 mg. of neodymium, 2 mg. of praseodym-
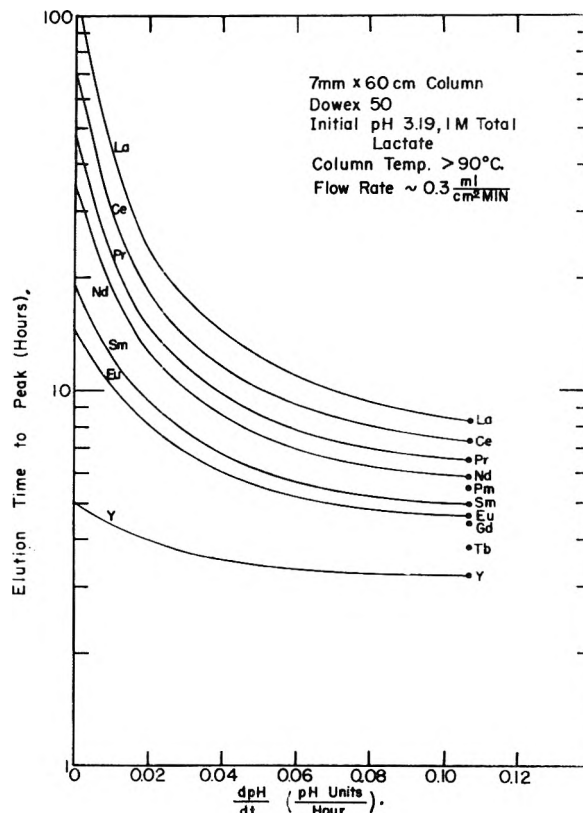


Fig. 4.—"Column operation time required for elution" *versus* "Average rate of change of $pH$" for several of the rare earths.

ium, and rare earth tracer activities were eluted with an average $dpH/dt$ of 0.11 $pH$ unit/hour. Here lutetium, ytterbium and thulium have the normal carrier-free peak shape. The yttrium peak is very wide and has the terbium "spike" as in Fig. 5. Europium also shows this saturation peak shape. The presence of relatively large amounts of europium carrier does not seem to affect the gadolinium–europium separation, but samarium is completely hidden under the back edge of the europium peak. Similarly, promethium is not affected by the presence of large amounts of neodymium carrier, but the neodymium–praseodymium peak separation is poor.

## IV. Conclusion

The elution curve of Fig. 3 indicates that an eluting agent with a continuously changing $pH$ may be used most effectively with a mixture of essentially carrier-free activities. The method is also of great aid when relatively large amounts of carrier are present, but greater caution must be taken to effect the desired separations. The curves shown here, however, suggest several general rules for operating an ion-exchange column with any given mixture of rare earth activities and carriers.

1.   Any mixture of carrier-free rare-earth activities may be separated completely and quickly without difficulty.

2.   Any essentially carrier-free rare earth may be easily separated from massive amounts of a rare earth of lower atomic number so long as there are no excessive massive amounts of a rare earth of
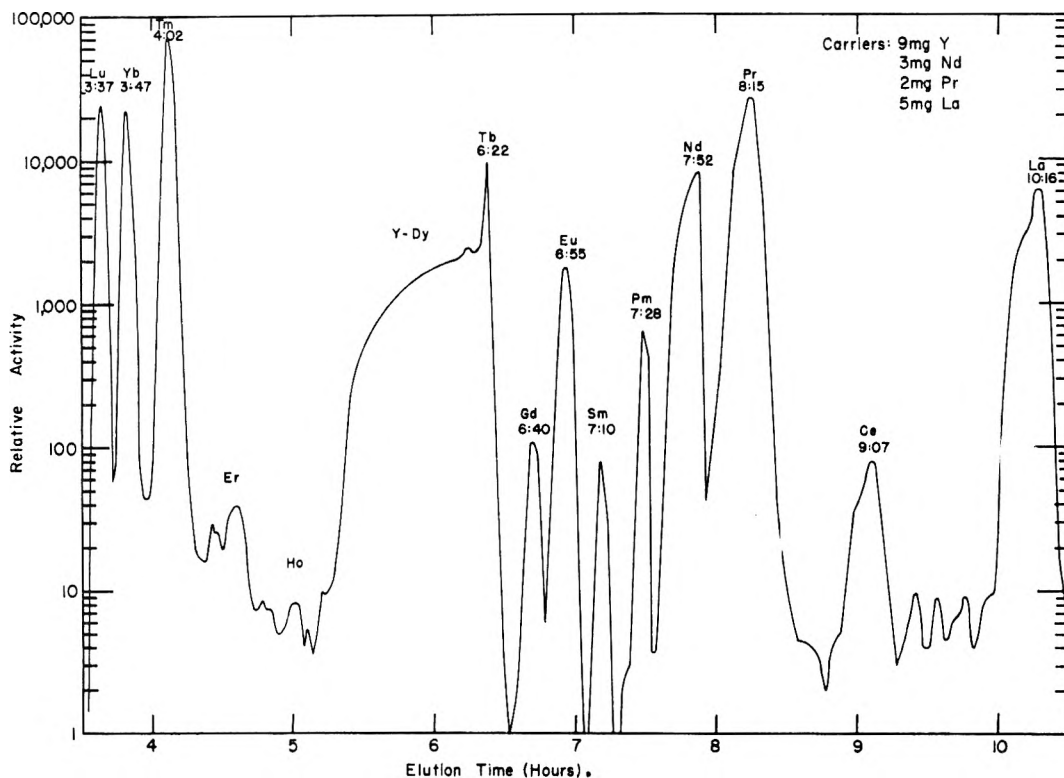
Fig. 5.—Elution curve of rare earth tracer activities plus 9 mg. of yttrium, 3 mg. of neodymium, 2 mg. of praseodymium and 5 mg. of lanthanum carriers, initial pH 3.19; pH changed continuously at 0.1 pH unit/hour.
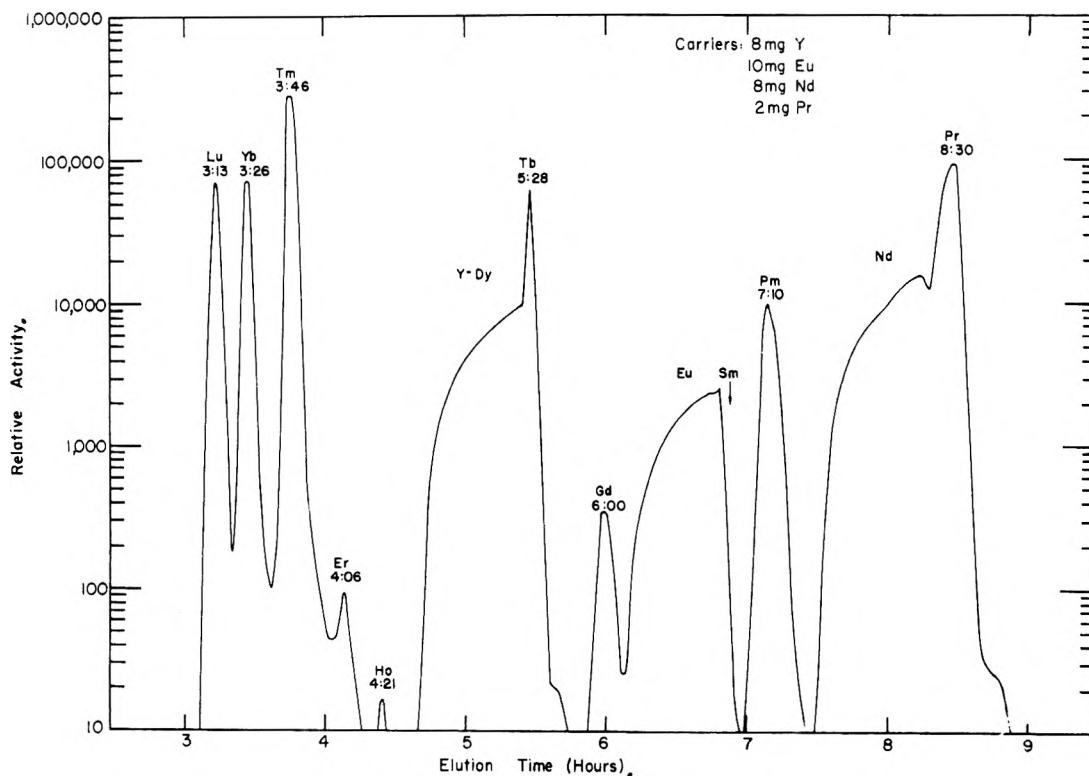


Fig. 6.—Elution curve of rare earth tracer activities plus 8 mg. of yttrium, 10 mg. of europium, 8 mg. of neodymium and 2 mg. of praseodymium carriers; initial pH 3.19; pH changed continuously at 0.1 pH unit/hour.

heavier atomic number present, *i.e.*, in Fig. 6 lutetium, ytterbium, thulium, erbium and holmium were separated from relatively large amounts of yttrium. Gadolinium was separated from europium but would not have been pure if larger amounts of yttrium carrier had been present.

3. If a small amount of one rare earth is to be separated from massive amounts of a rare earth of higher atomic number, the most effective method seems to be one in which the column is run under saturation conditions; i.e., the yttrium–terbium separation in Fig. 6. The terbium fraction was not completely free of yttrium after the first run, but the amount of yttrium carrier had been greatly reduced. A second column run on the terbium fraction should then give complete separation of the yttrium and terbium peaks without any significant loss in the total terbium activity.

4. When massive amounts of adjacent rare earth elements are present, the chemist has two choices if well-defined peaks are desired. He may either use a wider column to give an "unsaturated" rare earth carrier load per unit area of resin, or he may use a lower rate of change of $p$H (and a longer column operating time) to give total separation of the two peaks in question.

These general rules have been used effectively in this Laboratory to determine the experimental conditions under which a mixture of 10 mg. of each of seven of the rare earths (yttrium, europium, samarium, neodymium, praseodymium, cerium and lanthanum) containing uranium fission product activities could be separated completely on a routine basis. As an indication of how the curves of

Figs. 3 to 6 may be used to establish the operating conditions for optimum separation of a mixture of this type, the following line of reasoning was followed.

(a) From the curves of Fig. 5 and Fig. 6 an estimate of the saturation peak width versus carrier mass could be made. Thus, for 10 mg. of carrier, the peak would be approximately 60 minutes wide.

(b) Choosing the elements in the given mixture which were most difficult to separate, and allowing for the effects of carriers of these elements, the curves of Fig. 4 were used to estimate the highest $dp$H$/dt$ which would give the desired separation of the most difficult pair. In the given mixtures, the europium–samarium pair are hardest to separate because of the presence of carriers. Allowing for a generous error in the estimated carrier peak width (i.e., using a 120-minute europium–samarium peak separation instead of 60 minutes), a value of 0.01 $p$H unit per hour was chosen from Fig. 4. This rate of change of $p$H has proven to give excellent separation of this mixture of carriers with no detectable cross contamination of the peaks.

V. Acknowledgments.—The author wishes to thank Mr. D. Nethaway for his considerable assistance in assembling and operating the ion-exchange columns and Drs. P. C. Stevenson, H. G. Hicks and H. B. Levy for their aid in assaying the samples.

---

# SPECIFIC ADSORPTION

By Frank H. Dickey[1]

Contribution from the Gates and Crellin Laboratories of Chemistry, California Institute of Technology, No. 1848; Biokemiska Institutionen, Uppsala Universitet; and the Department of Chemistry of the University of California at Berkeley

Experiments that demonstrate a method for preparing specific adsorbents for predetermined substances have been repeated under conditions that give a more reproducible and more pronounced effect. This method consists simply of allowing the solid structure of the adsorbent to take form in the presence of the particular compound for which a specific adsorbent is sought. Thus, a large part of the surface of a silica gel prepared in the presence of methyl orange displays a greater than normal affinity for that dye and a small part of the surface attracts the dye very strongly. Such specific adsorbents were obtained with silica gel for a large variety of organic compounds but the effect is not observed with compounds that are not appreciably adsorbed from aqueous solution onto ordinary silica gel. Low $p$H, low electrolyte concentration, and low temperature favor the development of the specific adsorption property and also retard the loss of this property on aging. A part of the organic compound present during the preparation of a silica gel specific adsorbent is so strongly adsorbed that it can not be extracted from the product. Compounds in this condition show remarkable resistance to destruction by chemical agents and light but will undergo certain reactions that involve only minor changes in their structure.

An announcement of the finding that silica gels prepared in the presence of certain dyes show an increased capacity for the adsorption of the particular dye present during their preparation was published in 1949.[2]

The technique of preparing these "specific adsorbents" consisted simply of acidifying a silicate solution containing methyl orange or one of its homologs, drying the resulting gel, and then washing it thoroughly to remove as much of the dye as possible. Each such product was found to be a better adsorbent than ordinary silica gel for any one of the dyes but the effect was greatest for the dye actually used in the preparation and greater

for near members of the homologous series than for distant ones. Subsequently there have been confirmations of this work[3–5] but the original description of the experiments did not emphasize certain details of procedure that are now known to be critical, and several private reports of disappointing results have been received. The present investigation has been directed toward obtaining a more substantial and more easily reproduced demonstration of the effect as well as answering certain questions about the processes involved.

While the earlier work shows that the gels specifically attract the dyes that were present during their formation it gives no information about the strength of this attraction or about the amount

(1) (a) A. A. Noyes, Postdoctoral Fellow, 1949–1950; Guggenheim Fellow, 1950–1951. (b) Continental Oil Company, 135 Main Street, Seal Beach, California.

(2) F. H. Dickey, Proc. Nat. Acad. Sci., 35, 227 (1949).

(3) P. H. Emmett, private communication.

(4) R. Curti and U. Colombo, Gazz. chim. ital., 82, 491 (1952).

(5) S. Bernhard, J. Am. Chem. Soc., 74, 4946 (1952).

of attractive surface that is formed. In fact, there was some doubt that a modification of the silica surface is really responsible for the effect. A part of the dye used in the preparations cannot be washed out and is present during the adsorption measurements. Thus the possibility existed that this dye was in some way responsible for the modified adsorption properties of the gels.

The effects of various preparation methods and subsequent treatments have been investigated and also the question of what requirements a compound must meet in order to yield a silica gel specific adsorbent. It will be seen that many of the data reported here relate to gels that were not prepared and handled under the best conditions. In fact, the results point to methods of preparation that would be expected to yield better specific adsorbents than any actually prepared. The work is being reported at this stage because it is not possible to continue it at the present time.

### Experimental

The silica gels were prepared from commercial sodium silicate solution containing 1.4 moles of $Na_2O$ and 4.9 moles of $SiO_2$ per kg.: $d^{25}_4$ 1.40. C.P. or reagent grade inorganic chemicals were used and 99% methanol for the extractions but the dyes and other adsorbed compounds were obtained from various sources and generally used without special purification. Propyl orange and butyl orange were synthesized.

**Preparation of the Gels. A. Composition.**—Each of the gels described here has been prepared by one of three procedures designated as the acetic acid method, the hydrochloric acid method and the oxalate method. In the acetic acid method 30 ml. of the sodium silicate solution was diluted with 150 ml. of water and there was then stirred into it a solution obtained by diluting 30 ml. of glacial acetic acid with 125 ml. of water. In the hydrochloric acid method 42 g. of the sodium silicate solution was diluted to 200 ml. and 130 ml. of 5.7 N hydrochloric acid was added.

The oxalate method required first a more accurate determination of the composition of the sodium silicate. The sodium silicate was then diluted with a solution containing enough sodium oxalate to saturate the final mixture with sodium acid oxalate. Finally there was added a solution containing hydrochloric acid equivalent to the sodium in the sodium silicate and to half of the sodium in the sodium oxalate.

For example, the sodium silicate used in most of the preparations by the oxalate method was found to contain 1.40 moles (87 g.) of $Na_2O$ (titration to methyl orange endpoint) and 4.94 moles (296 g.) of $SiO_2$ (hydrochloric acid-insoluble residue) per kg. For each gel batch a 38.5-g. portion of this material, containing 0.108 equivalent of sodium, was diluted with a solution consisting of 0.016 mole of sodium oxalate in 150 ml. of water. To this mixture was added a solution of 10.00 ml. of 12.4 N hydrochloric acid in 60 ml. of water. The initial composition of these mixtures was as follows: $H_2O$, 241 g. (13.4 moles); $SiO_2$, 11.4 g. (0.190 mole); NaCl, 7.25 g. (0.124 mole); $NaHC_2O_4$, 1.79 g. (0.016 mole).

At the step where the silicate is acidified in each of the three methods it was necessary to mix quickly and thoroughly in order to avoid premature precipitation of a part of the silica. The dyes or other substances for which specific adsorbents were sought were generally introduced into the mixtures at this initial stage. The technique for doing this will be explained later.

**B. Drying and Extraction.**—The jellies that formed from the acidified silicate solutions were allowed to stand for several days and were then broken up on filter paper and dried in a slow stream of air in a fume hood. Finally, the resulting brittle particles were ground in a mortar, sieved, and the fraction between 48 and 200 mesh extracted with at least 30 l. of methanol. In the best extraction procedure the materials were packed in 10 mm. i.d. columns in a continuous extraction system that delivered 700 ml. of methanol per hour.

At the conclusion of the extraction the products were spread on filter paper, dried in air overnight, and sieved again to remove a small amount of material finer than 200 mesh formed during contact with methanol. The yield for each of the methods was 8 to 10 g. of dry silica per batch.

**C. Introduction of the Dye.**—The control gels were prepared simply as described above. For the specific adsorbents the contemplated adsorbate was dissolved in that one of the solutions to be combined in the gel preparation in which it was most soluble. For example, methyl orange was dissolved in the water or oxalate solution used to dilute the silicate, tyrosine was dissolved in the acid solution, and malachite green, being very soluble, was dissolved in any one of the component solutions. In preparing the alizarin gel, the hydrochloric acid method was modified by replacing 40% (by volume) of the water with an ethanol solution of that dye.

Generally 0.5 g. of adsorbate was taken whether or not this amount was soluble in the final gel mixture. Only 0.05 g. was used in preparing the vitamin $B_{12}$ gel.

In experiments in which the adsorbate concentrations were varied these concentrations were determined spectrophotometrically in the centrifuged gel mixtures before they had set. Particular concentrations were then obtained by blending with control gel mixtures. Similarly, the concentrations of dye in the completed gels were determined by dissolving a sample in 1.0 N base adding excess hydrochloric acid to a known volume and measuring the color before precipitation or setting occurred. The validity of these measurements was established by making similar measurements on control gel solutions to which known amounts of dye had been added.

**Special Treatments. A. Acid Washing.**—The acid washing procedure, found to preserve the specific adsorption property, consisted simply of suspending the gel sample in two or three successive portions of 1.0 N hydrochloric acid and allowing it to stand overnight in contact with this solvent, then extracting with methanol and drying in the usual way.

**B. Solutions.**—In studying the effects of various solutions on the gel properties small samples suitable for adsorption measurements were accurately weighed into mixing cylinders, 10-ml. portions of the indicated solutions were introduced, and the cylinders were shaken occasionally during the indicated time of treatment. The adsorption measurements immediately followed and were carried out in the usual way except that the samples were shaken for an hour with 5% acetic acid for a second time in the equilibration step described below under Adsorption Measurements.

**C. Chlorine and Ozone.**—The gel samples, 2–3 g., were packed between glass wool plugs in a 20 mm. i.d. glass tube and a stream of chlorine or ozonized oxygen (about 4 mole % ozone) at a rate of about 5 ml. per min. was passed through them. Afterwards the samples were spread out on filter paper in a gentle stream of air overnight and were then extracted for 40 hours with methanol in the apparatus used for the gel preparations.

The samples retained some capacity for decolorizing methyl orange, so that a modified procedure was required for measuring their adsorption and for determining their dye content. Allyl alcohol was found to prevent this decolorizing action and to give reliable results in test experiments with control gels and known amounts of dye. In the adsorption measurements 0.2 ml. of allyl alcohol was added to the solution before introduction of the dye sample. In determinations of dye content, 0.5 ml. of allyl alcohol was added to the water suspension of the gel before introducing the NaOH solution. No effect on the light absorption of the dye or on the adsorption of the dye is produced by these small amounts of allyl alcohol.

**D. Ultraviolet Light.**—In comparing the effects of ultraviolet light on the unextractable methyl orange and on methyl orange ordinarily adsorbed, samples of an aged (2 years) methyl orange gel prepared by the hydrochloric acid method and preserved by acid washing, containing 80 $\times 10^{-6}$ mole per kg. of unextractable dye and a sample of a similar control gel containing this amount of ordinarily adsorbed dye were placed in strips of about 1.0 mm. thickness and 6 mm. width alternately in a Petri dish. A narrow band of light from a high-pressure mercury arc (General Electric, AH 6) was allowed to fall across these strips until, after 5 hours, color could no longer be discerned on the

underside of the exposed portions of the control gel. No bleaching of the specific adsorbent could be detected.

**E. Heat.**—The gel samples heated to 110° for 24 and 48 hours were simply weighed into small glass tubes, sealed and placed in a drying pistol heated with toluene vapor.

**Adsorption Measurements.**—The procedure used for obtaining adsorption isotherms with methyl and ethyl orange will be given in detail. Only minor and obvious modifications were required for the reported measurements under different conditions and with other dyes.

Gel samples ranging from 0.1 to 2.5 g. were weighed into 10-ml. mixing cylinders to an accuracy of 1 mg. They were equilibrated by shaking with three successive 10-ml. portions of 5% aqueous acetic acid over a period of an hour. Then a fourth portion of this solvent was introduced, of such a weight that the subsequent introduction of a predetermined weight of dye solution made the whole weight of solution 10.00 g.

Dye solutions in the same solvent at concentrations of about $50 \times 10^{-6}$ mole per kg. were used except in the measurements at the highest concentrations when solutions (the methyl orange supersaturated) of twice this strength were required.

The cylinders containing solvent, dye and gel sample were shaken mechanically for 60 minutes at 20 to 22°, the supernatant solutions were decanted, centrifuged, and their dye concentrations determined spectrophotometrically. Readings at 5,100 Å., close to the absorption maximum of both dyes, were used for this purpose as follows: concentration in moles per kg. $\times 10^6$ of

$$\text{methyl orange}[6] = E \times 24.6$$
$$\text{ethyl orange} = E \times 50.2$$

## Adsorption Isotherms with Specific Adsorbents

**Observations and Reproducibility.**—Adsorption isotherms for methyl orange and ethyl orange on a control gel, a gel prepared with methyl orange, and a gel prepared with ethyl orange, respectively, are shown in Figs. 1, 2 and 3. In obtaining these data, the quantities of dye and gel were chosen, on the basis of earlier observations, to give final concentrations of dye in the supernatant solutions of approximately 1, 5, 15, 30 and $60 \times 10^{-6}$ mole per kg. Also, where possible, these quantities were so chosen that about 50% of the dye initially present was adsorbed. This procedure could not always be followed with the control because of the limited supply of gel, but in no instance was less than 15% of the dye adsorbed. Thus the error in the determination (by difference) of the concentration of the adsorbed dye is still of the same order as the error in the determination of the concentration of the dissolved dye. Duplicate determinations of these quantities generally agreed within a per cent. or two.
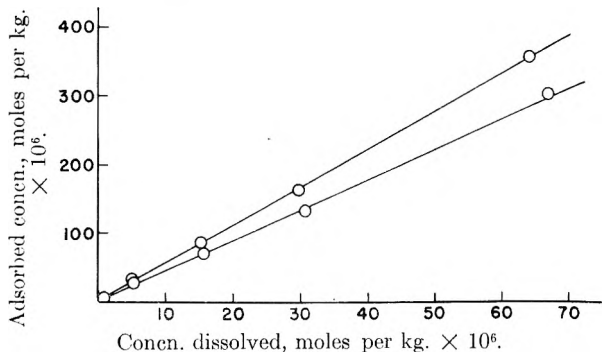


Fig. 1.—Adsorption of methyl orange (upper curve) and ethyl orange (lower curve) on control gel.

(6) The factor 20 was used for methyl orange solutions in hydrochloric acid encountered in measuring the dye content of gels.
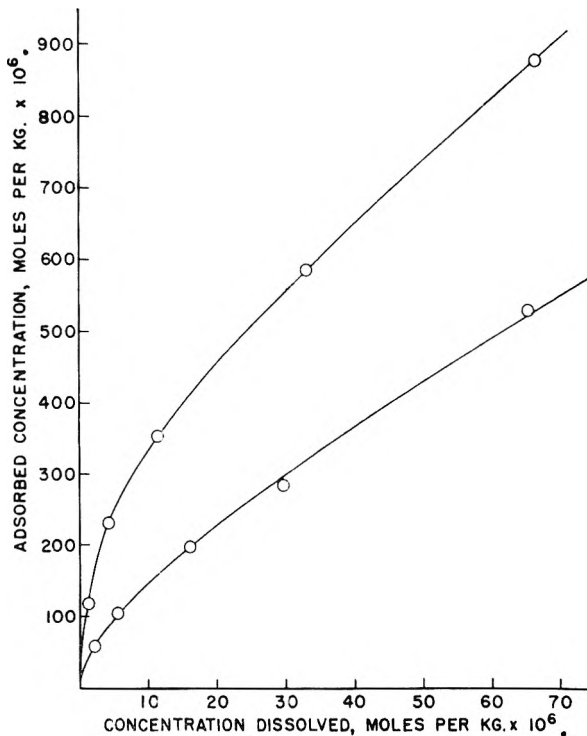


Fig. 2.—Adsorption of methyl orange (upper curve) and ethyl orange (lower curve) on methyl orange gel.
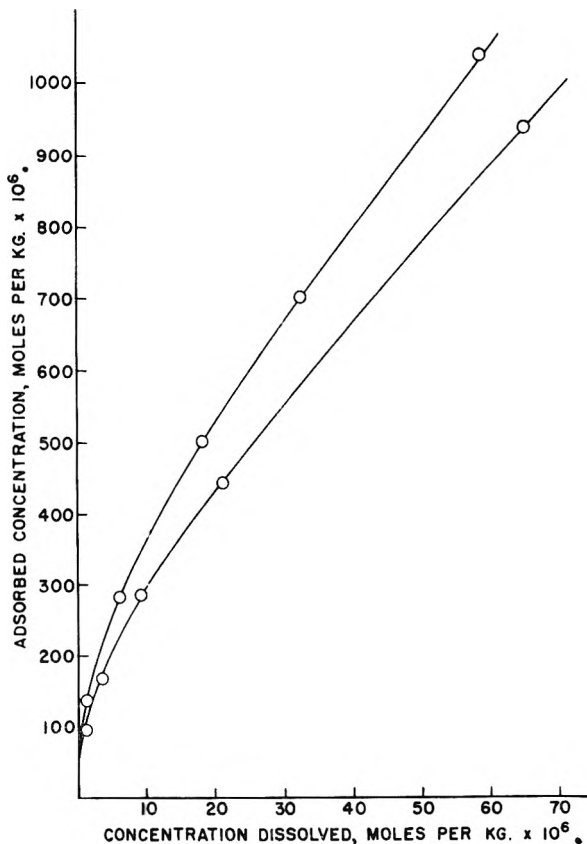


Fig. 3.—Adsorption of methyl orange (lower curve) and ethyl orange (upper curve) on ethyl orange gel.

The reproducibility of the gels, however, is of a much lower order. These gels were prepared by the oxalate method and they were not acid washed

on completion of the preparations. As shown in the following section, under these conditions very small differences in the composition, initial dye saturation, or age of the specific adsorbents could appreciably alter their adsorption properties, although the control gels are well reproduced. The shape and relative positions of the curves obtained with the specific adsorbents, respectively, have been regularly obtained in a large number of experiments but comparisons of absolute rather than relative measurements between two specific adsorbents are of little significance. For example, the fact that the upper (methyl orange) curve in Fig. 2 starts out above but eventually falls below the lower (methyl orange) curve in Fig. 3 would not be reproducible with different gel preparations.

**Interpretation of Isotherms.**—The isotherms in Figs. 1, 2 and 3 show that the gels prepared in the presence of a dye adsorb much more dye than the control gels over the whole concentration range studied.[7] Also the particular dye used in the preparation was subsequently the one more strongly adsorbed. Thus, in the case of the ethyl orange gel the "natural" order of adsorption strength was inverted.

The magnitude of these effects can be described in terms of the following three quantities

$$\text{specifically adsorbed dye} = G - G_0 \quad (1)$$
$$\text{adsorption power} = G/S \quad (2)$$
$$\text{relative adsorption power}[8] = G/G_c \quad (3)$$

for which interpolated values at corresponding concentrations are shown in Table I. In these expressions $G$ is the concentration of adsorbed dye at a concentration, $S$, of dissolved dye, expressed as moles per kg. $\times 10^6$ of adsorbent and solution, respectively. $G_c$ is the concentration of adsorbed dye on the control gel in particular at the same concentration of dissolved dye.

The isotherms obtained with the control gel are approximately straight lines, except in the lowest part of the range, for both dyes, while those with the specific adsorbents are sharply curved over much of the range, but became nearly straight at the highest part. Thus the adsorption powers are highest at the lowest concentrations but are nearly constant for the specific adsorbents, as well as for the control, at the highest concentrations. Correspondingly, the relative adsorption powers diminish rapidly at first but appear to be approaching a constant value, and the specifically adsorbed dye increases less rapidly but does not seem to be approaching a maximum value, as the concentration rises.

(7) The solubility of methyl orange in 5% aqueous acetic acid appears to be close to 60 × 10⁻⁶ mole per kg. It crystallizes so slowly, however, that it might be possible to extend these measurements to much higher concentrations. Ethyl orange is more soluble.

(8) It should be noted that this quantity is not the same as the "relative adsorption power" described in the first report of specific adsorption.² There it was the ratio of the adsorption power shown by a specific adsorbent to that shown by a control when the solution weight was 10 × the gel weight and the initial rather than the final dye concentrations were the same. Since the adsorption powers of the control gels are nearly constant over the concentration range studied, the relative adsorption powers so calculated were nearly the same as those calculated by the above formula. However, since the adsorption powers for the stronger adsorbents were determined at lower concentrations, where adsorption powers are higher, the specificities were magnified.

TABLE I

| | Conc.[a] | | Ads. | Rel. | Spec. |
|---|---|---|---|---|---|
| | Diss. | Ads. | power | ads. power | ads. dye[a] |
| MO on control gel | 1 | 10 | 10 | | |
| | 5 | 32 | 6.4 | | |
| | 15 | 86 | 5.7 | | |
| | 30 | 168 | 5.6 | | |
| | 60 | 332 | 5.5 | | |
| EO on control gel | 1 | 8 | 8.0 | | |
| | 5 | 25 | 5.0 | | |
| | 15 | 68 | 4.5 | | |
| | 30 | 136 | 4.5 | | |
| | 60 | 269 | 4.5 | | |
| MO on MO gel | 1 | 112 | 112 | 11.2 | 102 |
| | 5 | 250 | 50 | 7.8 | 218 |
| | 15 | 402 | 27 | 4.7 | 316 |
| | 30 | 559 | 19 | 3.4 | 391 |
| | 60 | 830 | 14 | 2.5 | 498 |
| EO on MO gel | 1 | 35 | 35 | 4.4 | 27 |
| | 5 | 95 | 19 | 3.8 | 70 |
| | 15 | 187 | 12.5 | 2.8 | 119 |
| | 30 | 296 | 9.9 | 2.2 | 160 |
| | 60 | 492 | 8.2 | 1.8 | 223 |
| MO on EO gel | 1 | 90 | 90 | 9.0 | 80 |
| | 5 | 207 | 41 | 6.4 | 175 |
| | 15 | 369 | 25 | 4.3 | 283 |
| | 30 | 555 | 18.5 | 3.3 | 387 |
| | 60 | 890 | 14.8 | 2.7 | 553 |
| EO on EO gel | 1 | 125 | 125 | 15.6 | 117 |
| | 5 | 255 | 51 | 10.2 | 230 |
| | 15 | 454 | 30 | 6.7 | 386 |
| | 30 | 672 | 22 | 5.0 | 536 |
| | 60 | 1070 | 17.8 | 4.0 | 801 |

[a] Moles per kg. $\times 10^6$.

Earlier experiments had disclosed the sharp decline in adsorption power with increasing concentration at low concentrations, which suggested that the specific gels differ from the controls only in possessing a small number of strongly attracting adsorption sites. Such an interpretation, however, is inconsistent with the observation that the isotherms are nearly straight lines at the highest concentrations, but with slopes greater on the specific gels than on the control. It must be that the adsorption properties of large fractions of the surface areas have been modified by the special method of preparation.

A reasonable interpretation of the isotherms would be that the specific adsorbents have been provided with a large number of different classes of adsorption sites distinguished by different degrees of affinity for the dyes, the more strongly attracting sites being the less numerous. The control gels, on the other hand, present surfaces that are largely uniformly weakly attracting, with only a few spontaneously occurring sites of stronger attraction. Such an interpretation does not suggest a simple equation for the curves. However, in studying this phenomenon it might prove valuable to have a method for giving a concise description of the adsorption properties over a range of concentrations.

This result can be obtained conveniently by treating the large number of different classes of

adsorption sites as but two classes, weakly attract-ing and strongly attracting. That is, the curves can be represented as the sums of pairs of Langmuir isotherms. Such equations would have the form

$$G = \frac{SC_1}{K_1 + S} + \frac{SC_2}{K_2 + S}$$

Here, $G$ and $S$ have their earlier meaning, $C_1$ and $C_2$ are the ultimate capacities for weakly and strongly attracting sites, respectively, expressed as moles of adsorbed dye per kg. $\times 10^6$ of adsorbent, and $K_1$ and $K_2$ can be best described as equilibrium constants for the dissociation of the dye–adsorbent combination. At unit concentration of dissolved dye ($1.0 \times 10^{-6}$ mole per kg.) $K_1$ and $K_2$ are ratios of unoccupied to occupied adsorption sites in the respective classes of adsorption sites.

Good fits to the six curves are obtained with the values for $K_1$ and $C_2$ shown in Table II, when $K_2$ and $C_1$ are given the constant values 1.5 and 8,000, respectively. It has been shown, although not with these samples in particular, that the surface areas of the specific adsorbents and controls, measured by $N_2$ adsorption, are the same.[3]

TABLE II

| Gel | Dye | $K_1$ | $C_2$ |
|---|---|---|---|
| Control | Methyl orange | 1430 | 10 |
| | Ethyl orange | 1800 | 11 |
| Methyl orange | Methyl orange | 800 | 270 |
| | Ethyl orange | 1100 | 80 |
| Ethyl orange | Methyl orange | 625 | 190 |
| | Ethyl orange | 525 | 250 |

The effect of preparing silica gel in the presence of these dyes may now be summarized as follows. The number of sites that attract the particular dye strongly has been increased by a factor of about 25 and the attraction strength of the weakly attracting main part of the surface has been in-creased by a factor of about 2.5. With respect to adsorption of the homologous dye, similar but substantially smaller effects are observed. While the specific adsorption property is most pronounced at low dye concentrations, the specificity persists to a considerable extent through the highest prac-tical concentrations, so that applications of the adsorbents are not limited to the treatment of traces of material.

Since only two dyes were employed in this study it could be argued that the observed alterations of the adsorption properties of the gels represent modifications of the gel structures that only happen to favor adsorption of the respective dyes, but are not, in fact, specifically directed toward their particular molecular structures. The fact that the effects are indeed specific was adequately demonstrated in the original announcement of this study.[2] In Table III are shown the results of similar measurements made with a series of gels prepared by the hydrochloric acid method.

## Factors in the Development and Persistence of the Specific Adsorption Property

**Methods of Gel Preparation.**—The most obvi-ous differences among the three gel preparation procedures lie in the $pH$ of the respective mixtures

TABLE III

| | | Relative adsorption power[a] for | | | |
|---|---|---|---|---|---|
| | | Methyl orange | Ethyl orange | Propyl orange | Butyl orange |
| Gel prepared with | Methyl orange | 17 | 8 | 3 | 2 |
| | Ethyl orange | 9 | 30 | 10 | 3 |
| | Propyl orange | 7 | 22 | 30 | 25 |
| | Butyl orange | 5 | 13 | 30 | 30 |

[a] Concentration in solution $0.5 \times 10^{-6}$ mole per kg., interpolated.

during the process. The excess acetic acid in the acetic acid method gives an initial mixture with a $pH$ of the order of 3.3 but during the drying proc-ess, as the acetic acid evaporates and the sodium acetate becomes more concentrated, the $pH$ rises. The $pH$ is very low in the hydrochloric acid method mixture and remains very low up to the extraction step.

The oxalate method was developed to keep the $pH$ at about 3 during the whole process. This is desirable because at higher $pH$ values the specific adsorption effect is appreciably reduced while, on the other hand, the use of an excess of a strong acid limits the choice of adsorbates to compounds that are stable in a strongly acid medium for a period of several days. The result is obtained by preparing a mixture in which the acid component is a saturating concentration of sodium acid oxalate which persists through the drying process.[9] How-ever, these mixtures are not really buffered and a small excess of silicate or hydrochloric acid may produce a substantial change in the $pH$ of the dried gel. Some of the variability in the products of the oxalate method may be explained in this way.

The results obtained with each of these methods for the dye methyl orange are shown in Table IV. They illustrate the general observation that the specific adsorption property is more pronounced in gels prepared at lower $pH$ values, but that there is little further change below $pH$ 3. The acetic acid gels appear to have much larger surface areas and adsorb more dye but the relative adsorption powers are very much less. The hydrochloric acid gels are only a little better than those prepared by the oxalate method and they have not been so thoroughly studied because it was desired to develop a method that could be used with com-pounds that are destroyed by strong acid.

Table IV also shows the effect of varying the amount of dye present during the preparation of the gel. The amount of dye specifically adsorbed at a given concentration will be seen to be roughly proportional to the amount present during its preparation. It was found that removal of sus-pended dye by centrifugation before the gels set does not appreciably affect their adsorption proper-ties. Accordingly, only dissolved dye is effective in producing a specific adsorbent but the mixtures after centrifugation are found to be supersaturated with methyl orange by a factor of about five.

After the gels have set they are broken up and allowed to dry in an air stream while their volumes shrink to about one tenth. This appears to be an essential step in the process. If it is omitted and the gels are extracted directly with methanol the

(9) The concentration of sodium acid oxalate will diminish as the gel drys until the liquid is saturated with sodium chloride as well.

## Table IV

| Method | Amount of dye present[a] | Concn.[b] Diss. | Ads. | Rel. ads. power | Spec. ads. dye[b] |
|---|---|---|---|---|---|
| Acetic | 11,000 | 0.5 | 145 | 3.5 | 200 |
| Hydrochloric | 11,000 | 0.9 | 112 | 13 | 100 |
| | | 2.8 | 214 | 8 | 195 |
| | | 8.6 | 400 | 5 | 320 |
| Oxalate | 9,000 | 1.2 | 118 | 12 | 110 |
| | | 4.1 | 231 | 8 | 200 |
| | | 11.2 | 352 | 5 | 285 |
| | | 33 | 587 | 3.2 | 400 |
| | | 66 | 880 | 2.4 | 520 |
| Oxalate | 4,500 | 2.1 | 71 | 3.7 | 50 |
| | | 8.1 | 149 | 3.1 | 100 |
| | | 33.5 | 330 | 1.6 | 140 |
| Oxalate | 900 | 1.8 | 28 | 1.7 | 10 |
| | | 4.4 | 49 | 1.6 | 20 |
| | | 31.8 | 250 | 1.4 | 70 |

[a] Moles per kg. of $SiO_2 \times 10^6$ in the reaction mixture from which the gel was prepared. [b] Moles per kg. $\times 10^6$.

absorption properties of the products are not different from those of the controls. In the same way failure results if, by using more concentrated solutions, the silica is obtained as a gelatinous precipitate rather than by allowing the whole mixture to set to a jelly. When this drying period was very long, two months instead of a few days, the specific adsorption effect was much reduced.

**Various Adsorbates.**—It has been found that compounds that are not appreciably adsorbed on silica gel under the conditions of gel preparation do not produce specific adsorbents. Furthermore, compounds that are weakly adsorbed under these conditions produce only a small effect on the adsorption properties of gels prepared in their presence. Table V illustrates these observations and also gives some results obtained with quite strongly adsorbed compounds. All of the gels in Table V were prepared by the hydrochloric acid method.

## Table V

| Adsorbate | Ads. power on control | Concn.[a] Diss. | Ads. | Rel. ads. power | Spec. ads. material[a] |
|---|---|---|---|---|---|
| Tyrosine | 0 | 55 | 0 | .. | 0 |
| Aurin | 0.3 | 8.9 | 10.6 | 4 | 8 |
| Orange II | 0.9 | 8.3 | 17.1 | 2.3 | 10 |
| Methyl orange | 6 | 8.6 | 400 | 5 | 320 |
| Butyl orange | 15 | 0.3 | 200 | 40 | 195 |
| Methyl red | 21 | 16 | 590 | 1.7 | 250 |
| Malachite green | 43 | 5.8 | 390 | 1.6 | 140 |

[a] Moles per kg. $\times 10^6$.

In addition to a large number of variously substituted aminoazobenzenesulfonic and carboxylic acids, the following compounds have been observed, at least qualitatively, to form specific adsorbents:

| | |
|---|---|
| Malachite green | Phenolphthalein |
| Brilliant green | Fluorescein |
| Crystal violet | Thymol blue |
| Orange II | Chrysamine |
| Alizarin | Aurin |
| Methylene blue | Vitamin B$_{12}$ |

**Aging of the Gels.**—The specific adsorption property is gradually lost on standing but the rate of loss is extremely sensitive to the conditions of preparation and storage. The data in Table VI are only typical findings. They show that aging is accelerated by heating the gel to 110° and is remarkably slowed by washing it with aqueous acid. It will also be seen that the rate of loss of the specific adsorption property declines as aging proceeds. Control gels did not change appreciably during storage or when heated to 110°.

## Table VI

| Age (months) | Treatment | Concn.[a] Diss. | Ads. | Rel. ads. power | Spec. ads. dye[a] |
|---|---|---|---|---|---|
| 0.25[b] | None | 20 | 460 | 4.1 | 350 |
| 2 | | 20 | 340 | 3.1 | 230 |
| 4[b] | | 23 | 256 | 2.0 | 125 |
| 9 | | 24 | 206 | 1.5 | 70 |
| 11[b] | | 26 | 165 | 1.2 | 20 |
| 9 | Acid wash at 2 mo. | 20 | 330 | 3.0 | 220 |
| 2 | Heated at 100-110° | | | | |
| | 24 hr. | 25 | 190 | 1.3 | 50 |
| | 48 hr. | 25 | 190 | 1.3 | 50 |
| 2 | Acid wash, then heated at 100-110° | | | | |
| | 24 hr. | 21 | 275 | 2.2 | 160 |

[a] Moles per kg. $\times 10^6$. [b] These observations were made on one gel batch. All of the other observations were made on another bath prepared by the same (oxalate) method at a different time.

Figure 4 shows the way in which the shape of the adsorption isotherm changes as the aging process reduces the adsorption power of the gel. While the curve is lowered at all points, there is a pronounced tendency for it to become straighter and to point toward the origin. That is, the gels lose their ability to adsorb dye at low concentrations more rapidly than their ability to adsorb it at high concentrations: the strongly attracting adsorption sites are more rapidly lost.

**Chemical Destruction of Specific Adsorbents.**—Chemical agents that react with silica, for example, aqueous sodium hydroxide, destroy the specific adsorption property very quickly. Strongly acid solutions have no immediate effect but there appears to be a slow destruction of the specific adsorption property, without any other manifestation of change in the gel structure, on treatment with certain substances toward which silica is relatively inert. For example, in one experiment, exposure to chlorine gas for 15 hours reduced the amount of methyl orange that a gel sample would adsorb in excess of its control by 20%.

Immersion in a buffer solution at a $p$H higher than about 3 is another example of a chemical treatment that appears to affect only the specific adsorption property. As shown in Table VII, the action is more rapid in more basic solutions and at $p$H 8 there is substantial destruction in a very short time, although such a solution does not dissolve an appreciable amount of silica. It was found that the specific adsorption power is not restored by subsequent treatment with strong acid for 24 hours. Table VII also shows that a buffer is

required.  Sodium chloride solution had very little effect and distilled water none at all.

**Mechanism of Specific Absorbent Formation.—** There are two processes, not wholly distinct, by which the presence of a dye molecule might induce the formation of a complementary structure in the gel.  First, the dye molecule might attract the components of the gel while they are in a fluid or flexible state and produce an attraction-favoring configuration of them that subsequently becomes a part of the rigid structure of the gel.  Second, an attraction-favoring configuration that occurs spontaneously might be more likely to survive to be a part of the final structure if a dye molecule is present and interferes with further reaction at that point.  That is, the dye might promote reactions that form strongly attracting configurations of the gel and it might suppress reactions that would destroy them.

It is not necessary to postulate a particular mechanism for the attraction between dye and gel in order to predict that a specific adsorbent will be formed.  Any change that the presence of the dye induces in the structure of the gel will be in such a direction as to stabilize their combination.  Probably several mechanisms of attraction play a part in the effects described here.  However, it is reasonable to suppose that van der Waals forces are primarily responsible for the ability of the specific adsorbents to effect a distinction between alkyl radicals.

The formation of silica gel in these experiments may be regarded as the elimination of water from orthosilicic acid to form a continuous polymer.  Each step in the process can be represented in this way

$$
\begin{array}{c}
\text{—O—Si—OH + HO—Si—O—} \longrightarrow \\[4pt]
\text{—O—Si—O—Si—O— + H}_2\text{O}
\end{array}
$$
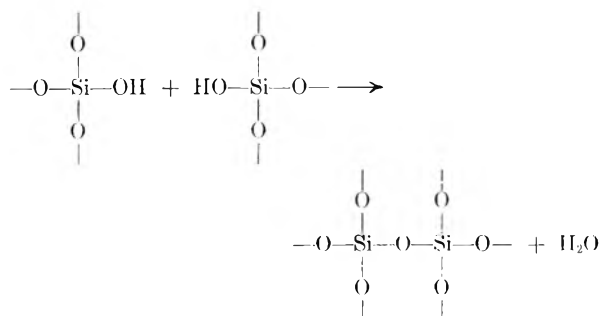
The reaction steps occur more or less randomly and initially, in a dilute solution, a large proportion of the hydroxyl groups remain unreacted when the polymer structure has become so extensive that a gel is formed.  As the gel dries and shrinks more bonds are formed, but at a diminishing rate until the quite rigid product is reached, in which, though a substantial number of unreacted hydroxyl groups are still present, reaction has nearly ceased.

It would be expected that the greater the proportion of bonds in the final product that were formed in the presence of the dye, the greater would be the relative adsorption power.  In addition, it might be expected that there would be an optimum rate of the gel-forming reaction, and also an optimum extent of that reaction.  If it proceeds too rapidly the influence of the dye in promoting favorable configurations of the unreacted gel components will

TABLE VII

| Treatment | Concn.[a] Diss. | Concn.[a] Ads. | Rel. ads. power | Spec. ads. dye[a] |
|---|---|---|---|---|
| None, before experiment | 1.7 | 108 | 7.2 | 93 |
| None, after experiment, 1.5 months later | 1.8 | 107 | 6.5 | 91 |
| 0.1 M phosphate–citrate buffer, pH 8.0, 1 hr. | 6.2 | 62 | 1.1 | 6 |
| 0.1 M phosphate–citrate buffer, pH 6.2, 4 hr. | 5.8 | 66 | 1.3 | 13 |
| None | 1.2 | 113 | 8.8 | 100 |
| 0.1 M acetate buffer, pH 4.7, 6 hr. | 2.6 | 99 | 3.4 | 70 |
| 0.1 M citrate buffer, pH 3.7, 7 hr. | 2.0 | 105 | 4.6 | 83 |
| None | 5.5 | 198 | 3.8 | 145 |
| 2.0 M NaCl, pH 7, 20 hr. | 6.0 | 176 | 3.1 | 120 |
| 2.0 M NaCl, 0.1 M HCl, 20 hr. | 5.5 | 197 | 3.8 | 145 |
| 0.1 M HCl, 20 hr. | 5.5 | 198 | 3.8 | 145 |
| Distilled water, pH 7, 20 hr. | 5.5 | 198 | 3.8 | 145 |

[a] Moles per kg. $\times 10^6$.

be lost.  If it proceeds too slowly the dye molecules will not suppress reactions that destroy favorable configurations that are already formed.  If the reaction does not go far enough, the gel structure will be flexible and unstable, and if it goes too far,
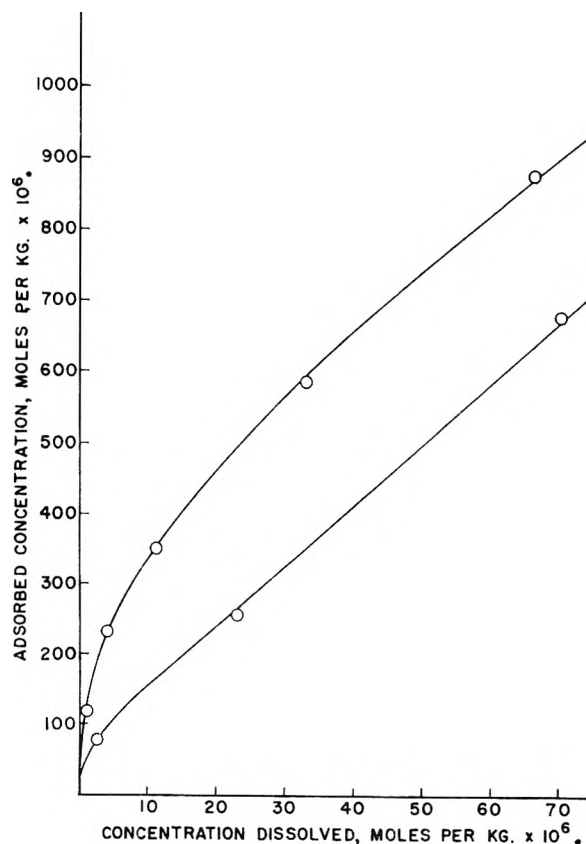


Fig. 4.—Adsorption of methyl orange on a methyl orange gel freshly prepared (upper curve) and four months later (lower curve).

a tendency toward a regular structure characteristic of silica may be entailed which would oppose

development of the special configurations favoring adsorption of the dye.

The suggested mechanisms for development of the specific adsorption property depend upon an attraction between dye and gel. This does not directly explain, however, the observation that compounds that are not ordinarily adsorbed do not produce specific adsorbents. Compounds that are not measurably adsorbed on a silica surface are nonetheless attracted to that surface, at least by van der Waals forces, and by obtaining specific adsorbents that distinguish between homologous dyes it has been shown that such weak forces are able to induce a significant modification of the silica surface.

It is more reasonable to say that unadsorbed dyes fail to give specific adsorbents because there is no mechanism for maintaining a constant position of the dye molecules with respect to the forming gel. If the dye were first adsorbed on the surface of another solid or combined with a dissolved substance of high molecular weight, ordinary adsorption on silica gel might not be necessary. That is, these findings do not preclude the possibility of preparing specific adsorbents for compounds not ordinarily adsorbed. Indeed, the need for a reasonably high molecular weight in an antigen might be an analogous phenomenon, and the methods used for obtaining antibodies to simple molecules[10] might be applied here as well.

Several explanations are possible for the lower relative adsorption powers observed with gels prepared under more alkaline conditions, and more than one factor may be important. There is direct evidence that the aging process is important. The observations recorded in Table VII indicate that gels prepared by the acetic acid method would age rapidly during their preparation and the finding that a long drying period leads to a poorer specific adsorbent shows that aging occurs even in the presence of the dye.

Aging might represent random rearrangements in the gel structure or a continuation of the gel-forming reaction. The observation that the effective surface areas of the control gels do not change on standing does not exclude the latter possibility. The atoms composing the gel could shift into arrangements permitting the formation of new linkages without appreciably affecting the gross structure on which surface area accessible to large dye molecules must depend. Apparently hydroxide ion does not directly catalyze the reaction responsible for aging. Rather, the gel is a weak cation exchanger that is subject to the aging reaction in its ionized form.

Only the red, acid form of methyl orange is appreciably adsorbed on ordinary silica gel and hence only this form would be expected to produce a specific adsorbent. The transition to the alkaline, yellow form begins around $p$H 3.3 so that the effective concentration of the dye was lower in the acetic acid mixtures. This is probably not an important factor, however, since the $p$H does not become high enough to convert more than a small part of the dye.

It was pointed out that an optimum rate and an optimum extent of the gel-forming reaction might be expected. Aging may represent too extensive reaction and the unsuccessful preparations from which the drying step was omitted might represent instances in which the reaction did not go far enough. The rate of the gel-forming reaction is strongly influenced by $p$H and passes through a minimum around $p$H 2. It is possible that in the acetic acid mixtures the reaction is too rapid for the dye molecules to be effective in modifying the gel structure. No adverse effect of too low $p$H has been observed but the reaction rate increases only slowly on the acid side of the minimum. Iler has shown that increase in the gel formation rate below $p$H 2 depends on traces of fluoride ion[11] and by introducing an appreciable concentration of fluoride rapid gel formation in an acid medium could be obtained. The effect of such a procedure on the specific adsorption property has not been investigated.

Setting of the silicate solution to a jelly is an essential step and the special configurations of the silica structure are probably assumed during the drying and shrinking of the jelly rather than at the time of setting. If the effective silica bonds are formed during the evaporation of the solvent, a high concentration of the dye will be maintained during their formation. In gels prepared in more alkaline media a higher proportion of the silica bonds are formed before drying since the reaction is more rapid. The greater surface area is one result. Under such conditions the concentration of dissolved dye would fall as the gel took form and adsorbed it.

### The Significance of the Unextractable Dye

In the foregoing considerations of the quantitative aspects of specific adsorption and the effects of various conditions on the properties of the adsorbents no mention has been made of that part of the dye present during the gel preparations that was not removed by extraction before the adsorption measurements. This retained dye plays no obvious role in these phenomena. Nevertheless it is a subject of considerable interest especially since its presence constitutes a logical flaw in the argument that a modified silica structure is responsible for the specific adsorption observations.

An alternative explanation was offered early in the investigation.[12] It was suggested that the dye is trapped in the gel in the form of micelles in such a way that the finished adsorbent presents a dye surface as well as a silica surface. Specific adsorption was then supposed to occur on this dye surface and its specificity to be a phenomenon akin to crystallization.

Other possible explanations would be that the dye molecules are surrounded by silica, that is, mechanically trapped, or that they are very strongly specifically adsorbed. The most direct route to a choice among these possibilities would be to remove the unextractable dye chemically and repeat the adsorption measurements on the clean gel. This proved quite difficult, however, and a considerable

(10) K. Landsteiner. *Biochem. Z.*, **104**, 280 (1920).

(11) R. K. Iler, THIS JOURNAL, **56**, 680 (1952).

(12) S. J. Singer, private communication.

study was required before a decision could be reached. The amount of dye that remains in the gel depends, of course, on how long the extraction process at the end of the preparation is continued. It is found, however, that the procedure previously described removes dye very slowly after the first few hours. After 40–48 hours an amount remains that is but little reduced on continuing extraction for several weeks and it is this material that is termed here the "unextractable dye."

The resistance to extraction is a result of the presence of the dye during the formation of the gel. That is, none of the dyes studied was so strongly adsorbed on a control gel that the extraction process did not effect essentially complete removal in 40 hours. However, there is a relationship between retention of a dye by the specific adsorbent and its ordinary adsorption, for dyes that are not appreciably adsorbed are completely extracted from gels prepared in their presence and the extent of ordinary adsorption proves to be a rough measure of the amount of dye that resists extraction. The phenomenon has been studied quantitatively only with methyl orange but it was observed that smaller amounts of weakly adsorbed dyes, fluorescein, orange II and aurin, are retained and much larger amounts of more strongly adsorbed dyes, butyl orange, methyl red and malachite green.

Since the magnitude of the specific adsorption effect has also been found to parallel ordinary adsorption, there is a correlation between this property and the amount of unextractable dye. This correlation has been shown qualitatively for the less strongly adsorbed dyes mentioned above and for the series methyl, ethyl, propyl and butyl orange. Only a few measurements have been made of the specific adsorption property of gels prepared with methyl red and malachite green, and they do not indicate that these gels are more powerful specific adsorbents than those prepared with methyl orange.

With a particular compound and different methods of gel preparation, the amount of unextractable material is found to parallel the magnitude of the specific adsorption effect. This observation is shown in Table VIII for the three standard gel preparation methods and for different ratios of dye to silica in preparations by the oxalate method.

Table VIII

| Preparation | | | |
|---|---|---|---|
| Method | Amount of dye present[a] | Rel. ads. power[b] | Unextractable dye[a] |
| Acetic | 11,000 | 1.2 | 10 |
| Hydrochloric | 11,000 | 7 | 80 |
| Oxalate | 9,000 | 7 | 40 |
| Oxalate | 4,500 | 4 | 20 |
| Oxalate | 900 | 1.6 | 3 |

[a] Moles per kg. $SiO_2 \times 10^6$.  [b] At a concentration in solution of $5 \times 10^{-6}$ mole of methyl orange per kg., interpolated.

**Stability.**—The most striking property of the unextractable dye is its chemical inertness. Silica gel samples colored in this way with methyl orange, methyl red, malachite green or crystal violet may show no appreciable fading after four years of

frequent exposure to light and to a laboratory atmosphere. Simply adsorbed on ordinary silica gel, these dyes persist for only a few weeks under such conditions.

The following chemical agents, that quickly destroy free or ordinarily adsorbed methyl orange, failed to destroy unextractable methyl orange: aqueous bromine, liquid bromine, sodium hydrosulfite in neutral or in weakly acid solution, a mixture of nitric and hydrochloric acid, a mixture of nitric and sulfuric acid at 50°, 30% hydrogen peroxide. In general, some bleaching was effected by an hour's contact with these agents, but it was estimated visually to be less than 10% in all cases. Furthermore, repeating the treatments produced a much smaller effect, so that it appeared that most of the dye would persist for weeks or months.

Unextractable methyl orange was not visibly changed by exposure to ultraviolet light under conditions where the dye, ordinarily adsorbed on silica gel, was wholly destroyed.

As will be described presently, it has been found that dyes in this condition will undergo certain chemical reactions. It has not been found possible, however, to separate the dye from the gel by any process that does not destroy one or the other.

**Removal of the Dye by Destruction of the Gel.**—On aging, the unextractable dye is gradually set free. Most of the dye that is removed by continuing extraction beyond 40 hours can be accounted for in this way. That is, about as much dye is obtained from a sample during the first few hours of extraction after a 30-day period of storage as is obtained by extraction during the whole period.

Processes that accelerate the loss of the specific adsorption property also accelerate the freeing of the unextractable dye. Thus, after heating to 110° or immersion in a neutral buffer solution for a few hours, methanol extraction will remove an additional portion of dye from a methyl orange gel, but each succeeding treatment produces a smaller effect. Also, like the loss of the specific adsorption property, the freeing of dye by aging or heat proceeds less rapidly in gels that have been well washed with acid. A methyl orange gel preserved in this way was found to set free only 5% of its dye during two years of storage.

While the specific adsorption property and the ability to retain dye respond in the same way to these various treatments, the latter is much more stable. Most of the dye remains unextractable when the specific adsorption property has been almost wholly destroyed.

**Destruction of the Dye.**—The methyl orange gels do not appear to be more effectively bleached by being placed in a vessel of chlorine gas than by the methods previously mentioned but when a stream of chlorine is passed through such a gel for several hours a substantial amount of dye is destroyed. Ozone is much more effective. These results are shown in Table IX for samples of a methyl orange gel prepared by the hydrochloric acid method.

It will be seen that the action of chlorine gas, like that of the less effective bleaching agents, is markedly diminished after a part of the dye has been destroyed. The same observation was made

TABLE IX

| Treatment of gel | Rel. ads. power[a] | Unextractable dye[b] |
|---|---|---|
| None | 6.0 | 80 |
| Cl₂ for 4 hours | .. | 30 |
| Cl₂ for 15 hours | 5.0 | 15 |
| O₃ for 2 hours | 5.6 | 3 |
| O₃ for 2 hours, contact with dye solution for 38 days | 5.6 | 15 |

[a] Concentration of dissolved methyl orange $5 \times 10^{-6}$ mole per kg. [b] Moles per kg. of $SiO_2 \times 10^6$.

visually in the ozone experiment, most of the decolorizing having taken place during the first 30 minutes.

Both gases produce some destruction of the specific adsorption property, but at least with ozone this effect is small in comparison with the destruction of the dye. No change in the adsorption properties of control gels subjected to these treatments was found. Gel destruction by chlorine and ozone was not studied further, but a phenomenon that may be related should be mentioned here. It was found that even after long exposure to air and thorough extraction with methanol, gels that had been exposed to either of these gases gradually decolorized methyl orange subsequently adsorbed on them. The details of these operations and the use of allyl alcohol to prevent the decolorizing action are described in the experimental section.

When the chlorine-treated and ozone-treated gel samples used in these adsorption experiments were washed with methanol the following day, the dye that they had adsorbed was quickly removed, and the gels were restored to their bleached condition. However, a sample of the ozone treated gel was allowed to stand in contact with a saturated, strongly acid solution of methyl orange for 38 days. At the end of this time 48 hour's methanol extraction left a considerable portion of the newly adsorbed dye as shown in Table IX. This new unextractable dye also resisted decolorization by chemical agents and light. Gels prepared with methyl red and with malachite green behave similarly although a yellow color remains in the latter after contact with ozone. Both of them acquire new unextractable color on long immersion in solutions of the respective dyes. Control gels, under exactly the same conditions do not take up an appreciable amount of dye that can not be readily extracted.

**Reactions in situ.**—While only these powerful oxidizing agents remove the unextractable dyes, certain dyes can be shown to undergo reaction while remaining attached to the silica. For example, it is observed that the red color of unextractable methyl orange is affected by the pH of solutions around it, being much brighter in strongly acid solutions. The color remains reddish up to pH 7, however, and at substantially higher pH values, where a more orange shade is observed, the dye is being set free at a considerable rate so that it is uncertain that the color change occurs in the adsorbed state. However, if the sample is immersed in pyridine, the dye changes to the yellow form without being extracted, in spite of the fact that methyl orange is very soluble in pyridine.

This change is rapid and reversible, and it is particularly interesting that methanol or distilled water will restore the red color although free methyl orange is yellow in these liquids.

Still more remarkable observations have been made on the behavior of other dyes in the unextractable state. Malachite green in aqueous solution changes from a green to a yellow form as the pH is lowered from about 2 to 1. Both forms are strongly adsorbed on ordinary silica gel, so that it is possible to compare the behavior of the unextractable dye with both the free and ordinarily adsorbed forms. Also, gels prepared with malachite green by the oxalate method are formed in the presence of the green form, while those prepared by the hydrochloric acid method are formed in the presence of the yellow form of the dye.

It is found that both the ordinarily adsorbed dye and the unextractable dye in the hydrochloric acid gel change color in the same pH range as the dissolved dye. The unextractable dye in the oxalate gel does undergo the color change, but it takes place in much more strongly acid solutions. Thus, the color remains green in 1.0 N hydrochloric acid, and it is incompletely changed in 6.0 N sulfuric acid. Concentrated hydrochloric acid or sulfuric acid changes the dye completely, but reversibly, to the yellow form.

Thus these three preparations, each consisting only of malachite green and silica gel, display sharply contrasting chemical behaviors. If a sample of the oxalate gel is turned yellow with concentrated hydrochloric acid, and samples of the hydrochloric acid gel and of ordinarily adsorbed malachite green are turned green by washing with distilled water or methanol, and to each of the three 1.0 N hydrochloric acid is added, the yellow sample turns green, and the green ones turn yellow. Addition of a trace of sodium hydrosulfite now has no effect on the green sample or one of the yellow ones, but the other yellow gel, containing the ordinarily adsorbed material, is bleached white.

A similar phenomenon was observed with an oxidation–reduction reaction using methylene blue. Gels prepared with this dye were strongly colored by it even after long extraction. Sodium hydrosulfite solution or hydriodic acid readily bleached them but the color was restored on exposure to air, or aerated water, and immediately on contact with hydrogen peroxide or nitric acid. Because the reduced form of the dye is so readily affected by air it was difficult to prepare a gel under comparable conditions in the presence of the reduced form. However, such a preparation was carried out in which nearly all of the dye present was reduced up to the methanol extraction step. This gel displayed the same characteristics as the others but was distinctly more easily reduced. Thus a concentration of hydriodic acid could be obtained that would decolorize this gel but would not affect the ones prepared in the presence of the oxidized form of the dye.

**The Strongly Specifically Adsorbed State.**—The dyes that are unextractably bound to silica have been found to react with chlorine and with ozone

under conditions where there is very little change in the gel structure and they can react with hydrogen ion and with various oxidizing and reducing agents under conditions where there is no evidence of change in the gel. These dyes must then be accessible to the solvents that do not extract them and the reagents that do not react with them. Of course, accessibility of the dye to small molecules does not prove that the large dye molecules are not mechanically prevented from escaping. Indeed, the facts that most of the ozone-destroyed dye is not replaced on subsequent contact with dye solution, and that the dye that is replaced requires much time for the process, suggest such mechanical obstruction. However, this picture affords no explanation for these findings: that compounds that do not form specific adsorbents are wholly extractable, that processes that destroy the specific adsorption property gradually remove the unextractable dyes, that the unextractable dyes are inert to ultraviolet light, and that under some circumstances they exhibit a modified response to chemical reagents.

The suggestion that the unextractable dye is responsible for the specific adsorption property is not supported by the observations. While there is a pronounced correlation between the amount of dye specifically adsorbed and that that is initially unextractable, these properties respond independently to treatments subsequent to gel preparation. Heating, exposure to buffer solutions, or simply long storage destroys the specific adsorption property but leaves most of the unextractable dye. On the other hand, ozone destroys most of the unextractable dye while hardly affecting the specific adsorption property.

Neither is there any evidence for a micellar disposition of the dye molecules. A micelle structure could not account for the chemical inertness of the dye. Furthermore, it is difficult to ascribe to the unextracted dye the role of attracting the dye that is to be specifically adsorbed when it is seen that more than one hundred times as much dye may be specifically adsorbed as is unextractably retained. In fact, the observation that destruction of the unextractable dye has little effect on the amount subsequently adsorbed suggests that it plays no part in the adsorption.

Only the hypothesis that the unextractable dye is strongly specifically adsorbed can explain its special properties. This viewpoint clearly accounts for the original correlation between unextractable dye and specific adsorption and for the fact that processes that destroy the specific adsorption property also gradually set free the unextractable dye.

The resistance of the dye to chemical agents as well as to light might simply reflect a high energy of combination with the gel. Those agents that do manage to effect reaction with the dye are of two types: first, are agents whose energy of reaction is large and might overwhelm the stabilizing effect of the gel; second, are agents whose reaction does not effect a large change in the dye structure so that only a small part of the energy of dye–gel combination is lost during the reaction.

It was observed that unextractable methyl orange in a gel prepared at a $p$H where this dye is in its red, acid form requires a much more basic medium for conversion to the yellow form than does the free dye. Similarly, malachite green in a gel prepared at a $p$H where it is in its green, basic form requires a much more acid medium for conversion to the yellow, acid form than does the free dye. Methylene blue also exhibits a tendency to retain the form initially present. These effects may be considered to reflect a stabilizing action by the gel for the original form of the dye, a stabilizing action of a much lower order than that which opposes reactions that destroy the dye molecule and completely abolish its energy of combination with the gel.

It has been previously suggested that these specific adsorbents are formed by the development of a silica surface comprising many different kinds of adsorption sites having many different strengths of attraction for the dye. It is not unreasonable to suppose that some of these sites should attract the dye so strongly that it is not extracted at an appreciable rate and the evidence presented here indicates that the strength of attraction may be great enough to suppress many chemical reactions as well. Such an effect would be expected for a strong specific adsorbent since the adsorption energy would supplement the activation energies of the reactions. It would not be expected for an ordinary strong adsorbent which might just as strongly attract the initial product of reaction. Only when the adsorption affinity is directed toward the exact structure of a molecule will all of the reactions of that molecule be restrained.

Some important questions remain. For example, it might seem unreasonable to postulate high energies of adsorption when, at least visually, the color of the dye is the same as it is in solution or ordinarily adsorbed. The picture of a large number of different kinds of adsorption sites offers a likely explanation. The dye molecules are affected by the strong forces of attraction but in many different ways so that the net result may be to make the light absorption less sharp but not to shift the maximum appreciably.

Since it has been shown that the strongest specific adsorption sites are more rapidly lost by aging, and since the sites of attachment of the unextractable dye are here supposed to be the strongest of all, it might have been expected that the unextractable dye would be rapidly set free on aging. However, as long as the dye molecules are present the silica structure will be stabilized by the same forces that render the dye resistant to chemical attack. The same idea might explain the finding that the ozone-destroyed dye is not readily replaced. That is, the very strongly attracting sites may rapidly deteriorate when the dye is removed. However, some of this dye is gradually replaced so that ozone treatment appears to uncover some sites that persist but function only with a substantial activation energy.

The observation that the acid form of malachite green is not stabilized with respect to the basic form requires special consideration. Malachite

green that cannot be extracted from a gel prepared in a strongly acid mixture was found to change color at the same $p$H, about 2, as the ordinarily adsorbed or free dye. A possible explanation will be described here because of its theoretical interest, although the experimental evidence does not justify offering it as a conclusion. The following reaction occurs when malachite green turns yellow in acid.
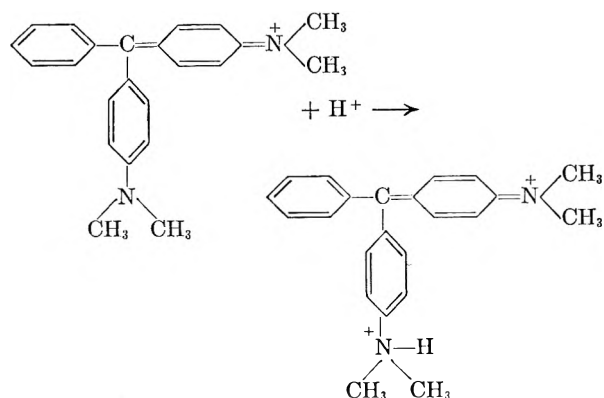


In the green form it will be seen that two of the rings have equivalent structures, and resonance will hold them in a strained planar arrangement. In the yellow form the dimethylamino group on one of these rings has acquired a proton, preventing its assumption of the quinoid structure, and it is free to rotate about the bond joining it to the central carbon atom. It is this latter structure that fails to be stabilized with respect to the former by the adsorbing gel.

The suggested explanation is that just as molecules that are not held in place by ordinary adsorption during the formation of the gel fail to yield specific adsorbents, those features of an adsorbed molecule that are not constant during the formation of the gel cannot contribute to the specificity. In other words, specificity can only be expected for rigid features of the molecules present during gel formation. In this instance, the specific adsorbent for the yellow form of malachite green adsorbs the green form equally well but the specific adsorbent for the green form tends to hold the rings in the same plane and thus to make that form abnormally stable.

From the standpoint of preparing a useful specific adsorbent, unextractable dye is a disadvantage. In the case of methyl orange it is a negligible disadvantage, for only a small part of the gel surface is so occupied. With compounds that are more soluble and more strongly adsorbed, however, the available surface might be seriously limited. There might prove to be an optimum degree of ordinary adsorption, an effect that would be analogous to the proposals of Pressman and Pauling[13] concerning the specificity of antibodies to difunctional antigens.

There is little experimental evidence for an adverse effect of too great ordinary adsorption but it will be noted that only rather feeble specific adsorbents have been obtained for methyl red and malachite green. Also, on aging under adverse

conditions the malachite green gels appear to become poorer adsorbents for this dye than are the controls.

### Conclusions

This phenomenon might be made the basis of new techniques both in analysis and in the isolation of natural products. Its advantages would lie in more subtle separations than are possible by other means. However, the requirement for some degree of ordinary adsorption before a specific adsorbent can be formed is a severe restriction on the usefulness of silica gel for such purposes. Silica gel can only be prepared conveniently in an aqueous medium and it has such a strong affinity for water that it is a quite feeble adsorbent for most compounds when water is present. For example, it would appear to be impossible to prepare silica gel specific adsorbents for amino acids or simple peptides because these compounds would not be appreciably adsorbed during the formation of the gel.

It is likely that this method can be used to give specific affinities to more versatile adsorbing materials but these studies suggest certain requirements that an alternative material must meet. In the first place, such a material must be amorphous, for a well-defined crystal structure would resist the imposition of a special surface configuration and would limit the number of accessible configurations. Then it must be stable, and formed by a reaction with which the prospective adsorbates will not interfere, and formed in a medium in which a high concentration of the prospective adsorbates can be presented. The formation of a jelly that shrinks on drying appears to be an important part of the silica gel process but may not be essential in general.

**Stabilized Reagents.**—Valuable applications might be found for organic reagents that can be obtained in that combination with a solid that has been termed here the strongly specifically adsorbed state. Several acid–base indicators, for example, when combined in this way with silica gel are remarkably stable and are able to function in chemical environments that destroy the free dyes. Moreover, they do not contaminate the solutions with which they come in contact but can be readily removed by filtering or decanting. A continuous indication of $p$H in a stream of liquid could be obtained with such a material. The experiments with methylene blue illustrate similar stabilization of an oxidation–reduction indicator and there are many other possibilities as well. The process appears to require that the reagent be adsorbed to some degree on the ordinary form of the adsorbent and that the reaction of the reagent entail only a small change in its structure. Within these limits it may have general applicability.

These considerations suggest that enzymes might be so preserved in a functioning state and a few tests of this possibility have been made. Gels were prepared containing urease, catalase[14] and muscle adenylic acid deaminase,[15] respectively, but in order to avoid destruction of the enzymes during

(13) D. Pressman and L. Pauling, *J. Am. Chem. Soc.*, **71**, 2893 (1949).

(14) Donated for this experiment by Dr. A. B. Pardee.

(15) Donated for this experiment by Dr. E. Bennett.

the preparation nearly neutral, $pH$ 6.0 solutions were used. More acid solutions have been found necessary for the development of strong specific adsorbents and, perhaps for this reason, no practical demonstration of the desired effect was obtained. On the other hand, it might be unreasonable to anticipate stabilization of such large molecules: the molecular weights of these substances are all greater than 300,000. In the cases of urease and catalase, detectable traces of the activity survived the gel preparations but persisted for only a day or two thereafter. The test with muscle adenylic acid deaminase showed no activity but was inconclusive since the free enzyme was found to be inactive in the presence of the gel or an aqueous extract of it.

In another similar test with cytochrome-c,[16] not an enzyme but a colored protein of molecular weight about 11,000, a degree of stabilization was obtained. The gel was prepared at $pH$ 4.6 and the test for persistence and function of the adsorbate was the color change that it undergoes on passing reversibly from the oxidized to the reduced form. The gel had the color of the free protein and exhibited the same responses to oxidizing and reducing agents. Moreover, these properties persisted for the two-month period of observation and were not destroyed by dry storage at room temperature, long extraction with acetone and methanol, or even contact for a few minutes with concentrated hydrochloric acid. However, after longer contact with acid or with distilled water for 10 days the

color had faded appreciably and no longer responded to reducing agents. This product was not tested as a specific adsorbent but it is unlikely that it had this property since all of the protein present during the preparation appeared to be retained.

**Biological Aspects.**—Many biological processes involve the operation of specific affinities like those that have been demonstrated here. The functioning of antibodies and enzymes provide the clearest examples but there are others of great interest. The procedure for preparing specific adsorbents can be regarded as an illustration of the mechanism proposed by Pauling[17] for the natural formation of antibodies and which was the basis for the manufacture of artificial antibodies reported by Pauling and Campbell.[18] On distinctly less firm grounds similar mechanisms have been proposed from time to time for the natural formation of certain enzymes and for the process by which genes are duplicated.

For none of these problems does specific affinity provide a complete answer. Binding of its antigen appears to be only a part of the functioning of an antibody and certainly enzymes do more than merely combine with their substrates. In the same way, while protein structures may be fabricated on templates that have the properties of specific adsorbents this would only be one element in a process that is otherwise obscure. Nevertheless, the study of that element could be a step toward a fuller understanding of the process as a whole.

(16) Donated for this experiment by Dr. J. B. Neilands.

(17) L. Pauling, *J. Am. Chem. Soc.*, **62**, 2643 (1940).

(18) L. Pauling and D. H. Campbell, *J. Exptl. Med.*, **76**, 211 (1942).

# INHIBITION OF ACID DISSOLUTION OF METALS.
# I. SOME GENERAL OBSERVATIONS

By A. C. MAKRIDES AND NORMAN HACKERMAN

*Institute for the Study of Metals, University of Chicago, Chicago, Illinois*
*Department of Chemistry, University of Texas, Austin, Texas*

A mechanism for inhibition of metal dissolution is given, and the important parameters are pointed out.

Recent studies[1-3] of inhibition of acid dissolution of metals by organic compounds have shown that adsorption of inhibitor on the metal to be protected is general and not decisively controlled by the (postulated) existence of local cells. There is little doubt that positively charged inhibitor molecules are adsorbed at the interface, but it appears that in addition neutral molecules are firmly adsorbed also.[3] The mechanism of adsorption of neutral molecules is clearly of importance since the extent of inhibition is expected to be some function of the extent of adsorption. Roebuck[4] found no correlation between dipole moment of organic

molecule and inhibition effectiveness. While a more exact treatment would bring in polarizabilities and bond lengths also, this lack of correlation strongly suggests that adsorption is not caused by a dipole type of interaction. The present authors have shown qualitatively that there is a relation between the electron "donor property" of the electronegative atom or group in the organic molecule and its inhibition effectiveness.[5] This relation is developed here more rigorously and a discussion of adsorption and inhibition is presented on this basis.

**Adsorption of Organic Molecules.**—As previously noted[5] organic compounds containing elements of groups Vb of VIb or functional groups of the type $-CN$, $-CNS$, $>CO$ and $-CHO$ are effective inhibitors. Similar compounds are

(1) T. P. Hoar, "Pittsburgh International Conference on Surface Reactions," The Corrosion Publishing Co., Pittsburgh, 1948, p. 127.

(2) L. Cavallaro and G. Bolognesi, *Acad. Sci. Ferrara*, **24**, No. 1 (1946–47).

(3) N. Hackerman and E. L. Cook, *J. Electrochem. Soc.*, **97**, 1 (1950).

(4) A. H. Roebuck, Thesis, University of Texas, 1949.

(5) N. Hackerman and A. C. Makrides, *Ind. Eng. Chem.*, **46**, 523 (1954).

strongly adsorbed by platinum and nickel catalysts and often act as poisons. Maxted[6] has suggested that adsorption in the latter case involves electron transfer from the adsorbate to the d band of the catalyst with probable elimination of electronic deficiencies in this band.

A mechanism for adsorption that applies to both systems was proposed by Matsen, et al.,[7] who applied the theory of the charge-transfer complex to chemisorption. The ground state of the complex is described as a linear combination of the wave functions for a no-bond state and a dative state in which an electron has been transferred from a Lewis base to a Lewis acid. For adsorption, the metal is the acid and the heat of adsorption at zero coverage is then given by

$$X_0 = \left[ -\left(I_B - \phi - \frac{e^2}{4R}\right) + \sqrt{\left(I_B - \phi - \frac{e^2}{4R}\right)^2 + 4\beta^2} \right] / 2 \quad (1)$$

Here $I_B$ is the ionization energy of the base, $\phi$ the work function of the metal, $e^2/4R$ the image energy, and $\beta$ the interaction integral.

The relation between heat and extent of adsorption can be derived from a theoretical isotherm for monolayer adsorption.[7] For our purposes we may use Fowler's[8] adsorption isotherm

$$\frac{\theta}{1-\theta} = \exp\left[\frac{X_0 + X_1\theta}{kT}\right] P \frac{Q_a}{Q_g} \quad (2)$$

Here $X_1$ is a molecular interaction constant which is negative for repulsion and the other symbols have their usual significance. We are interested in the dependence of $\theta$ on $X_0$ at constant $P$. From (2)

$$\frac{d\theta}{dX_0} = \frac{1/kT}{[1/\theta(1-\theta)] - X_1/kT} \quad \text{(constant } P, Q_a/Q_g) \quad (3)$$

For $-X_1/kT \sim 3$, $d\theta/dX_0$ is constant to within 10% for $0.3 < \theta < 0.7$ and to within 15% for $0.2 < \theta < 0.8$. The limits of constancy are narrowed with greater values of $-X_1/kT$.[9] Since $\theta$ is usually not known to an accuracy of better than 10% to 15% we may consider that $\theta$ and $X_0$ are linearly related over the main portion of the isotherm.

The value of the interaction integral $\beta$ is expected to be from 1 to 2 e.v. while its variation with adsorbate should be of the order of tenths of an electron volt. Since ionization energies of adsorbates usually differ by one or more electron volts, the effect of variation in $\beta$ is probably small when compared to the variation of $I_B$.[10] For a given metal then, the extent of adsorption is largely a function of the ionization energy of adsorbate.

(6) E. B. Maxted, J. Chem. Soc., 1987 (1949).

(7) F. A. Matsen, A. C. Makrides and N. Hackerman, J. Chem. Phys., 22, 1800 (1954).

(8) R. H. Fowler, "Statistical Mechanics," University Press, Cambridge, England, 1936.

(9) Values of $-X_1/kT$ greater than 3 are generally considered to have little physical significance. Here, however, since the adsorbed molecules are quasi ions and interaction is mainly electrostatic repulsion, values of $-X_1/kT$ greater than 3 have some plausibility.

(10) It is often assumed that $\beta$ is small compared to the other term under the square root and equation 1 is rearranged by retaining the first term of a binomial expansion. This is not permissible here since $\beta \sim 1$ or 2 e.v. and $(I_B - \phi - e^2/4R) \sim 4$ e.v. It should be noted that the argument presented above does not require that $\beta << (I_B - \phi - e^2/4R)$ but rather that the variation of $\beta$ is small when compared to the variation of $(I_B - \phi - e^2/4R)$.

Assuming that the extent of inhibition runs parallel to the extent of adsorption, nitrogen bases would be expected to be better inhibitors than corresponding oxygen compounds, as is found experimentally. Sulfur compounds have somewhat lower ionization potentials than corresponding nitrogen compounds, but their inhibition effectiveness is considerably greater. To account for this it is assumed that the interaction integral is larger. This is in line with the greater polarizability of the sulfur atom.

Differences in extent of adsorption between metals are accounted for by $\phi$ and $\beta$. Since transition metals in general adsorb more strongly it appears that $\beta$ is large only for metals with vacant d orbitals. A given inhibitor would then be expected to be more effective with iron or nickel than with zinc. Data are lacking but some results of King and Hillner[11] given in Table I are in agreement with this conclusion.

TABLE I[a,b]

| Compound | Concn. (M) | Fractional rate[c] | | |
| --- | --- | --- | --- | --- |
| | | Fe | Zn | Cd |
| Sodium gluconate | 0.01 | 0.03 | 0.56 | ... |
| Ethylenediaminetetracetic acid | Satd. soln. | 0.09 | 1.23 | ... |
| Citric acid | 0.01 | 0.055 | 0.95 | 0.57 |

[a] Calculated from data of King and Hillner.[9] [b] All solutions 0.02 M in HCl and 0.06 M in KNO₃. Five minute runs at 15,000 cm./min. at 30 ± 1°. [c] Comparative rates calculated on assigning for the rate of the uninhibited reaction the value of unity.

A detailed qualitative discussion of numerous cases was given previously;[5] it was shown that inhibition effectiveness runs parallel to the "electron donor property," which was considered to be influenced by substituents according to well established rules of the electronic theory of organic chemistry.

It may be added parenthetically that the data of Table I, combined with results obtained by the authors for a more conventional inhibitor (Table II), show conclusively that inhibitors function under strongly oxidizing conditions. This demonstrates that the mechanism of inhibition is not connected with "poisoning" of hydrogen deposition.

TABLE II[a]

| Concn. of FeCl₃ (M) | Wt. loss in absence of butyl-thiourea (mg.) | Wt. loss in presence of butyl-thiourea (mg.) | Fractional rate |
| --- | --- | --- | --- |
| ... | 5.0 | ... | 0.01 |
| 0.045 | 176 | 9.4 | 0.05 |
| 0.100 | 722 | 62 | 0.08 |
| 0.295 | 2700 | 229 | 0.08 |

[a] Mild steel at 30,000 cm./min.; 10 cm.² of exposed projected area in 10 min. runs; concentration of butyl thiourea, 15 mM.

**The Role of the Solvent.**—The distribution of adsorbate between adsorbed phase and solution is influenced not only by adsorbent–adsorbate interactions but also by solvent–adsorbent and solvent–adsorbate interactions. In a homologous series, e.g., the n-aliphatic amines, inhibition increases

(11) C. V. King and E. Hillner, J. Electrochem. Soc., 101, 79 (1954).

with increasing chain length. It has been suggested[12] that this is another application of Traube's rule, which has been found to hold for mobile monolayers of surface active compounds. Traube's rule is, of course, valid as an approximate statement of experimental facts. However, the inference drawn from it by Langmuir[13] as to molecular orientation at the interface has been challenged by Ward.[14] In the present instance, adsorption on the metal surface occurs through the polar group, and though the solid–solution interfacial tension must be lowered on adsorption as required by Gibb's equation, a discussion of chemisorption in these terms is, in a sense, artificial and does not appear to lead to any significant conclusions. Further, since interaction of adsorbent with given functional group should be largely independent of chain length, this approach does not account for an increase of adsorption, and hence of inhibition, with increasing chain length.

The work required to remove a component from solution to its standard state (pure liquid) depends only on its absolute activity which closely parallels the reduced concentration, $C/C_0$, where $C_0$ is the saturation value of $C$.[15] Thus for a given concentration adsorption should increase as $C_0$ decreases, or, in other words, adsorption for a homologous series should be a congruent function of the reduced concentration. This has been observed for adsorption of alcohols and acids on carbons.[16] This simple observation gives, then, a rational basis for Traube's rule.

It is interesting to examine the contributions of various factors to the heat of adsorption from solution in a manner somewhat analogous to Ward's[14] treatment for adsorption at liquid–air interfaces. The heat of adsorption is assumed to be separable into two parts. One is essentially the difference between the heat of adsorption of the polar group on the metal ($X_0$ given by (1)] and the sum of the heat of desorption of water and of the heat of removal of the polar group from solution (equal and of opposite sign to the heat of solution given by Butler[17]). This term is considered constant, to a first approximation, for a given functional group and independent of the hydrocarbon chain length. The second term is the heat change in transferring the hydrocarbon chain from solution to interface. If taken as equal and of opposite sign to that for placing the hydrocarbon chain in solution it can be calculated approximately by using Langmuir's "principle of independent surface action."[18] Experimentally it could be obtained directly if heats of adsorption for various members of homologous series were known.

(12) Shih-Jen Ch'iao and C. A. Mann, *Ind. Eng. Chem.*, **39**, 910 (1947).

(13) I. Langmuir, *J. Am. Chem. Soc.*, **39**, 1883 (1917).

(14) A. F. H. Ward. *Trans. Faraday Soc.*, **42**, 399 (1946).

(15) The use of reduced concentration is, of course, an approximation in the same way that use of $P/P_0$ (instead of fugacities) is for adsorption from the gaseous phase. Further, the activity at $C_0$ is not that of the pure liquid but of liquid solute saturated with water. For the higher homologs (pentyl, hexyl, etc.) these are not much different.

(16) R. S. Hansen and R. P. Craig, THIS JOURNAL, **58**, 211 (1954).

(17) J. A. V. Butler, *Trans. Faraday Soc.*, **33**, 239 (1937).

(18) I. Langmuir, "Colloid Symposium Monograph," Vol. III, Chemical Catalog Co., New York, N. Y., 1925, p. 48.

The meagerness of available experimental data makes impossible the application of a detailed analysis of this nature. Two points of immediate applicability are evident, however. Comparison of inhibitors with different functional groups must be made at equal activities, or approximately at equal reduced concentrations, if it is to be meaningful. Secondly, the smaller the solubility of inhibitor, the smaller the concentration required for protection. It follows that if the solvent is changed so as to increase the inhibitor solubility, the concentration–inhibition curve is shifted in the direction of larger concentrations for given inhibition. This has been observed for *sec*-diethylthiourea in water–methanol solutions.[19]

**Adsorption and Inhibition.**—Up to this point, the relationship of extent of adsorption to inhibition has not been considered. The functional form of this relation depends on the specific model adopted for the mechanism of inhibition. If, for example, it is assumed that the inhibitor is adsorbed at "cathodic areas" and that it functions by simply blocking off part of the available area for discharge of hydrogen ion, inhibition should be proportional to amount adsorbed.[12] This model is hardly satisfactory for reasons already pointed out by several authors.[1,2,5] There exists fairly conclusive evidence that the anodic reaction is also inhibited. This is to be expected if chemisorption occurs over the entire surface, as postulated above. If our adsorption mechanism is correct, a dipole layer with the positive end outermost is formed. Such a layer should retard the rate of escape of positive ions just as adsorbed dipole layers with the negative end outermost increase the work of extraction of electrons.

Another consequence of inhibitor chemisorption, of perhaps greater importance for inhibition, is the displacement of adsorbed anions and water molecules from the metal surface. The minimum activation energy for escape of positive ions is given by the sum of the latent heat of sublimation and of the energy of ionization of metal atoms, less the energy gained by returning the ionized electrons to the metal, and is of the order of 20 e.v. Although a favorable potential gradient will reduce this energy requirement, in the absence of the disruptive effect of adsorbed water (or anions) on metal to metal bonds, the rate of escape of positive ions at room temperature is zero. It is apparent then that the entities crossing the metal–solution interface are "partially hydrated or complexed" metal ions. This is the same description as given pictorially by the "crossing" of potential energy–distance curves for the ion in solution and the ion in the lattice; or this entity may be identified with the usual activated intermediate complex of chemical kinetics. In either case, a stable metal–inhibitor adsorption complex will decrease the anodic reaction rate.

In view of the above, inhibition may be described in terms of two more or less independent processes: (i) adsorption of positively charged inhibitor molecules; (ii) chemisorption of neutral inhibitor molecules. The first of these can be considered

(19) A. C. Makrides and N. Hackerman, *Ind. Eng. Chem.*, in press.

to decrease the rate of hydrogen ion discharge, while the second reduces both the anodic and cathodic reaction rates. Dissolution potentials[1,2] and polarization studies at small current densities[2] indicate that, at large inhibitor concentrations at least, the anodic reaction is inhibited to a somewhat greater extent. There is some evidence that at small inhibitor concentrations the reverse is true.[20] Since in this concentration region only a small fraction of the surface is covered with chemisorbed inhibitor, it is probable that process (i) is of greater importance.

**Dissolution Potentials and Polarization Studies.** —A method of establishing the inhibition effectiveness of various compounds consists in obtaining hydrogen overpotential curves at relatively high current densities.[12] It has been found that at equal potentials (constant overpotential) the relation

$$\% I = \frac{i_1 - i_2}{i_1} \times 100 \qquad (4)$$

correctly gives the inhibition effectiveness. Here $i_1$ is the current density in the absence of inhibitor, and $i_2$ is the apparent current density in its presence.

The success of the above equation has been cited as evidence that inhibitors function by being adsorbed as positive ions at "cathodic areas." This conclusion does not seem necessary. If adsorption of neutral molecules occurs, as the evidence referred to above suggests, it is probably little affected by applied potential. If now the surface available for hydrogen ion discharge is restricted to areas not covered by adsorbed inhibitor, the above relationship also results.

The simplest approximation that yields conclusions in reasonable agreement with observation

(20) L. Cavallaro, Soc. Roy. Belge Ing. Indust., No. 3, p. 15, 1952; L. Cavallaro and A. Indelli, Rev. Metall., 49, 117 (1952).

proposes that parts of the metal surface on which inhibitor has been chemisorbed are not available for either the anodic or the cathodic reaction. The potential determining reactions, however, do not change. It is then to be expected that the dissolution potential is not significantly affected on addition of inhibitor, though the dissolution rate may become essentially zero. This constitutes a fundamental difference between inhibitors and passivators. In the latter case, the potential determining reaction is altered and not simply restricted in area. In the case of iron and potassium chromate, for example, the reaction is no longer iron to ferrous ion, but iron to iron oxide with a consequent change of potential of about a volt. It is apparent that dissolution potential or polarization studies do not yield important results for the primary step in inhibition, i.e., adsorption. Therefore, by themselves they cannot provide a basis for an account of the inhibitive properties of organic compounds.

### Conclusion

A detailed mechanism for inhibition is not possible without an understanding of the adsorption process. Experimental values of quantities important in this respect are not available in general. Reported heats of adsorption are of doubtful value since in the indirect method used the rate of metal dissolution changes. Desorption studies at some fixed temperature would probably give more reliable results. Substitution of some other reaction for the relatively complex hydrogen ion discharge may simplify the interpretation of experimental results. Finally, a major disturbing factor common to most inhibition experiments is incomplete wetting resulting from the hydrophobic character of the adsorbed film. Wetting effects usually can be eliminated by simply adding a wetting agent. Work on some of these aspects will be reported in the near future.

---

# THE SOLVENT EXTRACTION BEHAVIOR OF INORGANIC COMPOUNDS: MOLYBDENUM(VI)[1]

By I. Nelidow and R. M. Diamond[2]

Contribution from the Department of Chemistry, Harvard University, Cambridge, Mass.

The distribution ratios of molybdenum(VI) between various organic solvents and certain aqueous acids were determined as a function of the acid concentration, the temperature and, in a few cases, the variation of the molybdenum concentration from $10^{-9}$ to $10^{-2}$ M. The results lead to the determination of better conditions for the extraction of molybdenum(VI) than the customary method from 6 M HCl using diethyl ether. A discussion of the nature of the extracting species is given, and it is suggested that there are four main factors involved in the mechanism of metal extraction systems such as this one and, for example, the iron(III)-hydrochloric acid-ether system. These factors are: 1, association and polymerization; 2, acid strength of species; 3, complex formation with halide ion, etc.; 4, solvation of species in the two phases.

The first mention of the ether extraction of molybdenum from a hydrochloric acid solution of an alkali molybdate was by Péchard,[3] in 1892. Blair[4] suggested the use of such a method in steel

(1) This work was supported by the U. S. Atomic Energy Commission.

(2) Department of Chemistry, Cornell University, Ithaca, New York.

(3) E. Péchard, Compt. rend., 114, 173 (1892).

(4) A. A. Blair, J. Am. Chem. Soc., 30, 1229 (1908).

analysis, and worked out a procedure. In a paper on the diethyl ether extraction of gallium(III) from 6 M HCl, Swift[5] lists other extracting elements and gives the extraction of molybdenum (VI) as being 80–90% for initially equal volumes of the two liquids. Sandell[6] quotes Perrin to the

(5) E. H. Swift, ibid., 46, 2375 (1924).

(6) E. B. Sandell, "Colorimetric Determination of Traces of Metals," 2nd Edition, Interscience Publishers, Inc., New York, N. Y., 1950, p. 455.

effect that molybdenum(VI) extraction into diethyl ether peaks sharply at 6 $M$ HCl and, at this optimum acid concentration, about 70% is extracted by an equal volume of ether. By evaporation of an ether extract of a hydrochloric acid solution of sodium molybdate, Péchard[3] obtained a crystalline product which he said was identical to that from the evaporation of an ether solution of the compound $MoO_2Cl_2 \cdot H_2O$ or $MoO_3 \cdot 2HCl$. This compound had been prepared by Debray[7] by passing anhydrous hydrogen chloride over molybdenum trioxide at 150–200°, at which temperature the $MoO_3 \cdot 2HCl$ sublimes. The molecular weight of this substance in ether, as determined by the elevation of the boiling point, is normal and monomeric, while that in water, as determined by the lowering of the freezing point, corresponds to dissociation into at least four or five ions.[8]

The previous paragraph gives most of the published data available concerning the extraction of molybdenum(VI). Yet this is an often used separation procedure, particularly in radiochemistry where solvent extraction methods are especially suitable for work with carrier-free activities. In order to determine better conditions for more complete extraction, and to obtain data to help in understanding the extraction process in general and this extraction system in particular, the distribution of tracer molybdenum(VI) was studied under varying conditions, that is, when changing the nature of the solvent, the nature and the concentration of the acid in the aqueous phase, and the temperature.

## Experimental

**Tracers and Counting.**—The radioactive tracer used in the major part of this study was $Mo^{99}$ obtained from Brookhaven National Laboratory. It was counted with a well-type NaI(Tl) scintillation counter in a manner eliminating interference from the $Tc^{99m}$ daughter. However, the samples of $Mo^{99}$ contained an unidentified long-lived radioactive impurity which amounted to about 2% of the total activity by the end of the two-week periods of experimentation. The last set of extraction measurements used $Mo^{93m}$ tracer. This activity was produced by irradiating $Nb^{93}$ metal foil with deuterons in the Massachusetts Institute of Technology cyclotron,[9] and separating from this target carrier-free $Mo^{93m}$ activity. Resolution of the decay curve of a sample of the $Mo^{93m}$ used showed but 0.4% foreign activity at the time the experiments with it were completed.

**Reagents.**—Reagent grade nitric, hydrofluoric, hydrochloric, hydrobromic, hydriodic, sulfuric and perchloric acids were used without further purification, as were the trifluoroacetic acid and the reagent grade lithium chloride, molybdenum trioxide, benzene, chloroform, carbon tetrachloride and anhydrous diethyl ether. Practical grade or C.P. $\beta,\beta'$-dichlorodiethyl, $\beta,\beta'$-dichlorodiisopropyl, diisopropyl and dibutyl ethers were used as obtained and also after distillation (a two degree cut was taken) with no apparent change in molybdenum distribution ratios. Practical grade diisopropyl ketone and isoamyl acetate were fractionated and a two degree cut used. In some cases practical, in others reagent grade, but usually C.P., methyl isobutyl ketone, tributyl phosphate, methyl benzoate, methyl salicylate, 2-ethylhexanol, diisobutyl ketone, nitrobenzene and o-dichlorobenzene were used without further purification.

**Analyses.**—Aliquots of ether equilibrated with hydrochloric or hydrobromic acid solutions containing molybdenum(VI) were pipetted into water, warmed to remove the

(7) M. H. Debray, *Compt. rend.*, **46**, 1098 (1858).

(8) A. Vandenberghe, *Z. anorg. Chem.*, **10**, 47 (1896).

(9) The authors gratefully acknowledge the kindness of Professor J. Irvine, Jr., and the help of the operating crew of the M.I.T. cyclotron.

ether, and then analyzed directly for chloride, molybdate and hydrogen ion. Hydrogen ion was determined by titration with sodium carbonate using brom cresol green as indicator or with sodium hydroxide using phenolphthalein. Molybdenum was determined gravimetrically as lead molybdate from a hot acetate buffered solution, and the halide in the filtrate was measured volumetrically with silver nitrate.

**Extraction Procedure.**—Ten ml. of the aqueous acid was added to 20 ml. of the organic solvent (except in the tributyl phosphate extractions where only 10 ml. of the solvent was taken) in 2 oz. glass-stoppered bottles. The tracer was added, usually in a volume of 25 microliters, and the bottles were shaken for two hours at room temperature on a mechanical shaker. They were then placed for a minimum of two hours in a constant temperature bath which for most experiments was set at 25.0 ± 0.5°. Usually satisfactory phase separation occurred immediately, but for a few difficult cases the mixture was centrifuged. Two-milliliter aliquots from each phase were pipetted into one-dram screw-cap vials and γ-counted using the well-type NaI(Tl) scintillation counter.

The ratio of the counting rates (corrected for background; no coincidence correction necessary at rates used) of the sample from the organic phase to that from the aqueous phase gives directly the value of the distribution ratio of molybdenum(VI) between the two phases

$$D = \frac{\text{c./m. of 2 ml. org. phase}}{\text{c./m. of 2 ml. aq. phase}} = \frac{\text{molybdenum molarity in org. phase}}{\text{molybdenum molarity in aq. phase}}$$

Duplicate trials from the same bottle showed that pipetting and counting errors were less than 3%. However, duplicate trials on the same system from different bottles showed a wider variation, though less than 10% except for tributyl phosphate extractions where $D$ is so large that the value is very sensitive to a few counts per minute in the aqueous phase and reproducible results were difficult to obtain. That equilibrium was reached in the two-hour shaking period used was shown by shaking for still longer times, overnight in a few cases, and obtaining the same values of $D$. Also the organic phase from one extraction (now containing tracer) was re-equilibrated with a fresh portion of aqueous phase, and again approximately the same value of $D$ resulted.

Experiments using the $Mo^{99}$ tracer showed gradually decreasing values of the distribution ratio, $D$, over intervals of several days due to the unidentified long-lived impurity which did not extract. However, these tracers were used only up to the time that the impurity amounted to less than 2% of the radioactivity. The maximum error from this cause when $D$ differed from unity by only an order of magnitude, as it usually did, would be when all the impurity was concentrated in the phase with the least amount of molybdenum, and then would amount to 20% at the end of the experimentation period. Resolution of the decay curve of the $Mo^{93m}$ tracer showed so little radioactive impurity as to be relatively negligible during its period of use.

In the experiments performed, none of the organic phases were pre-treated with aqueous acids.

## Results

The results of the measurements on the extraction of molybdenum(VI) from hydrochloric acid solutions into the ethers studied, diethyl, diisopropyl, $\beta,\beta'$-dichlorodiethyl (hereafter referred to as DDE), $\beta,\beta'$-dichlorodiisopropyl and dibutyl, are shown in Fig. 1, where the distribution ratio, $D$, is plotted against the acid molarity, using logarithmic scales. It may be noted that in dilute acid (below 6 $M$) the value of $D$ roughly decreases with increasing size and weight of the organic molecule. Furthermore, the larger ethers show a monotonic increase in $D$ with increasing acid concentration, while diethyl and diisopropyl ethers have maxima at 6.5 and 9 $M$ HCl, respectively. This parallels roughly the variation in the equi-
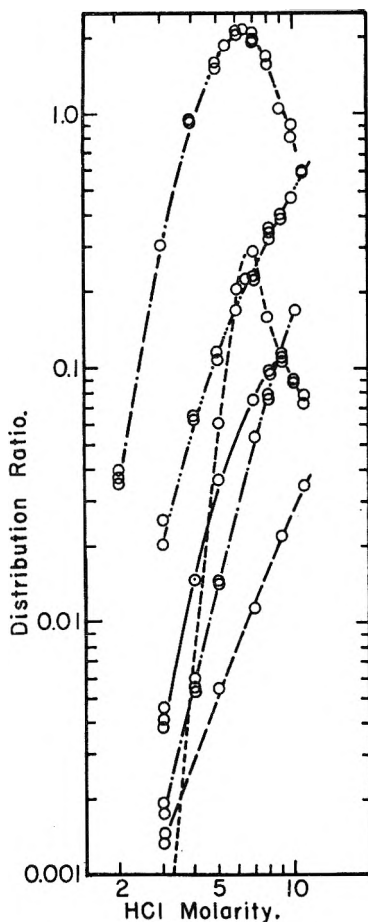
Fig. 1.—Plot of distribution ratio, $D$, against initial aqueous acid molarity for diethyl ether–HCl, — — ·; diisopropyl ether–HCl, ———; diisopropyl ether–HBr, – – –; $\beta,\beta'$-dichlorodiethyl ether–HCl, — ··; dibutyl ether–HCl, — ·; $\beta,\beta'$-dichlorodiisopropyl ether–HCl, — —; all at 25°.

librium aqueous acid concentration with initial concentration, which also shows a maximum for the latter ethers, Fig. 2.

In contrast to the ethers, negligible extraction of molybdenum(VI) was observed, even from 12 $M$ HCl, for carbon tetrachloride, chloroform, benzene and Fluorolube FS (a mixture of fluorocarbons) as indicated in Table I. This lack of solubility suggests that oxygenated solvents are required for successful extractions, and a further indication of this is given by a comparison of the values of $D$ for $o$-dichlorobenzene and nitrobenzene. From 12 $M$ HCl the former solvent shows a very low extraction, while that of nitrobenzene is significant. If, indeed, oxygenated solvents are necessary, other types of oxygen-containing organic compounds besides the ethers might be just as suitable, or more so, provided they are relatively immiscible with the aqueous acid phase and reasonably stable on contact with it. To test this, measurements were made on representative ketones, esters and an alcohol. Molecules containing six to nine carbon atoms were chosen, as they satisfy the above mentioned requirements and are of similar size and weight to compare with the ethers.

All of the compounds tried were better at extracting molybdenum(VI) than was the corresponding ether,
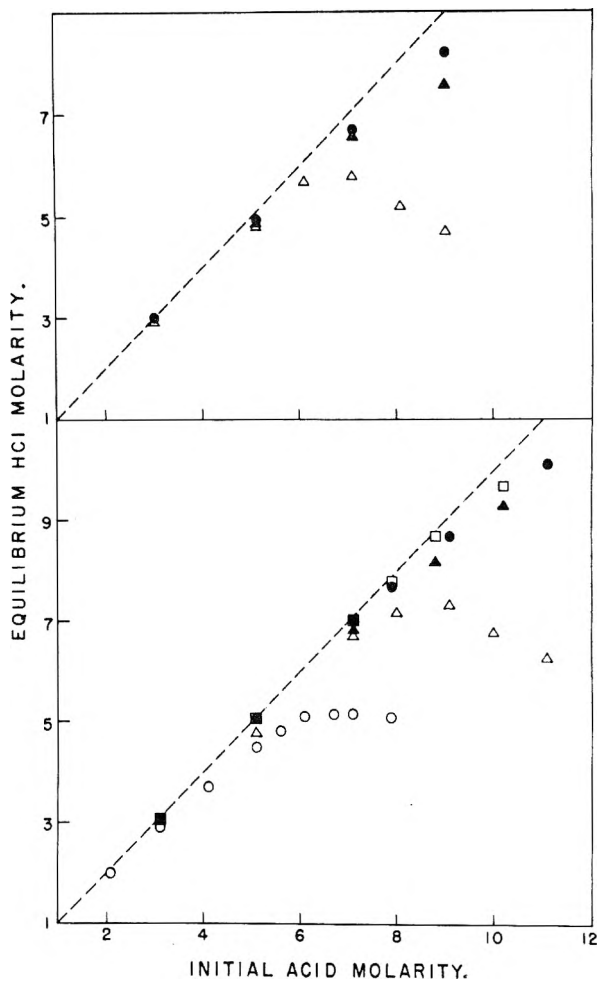


Fig. 2.—Plot of equilibrium aqueous HCl (lower figure) and HBr (upper figure) molarity against initial aqueous acid molarity when in contact at 25° with twice its volume of diethyl ether, ○○○; diisopropyl ether, △△△; diisopropyl ketone, ▲▲▲; $\beta,\beta'$-dichlorodiethyl ether, ●●●; dibutyl ether, □□□; — — — is line of unit slope.

and esters and the alcohol were the best, $i.e.$, isoamyl acetate > diisopropyl ketone > diisopropyl ether and 2-ethylhexanol ⩾ methyl benzoate > diisobutyl ketone > dibutyl ether (Table II). Plots of the logarithm of $D$ against the logarithm of the hydrochloric acid molarity for some of these solvents are shown in Fig. 3. It may be noted that, as with diethyl and diisopropyl ether, the plot of $D$ $vs.$ acid concentration passes through a maximum and then falls with increasing hydrochloric acid molarity for hexone, isoamyl acetate and 2-ethylhexanol.

The largest distribution ratios observed were obtained using tributyl phosphate as a solvent; the values of $D$ were so high at some hydrochloric acid concentrations, as to make the determinations inaccurate. Even from 1 and 2 $M$ HCl values of $D$ of 4.0 and 65, respectively, were obtained. Extractions into tributyl phosphate are therefore a very useful procedure for molybdenum(VI) if the solvent does not also extract undesirable impurities as well.

Another factor in the extraction process which can be varied besides the solvent and the concentration of hydrochloric acid is the nature of the

TABLE I

| Organic phase | Aqueous phase | Molybdenum, $M$ | $D$ |
|---|---|---|---|
| Carbon tetrachloride | 12 $M$ | $10^{-3}$ | <0.001 |
| Chloroform | 12 $M$ | $10^{-8}$ | .001 |
| Fluorolube FS | 12 $M$ | $10^{-4}$ | .000 |
| Benzene | 12 $M$ | $10^{-2}$ | .000 |
| o-Dichlorobenzene | 12 $M$ | $10^{-8}$ | .001 |
| Nitrobenzene | 12 $M$ | $10^{-8}$ | .22 |
| Diisobutyl ketone | 7 $M$ HCl | $10^{-4}$ | 1.5 |
| Methyl benzoate | 7 $M$ HCl | $10^{-4}$ | 2.4 |
| Methyl salicylate | 7 $M$ HCl | $10^{-4}$ | 0.072 |
| 2-Ethylhexanol | 7 $M$ HCl | $10^{-4}$ | 2.5 |
| Diisopropyl ketone | 7 $M$ HCl | $10^{-4}$ | 3.9 |
| Methyl isobutyl ketone | 7 $M$ HCl | $10^{-4}$ | 29 |
| Isoamyl acetate | 7 $M$ HCl | $10^{-4}$ | 18 |
| Diethyl ether | 7 $M$ HCl | $10^{-4}$ | 2.1 |
| Diisopropyl ether | 7 $M$ HCl | $10^{-4}$ | 0.076 |
| $\beta,\beta'$-Dichlorodiethyl ether | 7 $M$ HCl | $10^{-4}$ | .24 |
| $\beta,\beta'$-Dichlorodiisopropyl ether | 7 $M$ HCl | $10^{-4}$ | .011 |
| Dibutyl ether | 7 $M$ HCl | $10^{-4}$ | .054 |
| $\beta,\beta'$-Dichlorodiethyl ether | 7 $M$ LiCl | $10^{-4}$ | .000 |
| $\beta,\beta'$-Dichlorodiethyl ether | 7 $M$ HNO₃ | $10^{-4}$ | .003 |
| $\beta,\beta'$-Dichlorodiethyl ether | 7 $M$ H₂SO₄ | $10^{-4}$ | .033 |
| $\beta,\beta'$-Dichlorodiethyl ether | 7 $M$ HClO₄ | $10^{-4}$ | .05 |
| $\beta,\beta'$-Dichlorodiethyl ether | 7 $M$ HF | $10^{-4}$ | <0.001 |
| $\beta,\beta'$-Dichlorodiethyl ether | 7 $M$ HBr | $10^{-4}$ | 5.7 |
| $\beta,\beta'$-Dichlorodiethyl ether | 7 $M$ HI | $10^{-4}$ | 6.6ª |
| Diisopropyl ketone | 7 $M$ HNO₃ | $10^{-4}$ | 0.011 |
| Diisopropyl ketone | 7 $M$ H₂SO₄ | $10^{-4}$ | <0.017 |
| Diisopropyl ketone | 7 $M$ HClO₄ | $10^{-4}$ | 0.47 |
| Diisopropyl ketone | 7 $M$ HF | $10^{-4}$ | 0.001 |
| Diisopropyl ketone | 7 $M$ HBr | $10^{-4}$ | 29 |
| Diisopropyl ketone | 7 $M$ HI | $10^{-4}$ | 17ª |
| $\beta,\beta'$-Dichlorodiisopropyl ether | 5 $M$ HBr | $10^{-4}$ | 0.011 (0.005)ᵇ |
| 2-Ethylhexanol | 5 $M$ HBr | $10^{-4}$ | 0.83 (1.3)ᵇ |
| Diisopropyl ketone | 5 $M$ HBr | $10^{-3}$ | 2.7 (1.6)ᵇ |
| Diisobutyl ketone | 5 $M$ HBr | $10^{-4}$ | 0.78 (0.56)ᵇ |
| Methyl benzoate | 5 $M$ HBr | $10^{-4}$ | 1.7 (1.1)ᵇ |
| Methyl salicylate | 5 $M$ HBr | $10^{-4}$ | 0.41 (0.074)ᵇ |
| Methyl isobutyl ketone | 5 $M$ HBr | $10^{-4}$ | 17 (0.7)ᵇ |
| Dibutyl ether | 5 $M$ HBr | $10^{-4}$ | 0.035 (0.014)ᵇ |
| $\beta,\beta'$-Dichlorodiethyl ether | 5 $M$ HBr | $10^{-4}$ | 0.17 (0.11)ᵇ |
| Diisopropyl ether | 5 $M$ HBr | $10^{-4}$ | 0.061 (0.036)ᵇ |
| Diethyl ether | 5 $M$ HBr | $10^{-4}$ | 1.4 (1.6)ᵇ |
| $\beta,\beta'$-Dichlorodiethyl ether | 6 $M$ HCl | $\sim10^{-9}$ | 0.17 |
| $\beta,\beta'$-Dichlorodiethyl ether | 6 $M$ HCl | $\sim10^{-9}$ | .17 |
| $\beta,\beta'$-Dichlorodiethyl ether | 6 $M$ HCl | $10^{-8}$ | .17 |
| $\beta,\beta'$-Dichlorodiethyl ether | 6 $M$ HCl | $10^{-6}$ | .17 |
| $\beta,\beta'$-Dichlorodiethyl ether | 6 $M$ HCl | $10^{-4}$ | .17 |
| $\beta,\beta'$-Dichlorodiethyl ether | 6 $M$ HCl | $10^{-3}$ | .17 |
| $\beta,\beta'$-Dichlorodiethyl ether | 6 $M$ HCl | $10^{-2}$ | .17 |
| Methyl isobutyl ketone | 6 $M$ HCl | $\sim10^{-9}$ | 21 |
| Methyl isobutyl ketone | 6 $M$ HCl | $\sim10^{-9}$ | 21 |
| Methyl isobutyl ketone | 6 $M$ HCl | $10^{-8}$ | 21 |
| Methyl isobutyl ketone | 6 $M$ HCl | $10^{-6}$ | 21 |
| Methyl isobutyl ketone | 6 $M$ HCl | $10^{-4}$ | 21 |
| Methyl isobutyl ketone | 6 $M$ HCl | $10^{-3}$ | 20 |
| Methyl isobutyl ketone | 6 $M$ HCl | $10^{-2}$ | 24 |

ª Measured after 5.5 hours of shaking and standing.
ᵇ Values in parentheses are $D$ for 5 $M$ HCl.



Fig. 3.—Plot of distribution ratio, $D$, against initial aqueous hydrochloric acid molarity for methyl isobutyl ketone, ——; diisopropyl ketone, — ·; diisobutyl ketone, — —; methyl benzoate, — ··; methyl salicylate, — —·; 2-ethylhexanol, - - -; isoamyl acetate, — — ··; all at 25°.

aqueous phase itself. Other aqueous acids might also allow extraction of molybdenum(VI), so a survey of the extractions from 7 $M$ solutions of various acids into DDE and into diisopropyl ketone was done with the results shown in Table I. Nitric and sulfuric acids show little extraction, but strangely enough, a small amount of extraction does occur from perchloric acid. The hydrogen halides show an interesting order. Hydrofluoric acid is much worse than hydrochloric acid, and hydrobromic acid is much better. One might expect hydriodic acid to be still better. Unfortunately, the molybdenum(VI) apparently reacts with this acid, oxidizing it, and the value of the
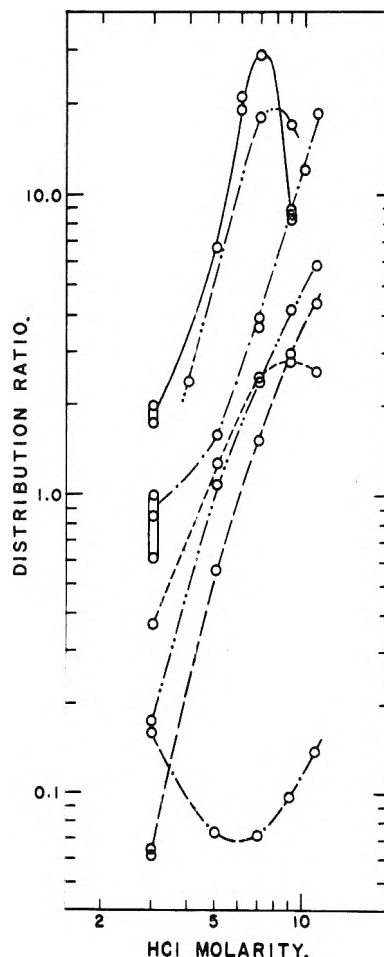
distribution ratio appears to decrease with the length of time the molybdenum has been in contact with the acid. The values given for the chloroether and the ketone, 6.6 and 17, are for separation after 5.5 hours shaking and standing; for separation after six days these values have dropped to 4.4 and 3.7, respectively. Perhaps intrinsically hydriodic acid would be better in molybdenum(VI) extractions than hydrobromic acid if it were stable. In any case, these results indicated that more complete extractions could be obtained using hydrobromic acid so studies were made with it. Various extractions from 5 $M$ HBr are shown in Table I, confirming this expectation. In Fig. 4, values of $D$ for the extraction into DDE from different concentrations of hydrobromic and hydrochloric acids are plotted. It may be noted that the curve for the former acid is steeper than that for the latter, so that above 4–5 $M$ acid HBr is the better acid to use, and that below this concentration, HCl gives the largest value of $D$. This behavior could very well be typical, as it is also observed with diisopropyl ketone and diisopropyl ether. With the latter solvent a maximum in $D$ is observed, as when using hydrochloric acid, but the maximum occurs now at 6.5–
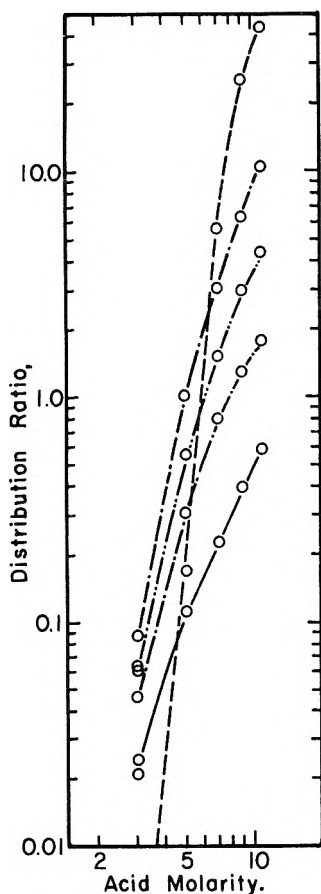
Fig. 4.—Plot of distribution ratio, $D$, against initial aqueous acid molarity for $\beta,\beta'$-dichlorodiethyl ether and HCl at 25°, ———; $\beta,\beta'$-dichlorodiethyl ether and HBr at 25°, — — —; and for diisobutyl ketone and HCl at 5°, — — ·; 25°, — · ·; 45°, — ·.

7 $M$ HBr instead of 9 $M$ HCl (Fig. 1). Diethyl ether extractions from hydrobromic acid also show their maximum value at a lower concentration than with hydrochloric, but this solvent is unusual in being the only one tried which did not yield more complete extractions, above 4 $M$ HBr, than with hydrochloric acid.

The effect of temperature on the extraction was also studied. Distribution ratios were measured at 5.0 ± 0.5° and 45.0 ± 0.5° in many cases, as well as at 25.0 ± 0.5°. With all the solvents tried except for 2-ethylhexanol, i.e., $\beta,\beta'$-dichlorodiethyl and $\beta,\beta'$-dichlorodiisopropyl ethers, diisopropyl and diisobutyl ketones, methyl benzoate, methyl salicylate and tributyl phosphate, and with hydrochloric acid concentrations from 1 to 11 $M$, the extraction was always more nearly complete at the lower temperature. This was also true in the few cases where the extractions from hydrobromic acid solutions were observed as a function of temperature. 2-Ethylhexanol extractions alone seemed to be independent of temperature over this range. From the distribution ratios at the three temperatures, values of the thermodynamic functions, $\Delta F°$, $\Delta H°$ and $\Delta S°$, can be calculated for the extraction, but since the change in temperature affects the solubility of hydrochloric acid in the solvents as well as that of the molybdenum, it is difficult to interpret these data without more

detailed work on the variation with temperature of the distribution of acid alone.

Information as to the nature of the extracting species can be obtained from distribution measurements. Ideally, if no HCl or LiCl dissolves in the organic phase so there is no change in its properties, the hydrogen ion dependence of the extracting species could be determined from the variation of $D$ with increasing hydrochloric acid concentration in the aqueous phase, keeping the ionic strength and chloride concentration constant with lithium chloride. Actually, at 6 $M$ total concentration the solubility of LiCl in DDE is negligible and that of HCl is very small ($\sim 0.002\ M$), so that the above-mentioned condition is approximated. The results of the extractions, given in Fig. 5, show only a slight increase in $D$ with an increase in hydrochloric acid from 0.6 to 6 $M$, indicating no significant hydrogen ion dependence and thus that the extracting species cannot be a strong acid. Comparison of the conductances of diisopropyl ether extracts of molybdenum(VI) and of iron(III) (which does extract as an acid, $H(H_2O)_5FeCl_4$[10]) from 6 $M$ HCl, and of diisopropyl ether extracts of 6 $M$ HBr, 6 $M$ HClO$_4$, 6 $M$ HNO$_3$, 6 $M$ HCl and 6 $M$ H$_2$SO$_4$, confirms this.
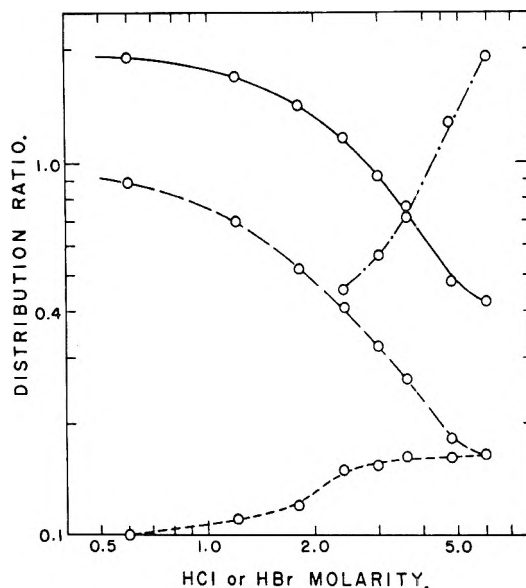


Fig. 5.—Plot of distribution ratio, $D$, against HCl molarity at a total ionic strength of 6 $M$ with LiCl and $\beta,\beta'$-dichlorodiethyl ether, — — —; with HClO$_4$ and $\beta,\beta'$-dichlorodiethyl ether, — —; with HClO$_4$ and methyl isobutyl ketone, — ·; plot of $D$ against HBr molarity at a total ionic strength of 6 $M$ with HClO$_4$ and $\beta,\beta'$-dichlorodiethyl ether, ———; all at 25°.

Similarly, the chloride dependence can be studied by varying the concentration of hydrochloric acid but keeping the hydrogen ion concentration constant with some other non-complexing strong acid. Trifluoroacetic and perchloric acids were tried. The trifluoroacetic acid was quite soluble in the chloroether, in fact 9 $M$ trifluoroacetic acid was miscible, so that the desired and necessary requirement of not affecting the environment of the organic phase was not even remotely approached.

(10) E. J. Goon, Ph.D. Dissertation, Rensselaer Polytechnic Institute, Troy, New York, 1953.

TABLE II

ANALYSES OF ETHER EXTRACTS (AVERAGE OF DUPLICATE TRIALS)

| | Diisopropyl ether | | Diethyl ether | | | | |
|---|---|---|---|---|---|---|---|
| Initial acid molarity | 6 M HCl | 9 M HCl | 3 M HCl | 6 M HCl | 9 M HCl | 6 M HBr | 6 M HCl |
| Initial vol. ratio ether:acid | 1:1 | 1:1 | 1.5:1 | 1.5:1 | 2.5:1 | 2:1 | 1.5:1 |
| Initial Mo molarity in acid | 0.1 | 0.1 | 0.1 | 0.02 | 0.1 | 0.1 | 0.04 |
| Acid solubility, mmoles/20 ml. ether | .11 | 1.56 | .008 | .14 | 0.96 | 0.07 | 0.14 |
| Mmoles H$^+$/20 ml. ether | .56[a] | 2.23[a] | .39[a] | .90[a] | 2.78[a] | 2.44[a] | 2.07[b] |
| Mmoles halide/20 ml. ether | .39 | 2.04 | .25 | .63 | 2.18 | 1.82 | 1.10 |
| Mmoles Mo/20 ml. ether | .14 | 0.22 | .13 | .25 | 0.60 | 0.84 | 0.48 |
| Cor. mmoles H$^+$/20 ml. ether | .45 | 0.67 | .38 | .76 | 1.82 | 2.37 | 1.93 |
| Cor. mmoles halide/20 ml. ether | .28 | 0.48 | .24 | .49 | 1.22 | 1.75 | 0.96 |
| Ratio Mo:H$^+$:halide | 1.0:3.2: 2.0 | 1.0:3.0: 2.2 | 1.0:2.9: 1.9 | 1.0:3.0: 2.0 | 1.0:3.0: 2.0 | 1.0:2.8: 2.1 | 1.0:4.0: 2.0 |

[a] Determined with Na$_2$CO$_3$ to brom cresol green end-point, pH 4–5.   [b] Determined with NaOH to phenolphthalein end-point, pH 9.

The results with 6 $M$ HClO$_4$ are perhaps more meaningful, for although perchloric acid is also much more soluble in the ether than hydrochloric acid, it is not as soluble as trifluoroacetic acid (6 $M$ HClO$_4$ is not miscible) and so conditions are closer to the desired ideal case. The extraction of molybdenum(VI) from 6 $M$ HClO$_4$ is low, $D \sim 0.02$, but rises rapidly with increasing hydrochloric acid, passes through a maximum, and then decreases to the value from 6 $M$ HCl alone (Fig. 5). Unfortunately not enough measurements were made in the low hydrochloric acid concentration region to fix accurately the position of the maximum, but it is somewhere between the points at 0.06 and 0.6 $M$ HCl. The decrease in $D$ from there to 6 $M$ HCl is about a factor of 6–10. The same type of measurements were carried out using mixtures of hydrobromic and perchloric acids of 6 $M$ total concentration. Again $D$ rises rapidly from the low value in 6 $M$ HClO$_4$ to a maximum and then decreases to its value in 6 $M$ HBr. In Fig. 5 the results are shown from about the maximum on. The curve is quite similar to that of the HClO$_4$–HCl extractions, except that the absolute values of $D$ are larger and the maximum may occur at a higher hydrogen halide concentration, that is not far below 0.6 $M$ HBr. Similar extractions from HCl–HClO$_4$ mixtures of 6 $M$ total concentration into hexone were also performed. 6 $M$ HClO$_4$ is miscible with hexone so only part of the curve is experimentally accessible, as in the case of trifluoroacetic acid and DDE, and, as in that system, $D$ is monotonically increasing with increasing hydrochloric acid concentration.

The effect of varying the molybdenum concentration also was studied. Using mixtures of the carrier-free Mo$^{93m}$ tracer[11] and inactive molybdenum prepared by volumetric dilution of a 0.0100 $M$ stock solution, 10-ml. aliquots of 6 $M$ HCl containing $\sim 10^{-9}$, $10^{-8}$, $10^{-6}$, $10^{-4}$, $10^{-3}$, $10^{-2}$ $M$ molybdenum(VI) were extracted with 20-ml. portions of DDE and of hexone. As shown in Table I, there was no variation in the values of $D$ over this range of molybdenum concentration.

A more direct sort of information about the extracting species is obtained by analyzing aliquots

of the organic phase for molybdenum, halide and hydrogen ion. The results of such analyses are given in Table II, and show that in these cases the ratio of molybdenum to halide ion is 1 to 2 (assuming that the amount of free acid in the ether is the same whether or not extracted molybdenum is present). Titration of hydrogen ion with Na$_2$CO$_3$ to the brom cresol green end-point yields a hydrogen ion to molybdenum ratio of 3, and with NaOH to the phenolphthalein end-point gives a ratio of 4.

## Discussion

The distribution experiments for molybdenum (VI) show in general the same pattern of behavior as those for iron(III),[10,12–17] gallium(III)[5,18,19] gold(III),[20] thallium(I),[19] thallium(III),[19] antimony(V),[21] indium(III),[19] when the same solvents are compared. That is, extractions from hydrochloric or hydrobromic acid solutions up to concentrations of about 5 $M$ all show an increase in $D$ with increasing acid concentration. For diethyl and diisopropyl ethers, maxima occur followed by a decrease in $D$ with increasing acid concentration, while for DDE there is a continuous increase in $D$. In other respects there are differences in the extractions. The authors would like to suggest that the behavior of these metal ion–acid–solvent systems all depend on the following four main factors, although to varying degrees for the different systems.

1. The extracting species, if ionic, may associate in the organic phase to ion-pairs, ion-triplets, and to higher clusters, or, if non-ionic, dimerize, trimerize, etc., in either, or both, phases. For species which ionize in the organic solvent, an increase in concentration will promote ion-pairing,[22]

(11) Spectroscopic analysis of a sample of the niobium metal foil that was used to produce the Mo$^{93m}$ tracer indicated a molybdenum content of 0.004%. This corresponds to a $10^{-9}$ $M$ concentration of molybdenum in the 10 ml. of aqueous solution used in each extraction.

(12) R. W. Dodson, G. J. Forney and E. H. Swift, *J. Am. Chem. Soc.*, **58**, 2573 (1936).

(13) N. H. Nachtrieb and S. G. Conway, *ibid.*, **70**, 3547 (1948).

(14) N. H. Nachtrieb and R. E. Fryxell, *ibid.*, **70**, 3552 (1948); **74**, 897 (1952).

(15) J. Axelrod and E. H. Swift, *ibid.*, **62**, 33 (1940).

(16) R. J. Myers, D. E. Metzler and E. H. Swift, *ibid.*, **72**, 3767 (1950).

(17) D. E. Campbell, Ph.D. Dissertation, Rensselaer Polytechnic Institute, Troy, N. Y., 1952.

(18) N. H. Nachtrieb and R. E. Fryxell, *J. Am. Chem. Soc.*, **71**, 4035 (1949).

(19) H. M. Irving and F. S. C. Rossotti, *The Analyst*, **77**, 801 (1952).

(20) W. A. E. McBryde and J. H. Yoe, *Anal. Chem.*, **20**, 1094 (1948).

(21) F. C. Edwards and H. F. Voigt, *ibid.*, **21**, 1204 (1949).

(22) R. M. Fuoss and C. A. Kraus, *J. Am. Chem. Soc.*, **56**, 1019 (1933).

and the latter will cause an increase in the distribution ratio. This is very likely the reason for the increase in $D$ observed with the iron(III)–HCl–ether and gallium(III)–HCl–ether systems with increase in metal ion concentration above $10^{-2}$ $M$.[16] Likewise, if polymerization occurs, an increase in metal ion concentration will favor distribution to that phase in which polymerization is greatest.

2. The extracting species may be an acid whose distribution between the two phases then depends on the concentration and acid strengths of the other acids present in the system. That is, if the extracting species is a strong acid even in the solvent phase, its distribution ratio will depend upon the distribution and strengths of the other acids present, being larger when the other acids are relatively insoluble and undissociated in the organic layer, and smaller when the other acids are quite soluble and also dissociated in the organic phase. (It must be remembered that acids normally considered "strong" in aqueous solutions, i.e., hydrochloric acid, may be but little dissociated in solvents such as ether.)

3. The extracting species is a chloro compound (or bromo, etc.) whose distribution between the two phases then depends on the concentration and degree of dissociation of the other chloride (or bromide, etc.) containing compounds present in the system.

4. The extracting species is solvated in one or both phases so that its distribution is dependent on the nature and availability of solvate in the two phases.

There are certainly other factors, but these four seem sufficient to explain a considerable amount of the data available on the extraction of metals.[23]

In the molybdenum(VI)–HCl–organic solvent systems under study in this work, the first factor above is unimportant, as conductance studies indicate that the extracting molybdenum species is relatively undissociated, and there is indirect evidence that it is monomeric. This is obtained from the distribution experiments in which the molybdenum concentration was varied from $10^{-9}$ to $10^{-2}$ $M$. The constancy in the distribution ratio of the molybdenum(VI) between 6 $M$ HCl and DDE and between 6 $M$ HCl and hexone in these experiments shows that the extracting species and predominant aqueous forms have the same number of molybdenum atoms per molecule. If these forms were polymeric, their degree of polymerization would be expected to change over such a large concentration range, and the constant distribution ratios observed would require identical changes in the organic and aqueous phases over this range. Such behavior for both solvents seems somewhat problematical, and the simplest (though not necessarily correct) solution is to assume the species monomeric. It will be interesting to repeat these distribution experiments at a lower hydrochloric acid concentration, say 2 $M$, to see if a constant value of $D$ is again obtained, for it has been suggested as a result of oxidation–reduction

potential measurements that molybdenum(V) and molybdenum(VI) form dimeric species in hydrochloric acid solutions below 6 $M$.[24] This suggestion has appeared to be confirmed for the (V) state by magnetic susceptibility measurements.[25]

In the systems under study in this work, factor 2 is also unimportant, as the extracting molybdenum (VI) species either is not an acid or is a weak one. This is shown by the small variation observed in the distribution ratios from mixed HCl–LiCl solutions at 6 $M$ total concentration, indicating little hydrogen ion dependence, Fig. 5. However, this factor is important in the iron(III), gallium (III), thallium(III) and indium(III) systems with the hydrogen halides, as in these cases the extracting species are strong acids, dissociating to varying degrees (but more than the hydrogen halides) in different organic solvents of differing dielectric constants.

On the other hand, the third factor above is important, as analyses of the organic phase (Table II) show that the extracting species is indeed a chloro (or bromo) compound, $MoO_2Cl_2$, with an undetermined amount of water and solvent also involved. Such a compound gives the observed hydrogen ion to molybdenum ratios by the following hydrolytic processes

$$7MoO_2Cl_2 + 20OH^- \rightleftarrows Mo_7O_{24}^{-6} + 14Cl^- + 10H_2O$$
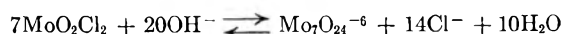
at the bromocresol green end-point, $pH \sim 4$–5, and

$$MoO_2Cl_2 + 4OH^- \rightleftarrows MoO_4^- + 2Cl^- + 2H_2O$$

at the phenolphthalein end-point, $pH \sim 9$. Starting with a very dilute hydrochloric acid solution and increasing its chloride concentration must increase the proportion of $MoO_2Cl_2$ to other (less chloride-containing) molybdenum species in the aqueous phase by a mass-action effect. As the rest of the molybdenum in the less chloride-containing, possibly polymeric, forms is non-extracting, the increase in the percentage of $MoO_2Cl_2$ will cause a rise in the distribution ratio of the metal into the organic solvent. At some high hydrochloric acid concentration, the proportion of neutral dichloride in the aqueous phase will start to decrease due to the increasing amount of molybdenum(VI) transforming into anionic complexes of higher chloride content such as, perhaps, $MoO_2Cl_3^-$ or $MoO(OH)_2Cl_3^-$ and $MoO_2Cl_4^=$.[26] However, since the distribution ratios observed with most solvents increase monotonically with increasing acid concentration up to 11–12 $M$ HCl, either the amount of higher complexes formed is small, or they, too, extract. Certainly the mass-action effect of increasing chloride ion concentration on the extractable molybdenum(VI) dichloride is one of the

(24) A. R. Tourky and H. K. El-Shamy, J. Chem. Soc., 140 (1949); H. K. El-Shamy and A. M. El-Aggan, J. Am. Chem. Soc., 75, 1187 (1953).

(25) L. Sacconi and R. Cini, ibid., 76, 4239 (1954).

(26) Preliminary cation and anion exchange resin work shows that even at moderate concentrations (2–6 $M$) of hydrochloric, hydrobromic, hydrofluoric and sulfuric acids anionic species of molybdenum (VI) are present, and in increasing amounts as the acid concentration is raised. On the other hand, molybdenum tracer in 2 $M$ HClO₄ is not anionic, although the cationic species may be polymeric even at the molybdenum concentrations used, $10^{-3}$ to $10^{-6}$ $M$.

(23) A later paper will consider the appropriate equilibrium equations for the general case, and discuss other metal systems on this basis.

principal factors for the increasing distribution ratios observed for most solvents. This is also true for the other metal chloride–hydrochloric acid systems, where, in fact, the chloride dependence may be even greater due to a higher chloro complex being the extracting species, for example, $HFeCl_4$.

With increasing acid concentration, the fourth factor becomes increasingly important. In dilute acid solution, the hydronium ion, $H_3O^+$, has a primary hydration shell of possibly four waters. Some evidence for this comes from determination of the number of waters of hydration of the sulfonic acid groups of a strong acid-cation-exchange resin such as Dowex-50,[27] but more readily from analyses and conductance studies on iron(III), ($HFeCl_4$), extracted from aqueous hydrochloric acid solutions into diisopropyl ether.[10] It was found by direct analysis of ethereal water that five moles of water was carried into the ether for each mole of $HFeCl_4$, and that the water was associated with the $H^+$, i.e., $H_3O(H_2O)_4^+$, since electrolysis of the ether phase produced five moles of water at the cathode for each mole of hydrogen ion reduced there. If the acid concentration is increased, more and more of the water in the aqueous phase is tied up in solvating the acid (the chloride ion is also hydrated, though not as highly) until a point is reached where even the primary hydration shells of all the ions cannot be satisfied. Evidence for such "ion dehydration" in solutions of concentrated acids (or other electrolytes) has appeared in ion-exchange studies[28] and also in the above-mentioned work on the iron(III)–hydrochloric acid–water–isopropyl ether system.[10] In these latter studies it was found that the average number of water molecules associated with the $HFeCl_4$ complex in ether fell to around four when the aqueous phase was initially 8 $M$ HCl and to about three when the acid was initially 10 $M$. Presumably the decreasing solvation of the hydrogen ion in the extracting $HFeCl_4$ was at least partially compensated for in the organic phase by solvation with ether.

It seems to the present authors that a large factor in the marked extraction of iron(III), gallium(III), gold(III), thallium(III) and indium (III) from strong hydrohalic acid solutions is this gradual decrease in availability of water for ion hydration in the aqueous phase with increasing acid concentration, that is, that part of the driving force for the extraction into the solvent comes from the pushing of hydrogen ion into the organic phase to solvate there with oxygenated organic molecules. To conserve electroneutrality, the hydrogen ion drags with it across the phase boundary the anion containing the metal, i.e., $FeCl_4^-$, $GaCl_4^-$, etc. Similarly this "dehydrating effect" of increasingly concentrated acid solutions tends to drive the molybdenum(VI) species into the organic phase to coördinate there with oxygenated molecules. In this case, the driving force is less, as $MoO_2Cl_2$ is not a strong acid and so does not involve the strongly solvated hydrogen ion. But the $MoO_2Cl_2$ molecule as a whole can be solvated, though more weakly perhaps, and there are several reasons for

considering the extracting species to contain molecules of water and/or solvent. $MoO_2Cl_2$ itself is soluble in anhydrous ethyl ether, and apparently unstable etherates are obtained upon evaporation of the solution. Similarly, Pechard[3] observed ether containing compounds upon evaporating ether solutions of $MoO_2Cl_2 \cdot H_2O$. Furthermore, the negligible extraction shown by non-oxygenated solvents such as carbon tetrachloride, chloroform, benzene, and especially the contrast between o-dichlorobenzene and nitrobenzene suggest that there is coördination of the solvent molecule through its oxygen atom with the molybdenum(VI) species. It is not solely a question of relative dielectric constants, either, as chloroform and o-dichlorobenzene have constants larger than diethyl ether, for example. Also, comparison of the distribution ratios with methyl benzoate and methyl salicylate above 7 $M$ HCl shows that the former ester has values 40 times greater than those of the latter, a result which is explicable on the assumption that the carbonyl group in the latter ester is somewhat blocked from coördination with molybdenum by internal hydrogen bonding with the ortho hydroxyl group, thus contributing to a lower $D$. (No explanation can be offered for the anomalous decrease in $D$ for methyl salicylate with increasing HCl concentration from 3 to 6 $M$, nor was such behavior observed for any other solvent tried.)

The order of decreasing extraction of molybdenum with the ethers tried, diethyl $> \beta,\beta'$-dichlorodiethyl $>$ diisopropyl $>$ dibutyl $> \beta,\beta'$-dichlorodiisopropyl, parallels roughly the expected order of decreasing base strength and steric availability of the ether oxygen. Furthermore, the oxygen atoms of the respresentative 6–8 carbon esters, ketones and alcohol tried are more basic and sterically more available for coördination than those of the corresponding diisopropyl and dibutyl ethers, and the results show that the distribution ratios are correspondingly greater, again suggesting coördination of the molybdenum with the solvent oxygen.

The "dehydration effect" is very likely the principal cause for the salt-effects observed with molybdenum extractions from mixed HCl– chloride salt solutions.[29] If samples of a molybdenum(VI) solution are made sufficiently acid to get beyond the polymolybdate region ($> 1$–2 $M$ HCl), an equivalent amount of a metal chloride, ammonium, calcium, or aluminum, added, and then the samples are equilibrated with ethyl ether, it is found that the distribution ratios for the molybdenum vary considerably for the same initial chloride concentration, being smallest for the solution containing ammonium ions and largest for that containing aluminum. This order is the inverse order of the water activity in these solutions, ammonium ion being the least, and aluminum ion the most, strongly hydrated. On the basis of the mechanism suggested, the former ion should cause the smaller "salting out" of molybdenum into the ether, the latter ion the greater, as is observed experimentally.

If, however, the oxygenated organic solvent

(27) K. W. Pepper and D. Reichenberg, Z. Elektrochem., 57, 183 (1953).

(28) R. M. Diamond, J. Am. Chem. Soc., 77, 2978 (1955).

(29) G. H. Morrison and R. P. Taylor, unpublished work quoted by G. H. Morrison in Anal. Chem., 22, 1388 (1950).

molecules are relatively small, they may, with increasing acid concentration in the aqueous phase, be pulled into that phase to a considerable extent to help solvate the ions there. Hydrochloric and hydrobromic acid solutions act in this manner with diethyl and diisopropyl ethers and with hexone, and very noticeable phase volume changes occur in these systems with increasing acid concentration. For example, originally equal volumes of 6 $M$ HCl and diethyl ether when equilibrated together will show a final volume ratio of approximately two (aqueous phase to organic phase), and the value is even larger for 6 $M$ HBr, and becomes increasingly so with increasing acid concentration. This behavior is the probable cause for the maximum and subsequent decrease in the distribution ratio of molybdenum with increasing acid concentration observed for diethyl and diisopropyl ethers and hexone; the solution of these organic molecules in the aqueous phase at high acid concentrations allows for solvation of the acid and of the molybdenum species there without the necessity of going into the organic phase. Furthermore, the diisopropyl ether molecule, being larger and more hydrocarbon-like than that of diethyl ether, would be expected to dissolve less readily in the acid, and indeed Fig. 1 shows that the maximum for diisopropyl ether occurs at about 9 $M$ HCl in contrast to the earlier appearance at 6.5 $M$ HCl with diethyl ether. The similar extraction behavior of other metal chlorides with these two ethers shows that these maxima are connected with the nature of the solvent and not with the particular metal chloride.

Another indication that this is the correct interpretation is furnished by comparison of the position of the maximum with hydrochloric acid with that of hydrobromic acid. A solution of several molar hydrobromic acid has a lower water activity than a solution of hydrochloric acid of the same concentration. It would be expected then that a hydrobromic acid solution would pull the organic molecules into the aqueous phase more readily than a hydrochloric acid solution of corresponding concentration so that the maximum in the plot of $D$ vs. acid concentration for diethyl and diisopropyl ethers and for hexone would occur sooner than with hydrochloric acid. This is what is observed as shown in Fig. 1 for diisopropyl ether. The maximum with hydrobromic acid is at 6.5–7 $M$; with hydrochloric acid it is at 9 $M$.

Another aspect of this situation is that the large solubility of these particular organic solvents in high concentrations of the halogen acids dilutes the aqueous phase, and thus reduces the molarity of the acid in this phase. The equilibrium acid molarity actually goes through a maximum and then decreases when plotted against the initial acid concentration, as is shown in Fig. 2. These maxima occur at about the same initial acid concentration as the maxima in the molybdenum distribution ratios, indicating that the influence of

the dissolved organic molecules in causing the latter maxima can be both through the decrease in chloride ion concentration, factor 3, as well as through the "dehydrating effect," factor 4, discussed above.

The larger ethers, esters and ketones, due to their increased size, hydrocarbon-like nature, and lower basicity, dissolve much less of, and are less soluble in, hydrochloric and hydrobromic acids, and no significant phase volume changes or maxima in the distribution ratios are observed. That is, the value of $D$ increases monotonically with increasing acid concentration, at least up to 11 $M$ HCl and 9 $M$ HBr for DDE, dibutyl and $\beta,\beta'$-dichlorodiisopropyl ethers, diisopropyl and diisobutyl ketones, and methyl benzoate.

In all of the systems studied, however, the concentration of acid in the organic phase increases with increasing initial concentration of aqueous acid, and this may lead in certain systems to phase volume changes opposite in nature to those just described. That is, in these systems it is the organic phase that swells at the expense of the aqueous. Examples are 2-ethylhexanol and isoamyl acetate with hydrochloric acid. In these two systems, the value of the molybdenum distribution ratio passes through a maximum at 9 $M$ HCl and $\sim 8$ $M$ HCl, respectively, where the volume changes become pronounced. In these cases, however, where the acid itself goes into the organic phase more readily than the organic molecules dissolve in the aqueous acid, the decrease in the molybdenum distribution ratio at high acid concentrations may be due to a decreasing availability of the oxygenated organic molecules to solvate the extracted molybdenum species; the alcohol and ester molecules may be increasingly tied up with hydrogen ions as oxonium ions in the organic phase.

Finally, from the distribution measurements performed, it can be seen that the customary procedure of extracting molybdenum(VI) from 6 $M$ HCl with diethyl ether, though giving the optimum results if one is limited to hydrochloric acid–diethyl ether systems, is inferior to extraction by certain immisicible esters, alcohols and ketones. A useful solvent is the readily available methyl isobutyl ketone (hexone). By far the largest distribution ratios were obtained using tributyl phosphate, and when it is known that coextracting elements are not present, (as in the preparation of the carrier-free $Mo^{93m}$ tracer used in this work) this is therefore the solvent to use. With all the oxygenated solvents tried, extraction was more nearly complete from hydrobromic than from hydrochloric acid solutions (with the exception of diethyl ether), and was improved by lowering the temperature of the system (with the exception of 2-ethylhexanol).

# ION-EXCHANGE EQUILIBRIA INVOLVING RUBIDIUM, CESIUM AND THALLOUS IONS

By O. D. Bonner[1]

*Department of Chemistry of the University of South Carolina, Columbia, South Carolina*

*Received February 18, 1955*

Equilibrium studies involving rubidium, cesium and thallous ion on Dowex 50 resins of approximately 4, 8 and 16% divinylbenzene content have been made while maintaining a constant ionic strength of approximately 0.1 molar. The characteristic maximum water uptake of the resin in these ionic forms has been measured. These results are correlated with those reported previously for other univalent ions.

## Introduction

The results of studies of ion-exchange equilibria on Dowex 50 resins of 4, 8 and 16% DVB content involving the common univalent cations with the exception of rubidium, cesium and thallous ion have been reported previously.[2-4] The pyridinium ion, substituted ammonium ions such as tetramethylammonium, hydroxylammonium, etc., and other complex univalent ions have not been included in these studies. The results reported herewith of equilibrium studies involving rubidium, cesium and thallous ion may be correlated with those reported previously to yield a more precise and complete experimental evaluation of certain characteristics of the ion exchange process such as (1) the relative affinities of the various common univalent ions for the resin, (2) the relationship between the maximum water uptake of the resin in a particular ionic form and the affinity of that ion for the resin, and (3) the variation of the ion–resin affinity with resin loading and with resin divinylbenzene content. It has been recognized by many workers, however, that a quantitative theoretical interpretation of ion exchange equilibria will not be possible until the osmotic properties of concentrated solutions of mixed electrolytes have been more thoroughly investigated.

## Experimental

The methods of equilibration and separation of the aqueous and resin phases have been described in detail.[2] The compositions of both phases at equilibrium were determined by quantitative analysis for each ion in each phase for all of the exchange reactions which were studied. Concentrations of hydrogen ion in the aqueous were determined volumetrically by titration with standard alkali. Rubidium and cesium ion concentrations were determined by weighing directly as the chloride, after evaporation of an accurately measured portion of the solution and drying to constant weight at 120–130°. Thallous ion concentrations were determined volumetrically by titration with standard potassium bromate solution in the presence of hydrochloric acid, methyl orange serving as an indicator. Resin compositions were determined in a similar manner except that an aliquot of the resin, dried to an arbitrary moisture content, was analyzed directly for hydrogen ion content. The remaining resin having the same moisture content and constituting a known fraction of the whole quantity of equilibrated resin, was then eluted completely with ammonium nitrate solution if thallous ion were present or hydrochloric acid if rubidium or cesium ion were present, and the eluent analyzed as before. The determination of the concentrations of cesium and lithium ion in the presence of each other, as was the case for cesium–lithium exchanges, was accomplished

by titration of one aliquot of the equilibrium solution containing both cesium and lithium chloride with standard silver nitrate to determine the total ionic concentration. The evaporation, drying and weighing of the cesium and lithium chloride in another aliquot enabled the calculation of the concentration of each ion. The equilibrium resin sample was completely eluted with hydrochloric acid. The resulting solution was then evaporated to dryness and heated overnight at 120–130°. The residue was then diluted and analyzed in the same manner as the equilibrium solution.

## Discussion and Results

The experimental data for these exchanges are presented graphically in Figs. 1–4 as a plot of $k$, the concentration equilibrium quotient or selectivity coefficient as a function of the resin composition. The thermodynamic equilibrium constants or mass action constants have been calculated from the equation[5,6]

$$\log K = \int_0^1 \log k \, dN$$

For the purpose of this calculation the standard state for the aqueous solution is taken as the hypothetical one molal solution in which the electrolyte behaves as it does at infinite dilution and the standard state for the resin phase is each "pure" resin with its characteristic maximum water content.[4,7] These mass action constants which are in reality average values of the selectivity coefficients, are listed in Table I. The data representing the maximum water uptake of these resins in these ionic forms and the selectivity of the resins for the ions relative to lithium ion taken as unity are presented in Tables II and III. The data for the other univalent ions are also given for convenience of comparison. It is believed that the maximum error in these data is of the order of 2%.

It is apparent from these data that rubidium and cesium ion are very similar to potassium ion in average affinity for the resins and in water uptake when associated with the resins. Although the ion–resin affinity of these three ions is nearly identical in the 16% DVB resin, the relative selectivities are in the expected order for the lower cross-linked resins.

The variation of the selectivity coefficient with resin composition for exchanges between hydrogen ion and the ammonium or alkali metal ions is of unusual interest. This variation becomes more marked as the series progresses from sodium to

(1) These results were developed under a project sponsored by the United States Atomic Energy Commission.

(2) O. D. Bonner and V. Rhett, This Journal, **57**, 254 (1953).

(3) O. D. Bonner and W. H. Payne, *ibid.*, **58**, 183 (1954).

(4) O. D. Bonner, *ibid.*, **58**, 318 (1954).

(5) E. Hogfeldt, E. Ekedahl and L. G. Sillen, *Acta Chem. Scand.*, **4**, 1471 (1950).

(6) O. D. Bonner, W. J. Argersinger and A. W. Davidson, *J. Am. Chem. Soc.*, **74**, 1044 (1952).

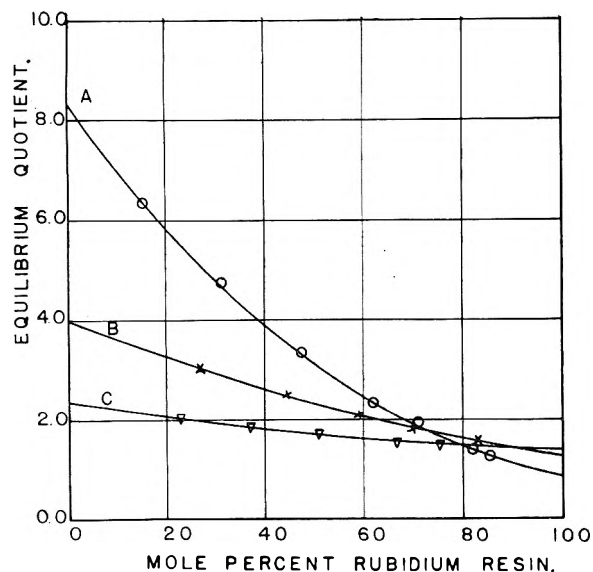(7) A. W. Davidson and W. J. Argersinger, *Ann. N. Y. Acad. Sci.*, **57**, 105 (1953).

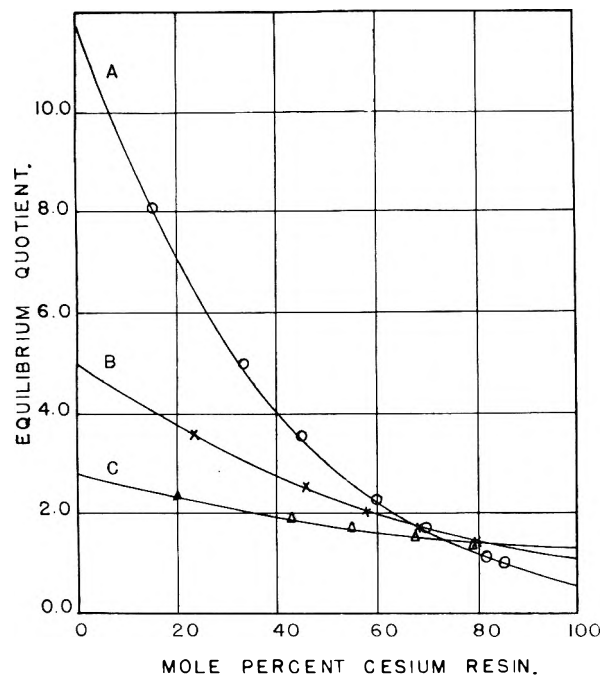Fig. 1.—Rubidium–hydrogen exchange: A, 16% DVB; B, 8% DVB; C, 4% DVB.



Fig. 2.—Cesium–hydrogen exchange: A, 16% DVB; B, 8% DVB; C, 4% DVB.



Fig. 3.—Thallous–hydrogen exchange: A, 16% DVB; B, 8% DVB; C, 4% DVB.



Fig. 4.—A, Cs–Li, 16% DVB; B, Cs–H, 16% DVB.

cesium ion. Gregor[8] and others have advanced a qualitative explanation for this variation based on the swelling properties of the resin. This theory does not explain, however, the reversal in selectivity which occurs when highly cross-linked resins are 80% or more in the salt form. Reichenberg,[9] et al., have suggested that this reversal might be due to the presence of weak acidic groups such as carboxyl in the highly cross-linked resins. The substitution of lithium ion for hydrogen ion in an exchange reaction with one of the heavier alkali metal ions such as cesium on a highly cross-linked resin

(8) H. P. Gregor, J. Am. Chem. Soc., **73**, 643 (1951).

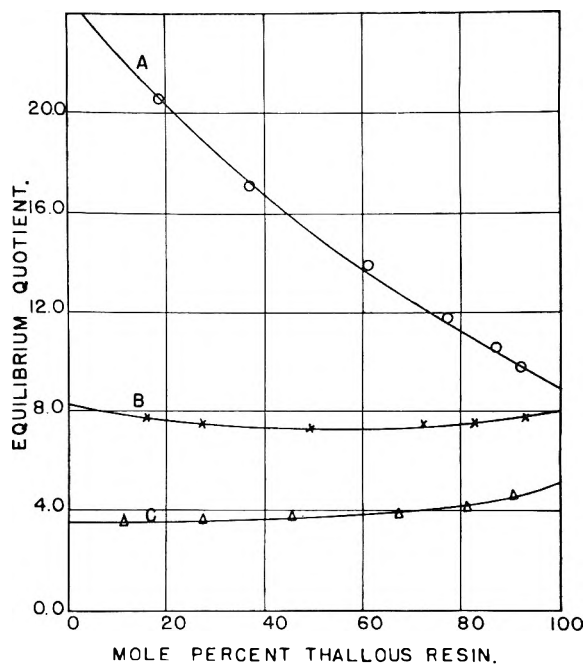(9) D. Reichenberg, K. W. Pepper and D. J. McCauley, J. Chem. Soc., 493 (1951).

should be significant since lithium ion should not form covalent bonds with carboxyl groups as readily as hydrogen ion. It is uncertain whether there was actually a reversal of selectivity when this exchange reaction was carried out using 16% DVB resin, because of the uncertainties in the analysis of solutions containing mixtures of cesium and lithium salts, especially when only a small amount of lithium salt is present. The rapid change of selectivity coefficient with composition suggests, however, that a reversal might occur on a higher cross-linked resin if it did not occur on this one. It appears, thus, that an alternative expla-

### TABLE I
### TABLE OF EQUILIBRIUM CONSTANTS

| Resin sample | Exchange | Equilibrium constant |
|---|---|---|
| 4% DVB | Rb–H | 1.71 |
|  | Cs–H | 1.82 |
|  | Tl–H | 4.00 |
| 8% DVB | Rb–H | 2.29 |
|  | Cs–H | 2.31 |
|  | Tl–H | 7.67 |
| 16% DVB | Rb–H | 2.89 |
|  | Cs–H | 2.86 |
|  | Tl–H | 15.3 |
|  | Cs–Li | 4.16 ± 2% |
|  | Cs–Li | 4.15[a] |

[a] Calculated from ratio of cesium–hydrogen and hydrogen–lithium exchanges.

### TABLE II
### MAXIMUM WATER UPTAKE OF DOWEX 50 RESINS IN VARIOUS IONIC FORMS (G./EQUIV.)

|  | 4% DVB | 8% DVB | 16% DVB |
|---|---|---|---|
| $Li^+$ | 418 | 211 | 130 |
| $H^+$ | 431 | 200 | 136 |
| $Na^+$ | 372 | 183 | 113 |
| $NH_4^+$ | 360 | 172 | 106 |
| $K^+$ | 341 | 163 | 106 |
| $Rb^+$ | 342 | 159 | 106 |
| $Cs^+$ | 342 | 159 | 102 |
| $Ag^+$ | 289 | 163 | 102 |
| $Tl^+$ | 229 | 113 | 85 |

nation is probably necessary to account for reversals of selectivity.

### TABLE III
### SELECTIVITY SCALE FOR DOWEX 50 RESINS

|  | 4% DVB | 8% DVB | 16% DVB |
|---|---|---|---|
| $Li^+$ | 1.00 | 1.00 | 1.00 |
| $H^+$ | 1.30 | 1.26 | 1.45 |
| $Na^+$ | 1.49 | 1.88 | 2.23 |
| $NH_4^+$ | 1.75 | 2.22 | 3.07 |
| $K^+$ | 2.09 | 2.63 | 4.15 |
| $Rb^+$ | 2.22 | 2.89 | 4.19 |
| $Cs^+$ | 2.37 | 2.91 | 4.15 |
| $Ag^+$ | 4.00 | 7.36 | 19.4 |
| $Tl^+$ | 5.20 | 9.66 | 22.2 |

The tabular and graphical data indicate that thallous ion is similar in behavior to silver ion, although its selectivity coefficient is appreciably higher and the characteristic water uptake lower. The equilibrium quotients for thallous–hydrogen exchanges, like those of the silver–hydrogen exchanges, are relatively independent of resin composition between 10 and 90% thallous resinate for the lower cross-linked resins. In this respect silver and thallous ion differ greatly from the alkali metal and ammonium ion in exchange reactions with hydrogen ion. It appears that the contribution of the activity coefficients of the resinates to the selectivity coefficient is much greater than that of the pressure–volume term for these exchanges. The positions of these "heavy metal" ions in the selectivity scale is that which one would predict from comparisons of activity coefficients of aqueous solutions of silver, thallous and the alkali metal salts.

---

# KINETICS OF THE HYDROGEN–OXYGEN–METHANE SYSTEM.
# I. INHIBITION OF THE SECOND EXPLOSION LIMIT[1]

BY ARTHUR LEVY

*Battelle Memorial Institute, Columbus, Ohio*

Hydrocarbons commonly interfere with the combustion of hydrogen and oxygen. The purpose of this investigation was to determine the manner by which this inhibition occurs. Methane at low concentrations reduces the pressure at the second explosion limit in hydrogen–oxygen mixtures by an amount directly proportional to the mole fraction of methane added. At a certain concentration, referred to as the critical methane concentration, there is a sharp break in the explosion pressure-methane concentration curve and the explosion reaction is completely inhibited. This effect has been studied in the temperature range 490–550° for mixtures with $H_2:O_2$ ratios of 4, 2, 1 and 0.5; KCl-coated Pyrex and clean Vycor reaction vessels have shown similar results. Analysis of the results indicates that the reduction in explosion pressure is related to a methane–hydrogen atom reaction step, and that total inhibition is probably related to a formaldehyde chain-termination step.

Studies of the combustion of mixed fuels have revealed that, when two or more fuels are burned together, each fuel promotes the combustion process no more than to the extent to which it adds its own heat of combustion to the reaction. It is usually observed, furthermore, that two or more fuels burning together in rich mixtures inhibit the over-all combustion process. Therefore the LeChatelier principle, by which the upper or lower limit of in-

flammability of many mixtures of gaseous fuels may be calculated, cannot be applied to rich mixtures.[2]

Interactions in the oxidation processes of mixed fuels have also been observed in the studies of Foord and Norrish.[3] In studying the kinetics of the hydrogen–oxygen reaction catalyzed by nitrogen dioxide, they observed that an exceedingly small concentration of methane, as low as one part in a thousand, was sufficient to suppress ignition in $H_2$–$O_2$–$NO_2$ mixtures, indicating that the hydro-

(2) H. F. Coward, C. W. Carpenter and W. Payman, *J. Chem. Soc.*, **115**, 27 (1919).

(3) S. G. Foord and R. G. W. Norrish, *Proc. Roy. Soc. (London)*, **A152**, 196 (1935).

carbon was exerting a strong influence on the normal chain-branching and chain-breaking processes in the hydrogen–oxygen reaction.

To understand these phenomena more fully, studies have been made on the combustion of mixed fuels for the purpose of determining the extent and nature of the interactions between fuels in burning. This paper describes a part of this research program covering studies of the reduction and inhibition of the second explosion limit of hydrogen and oxygen by methane.
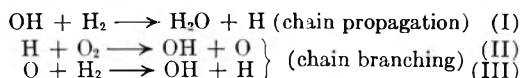
**Theory of the Hydrogen–Oxygen Reaction.—** Hydrogen and oxygen react by a chain mechanism involving the atoms and radical, H, O and OH. When the rate of formation of these active particles exceeds their rate of destruction, an explosion occurs. In the temperature range of 400 to 560° there are three explosion limits, which are dependent mostly on the pressure of the reacting system. The first explosion limit occurs at very low pressures of less than 4 mm. The second explosion limit for stoichiometric hydrogen–oxygen mixtures in KCl-coated Pyrex vessels is in the pressure range of 4 to 300 mm.
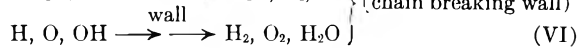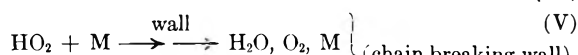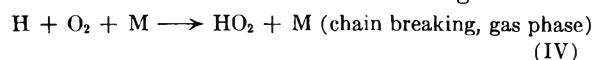
Between the first and second pressure limits the hydrogen–oxygen mixture will explode. At the higher pressures, between the second and third explosion limits, no explosion will occur.

A chain reaction theory of the mechanism for the explosion reaction of hydrogen and oxygen at the second explosion limit has been worked out in detail by Lewis and von Elbe.[4] This theory fits experimental observations well and is the one studied here.

It is proposed by this theory that the rate of chain branching is equal to the rate of chain breaking at the explosion limit. A chain propagating reaction and two chain branching reactions are illustrated below.

$$OH + H_2 \longrightarrow H_2O + H \text{ (chain propagation) (I)}$$
$$\left. \begin{array}{l} H + O_2 \longrightarrow OH + O \\ O + H_2 \longrightarrow OH + H \end{array} \right\} \text{ (chain branching) } \begin{array}{l} (II) \\ (III) \end{array}$$

The chain breaking reactions, by which the radical and atoms produced in reactions I, II and III are consumed, occur both in the gas phase and at the wall. Some of these reactions are given below.

$$H + O_2 + M \longrightarrow HO_2 + M \text{ (chain breaking, gas phase)}$$
$$\text{(IV)}$$

$$HO_2 + M \xrightarrow{\text{wall}} \longrightarrow H_2O, O_2, M \left.\begin{array}{l} \\ \\ \end{array}\right\} \text{ (chain breaking wall)} \begin{array}{l}(V)\end{array}$$
$$H, O, OH \xrightarrow{\text{wall}} \longrightarrow H_2, O_2, H_2O \left.\right\} \text{ (VI)}$$

Since reactions in the region of the second explosion limit are primarily homogeneous, gas phase reactions, reactions V and VI at the wall surface are disregarded and reaction IV is assumed irreversible for the purposes of this study. M denotes any third molecule that stabilizes the combination of H and $O_2$.

Applying these assumptions, a simplified rate equation for the pressure, $P$, at the second explosion limit can be derived. Let $r_2$, $r_3$ and $r_4$ be rates of reactions II, III and IV, respectively. Then under steady-state conditions the concentration of

(4) B. Lewis and G. von Elbe, "Combustion, Flames and Explosions of Gases," Academic Press, Inc., New York, N. Y., 1951, Chapter 2.

intermediates, H, O, OH and $HO_2$, is constant, so that just prior to explosion, the rate of the chain breaking reaction is equal to the combined rates of chain branching reactions, that is

$$r_4 = r_2 + r_3 \qquad (1)$$

Furthermore, since the concentration of oxygen atoms must be constant at any instant under these steady-state conditions, and since oxygen atoms are generated by reaction II and destroyed by reaction III, then

$$r_2 = r_3 \qquad (2)$$

For any constant $H_2/O_2$ ratio, equation 1 may then be rewritten as

$$2k_2(H)(O_2) = k_4P_0(O_2)(H) \qquad (3)$$

where the concentrations of the reactants are expressed by enclosing their symbols in parentheses, $k_2$ and $k_4$ are specific rate constants for the reactions indicated by their subscripts, and $P_0$ is the total pressure, which is proportional to (M) in reaction IV.

By rearranging equation 3, the explosion pressure, $P_0$, may be expressed as

$$P_0 = 2k_2/k_4 \qquad (4)$$

With methane present other chain-breaking steps besides reaction 4 are also made possible. Methane may react with any of the active centers produced in the reaction in the manner

$$CH_4 + H = CH_3 + H_2$$
$$CH_4 + O = CH_2 + H_2O$$
$$CH_4 + OH = CH_3 + H_2O$$
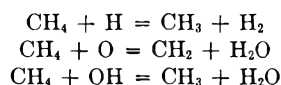
The methyl and methylene radicals may rapidly terminate the chains by forming formaldehyde, in reactions such as

$$CH_3 + O_2 \longrightarrow HCHO + OH \longrightarrow CHO + H_2O$$
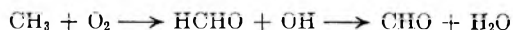
The chain terminating reactions are generalized as

$$CH_4 + X = CH_3 + HX \qquad (VII)$$
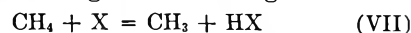
where X represents any one of the atoms or radical. Any reactivity of the $HO_2$ radical has been neglected in this simplified development because of its short lifetime. Its possible importance in these reactions is discussed later in the section devoted to the water vapor effect.

Applying steady-state theory again to these reactions, an explosion equation can be developed

$$P_{CH_4} = P_0 - \frac{k_5(CH_4)(X)}{k_4(O_2)(H)} \qquad (5)$$

where $P_0$ is the uninhibited explosion pressure for methane-free hydrogen–oxygen mixtures and $P_{CH_4}$ is the explosion pressure for the hydrogen–oxygen mixture containing methane.

For the case where X refers to hydrogen atoms as the active species in the interaction, equation 5 reduces to

$$P_{CH_4} = P_0 - \frac{k_5}{k_4}\frac{x_{CH_4}}{x_{O_2}} \cong P_0 - k_a x_{CH_4} \qquad (5a)$$

where $x$ represents mole fraction. Equation 5a is in general agreement with a similar development by Baldwin.[5] Baldwin has inferred however that the linear decrease of explosion pressure should only come about from interactions with hydrogen atoms.

(5) R. R. Baldwin, *Fuel*, **31**, 312 (1953).

Although subsequent arguments in this paper support the importance of the methane–hydrogen atom reaction, it is the opinion of the author that interactions with the hydroxyl radical and oxygen atom must also be considered. Approximately linear equations similar to Equation 5a are also obtained when small concentrations of hydrocarbon are considered in the interactions with OH and O. The steady state concentration of OH radicals from reactions I, II, III, IV, and VII is

$$\text{OH} = \frac{2k_2(\text{H})(\text{O}_2)}{k_1(\text{H}_2) + k_5(\text{CH}_4)} \qquad (6)$$

When this expression is substituted into equation 5 it is then apparent that low concentrations of methane may still cause a reduction of the explosion pressure that is approximately linear with respect to methane mole fraction. The case for interactions with oxygen atoms is similar.

The development of the reduced-explosion equation, as performed here or in Baldwin's study,[5] is of necessity a rather simplified one. Besides being based on only a minimum number of interactions, it also has been assumed that the addition of the third reactant into the hydrogen–oxygen reaction has only a negligible effect on the role of M in reaction IV. As pointed out by Walsh[6] the efficiency of the third body in reaction IV increases with the frequency of collisions and with the ability of the colliding molecules to take up the vibrational energy from $\text{HO}_2^*$. It is probably safe to assume that the concentration of methane is sufficiently low that its effect on the collision frequencies is not significantly large. The ability of methane to take up the vibrational energy of $\text{HO}_2^*$ is difficult to approximate however. It has been assumed therefore that the total effect of methane in reaction IV, although not readily calculable, is sufficiently low that the general conclusions are not seriously in error.

### Experimental

**Apparatus.**—These studies were performed in a conventional high-vacuum system. Apiezon grease, Type N, was used on all the joints except those in the vicinity of the furnace, where Apiezon, Type T, was used at the joint between the reaction vessel and the feed line; aluminum stearate was added to the Apiezon T to form a heavier grease which would not channel at temperatures of 80°.

The furnace was made from a 15-inch length of brass tubing, 4¼ inches in diameter, and was wound with No. 20 Chromel A wire, using one large central winding and two smaller end windings. Temperatures were recorded by means of a Chromel–Alumel thermocouple, located at the junction of the capillary inlet tube and the reaction vessel, and connected to a Leeds and Northrup potentiometer, Model 8657-C. The temperature was held constant to ±1° by means of two fine-control, external rheostats in series with two Variacs.

All data reported are for reactions in spherical, 200-cc., KCl-coated Pyrex vessels, or uncoated Vycor vessels, 7.4 cm. in diameter.

**Materials.**—The methane was 99% pure, Matheson, C.P. grade. It was charged into the gas reservoir after drying over $\text{CaCl}_2$ and $\text{P}_2\text{O}_5$, and passing through a Dry Ice trap. The hydrogen was Matheson electrolytic grade, 99.8% pure. It was purified further by passing over $\text{CaCl}_2$, platinized-asbestos at 250°, and $\text{P}_2\text{O}_5$, and finally through a Dry Ice trap. The oxygen was prepared by warming $\text{KMnO}_4$ gently and passing the gas over $\text{CaCl}_2$ and $\text{P}_2\text{O}_5$.

**Procedure. KCl Surface Coating.**—The vessels were cleaned in hot dichromate cleaning solution, rinsed several

times with distilled water, washed again with a soap solution, rinsed with distilled water many times, and finally rinsed with a saturated, aqueous solution of KCl. After gentle drying with a water aspirator, the vessel was placed on the vacuum line and pumped dry at 400°. This procedure gave a uniform, translucent, KCl coating.

**Operation.**—To determine the explosion pressures, the reaction vessel was evacuated first to less than $10^{-3}$ mm. pressure, flushed with hydrogen, and re-evacuated. Next, the reaction vessel was refilled with hydrogen to a pressure near or above the second explosion limit. Then the oxygen was transferred rapidly into the hydrogen-filled reaction vessel until the desired total pressure was reached. In approaching the explosion limit, the pressure was reduced rapidly to about 5 mm. above the explosion pressure, and then more slowly at a rate of about 1 mm. in 3 seconds, until explosion occurred. The explosion was characterized by a sharp pressure decrease, a flash, and an audible click when working at higher pressures. In any series of tests of the effect of methane concentration on the explosion limit, the $\text{H}_2 : \text{O}_2$ ratio was held constant while the methane concentration was increased.

**Observation of the Limit.**—Although the second explosion limit is determined essentially by gas-phase reactions, and for this reason is relatively independent of the nature of the reaction vessel, it has been shown[4,7] that different coatings may cause variations in the explosion data. Two identical Pyrex reaction vessels were made for these studies and both were coated using the same procedure. Some difference was found, nevertheless, in the results from the two vessels, especially for the oxygen-rich mixtures. For example, with mixtures having $\text{H}_2 : \text{O}_2$ ratio of 1:2, at temperatures of 490, 510, and 530°, the reactions in vessel 2 required about 1% less methane for inhibition than the reactions in vessel 1, and about 3% less methane at 550°. The results checked reasonably well for explosion in the range where the $\text{H}_2 : \text{O}_2$ ratios varied from 4:1 to 1:1.

It is important in these studies to condition the reaction vessel to avoid obtaining false (low) methane-inhibition values. It was necessary to run off several preliminary explosions before determining the critical methane concentration that caused complete inhibition of explosion. Otherwise a slight error was noticeable to the extent of 0.4% methane in a mixture requiring 12.8% methane.

### Experimental Results

The results of the studies performed in the two KCl-coated Pyrex vessels were essentially the same, except for the variations reported above. Figure 1 presents graphically the results observed in vessel 1. A similar set of results for the reactions in vessel 2, have been recorded in Table I.[8] Table I also includes results on 3:2 $\text{H}_2 : \text{O}_2$ mixtures, not shown in Fig. 1. In general, the sensitivity of the methane additions was such that a further increase in methane mole fraction of 0.001 was sufficient to inhibit explosion completely.

A comparison of the data obtained from vessels 1 and 2 shows good reproducibility for the hydrogen-rich and the stoichiometric mixtures.

Since Warren was able to show such pronounced effects of some surface coatings on the second explosion limit,[7] a brief investigation of the methane interactions in clean Vycor vessels was also made. Table II shows these results and compares them with the previous results obtained in KCl-coated Pyrex vessels. The data refer to stoichiometric $\text{H}_2$–$\text{O}_2$ mixtures, to which methane was added

---

(6) A. D. Walsh, *Fuel.*, **33**, 247 (1954).

(7) D. R. Warren, *Proc. Roy. Soc. (London)*, **A204**, (1951); **A211**, 86, 96 (1952).

(8) Table I has been deposited as Document number 4533 with the ADI Auxiliary Publications Project, Photoduplication Service, Library of Congress, Washington 25, D. C. A copy may be secured by citing the Document number and by remitting $1.25 for photoprints, or $1.25 for 35 mm. microfilm in advance payment by check or money order payable to: Chief, Photoduplication Service, Library of Congress.
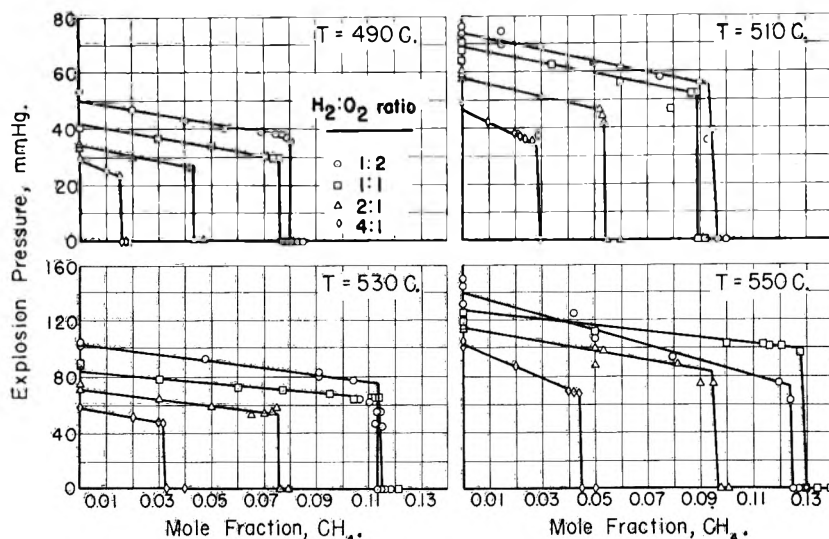
Fig. 1.—The inhibition of the $H_2$–$O_2$ explosion by methane in a KCl-coated Pyrex vessel (Vessel 1).

until explosion was completely inhibited. $P_0$ represents the methane-free $H_2$–$O_2$ explosion limit pressure and $x^*_{CH_4}$ represents the critical methane mole fraction required for total inhibition of explosion at each temperature.

TABLE II

EXPLOSION PRESSURES FOR STOICHIOMETRIC $H_2$–$O_2$ MIX-TURES AND CRITICAL METHANE CONCENTRATIONS FOR TOTAL INHIBITION OF EXPLOSION

| Temp., °C. | KCl-coated Pyrex $P_0$, mm. | $x^*_{CH_4}$ | Uncoated Vycor $P_0$, mm. | $x^*_{CH_4}$ |
|---|---|---|---|---|
| 470 | ... | ... | 27.0 | 0.026 |
| 490 | 35.0 | 0.043 | 38.2 | .045 |
| 510 | 55.5 | .056 | 60.6 | .057 |
| 530 | 76.0 | .076 | 83.2 | .070 |
| 550 | 117.5 | .095 | 127 | .078 |

### Discussion of Results

**Reduction of the Explosion Limit by Methane.—** Figure 1 has shown that the pressure at the second explosion limit decreases linearly for all $H_2$/$O_2$ ratios with increasing mole fraction of added methane. The simplified analysis of the primary inhibition reactions of methane presented earlier predicts that the reduction of the explosion limit should be linear, but equation 5a also indicates that the pressure of the limits should fall continuously to zero pressure. The complex nature of the methane interaction thus becomes apparent, because all the curves drop abruptly to zero pressure (no explosion) at a so-called critical methane concentration. Above the critical methane concentration, capture of active radicals by the reaction

$$CH_4 + X = CH_3 + HX \qquad (VII)$$
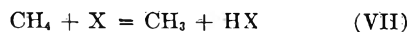
cannot be the sole inhibiting reaction of methane.

Two strong inhibitors in the explosion reactions are water vapor and formaldehyde. As will be shown in the following section, water vapor causes a reduction but does not completely inhibit explosion, at least up to concentrations of 40 mole per cent. water vapor. Formaldehyde is the chain-termina-

tor which is probably produced in the pre-explosion reaction

$$CH_3 + O_2 = HCHO +$$
$$OH = CHO + H_2O$$
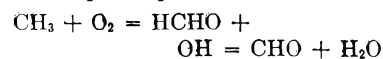
This reaction probably does not become predominant until the methane reaches a concentration capable of forming that concentration of formaldehyde necessary to suppress further chain branching.

Methane is the only hydrocarbon that exhibits the abrupt break in the explosion pressure curve. Propane, for example, causes an almost linear and continuous decrease in the second explosion limit.[9] Why then is the abrupt break observed for methane additions, attributed to formaldehyde formation, when higher hydrocarbons produce formaldehyde at an even greater rate at these temperatures? As shown by Baldwin,[5] the rate of decrease of the explosion pressure with hydrocarbon concentration increases with hydrocarbon chain length; and propane is approximately thirty times more effective than methane in completely inhibiting explosion.[9] As a result the explosion pressure is reduced so readily by the combination of water vapor and formaldehyde produced in the preexplosion reactions, that there is no opportunity to build up a critical concentration of formaldehyde, as can be done in the methane system.

**Reduction of the Explosion Limit by Water Vapor.—**Whereas the role of formaldehyde has been postulated by the author, Baldwin,[5] and others, on the basis of most probable reaction steps, the effect of water vapor on the second explosion limit has been well-established experimentally. The similarity in the effects of water vapor and of methane has been reported earlier.[10] Figure 2, reproduced from the previous study, illustrates this similarity. Until the point of discontinuity is reached, both methane and water vapor show identical effects on the chain breaking and chain branching pressures causing explosion in hydrogen–oxygen mixtures. This similarity in the effects of the two additives also extends to slow reaction processes.[10,11]

Consideration of these similarities has led to the following proposed mechanisms for these interactions

$$CH_4 + HO_2 = CH_3 + H_2O_2$$
$$CH_3 + O_2 = HCHO + OH = CHO + H_2O$$
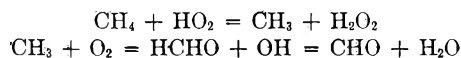
The first of these steps is analogous to the step proposed by Voevodskii for the accelerating effect of water vapor on the combination of hydrogen and oxygen.[12] Since the stability of the $HO_2$ radical is questionable at the temperatures of these studies the reactivity of the $HO_2$ radical was neglected in the de-

(9) A. Levy, Fifth Symposium (International) on Combustion, Paper No. 17.

(10) A. Levy, J. Chem. Phys., **21**, 2132 (1953).

(11) A. Levy and J. F. Foster, THIS JOURNAL, **59**, 727 (1955).

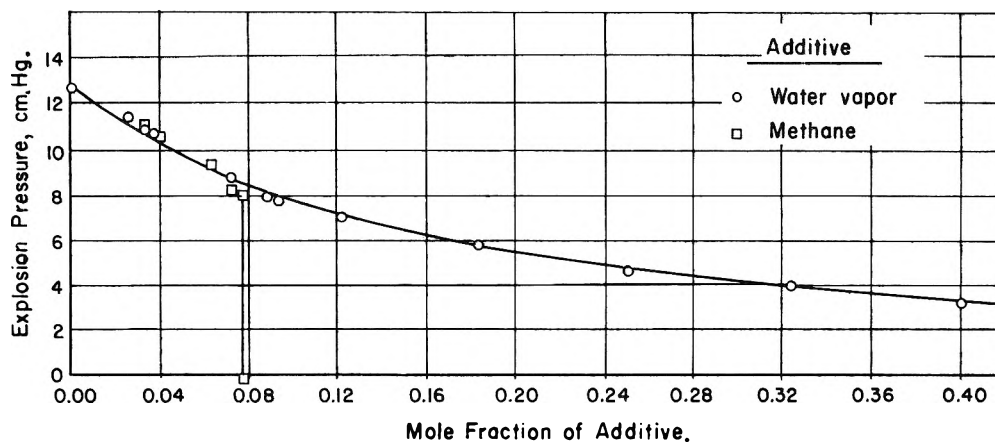(12) V. V. Voevodskii, J. Phys. Chem. (USSR), **22**, 457 (1948).

Fig. 2.—The inhibition of the second explosion limit of stoichiometric $H_2:O_2$ mixtures by methane and water vapor; Vycor vessel, $T = 560°$.

velopment of the reduced-explosion equation. Alternatively, the $HO_2$-reaction step may be included in the manner proposed by Prettre,[13] that is, as a rapid succession of two reactions

$$H + O_2 + M = HO_2 + M$$
$$CH_4 + HO_2 = CH_3 + H_2O_2$$
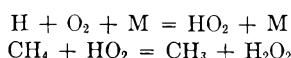
These equations may then be combined and written as

$$CH_4 + H + O_2 = CH_3 + H_2O_2$$
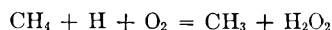
This reaction step, as written, represents the observed dependence of the reduction of the second explosion limit on the hydrogen atom concentration, without the necessity of assuming direct dependence on the elusive $HO_2$ radical.

**Difficulties Inherent in Interpretation of Variations of the Critical Methane Concentration.**—An analytical interpretation of the experimental results is difficult for two reasons. First, it has already been shown that the simplified development of the explosion pressure equation predicts a continuously decreasing explosion pressure as the hydrocarbon concentration is increased. This is found in all hydrogen–oxygen–hydrocarbon mixtures except methane. Thus, the analytical basis for interpreting the results is incomplete.

Second, surface effects appear to cause major problems in attaining complete reproducibility of the data for oxygen-rich mixtures.

This is illustrated in Fig. 3 where the oxygen mole fraction is correlated with the critical methane mole fraction for studies in two KCl-coated Pyrex vessels. Although the critical methane mole fractions are in close agreement for the two vessels up to $x_{0_2} \cong 0.45$, they do not agree as well above $x_{0_2} = 0.45$, and also above this point there is a sharp change in the relationship of the two variables.

The poor reproducibility of the experimental data in the oxygen-rich mixtures, $x_{0_2} > 0.45$, is probably related to increased pre-explosion reactivity of these mixtures, and a resulting enhanced effect of the withdrawal rate on the observed pressure at the explosion limit. Lewis and Von Elbe have shown that the shift from slow reaction to explosion is a continuous process.[4] Therefore, although the water formed initially may suppress explosion, the water is also responsible for an increased rate of combina-

tion of the hydrogen and oxygen in the slow reaction.[11] As a result the rate at which the gases are withdrawn from the explosion vessel becomes critical if the experimental error is to be minimized. Egerton and Warren[14] have observed, in an investigation of the effect of the withdrawal rate on the second explosion limits, that the effect was negligible with rich mixtures and quite noticeable with lean mixtures.
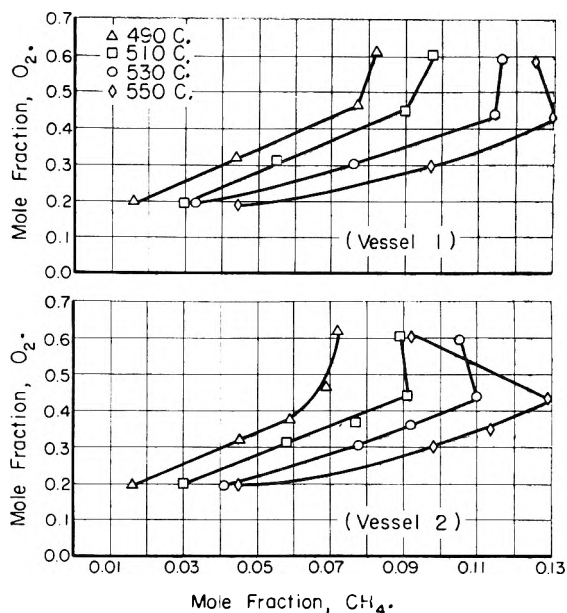


Fig. 3.—The dependence of the critical methane concentration on the oxygen concentration.

Two mechanisms that may affect the explosion pressure have been described. Baldwin and Precious[15] have suggested that quadratic branching reactions such as $H + HO_2 = 2OH$ are responsible. Egerton and Warren disagree with this explanation and suggest instead that the net branching factor is reduced to zero by the products formed during the initial stages of explosion. Although neither mechanism can be proved to complete satisfaction, the present studies lend support to Egerton and Warren's suggested mechanism.

(13) M. Prettre, *J. chim. phys.*, **33**, 189 (1936).

(14) A. C. Egerton and D. R. Warren, *Nature*, **170**, 420 (1952).

(15) R. R. Baldwin and R. M. Precious, *ibid.*, **169**, 290 (1952).

**Temperature Dependence of the Explosion Reactions.**—The temperature dependence of the explosion reactions also indicates sharp differences between the reactions of rich and lean mixtures. Grant and Hinshelwood[16] describe the second explosion limit of hydrogen and oxygen by the expression

$$p_{H_2} + a p_{O_2} = K \qquad (7)$$

where $K$ is a constant which is proportional to the branching probability of the active radicals in the reaction. As such, $K$ depends upon the frequency and energy of the collisions between particles, and varies with temperature according to the Arrhenius equation. The coefficient $a$, on the other hand, which reflects chain breaking via three-body collisions in the gas phase, increases gradually with temperature. This suggested to these authors that the chains are being broken in the gas phase by three-body reactions of the type

$$X + O_2 + M \longrightarrow \text{products}$$
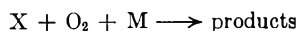
where X is a chain carrier and M is any molecule, including the excess oxygen and water vapor.

Figure 4 is a plot of the hydrogen pressure against the oxygen pressure at the second explosion limit. The solid lines represent hydrogen–oxygen mixtures with no methane present, and the dashed lines represent mixtures containing methane at the critical concentration just prior to complete inhibition of explosion. The methane-free data (solid lines) show that equation 7 is satisfied at 530 and 550°. At 490 and 510°, there is some curvature, signifying that the three-body gas phase collision is less predominant at these lower temperatures and that the importance of wall destruction is increasing.
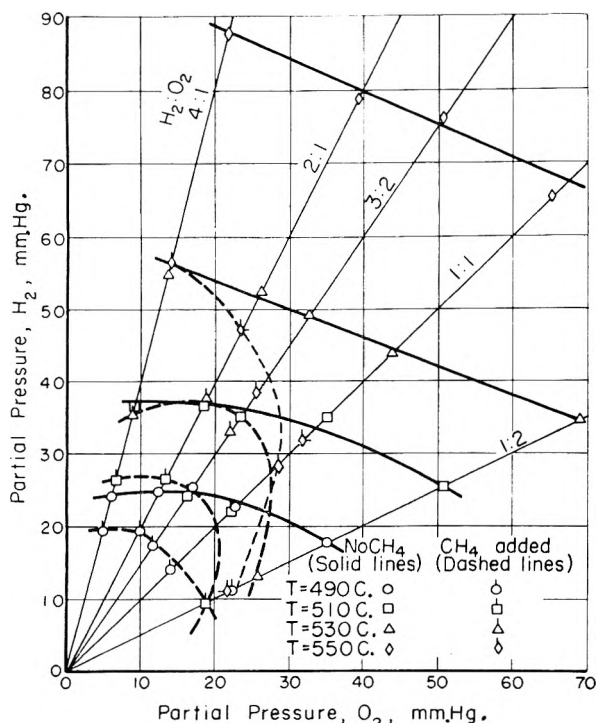


Fig. 4.—The relationship between the hydrogen and oxygen pressures at the second explosion limit.

(16) G. H. Grant and C. N. Hinshelwood, Proc. Roy. Soc. (London), A141, 29 (1933).

The extreme curvature of the dashed lines in Fig. 4 signifies that methane is not acting solely as a third body upon which the chains may be broken, but is participating in some other way. The locus of maximum curvature occurs in the portion of the graph bounded by the 3:2 and 1:1 $H_2:O_2$ constant ratio lines. This is the same observation as was shown in Fig. 3 where the proportionality between $x_{O_2}$ and $x^*_{CH_4}$ ends at $x_{O_2} = 0.45$.

A standard method for calculating the activation energy of the hydrogen–oxygen explosion reaction is from a consideration of the temperature dependence of the branching probability term, $K$. Table III lists the values of $a$ and $K$ for equation 7 obtained from the experimental data for methane-free mixtures. The values of $a$, the coefficient for three-body, gas-phase collisions, are shown to increase fairly uniformly with temperature, but at a much slower rate than $K$. The activation energy, $E_0$, obtained from these data for the methane-free explosion is 22,600 cal. per mole. This agrees well with values between 20 and 26 kcal. obtained by others.[15-18]

TABLE III

EXPERIMENTAL VALUES OF $a$ AND $K$

| Temp., C. | 490 | 510 | 530 | 550 |
|---|---|---|---|---|
| $a$ | 0.30 | 0.34 | 0.40 | 0.45 |
| $K$ | 30.8 | 44.9 | 62.0 | 97.6 |

Since one cannot justify such a plot for the hydrogen–oxygen–methane mixtures, apparent activation energies were determined from the temperature dependence of the slopes in Fig. 1. These results are shown in Table IV.

TABLE IV

THE TEMPERATURE DEPENDENCE OF THE SECOND EXPLOSION LIMIT IN $H_2$–$O_2$–$CH_4$ MIXTURES

| $H_2:O_2$ ratio | 4:1 | 2:1 | 1:1 | 1:2 |
|---|---|---|---|---|
| Apparent activn. energy, kcal./mole | 15.7 | 15.6 | 9.4 | Indeterminate |

Whereas the activation energy of the reaction in methane-free mixtures is independent of stoichiometry, activation energy in the ternary mixtures appears to be especially sensitive to excess oxygen. The fuel-rich mixtures, $H_2:O_2$ 4:1 and 2:1, give essentially the same value. The 1:1 $H_2:O_2$ mixtures on the other hand appear to have a much lower apparent activation energy, and in the case of the 1:2 $H_2:O_2$ mixture the reciprocal temperature plot of the explosion pressure slopes was too nonlinear for even an approximation of an apparent activation energy.

**Summary and Conclusions**

An equation has been developed, based on the principal chain-branching and chain-breaking steps of the hydrogen–oxygen mechanism, which describes the linear reduction of the second explosion limit by methane. The linearity in the pressure–concentration curve, and the similarity of methane and water vapor in this regard, suggest that the

(17) H. P. Broida and O. Oldenberg, J. Chem. Phys., 19, 196 (1951).

(18) A. A. Frost and H. N. Alyea, J. Am. Chem. Soc., 55, 3227 (1933).

principal methane termination step involves inter-action with the hydrogen atom. The break in the pressure–concentration curve, which is not predicted by this mechanism, is probably related to the formation of formaldehyde. For fuel-rich mixtures, the critical methane concentration correlates

linearly with the oxygen mole fraction, and the apparent activation energies are constant. Excess oxygen however destroys both of these correlations, suggesting that under such conditions the oxidation of methane is also occurring to an appreciable extent.

# KINETICS OF THE HYDROGEN–OXYGEN–METHANE SYSTEM. II. THE SLOW REACTION[1]

By Arthur Levy and John F. Foster

*Battelle Memorial Institute, Columbus, Ohio*

*Received February 18, 1955*

The slow reaction of hydrogen–oxygen–methane mixtures has been studied to explain more fully some of the anomalous results that are obtained in the region of the second explosion limit. Studies at 560° and 360–480 mm. pressure show that methane increases the initial rate of combination of hydrogen–oxygen mixtures. The maximum rate of reaction, however, may be either increased or decreased by the addition of methane, depending upon the oxygen concentration of the mixture. A similar dependence on oxygen concentration is also found in determinations of the orders of reaction. The composition of the reaction products indicates that the two mixed fuels are oxidized simultaneously at approximately equivalent rates. The general conclusion from these rate studies and from previous studies of the explosion reaction is that water vapor produced in the early stages of reaction serves as a homogeneous catalyst.

In a preceding paper the effect of methane on the explosion reaction of hydrogen and oxygen has been related to probable reactions with the active centers.[2] In the present study the slow reaction in $H_2$–$O_2$–$CH_4$ systems is investigated to determine which pre-explosion reactions may influence the interaction of methane on the second explosion limit of hydrogen and oxygen.

Complex chain reactions of this type are not readily measured in terms of the rate functions of classical kinetics, so that other, less direct, analyses must be applied. Two different reaction rates are considered here, namely, the initial rate and the maximum rate of reaction. Each is determined from the time rate of decrease of total pressure in the system.

## Experimental

**Apparatus.**—The apparatus and materials are the same as those described in the previous article, except that the oxygen used in these studies was Matheson Extra-Dry grade. It was found that this substitution was unimportant because there was no difference in results from those which were obtained using oxygen prepared by the $KMnO_4$ method.

A one-liter sampling bulb and a Toepler pump have been added to the line for the purpose of withdrawing the partial-reaction products at various times during an experiment.

**Procedure.**—The rate studies are performed in the following manner. Hydrogen and methane are first introduced into the reaction vessel, and then oxygen is added as rapidly as possible until the desired total pressure is reached. Reaction time is measured from the beginning of the addition of the oxygen, which requires about 10 seconds, although most of the oxygen is added within five seconds. Except for the extremely rapid reactions, however, the timing error is much less than other experimental errors. The course of the reaction is followed by measuring on a Hg manometer the rate of decrease in pressure as water vapor is formed. To prevent any condensation of water vapor in the line connecting the reaction vessel to the manometer, the line is kept at 70° by a wire-wound resistance heater.

The initial reaction rate is reported either as the time required to reach 10% reaction, $t_{10\%}$, or as the time required to reach maximum rate, $t_{max}$. The maximum rate is reported as the rate of pressure decrease in the system in mm. per minute.

Proper conditioning of the reaction vessel to attain acceptable reproducibility is a difficult experimental problem in slow reaction studies. Fairly good success was obtained by producing one or two preliminary explosions in the reaction vessel and by following these with two preliminary slow-reaction runs, before preceding to the actual series of experiments scheduled for that day. Although the procedure works quite well, a definite trend toward a more active vessel surface (*i.e.*, faster reaction rates) was observed over a period of time.

## Experimental Results of Slow Reaction Studies

A compilation of the results of the slow reaction studies performed in a KCl-coated Pyrex vessel, has been recorded in Table I.[3] Table I lists the maximum and initial rates at $T = 560°$ of 68 mixtures at total pressures of 360, 390, 420, 450 and 480 mm. The experimental run numbers, which were assigned in chronological sequence are also shown, to give some indications of the reproducibility of the data. As pointed out above, it is important to eliminate any surface conditioning effects, and thus to make certain that a change in reaction rate is the result of gas phase reaction and not of surface reaction. An example of surface conditioning is shown by comparing the identical runs 84 and 134 at 390 mm. pressure in Table I. These runs were made with stoichiometric hydrogen–oxygen mixtures, containing no methane. The maximum rates for runs 84 and 134 were 7.5 and 9.0 mm. per minute, respectively, and the initial rates were 11.5 and 8.5 minutes to reach maximum rate, respectively. A period of three weeks separated these runs and the rates showed a decided increase at the end of the

period. Therefore one run was repeated daily to give a reference rate that would cancel out any time-conditioning effects in these studies.

**The Effect of Added Methane on the Order of Reaction in Stoichiometric $H_2$–$O_2$ Mixtures.—** Figure 1 is a plot of the data from Table I for runs with varying amounts of methane added to stoichiometric $H_2$–$O_2$ mixtures. The "No $CH_4$" curve may be considered as the reference curve, and curves A, B and C show the effect of adding methane on the time required to reach maximum rate.
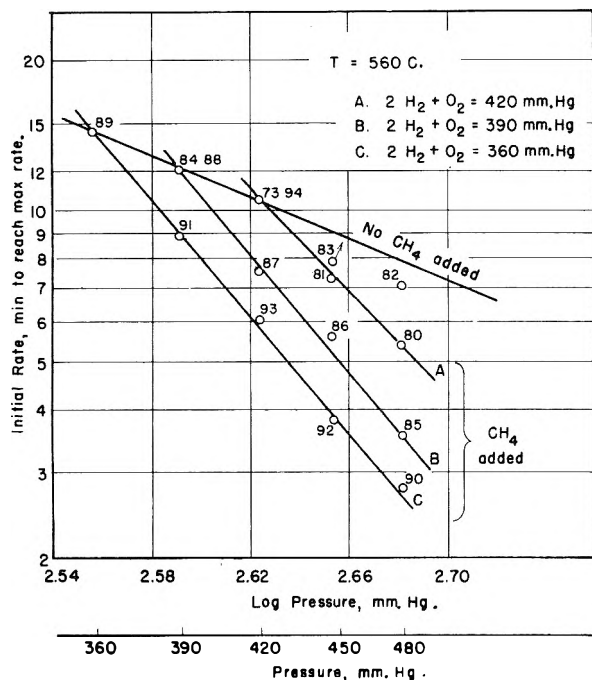


Fig. 1.—Effect of methane on the order of reaction of stoichiometric $H_2$–$O_2$ mixtures.

The order of a reaction is the dependence of the reaction rate on the total pressure of a system or on the pressure of individual reactants. It can be expressed as

$$R = kP^m \qquad (1)$$

or as

$$R = k'(A)^a(B)^b(C)^c \qquad (2)$$

where $R$ is a rate function, $P$ is the total pressure, and $(A)$, $(B)$ and $(C)$ are pressures of individual reactants in the system. The exponents $m$, $a$, $b$ and $c$, are the orders of reaction with respect to P, A, B and C, respectively. The values of the exponents are readily obtained from the slope of a plot of $\log R$ against the logarithm of one of the pressure terms.

As is apparent in Fig. 1, the order of the reaction is increased greatly with the addition of methane. The reaction order based on the initial reaction rate is approximately 2.5 for the methane-free $H_2$–$O_2$ mixture, while curve C yields an order of 5.3 for the $H_2$–$O_2$–$CH_4$ system in this pressure and concentration range. The almost-parallel slopes of curves A, B and C show a relatively constant effect of methane regardless of the initial $H_2$–$O_2$ concentration.

Figure 2 represents the same type of analysis for the maximum rate of reaction. The effect of methane is not nearly as pronounced here. In addition, the data show a slight falling off of the rate as the methane concentration is increased, i.e., the effect of methane under these conditions is to reduce the over-all order of reaction.
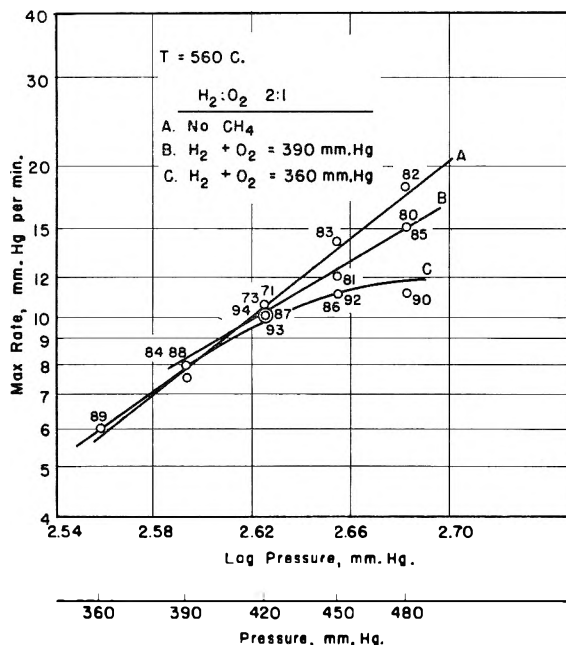


Fig. 2.—The variation of maximum rate with pressure for $H_2$–$O_2$–$CH_4$ mixtures.

**The Effect of Methane on the Order of Reaction with Varying $H_2$–$O_2$ Concentrations.—**The order of reaction for $H_2$–$O_2$ mixtures is a varying quantity, increasing with increasing temperature and pressure. Over a relatively small pressure range at constant temperature, however, the order is fairly constant and can be approximated from the slope of a log rate–log pressure graph. To learn more the dependence of the reaction rates on the concentrations of hydrogen and oxygen, reaction orders were determined for varying $H_2$–$O_2$ concentrations with fixed methane concentrations. The studies were made at 560° in the pressure range 360 to 480 mm.

Table II summarizes the results of these studies. The reaction order has been determined both in terms of the initial rate of reaction, $t_{10\%}$, and of the maximum rate of reaction. The data in Figs. 1 and 2 have already shown the effect of varying the methane concentration. In the studies shown in Table II, mixtures containing no methane are compared with those in which the methane concentration is constant at 30 mm.

The effect on the order of reaction is determined with respect to the hydrogen, the oxygen, and the total pressure as variables. The first column indicates the variable with respect to which the order was obtained. The symbol $P_T$ refers to the fact that the order was obtained with respect to the total pressure which was controlled by changing the concentration of hydrogen, oxygen or both, as shown in the last column. As will be shown subsequently,

this information is important since the reaction order is dependent on the over-all stoichiometry.

Table II

The Effect of Methane on the Reaction Order for Varying $H_2$–$O_2$ Concentrations, $T = 560°$

| Variable[a] | Reaction order Initial rate | Max. rate | Concn. range studied, mm. |
|---|---|---|---|
| $H_2$ | 1.8 | 2.8 | $H_2$ 220–340 |
| $P_T$ | 3.6 | 4.2 | $O_2$ 140, $CH_4$ 0 |
| $H_2$ | 1.2 | 2.0 | $H_2$ 190–310 |
| $P_T$ | 2.0 | 3.3 | $O_2$ 140, $CH_4$ 30 |
| $O_2$ | 0.8 | 0.8 | $O_2$ 120–240 |
| $P_T$ | 1.8 | 1.7 | $H_2$ 240, $CH_4$ 0 |
| $O_2$ | 0.9 | 1.8 | $O_2$ 120–210 |
| $P_T$ | 2.4 | 3.5 | $H_2$ 240, $CH_4$ 30 |
| $P_T$ ($H_2/O_2 = 2$) | 2.3 | 3.9 | $P_T$ 360–480, $CH_4$ 0 |
| $P_T$ ($H_2/O_2 = 2$) | 2.3 | 3.9 | $P_T$ 360–480, $CH_4$ 30 |
| $P_T$ ($H_2/O_2 = 3$) | 2.4 | 3.2 | $P_T$ 360–480, $CH_4$ 0 |
| $P_T$ ($H_2/O_2 = 3$) | 2.9 | 3.4 | $P_T$ 360–480, $CH_4$ 30 |
| $P_T$ ($H_2/O_2 = 1$) | 2.0 | 3.6 | $P_T$ 360–480, $CH_4$ 0 |
| $P_T$ ($H_2/O_2 = 1$) | 2.1 | 5.1 | $P_T$ 360–480, $CH_4$ 30 |

[a] $H_2$ = Hydrogen pressure, $O_2$ = oxygen pressure, $P_T$ = total pressure.

Figures 3 and 4 illustrate the type of rate curves obtained in these studies and the type of graph from which the orders of reaction shown in Table II were calculated.

The results in Table II show that the effect of methane on reaction order at the maximum rate is rather small in stoichiometric and 3:1 $H_2$–$O_2$ mixtures, and rather large in 1:1 $H_2$–$O_2$ mixtures.
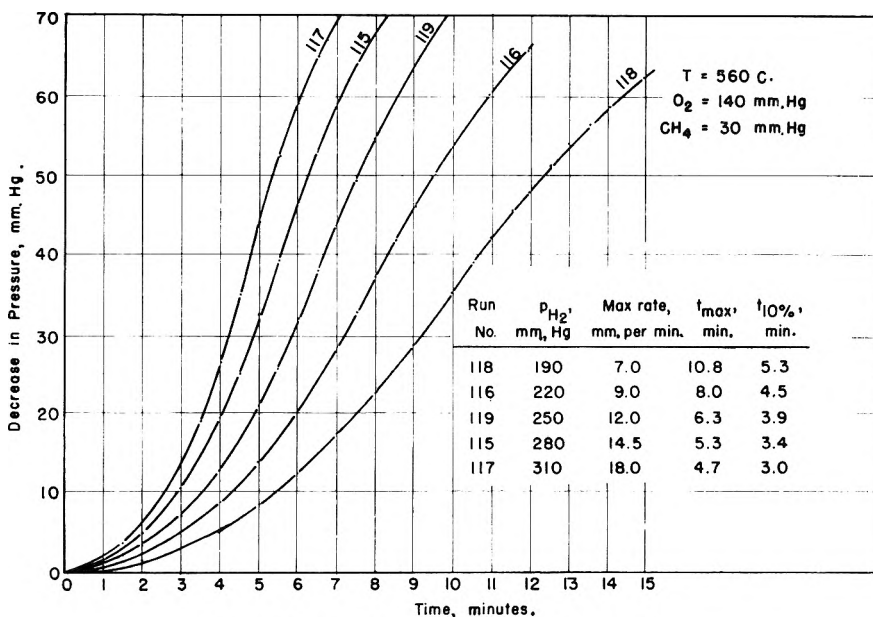


Fig. 4.—Pressure dependence of reaction rates for $H_2$–$O_2$–$CH_4$ mixtures.



Fig. 3.—Rate curves for $H_2$–$O_2$–$CH_4$ mixtures.

| Run No. | $P_{H_2}$, mm. Hg | Max rate, mm. per min. | $t_{max}$, min. | $t_{10\%}$, min. |
|---|---|---|---|---|
| 118 | 190 | 7.0 | 10.8 | 5.3 |
| 116 | 220 | 9.0 | 8.0 | 4.5 |
| 119 | 250 | 12.0 | 6.3 | 3.9 |
| 115 | 280 | 14.5 | 5.3 | 3.4 |
| 117 | 310 | 18.0 | 4.7 | 3.0 |

The presence of methane causes a decrease in reaction order when hydrogen is the variable, in contrast with an increase in reaction order when oxygen is the variable. This is observed with respect to both initial and maximum reaction rates.

**Rate Studies in Terms of Over-All Stoichiometry.**—The increased reactivity imparted by methane to $H_2$–$O_2$ mixtures containing excess oxygen
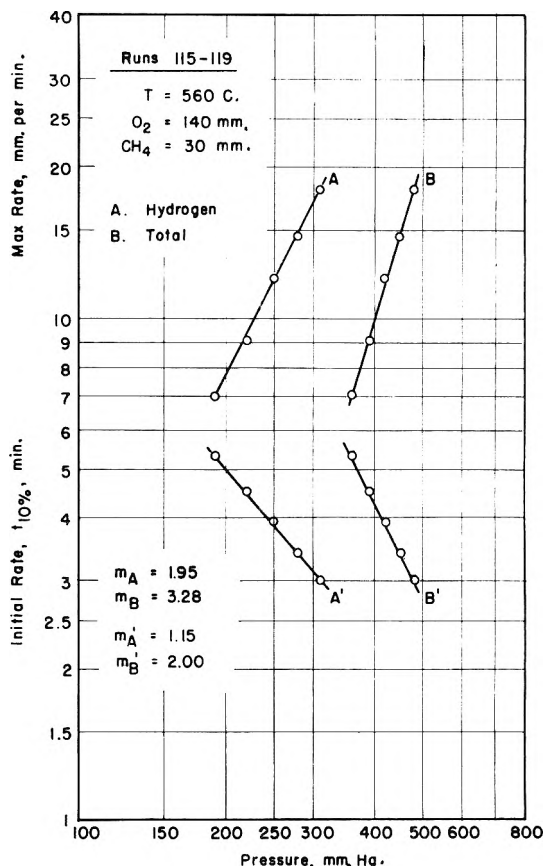
suggests that the rate of reaction may be a function of the over-all stoichiometry, or is at least dependent on the presence of sufficient oxygen in the system for the oxidation of both hydrogen and methane. A series of studies was performed at constant temperature and constant total pressure, $T = 560°$ and $P = 420$ mm., to investigate this further. The results of these studies are shown in Tables III and IV.

Table III shows the results of experiments in which the [$H_2 + CH_4$] concentration and the oxygen concentration are kept constant while varying the $H_2$ to $CH_4$ ratio. The maximum rate of reaction under these conditions was found to be independent of the methane concentrations, although the initial rate, expressed in terms of $t_{max}$, varies almost linearly with the methane concentration.

Table IV presents an entirely different picture. In these studies the hydrogen concentration is kept constant in each series of experiments while the proportions of $O_2$ to $CH_4$ are varied. As before, the

### TABLE III

REACTION RATES FOR VARYING $H_2$-$O_2$-$CH_4$ MIXTURES WITH
CONSTANT FUEL CONCENTRATIONS

$T = 560°, P = 420$ mm.

| Initial partial pressure, mm. | | | Max. rate, mm./min. | Initial rate, $t$, min. to reach max. rate |
|---|---|---|---|---|
| $CH_4$ | $H_2$ | $O_2$ | | |
| 0 | 280 | 140 | 11 | 9.7 |
| 30 | 250 | 140 | 11 | 7.7 |
| 60 | 220 | 140 | 12 | 5.5 |
| 90 | 190 | 140 | 12 | 4.7 |
| 120 | 160 | 140 | 11 | 3.5 |
| 10 | 310 | 100 | 7 | 7.5 |
| 30 | 290 | 100 | 7 | 6.7 |
| 60 | 260 | 100 | 7 | 5.0 |
| 90 | 230 | 100 | 7 | 4.5 |
| 120 | 200 | 100 | 7 | 3.7 |

### TABLE IV

REACTION RATES FOR VARYING $H_2$-$O_2$-$CH_4$ MIXTURES WITH
CONSTANT HYDROGEN CONCENTRATIONS

$T = 560°, P = 420$ mm.

| Initial partial pressure, mm. | | | Max. rate, mm./min. | Initial rate, $t$, min. to reach max. rate |
|---|---|---|---|---|
| $CH_4$ | $H_2$ | $O_2$ | | |
| 0 | 200 | 220 | 6.0 | 9.5 |
| 15 | 200 | 205 | 9.5 | 10.5 |
| 30 | 200 | 190 | 13.0 | 8.0 |
| 60 | 200 | 160 | 14.0 | 5.0 |
| 70 | 200 | 150 | 13.0 | 5.8 |
| 90 | 200 | 130 | 11.0 | 5.0 |
| 105 | 200 | 115 | 8.0 | 4.3 |
| 120 | 200 | 100 | 6.3 | 4.0 |
| 120 | 200 | 100 | 6.1 | 3.7 |
| 0 | 160 | 260 | 4.0 | 15.5 |
| 40 | 160 | 220 | 12.0 | 7.7 |
| 60 | 160 | 200 | 14.5 | 6.5 |
| 60 | 160 | 200 | 15.0 | 6.5 |
| 75 | 160 | 185 | 15.2 | 5.0 |
| 90 | 160 | 170 | 13.0 | 4.5 |
| 120 | 160 | 140 | 10.5 | 4.0 |
| 165 | 160 | 95 | 6.8 | 3.5 |

trend is for the initial rate of reaction to increase (in spite of some irregularities) with increasing amounts
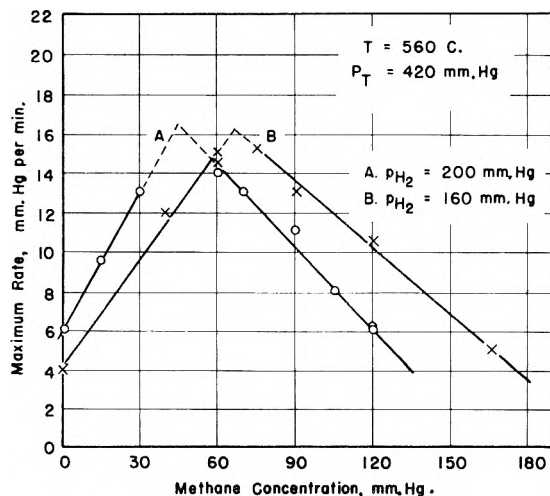
Fig. 5.—The variation of the maximum rate of reaction with the $H_2 + CH_4$ concentration.

of methane. The maximum rate however varies in a more unique manner. The maximum rate is found to increase to a maximum and to decrease as methane is increased.

Figure 5 shows more clearly the behavior of the maximum rate in relation to methane concentration. The best straight lines have been constructed through the data.

Figure 6 is a plot of the same data from Table IV in terms of oxygen concentration. The right-hand portions of the two curves are almost coincident, indicating that in rich mixtures the maximum rate is primarily a function of the oxygen concentration, and not of methane.
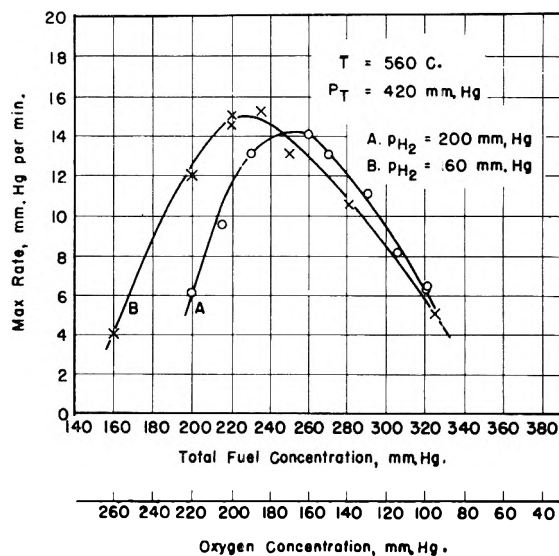
Fig. 6.—The correlation of the maximum rate with the total fuel concentration.

**Analysis of Reaction Gases.**—Since reaction rates derived from pressure measurements can refer only to the over-all changes during reaction, three experiments were performed for the purpose of determining to what extent each of the reactants entered into the reaction. A one-liter sampling bulb was attached to the apparatus for this purpose. The studies were made at 560° and 420 mm. initial total pressure. The procedure was to react the gases for a definite period of time and then to expand the reaction gases into the sampling bulb. The expansion reduced the pressure by a factor of twelve, thus virtually stopping the reaction. The gas samples were collected over mercury and analyzed on a micro-Orsat apparatus for oxygen, carbon monoxide and carbon dioxide. The composition of the partially reacted mixture was then calculated by assuming only the following three reactions, and using the stoichiometric relationships in conjunction with the Orsat analyses.

$$2H_2 + O_2 = 2H_2O$$
$$CH_4 + 1.5O_2 = CO + 2H_2O$$
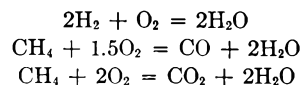$$CH_4 + 2O_2 = CO_2 + 2H_2O$$

Table V is a tabulation of the results of these experiments.

In the temperature region of 560°, rate equations have been written for the homogeneous oxidation

of hydrogen[4a] and of methane[4b] as

$$Rate_h = k_h(H_2)^2(O_2)P$$
$$Rate_m = k_m(CH_4)^2(O_2)P$$

where the subscripts h and m refer to hydrogen and methane oxidations, respectively. Since the oxygen and the total pressure terms of the two rate equations are common to both fuels, the ratio[4] of the rates of oxidation of the hydrogen and methane is

$$\frac{r_h}{r_m} = \frac{k_h(H_2)^2}{k_m(CH_4)^2} = k\left[\frac{H_2}{CH_4}\right]^2$$

TABLE V

ANALYSIS OF REACTION PRODUCTS IN $H_2$-$O_2$-$CH_4$ MIXTURES

| Expt. No. | Initial pressures, mm. | | | Pressure decrease at time of sampling, mm. | Calcd. ratios | |
|---|---|---|---|---|---|---|
| | $H_2$ | $CH_4$ | $O_2$ | | $(P_{H_2}/P_{CH_4})^2$ | $\Delta P_{H_2}/\Delta P_{CH_4}$ |
| A1 | 160 | 60 | 200 | 29 | 7.1 | 9 |
| A2 | 250 | 60 | 100 | 23 | 17.2 | 11.5 |
| A3 | 200 | 60 | 160 | 58 | 11.1 | 12.2 |

Final pressures, mm. (calcd. from Orsat analyses)

| Expt. No. | $CO_2$ | $O_2$ | CO | $H_2$ | $CH_4$ | $H_2O$ |
|---|---|---|---|---|---|---|
| A1 | 2.3 | 157 | 4.6 | 97 | 53 | 77 |
| A2 | 2 | 70 | 2 | 204 | 56 | 54 |
| A3 | 4 | 82 | 6 | 78 | 50 | 142 |

In the absence of interfering interactions, the ratio of the hydrogen to methane consumed would be proportional to the ratio of the squares of the initial hydrogen and methane concentrations in the system. This comparison is made in the last two columns of Table V. The experiments are too few in number to be definitive, but the results of experiments A1 and A3 indicate some confirmation of the predicted correlation under the conditions shown.

**The Water Vapor Effect on the Combustion of Hydrogen and Oxygen.**—The strong accelerating action of water vapor and its relation to the influence of methane on the $H_2$-$O_2$ reaction were discussed in some detail elsewhere.[5] It was shown that water vapor in $H_2$-$O_2$-$H_2O$ mixtures increased both the initial and maximum rates of reaction. Furthermore, it was shown that the initial rate in a $H_2$-$O_2$-$H_2O$ system is equal to the reaction rate in a partially reacted $H_2$-$O_2$-$CH_4$ system, after the reaction in the methane system has progressed to the point where the water vapor in the two systems is equal.

The results of Chirkov[6] also showed that the initial velocities of several $H_2$-$O_2$-$H_2O$ mixtures corresponded to velocities of partially reacted $H_2$-$O_2$ mixtures, initially free of water vapor, after equivalent quantities of water vapor had been formed. Chirkov described these results by the equation

$$Rate = k(H_2)^2(H_2O)$$

where the rate constant, $k$, is a function of the $O_2/H_2$ ratio.

(4) W. Jost, "Explosion and Combustion Processes in Gases," McGraw-Hill Book Co., New York, N. Y., 1946: (a) work of Prettre, p. 310; (b) work of Norrish, p. 417.

(5) A. Levy, *J. Chem. Phys.*, **21**, 2132 (1953).

(6) N. Chirkov, *Acta Physicochim.*, USSR, **6**, 915 (1937).

The present studies suggest that the same type of rate equation exists for systems containing methane. The entire equation becomes considerably more complex however. The rate constant, $k$, becomes a function of the $O_2/CH_4$ ratio and probably the $H_2/CH_4$ ratio in addition to the $O_2/H_2$ ratio, and the water vapor term is now a function of all three components.
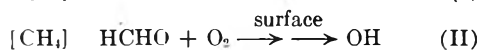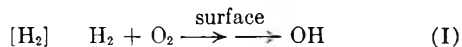
In the oxidation of methane the pressure of the system increases before decreasing. Since the rate data in these studies show only a *decrease* of the total pressure in the system with time, it becomes apparent that the accelerating effect of methane in these studies cannot be explained solely by the simultaneous, independent oxidations of methane and hydrogen. These facts therefore point to the strong accelerating effect of water vapor on the rate of combination of hydrogen and oxygen, which would mask any potential pressure increase and further accelerate the rate of pressure decrease. These studies of the $H_2$-$O_2$-$H_2O$ and $H_2$-$O_2$-$CH_4$ systems corroborate earlier postulations that methane enters reactions which increase the initial rate of water formation. These same reactions are then responsible for the reduction of the second explosion limit (Fig. 2 in Part I)[2] and for the acceleration of the slow reaction (Fig. 3).
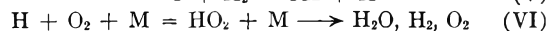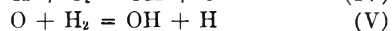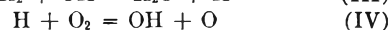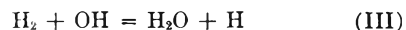
## Discussion

Methane affects the slow reaction between hydrogen and oxygen in various ways. To review briefly, for systems of varying composition at constant total initial pressure: the initial rate increases with increasing amounts of methane for all $H_2/O_2$ ratios; the maximum rate (1) is reduced when methane replaces both $H_2$ and $O_2$ in rich and stoichiometric $H_2$-$O_2$ mixtures, (2) is increased when methane replaces both hydrogen and oxygen in lean $H_2$-$O_2$ mixtures, (3) is unchanged when methane replaces only the hydrogen in a rich mixture, and (4) passes through a maximum when methane replaces only the oxygen in a mixture; the over-all order of reaction (1) is practically unchanged by adding methane to rich and stoichiometric $H_2$-$O_2$ mixtures, and (2) is increased by adding methane to lean $H_2$-$O_2$ mixtures.

**The Initial Rate.**—The similarity in the mechanisms for the homogeneous oxidation of methane and of hydrogen separately is quite apparent from the main reaction steps listed below.

Initiation

$$[H_2] \quad H_2 + O_2 \xrightarrow{surface} \longrightarrow OH \qquad (I)$$

$$[CH_4] \quad HCHO + O_2 \xrightarrow{surface} \longrightarrow OH \qquad (II)$$

Oxidation of $H_2$

$$H_2 + OH = H_2O + H \qquad (III)$$
$$H + O_2 = OH + O \qquad (IV)$$
$$O + H_2 = OH + H \qquad (V)$$
$$H + O_2 + M = HO_2 + M \longrightarrow H_2O, H_2, O_2 \qquad (VI)$$

Oxidation of $CH_4$

$$CH_4 + OH = CH_3 + H_2O \qquad (VII)$$
$$CH_3 + O_2 = HCHO + OH \qquad (VIII)$$
$$HCHO + OH = CHO + H_2O \longrightarrow CO, CO_2, H_2O \qquad (IX)$$
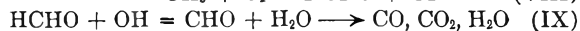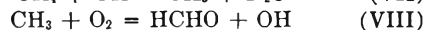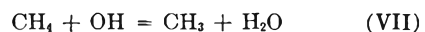
Although both hydrogen and methane appear to propagate their chains through reactions with the

hydroxyl radical when reacting separately, the explosion studies indicated that the interactions of hydrogen and methane apparently occur through hydrogen atom reactions. Since the acceleration by water vapor of the initial and maximum rate of the slow reaction has been shown by Voevodskii[7] to be due to a build-up of $HO_2$-radical concentration by the reaction
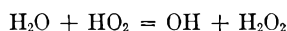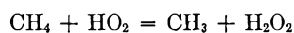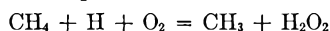
$$H_2O + HO_2 = OH + H_2O_2$$

the analogous reaction was proposed for methane acceleration[5]

$$CH_4 + HO_2 = CH_3 + H_2O_2$$

or as stated in the previous article

$$CH_4 + H + O_2 = CH_3 + H_2O_2$$

The observed increase in the initial rate of reaction is possibly caused by an increased rate of appearance of hydrogen peroxide and resulting higher steady-state concentrations of the hydrogen peroxide and the hydroxyl radical.

**The Maximum Rate.**—It was shown in Table II that the reaction order with respect to the maximum rate increased from 3.6 to 5.1 when 30 mm. of methane was added to $1:1$ $H_2$–$O_2$ mixtures. When the same quantity of methane was added to $2:1$ and $3:1$ $H_2$–$O_2$ mixtures there was no appreciable change in the reaction order. The effect of methane on the maximum rate thus appears to be hidden or non-existent when oxygen is deficient in the ternary mixture.

The maximum rate also remained unchanged (Table III) when methane replaced hydrogen and the oxygen concentration was kept constant. The results in Table II represent ternary mixtures deficient in oxygen, so the absence of a change in maximum rate conforms with the lack of a change in reaction order in oxygen-deficient mixtures.

In the other instance, when oxygen is in excess with respect to the hydrogen and the methane, the substitution of methane for hydrogen increases the maximum rate rather markedly. The lean (left-hand) portions of the curves in Fig. 6 illustrate this point quite clearly, in that curve B for mixtures containing more methane falls above curve A. Although the fuel-rich sides of these two curves do not coincide exactly, they do fall close together, and thus they conform generally with the absence of a methane effect in rich ternary mixtures. The range of variation in the hydrogen–methane concentrations of Table III is much wider than those of Fig. 6. Probably the deviation in Fig. 6 is due to the difficulty of reproducing data on an absolute basis over a period of time.

It was likewise noted in Fig. 5 that the maximum reaction rates passed through a maximum (the "peak rate") as the methane/oxygen ratio was varied at constant total and hydrogen pressures. This also suggests that the maximum rate is a function of the oxygen available to both fuels in the system.

If one assumes only the following reactions

$$2H_2 + O_2 = 2H_2O$$
$$CH_4 + 1.5O_2 = CO + 2H_2O$$
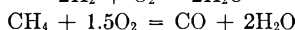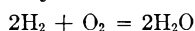
it is observed that the peak rates occur when there is just about sufficient oxygen to satisfy the needs of

the hydrogen and methane. The extrapolated peak-rate concentrations expressed in mm. are: A, 200 $H_2$, 45 $CH_4$ and 175 $O_2$; B, 160 $H_2$, 66 $CH_4$, and 194 $O_2$.

Although these peak mixtures are approximately stoichiometric in the relative concentrations of hydrogen, oxygen and methane, the two curves by themselves offer insufficient evidence that the rate depends primarily on stoichiometry. If, in accord with Chirkov's views, the peak mixtures are those that give a maximum of the product of $k(H_2)^2(H_2O)$, then, since the water vapor concentration is dependent on the methane and the hydrogen concentrations, the maximum of this product probably occurs near the region of the over-all stoichiometric mixture.

How a Chirkov-type equation might explain the constant rates of Table III for rich ternary mixtures is not evident in these studies, although an explanation which suggests itself is that the equation may be expressed as

$$\text{Rate} = k(H_2 + CH_4)^2(H_2O)$$

Such an explanation would not contradict any of the previous deductions on the peak rates, and would be in agreement with the maximum rate results of Table III. Confirmation of this postulate would require a detailed analytical study of the consumption and formation of all the constituents in the mixture as a function of time. The present study has only presented three such analyses for the purpose of illustrating the manner by which methane is also oxidized.

It has been stated that Chirkov's results are difficult to explain, except as the result of a special wall effect.[8] However in the light of the evidence presented here from both explosion and slow-reaction phenomena, the effects seem to be too closely related to the homogeneous reactions of methane in the presence of hydrogen to be primarily "special wall effects."

**Relation between the Slow Reaction and the Explosion Results.**—The marked effect of methane in increasing the reaction rate of lean $H_2$–$O_2$ mixtures now explains certain anomalous explosion inhibition results in lean $H_2$–$O_2$–$CH_4$ mixtures observed in the preceding article. It was found in previous studies that the critical methane concentration for total inhibition of explosion varied directly with the oxygen mole fraction up to $x_{O_2} \cong 0.45$. Above this value a sharp reduction in the critical methane concentration was observed. Since the rate of water formation is increased rather markedly in these lean mixtures, water vapor is probably formed in the short period in which oxygen is being admitted to the reaction vessel. The result is that the explosion reaction is inhibited in lean mixtures by both the "slow reaction" that forms water vapor and the fast, chain reactions that produce formaldehyde near the explosion limit. In effect, this is similar to the explanation for the reduced, critical methane concentrations in Vycor reaction vessels, the difference being that in the latter case the increased reaction rate is due to surface-accelerated reactions.

(7) V. V. Voevodskii, *Acta Physicochim.*, **22**, 457 (1948).

(8) W. Jost, ref. 4, p. 309.

This same effect is observed, but shown in another manner, in Fig. 4 of the article on the explosion studies.[2] There the $H_2$–$O_2$–$CH_4$ curves reverse near the critical methane concentration just prior to complete inhibition of the explosion reaction. The reversal in direction of these curves occurs when the $H_2$:$O_2$ ratio is between 2:1 and 1:1, and is analogous to the shape of the maximum rate curves of Fig. 6 of this article. In both instances the reversal of direction is probably related to the water vapor effect by the fact that water vapor accelerates the combination of hydrogen and oxygen in the early stages of reaction, and then decelerates the reaction when sufficient water vapor has been formed.

In general, water vapor appears to influence the oxidation of all hydrocarbons and hydrogen. To name only a few instances of this accelerating effect of water vapor in addition to those already cited, there is the well-known effect on carbon monoxide oxidation,[9] on methane oxidation,[10] and on ethane oxidation.[11] In more recent studies an indirect water vapor effect has also been shown in reactions where the rate of oxidation of carbon monoxide is increased by small additions of methane, and decreased by large additions.[12] These same workers have also noted a widening of the carbon monoxide explosion peninsula upon adding small quantities of methane to the $CO$–$O_2$ mixture. Along this same line it has also been shown that one can relate the stability of carbon monoxide–methane–air and carbon monoxide–propane–air flames to the water vapor produced by the hydrocarbon in preflame reactions.[13]

(9) G. Hadman, H. W. Thompson and C. N. Hinshelwood, *Proc. Roy. Soc. (London)*, **A138**, 297 (1932).

(10) M. Vanpee, *Am. Mines Bdge.*, **47**, 111 (1947–48).

(11) N. Chirkov, *Doklady Akad. Nauk, USSR*, **45**, 244 (1944).

(12) D. E. Hoare and A. D. Walsh, *Trans. Faraday Soc.*, **50**, 37 (1954).

(13) A. Levy and P. F. Kurz, *J. Am. Chem. Soc.*, **77**, 1489 (1955).

# PHOTOLYSIS WITH A HIGH INTENSITY SPARK

By Gilbert J. Mains,[1] John L. Roebber and G. K. Rollefson

*Contribution from the Department of Chemistry and Chemical Engineering, University of California, Berkeley, Calif.*

An apparatus is described in which a capacitance ranging up to 10 microfarads charged to 20,000 volts is discharged between magnesium electrodes in a low pressure chamber. The light from such a source was found to be predominantly that of the magnesium spark with a particularly high intensity of the doublet near 2800 Å. Hence for many photochemical reactions this spark can be used as essentially a monochromatic source of this wave length. The intensity of the light has been studied as a function of the discharge potential, inductance and capacitance. The duration of the discharge is also dependent on these quantities. The maximum average intensity incident on a 100-cc. reaction vessel was found to be $10^{21}$ quanta per second. The apparatus was used to study the photolysis of acetaldehyde. The principal products under these conditions were carbon monoxide, ethane, methane and hydrogen. It is shown that the results are in accord with the idea that all the methyl radicals formed by the primary action of the light on the aldehyde react to form ethane. The ethane yield does not vary appreciably with a thirty-fold change of intensity which indicates that competition between the reaction of methyl radicals with acetaldehyde to form methane and the combination to form ethane is not important at these intensities.

During the last few years there has been considerable interest in the effects produced by the illumination of gases and solutions by light of high intensity. The usual method for producing the light has been to charge a condenser and then discharge it through a tube filled with a gas at low pressure.[2-4] The light obtained in this manner was of high intensity, usually lasted for a period of the order of milliseconds, and gave a continuous spectrum. Such a source is useful for the production of relatively high concentrations of intermediates in photochemical reactions such as radicals or atoms. Thus it becomes possible to greatly increase the importance of reactions of radicals with each other as compared to their reactions with other molecules. For example, Kahn, Norrish and Porter[2b] showed that considerable amounts of ethane were formed by the combination of methyl radicals in acetaldehyde illuminated in this manner whereas with low intensities no appreciable amount

of ethane is produced. The principal difficulties with sources of this kind in the study of photochemical reactions are: (1) the light is not monochromatic and in many reactions the behavior is a function of the wave length of the light absorbed, (2) the large amount of energy absorbed from each flash raises the temperature to an extent which is difficult to determine and which may often materially affect the results. Both of these effects make it difficult to compare the work of different observers except in a qualitative way. In this paper we wish to describe an apparatus which will give high intensity flashes of essentially monochromatic light sufficient to make the reactions between radicals of dominant importance and still keep the total energy absorbed by the system low enough so that there is no significant change of temperature.

A light source with a line emission can be obtained if the gas discharge tube used by previous investigators is replaced by a spark gap of suitable electrode material. In our experiments we have used magnesium electrodes. The light emitted from a spark between such electrodes is made up primarily of the two lines at 2795.5 and 2802.7 Å. Such a wave length is convenient for the study of

(1) General Electric Fellow 1953–1954; du Pont Fellow 1952–1953.

(2) (a) G. Porter, *Proc. Roy. Soc. (London)*, **A200**, 284 (1950); (b) M. A. Kahn, R. G. W. Norrish and G. Porter, *ibid.*, **A219**, 312 (1953).

(3) N. Davidson, R. Marshall, A. E. Larsh, Jr., and T. Carrington, *J. Chem. Phys.*, **19**, 1311 (1951).

(4) G. Herzberg and D. A. Ramsay, *ibid.*, **20**, 347 (1952).

many photochemical reactions such as are observed with the aldehydes and ketones. If other wave lengths are desired the electrodes can be changed. For example, aluminum or zinc electrodes will supply light of shorter wave lengths. Sources of this kind are not as efficient as the gas discharges when considered from the standpoint of total radiation but they possess the advantage that the radiation which is supplied is in lines rather than a continuum and therefore more useful for the study of systems in which there is a wave length dependence. Also the smaller total energy involved means that there will be far less heating of a reaction mixture and thus undesirable temperature effects are avoided, or on the other hand definite temperature effects can be studied.

Earlier work on the production of high intensities of light[5,6] has shown that the light intensity follows the current approximately during a discharge. High currents are therefore essential to the production of high light intensity. Preliminary experiments with a magnesium spark showed that for a given voltage the duration of the spark increases with the capacity in the circuit. This fact tends to limit the intensity of the discharge. As a result we decided to devise an apparatus in which a discharge would occur simultaneously through several spark gaps.

In order to limit the radiation from the spark gaps to that characteristic of the electrodes, the pressure in the spark chamber was reduced as low as possible by an oil pump. Under these conditions the condensers could not be connected directly to the electrodes during charging because of the low breakdown potential in the chamber. Hence another spark gap which operated at atmospheric pressure was placed in series with the magnesium electrodes. This auxiliary gap was adjusted so as not to break down at potentials below 25,000 volts and was triggered to set off the discharge.

The circuit finally adopted is shown in Fig. 1. Ten magnesium spark gaps, $G_1$, were enclosed
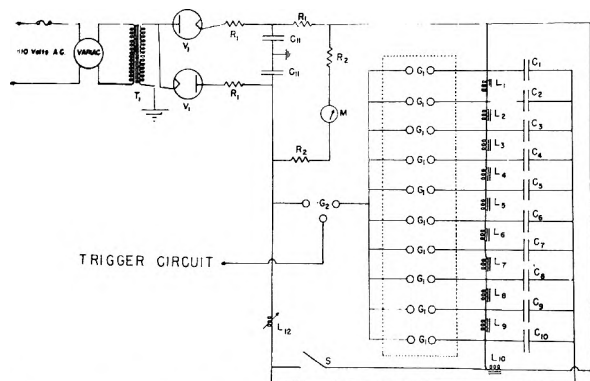


Fig. 1.—Condensed spark discharge circuit: $C_1$ - - - - - $C_{10}$, 1 μf., 25 kv. condensers; $C_{11}$, 0.1 μf., 15 kv. condenser; $L_1$ - - - - - $L_{10}$, 1 mh. R.F. choke; $L_{12}$, 1.05 mh. variable inductance; $G_1$, Mg electrodes, 3 cm. spacing, vacuum gap; $G_2$, Cr plated spheres, air gap; M, milliammeter; $R_1$, 160,000 ohm, 195 watt resistance; $R_2$, 20 megohms, 20 watt resistance; $T_1$, 25 kv. secondary, Thordarson transformer; $V_1$, 371 B vacuum tube; S, shorting switch.

(5) H. Edgerton and P. M. Murphy, J. Appl. Phys., **12**, 848 (1941).
(6) J. N. Aldington, et al., J. Inst. Elec. Eng., **95**, Pt. 2, No. 48 (1948).

in the spark chamber indicated by the dashed line. The condensers, $C_1$-$C_{10}$, were charged to the desired potential by the power supply made up of $T_1$, $V_1$, $R_1$ and $C_{11}$. When the desired voltage had been reached, in the range 10 to 25 kilovolts, the atmospheric gap, $G_2$, was triggered. This caused an overvoltage of several hundred per cent. on each magnesium gap, $G_1$. Because of this high overvoltage, the statistical time lag of these gaps was so small that each condenser began discharging within a fraction of a microsecond. The small R. F. chokes, $L_1$-$L_{10}$, prevented all the condensers from discharging through a single gap. Hence the net effect of the triggering was to simultaneously discharge each of the condensers through its own magnesium gap and thus produce a high intensity of light in the spark chamber.

The apparatus was set up in a space approximately nine feet long, six feet wide, and seven and one-half feet high, which was surrounded by a grounded screen except at one corner where the control panel was located. The condensers were placed on four shelves which lined the inside of the space. The spark chamber was mounted on a stand equipped with casters so that it could be placed in the middle of the space or rolled out to permit maintenance work on the condensers or their connections. The control panel was arranged to permit variation of the charging potential, the discharging potential and the inductance in the circuit. In addition the standard switches, pilot lights and fuses for each portion of the apparatus were situated here. The power supply was mounted on a fifth shelf high above the condensers for convenient access.

The power supply made use of a voltage doubling technique. By this arrangement one side of the condensers was charged positive relative to ground and the other negative. Although this device has the disadvantage that both leads must be insulated this is offset by the much lower insulation requirements. The primary potential of the transformer, $T_1$, was adjusted by means of a variac. The secondary of the transformer was connected, as shown, to the diode rectifiers, $V_1$, and then into the resistor-capacitor combination, $R_1$, $C_{11}$, which smoothed the pulsating DC signal and also served to protect the diodes from the oscillations of the main condenser discharge. Under normal operating conditions the variac was adjusted to supply 30 kv. to the condensers. While these conditions resulted in the charging resistors, $R_1$, operating quite warm to the touch, it permitted the apparatus to be operated at a rate of three to four cycles per minute.

The condensers used were Cornell–Dubilier 1 microfarad at 25 kv. d.c. Since these are quite large the total capacitance which could be used was limited by the space available. Early experiments showed that the condensers could not be repeatedly charged to their rated d.c. voltage and rapidly discharged since this led to a breakdown of the dielectric oil. Presumably this breakdown was the result of local dielectric heating since the body of the condensers at no time showed signs of heating. Because of this instability the condensers were

connected in groups of four to give 1 microfarad for each group. In all we used forty condensers for a total capacitance of 10 microfarads.

Because it was often necessary to expose a sample to many flashes to get sufficient photochemical decomposition for accurate analysis, an arrangement was made which triggered the gap, $G_2$, after the condensers had been charged and counted the number of times the cycle had been repeated. The circuit used for this purpose is shown in Fig. 2. A lead from the plus side of the condensers being charged produced a potential drop across $R_3$ and $R_4$ which increased as the charge in the condensers increased. By varying $R_3$ it could be arranged that this potential would be 105 volts when the condensers had been charged to the desired voltage. At this potential $V_2$ began to conduct a current which actuated the relay, $L_{11}$, and thus sent a 300 volt pulse to the counter and turned on the Tesla coil. When the condensers discharged the 105 volt potential was removed from the grid of $V_2$ and the relay opened. The charging current was too small to keep the spark gaps conducting so the circuit began a new cycle. Both the relay circuit and the Tesla coil were found to be quite reliable. The discharge potential was constant to at least 1%. The relay contacts had to be cleaned and readjusted periodically but no further maintenance was necessary during the course of ten thousand discharges.
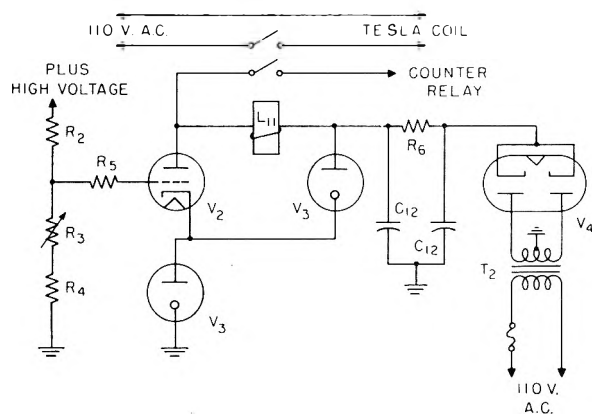


Fig. 2.—Relay circuit: $C_{12}$, 8 $\mu f$., 300 volt condenser; $L_{11}$, d.c. relay; $R_2$, 20 megohms, 20 watts resistance; $R_3$, 250,000 ohm potentiometer; $R_4$, 150,000 ohm, 1 watt resistance; $R_5$, 1 megohm, $1/2$ watt resistance; $R_6$, 1 megohm; $T_2$, 480 volt, C.T. transformer; $V_2$, 6 SN 7 vacuum tube; $V_3$, V.R. 105 gas tube; $V_4$, 5 Y 3 vacuum tube.

In some experiments the Tesla coil was replaced by a thyratron circuit shown in Fig. 3. The condenser, $C_{13}$, was charged along with the condensers, $C_1$–$C_{10}$ (Fig. 1). The center chromium sphere of the gap, $G_2$, remained at essentially ground potential. The distances between the center sphere and the upper and lower spheres just exceeded the critical value for breakdown. When all the condensers were charged to the desired potential the thyratron, $V_5$, was pulsed grounding the positive side of $C_{13}$. The center sphere instantly became negative with respect to ground thus placing almost 100% overvoltage across the upper spark gap which caused it to discharge. This discharge in turn

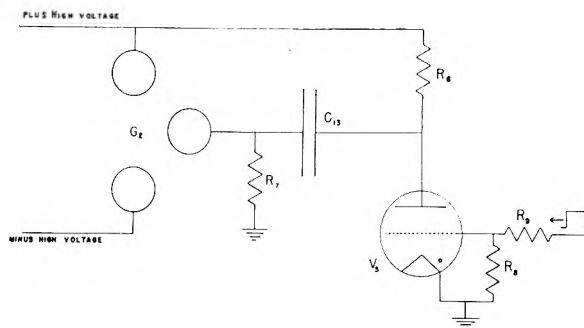caused the lower gap to discharge. In practice the two gaps seemed to fire simultaneously.



Fig. 3.—Thyratron trigger circuit: $C_{13}$, 0.001 $\mu f$., 25 kv. condenser; $G_2$, Cr plated spheres, air gap; $R_6$, 25,000 ohms; $R_7$, 50 megohms; $R_8$, 100,000 ohms; $R_9$, 5,000 ohms; $V_5$, 5 C 22 Thyratron.

The spark chamber which housed the ten pairs of magnesium electrodes was constructed of Plexiglass in the form of a right cylinder. Preliminary experiments showed that bakelite could not stand the electrical strain and polystyrene was too brittle. Plexiglass was found to have both the mechanical and electrical strength required. The electrodes were mounted symmetrically around a 32-mm. quartz tube which extended axially through the cylinder. The cylinder was ten inches in diameter and twelve inches long and was evacuated to a pressure of about five millimeters through a 15 mm. tube. The chamber was mounted on a stand three feet high which was equipped with casters so that it could be rolled in and out of the condenser room. This stand also supported a glass vacuum system for loading the reaction vessel.

The magnesium electrodes were quarter inch rods obtained from the Amend Chemical Company. The electrode gaps were staggered so as to provide relatively uniform illumination of the quartz reaction tube. Behind each gap was a chromium plated reflector bent to fit an ellipse with the spark gap and the reaction tube at the foci. During the course of ten thousand discharges the reflectors became coated with magnesium oxide but this did not interfere with the reflection of the ultraviolet. The oxide also coated the quartz tube; this coating was removed periodically.

The reaction tube was a 22-mm. quartz tube approximately thirty centimeters in length which was inserted in the quartz tube mentioned above. It was attached to a vacuum system mounted on the rolling stand previously described. The sample for photolysis was expanded into the reaction vessel from a side tube attached to the vacuum line. After the photolysis the gas was toeplered from the reaction tube into a bulb for analysis.

**Characteristics of the Spark Discharge.**—Photographs of the spectrum of the spark produced in the apparatus just described showed only lines characteristic of magnesium. The two lines near 2800 Å. were by far the strongest and were the only ones that would be of importance photochemically. The next most intense lines were the group at 3830 Å. but these were considerably weaker than the others. However, they did contribute some to the light measured by actinometry.

The total yield of photochemically active light from the source was determined by means of the potassium ferrioxalate actinometer described by Parker.[7] In this method the ferrioxalate is decomposed by radiation into ferrous ion and carbon dioxide. The ferrous ion is complexed with orthophenanthroline and the concentration of the complex determined using a Beckman D.U. spectrophotometer.

The light yield was studied as a function of the discharge potential, capacitance and inductance. From Fig. 1 it is apparent that each time one of the condensers, $C_1$–$C_{10}$ is removed from the circuit its corresponding spark gap is also removed. Hence it is not surprising that the amount of reaction produced per flash in the actinometer solution varied almost linearly with the capacity. The slight deviations from linearity were believed to be caused by variations in the condensers.

The variation of the light yield per flash as a function of the discharge potential is shown in Fig. 4. The data are shown in the form of optical density of the solution of the ferrous complex since this quantity is proportional to the number of quanta acting on the solution. The particular set of values shown were obtained with a capacity of 10 microfarads. The points are fitted with a curve varying as $V^{1.8}$ ($V$ is the potential). This exponent is significantly different from the value of 2.4 to 4 reported by Kornetski[8] for sparks at atmospheric pressure. Furthermore Kornetski used a phototube which was sensitive to a much wider range of wave lengths than the actinometer solution used in our experiments. These differences in conditions may account for the lower dependence on the discharge potential in our experiments but we have not investigated the point further.
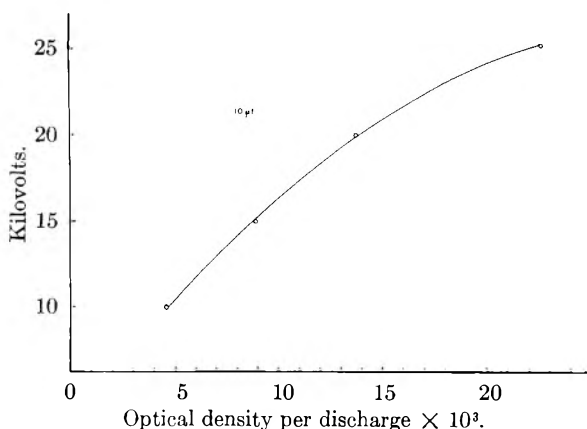


Fig. 4.—Variation of light output per flash with voltage.

The effect of adding inductance to the discharge circuit was to decrease the light yield per flash. The decrease was close to linear and amounted to a factor of 1.8 for the introduction of 1.05 millihenry in a circuit in which the capacity was 10 microfarads.

As a result of these studies it can be said that the total light yield per flash is given by $Y = aCV^n -$

(7) C. A. Parker, *Proc. Roy. Soc. (London)*, **A220**, 104 (1953).

(8) M. Kornetski, V. Formin and R. Steinitz, *Z. tech. Phys.*, **14**, 274 (1933).

$bL$. In this equation $a$ and $b$ are positive constants, $C$ is the capacitance, $L$ the inductance, $V$ the potential to which the condensers were charged and $n$ a constant which in our experiments was 1.8. This equation differs from one given by Kornetski in the addition of the second term and, as previously mentioned, a smaller value of $n$.

The intensity of the light produced by a discharge is of major interest as well as the total yield of light. For example, the concentration of radicals produced by a flash depends primarily on the intensity of the light. We have studied the intensity as a function of time by means of a phototube and oscilloscope. A 931A phototube with a 10,000 ohm load resistor was coupled to a 6J6 cathode follower. The cathode resistance of the latter was 1,000 ohms. The cathode signal was traced on a model 513 Tektronix oscilloscope using the signal itself to trigger the sweep. The gain applied to the signal was varied to use as much of the oscilloscope face as possible and no attempt was made to get an absolute calibration in terms of intensity. Therefore the traces which were photographed showed only the variation in intensity with time for single flashes. The curves shown in Fig. 5 represent typical traces. It is apparent that we are dealing with a damped oscillating discharge. The life-time of the discharge can be defined as the time necessary for the envelope of the oscillations to fall to $1/e$ of its initial peak value. The envelope is not easily determined because of the irregularities in the peaks and, in the case of high energy flashes, there was some interference with the time base of the oscilloscope. Hence the lifetimes for the high energy discharges are probably not accurate to better than ten per cent. Lower energy discharges did not affect the oscilloscope appreciably so in those cases the lifetimes are somewhat more accurate. The lifetime was studied as a function of the atmospheric spark gap spacing, the discharge potential, the capacitance and the inductance.
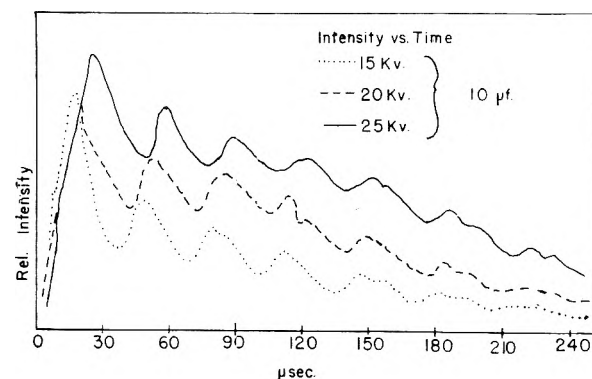


Fig. 5.—Variation of intensity of the flash with time.

Variation of the spacing in the atmospheric spark gap had no effect on the lifetime of the discharge within the limitations cited above. On the other hand an increase in the discharge potential caused an increase in the lifetime. This effect is apparent qualitatively in Fig. 5. To show it more clearly some of the data are plotted in Fig. 6. The variation seems to be essentially linear. Increase in

capacitance at a fixed voltage showed the variation in lifetime given in Fig. 6. Similar results were obtained at other voltages. In order to determine the effect of inductance on the lifetime a coil of No. 10 braided wire was wound on a glass cylinder six and one-half inches in diameter and thirty inches long. A lead was soldered on the coil every three inches so that various amounts of inductance could be used. This inductance is $L_{12}$ in Fig. 1. The resistance of the coil was less than 0.05 ohm and the total inductance at one kilocycle/second was 1.05 mh. With a discharge rate of four times per minute the coil became only slightly warm to the touch. On theoretical grounds it may be expected that the lifetime will be proportional to the inductance and inversely proportional to the resistance. The experimentally observed variation with inductance is shown in Fig. 7. The curvature is probably caused by the non-ohmic character of the spark gaps. To test the effect of added resistance 6.8 ohms was inserted in the circuit which also contained 1.05 mh. of inductance and it was found that the lifetime was reduced from 2.4 milliseconds to a few tenths of a millisecond in accordance with expectations. Under such conditions the light yield is reduced since a considerable amount of the energy which might be radiated is dissipated as heat in the resistance.



Fig. 7.—Duration of the discharge as a function of the inductance in the circuit.
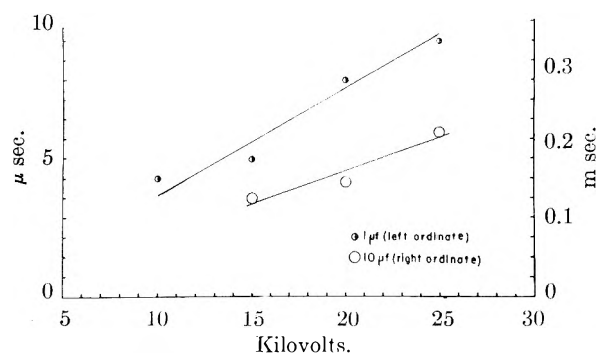


Fig. 6.—Duration of the discharge as a function of the discharge potential.

The curves in Fig. 5 show that the intensity varies over a wide range during any given flash. However, each flash can be characterized by an average intensity which we shall define as the quantum output per flash divided by the lifetime as defined above. An exact value for the quantum output cannot be obtained from our actinometer measurements because we do not know the distribution of energy among the lines in the spectrum of the flash and the quantum yield of the ferrioxalate reaction depends to some extent on the wave length. For purposes of discussion we will assume that the only light which affected the actinometer is that in the doublet at 2800 Å. The error involved cannot be more than 5%. For this wave length Parker reports a quantum yield of 1.23 (the next strongest lines which might be effective, at 3830 Å., give a quantum yield about 1.13). On the basis of this value and the values of the extinction coefficient of the ferrous–orthophenanthroline complex and the length of the absorption cell used in the analyses, we can calculate quantum output from our actinometer measurements. We
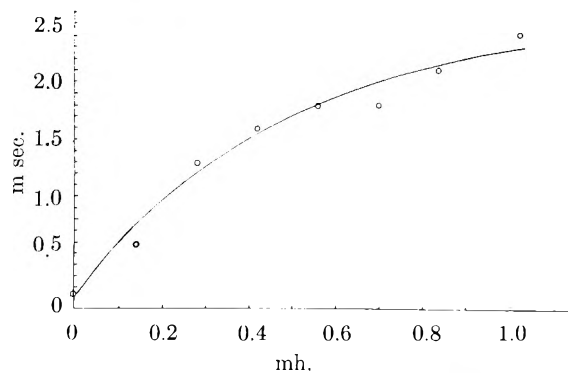
find $8.7 \times 10^{18}$ times the optical density observed. This leads to an average intensity of $8.7 \times 10^{21}$ times the ratio of the optical density to the lifetime in milliseconds. The maximum average intensity observed was approximately $10^{21}$ quanta per second in our 100-cc. reaction vessel. This value is less by a factor of approximately one hundred than the values given by Knox, Norrish and Porter.[9] However, their flashes gave light of a continuous spectrum and the intensities they quote are for the entire range of frequencies. Such conditions are satisfactory when the object is to produce the maximum number of radicals but they are not suitable for the study of effects which depend on the wave length of the light absorbed. Furthermore, since their flashes were of longer duration than ours the total energy put into the absorbing gas per flash was so much higher that it caused disturbing rises in temperature unless an inert gas were present in relatively large amount. In photolysis experiments with our apparatus we have never had any evidence of a significant temperature rise. Each apparatus has its advantages for particular purposes. We believe that ours is particularly suited for the study of reactions in which the results are dependent on temperature or frequency or both.

We have studied the average intensity as a function of discharge potential, capacitance and inductance. Variation of the first two produced no significant effect as might be predicted from the data presented in the previous paragraphs. The variation of intensity with inductance is shown in Fig. 8. It is apparent that when it is desirable to vary the intensity this can be done easily by varying the inductance.

**Photolysis with the High Intensity Spark.—** Acetaldehyde was chosen for the first experiments with the source just described because this substance has been the subject of extensive investigations at low light intensities. The adsorption of light causes a molecule to decompose by either of two paths

$$CH_3CHO + h\nu \longrightarrow CH_4 + CO \qquad (a)$$
$$CH_3CHO + h\nu \longrightarrow CH_3 + CHO \qquad (b)$$
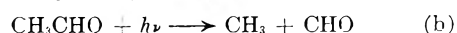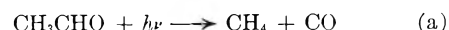
The quantum yield of (a) increases relative to that for (b) as the wave length is decreased. The

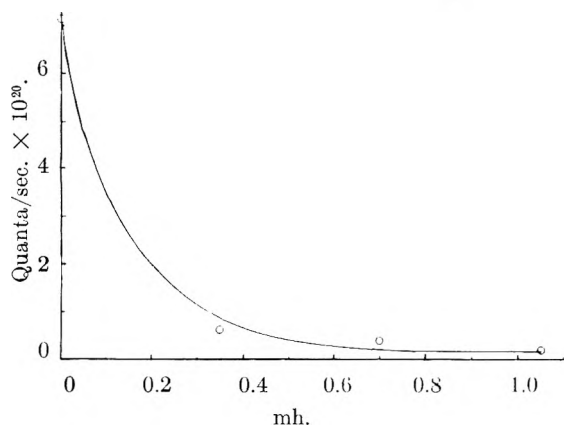(9) K. Knox, R. G. W. Norrish and G. Porter, J. Chem. Soc., 1477 (1952).

Fig. 8.—Average intensity of the discharge as a function of the inductance.

principal products of the reactions[10] are methane and carbon monoxide with small amounts of other substances such as biacetyl. At room temperature with the usual intensities it has not been possible to find ethane with a mass spectrometer. At temperatures exceeding 100° some ethane has been reported on the basis of mass spectrometer analyses.[11] On the other hand Kahn, Norrish and Porter[2b] found considerable quantities of ethane produced by their high intensity gas discharge.

Acetaldehyde was photolyzed under the two extremes of average intensity given by the data in Fig. 8. The highest and lowest intensities differed by a factor of thirty. Mallinckrodt acetaldehyde was used without further purification. Some of the liquid was put into a side tube on the portable vacuum system, cooled by a Dry Ice–acetone bath, and evacuated. When the permanent gas pressure, as read by a McLeod gage protected by a liquid nitrogen trap, read less than 10⁻⁵ mm. the reaction vessel and the side tube were cut off from the rest of the system and the Dry Ice–acetone bath removed. When the pressure in the reaction vessel was about 20 cm., as shown by a manometer attached to the system, the reaction vessel was cut off from the supply and subjected to the light from the desired number of discharges. The excess acetaldehyde and the photolysis products were toeplered out of the reaction vessel into a bulb for transfer to a more conveniently located vacuum system.

The gas mixture from the reaction vessel was passed three times through a glass spiral kept at the melting point of ethyl bromide. This removed most of the excess acetaldehyde. The uncondensed gas was pumped into a bulb and analyzed by means of a mass spectrometer. The total amount of gas was not determined accurately but was, in general, less than 0.003 cc. at STP. Since the total amount of gas was not determined the amounts of the various products are given relative to the carbon monoxide. The data are collected in Table I. The results obtained with no inductance are those for high intensity, those with inductance for low.

(10) F. E. Blacet and J. N. Pitts, *J. Am. Chem. Soc.*, **74**, 3382 (1952). This paper contains references to essential earlier work.

(11) C. J. Danby, A. S. Buchanan and I. H. S. Henderson, *J. Chem. Soc.*, 1426 (1951).

### TABLE I

#### ACETALDEHYDE PHOTOLYSIS PRODUCTS
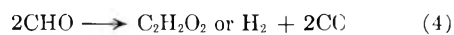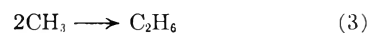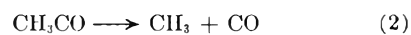
20 kilovolts; 10 μf.; no inductance
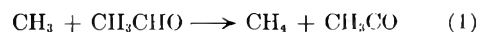
| No. discharges | CH₄/CO | C₂H₆/CO | CH₄/H₂ | CH₄/C₂H₆ |
|---|---|---|---|---|
| 50 | 0.51 | 0.32 | 4.1 | 1.6 |
| 100 | .54 | .28 | 4.7 | 1.9 |
| 200 | .55 | .34 | 4.2 | 1.6 |
| 300 | .54 | .34 | 4.5 | 1.6 |
| 300 | .55 | .31 | 4.3 | 1.8 |
| 50 | .48 | .30 | 4.2 | 1.6 |
| 100 | .49 | .30 | 4.4 | 1.6 |
| 100 | .51 | .33 | 4.6 | 1.6 |
| 100 | .49 | .31 | 4.5 | 1.6 |
| 100 | .51 | .32 | 4.6 | 1.6 |
| 100 | .52 | .39 | 4.1 | 1.4 |
| Av. | .52 | .32 | 4.4 | 1.6 |
| Av. dev. | .02 | .02 | 0.2 | 0.07 |

20 kilovolts; 10 μf.; 1.05 mh. inductance

| No. discharges | CH₄/CO | C₂H₆/CO | CH₄/H₂ | CH₄/C₂H₆ |
|---|---|---|---|---|
| 100 | 0.59 | 0.34 | 6.3 | 1.8 |
| 300 | .50 | .28 | 6.6 | 1.8 |
| 200 | .46 | .27 | 5.6 | 1.7 |
| 300 | .44 | .26 | 6.7 | 1.7 |
| 300 | .48 | .28 | 5.0 | 1.8 |
| Av. | .49 | .29 | 6.0 | 1.8 |
| Av. dev. | .04 | .02 | 0.6 | 0.04 |

The results show that the methane/ethane ratio is essentially independent of the intensity of the light when this intensity is varied about thirty-fold. Our value for this ratio, 1.6, is lower than that reported by Kahn, Norrish and Porter, which was 2.2. This difference is almost certainly caused by the difference in the light sources. Their source gave a continuous spectrum which extended to shorter wave lengths than the 2800 Å. available with ours and at these wave lengths the direct production of methane is favored which results in the higher ratio.

In order to compare our results with what might be expected on the basis of previous work it is necessary to consider the probable mechanism of the reaction, especially with reference to the fate of the radicals produced according to reaction (b) above. The most commonly assumed reactions of this type are

$$CH_3 + CH_3CHO \longrightarrow CH_4 + CH_3CO \quad (1)$$

$$CH_3CO \longrightarrow CH_3 + CO \quad (2)$$

$$2CH_3 \longrightarrow C_2H_6 \quad (3)$$

$$2CHO \longrightarrow C_2H_2O_2 \text{ or } H_2 + 2CO \quad (4)$$

$$CH_3 + CHO \longrightarrow CH_3CHO \text{ or } CH_4 + CO \quad (5)$$

The second reaction is believed to require somewhat elevated temperatures to be significant; at room temperature these radicals combine with each other and thus account for the biacetyl which has been reported as a product. The important competition for methyl radicals is between reactions (1) and (3). The latter is supposed to proceed at every collision but reaction (1) requires an activation energy which has been estimated by various in-

vestigators at from 7.5 to 10.7 kcal.[12-18] The ratio of the rates of (1) and (3) is given by $k_1(CH_3CHO)/k_3(CH_3)$. If it is assumed that the only difference between $k_1$ and $k_3$ is the exponential factor including the energy of activation of (3) the ratio of the rates can be calculated if we can estimate the concentration of methyl radicals The latter can be estimated by equating the rate at which light quanta are supplied to the rate of combination of the radicals. We have stated that the maximum number of quanta put into the reaction vessel per second was $10^{21}$, since the volume of the vessel was 100 cc. this is $10^{22}$ per liter. At the pressures used about half of this light is absorbed by the acetaldehyde and of that about one-sixth, according to Blacet and Loeffler,[15] produces methyl radicals. It follows that the rate of production of methyl radicals is 0.0016 mole per liter per second. Combined with the value of $k_3$ given by Gomer and Kistiakowsky[12] as $4.5 \times 10^{10}$ this rate gives a steady-state concentration of methyl radicals of $2 \times 10^{-7}$ mole per liter. Since the concentration of acetaldehyde is approximately 0.01 mole per liter the ratio of the rates of (1) and (3) can be calculated on the assumption stated above and we find that it must lie between 0.2 and 0.001, depending on what value is selected for the activation energy of (1). Actually if (1) proceeds like other hydrogen abstraction reactions it can be expected to have a steric factor of the order of 0.001, which would reduce the values just given by that factor. Under such conditions reaction (1) does not proceed to an appreciable extent in the experiments with high intensity so the possibility of the formation of methane in that way can be neglected.

The remaining possibilities for the formation of methane are reactions (a) and (5) although the latter may be simply the recombination of the radicals. If we assume that there is no formation of methane by (5) the methane/ethane ratio is given by

$$(CH_4)/(C_2H_6) = 2\phi_a(1 + k_5/(k_3k_4)^{1/2}/\phi_b) \qquad (1)$$

On the other hand if methane is considered to be formed by (5) the ratio is

$$(CH_4)/(C_2H_6) = 2(\phi_a + \phi_b/(1 + (k_3k_4)^{1/2}/k_5)$$
$$(1 + k_5/(k_3k_4)^{1/2})/\phi_b) \qquad (2)$$

The values for $\phi_a$ and $\phi_b$ have been given by Blacet and Loeffler[15] as 0.17 and 0.43, respectively, for a

(12) R. Gomer and G. B. Kistiakowsky, *J. Chem. Phys.*, **19**, 85 (1951).

(13) D. H. Volman and R. K. Brinton, *ibid.*, **20**, 1764 (1952).

(14) R. E. Dodd, *Trans. Faraday Soc.*, **47**, 56 (1951).

(15) F. E. Blacet and D. E. Loeffler, *J. Am. Chem. Soc.*, **64**, 893 (1942).

(16) D. C. Grahame and G. K. Rollefson, *J. Chem. Phys.*, **8**, 98 (1940).

(17) J. Leermakers, *J. Am. Chem. Soc.*, **56**, 1537 (1934).

(18) E. I. Akeroyd and R. G. W. Norrish, *J. Chem. Soc.*, 890 (1936).

wave length of 2804 Å., which is essentially what we are using. If we substitute these values in equation 1 above and assume that reactions (3), (4) and (5) proceed at every collision the methane/ethane ratio is found to be 1.6 in agreement with our results. With the same assumptions equation 2 gives 3.6 for the ratio. The constants $k_3$, $k_4$ and $k_5$ are most likely to be equal if they correspond to combinations of pairs of radical. If $k_5$ corresponds to the alternative process which forms methane and carbon monoxide it is apt to be smaller than the other two constants for two reasons. In the first place, such a reaction involves the breaking of a bond and is apt to have an energy of activation. Second, Steacie has found that hydrogen abstraction reactions usually have a steric factor such that only about one collision in a thousand of those with the necessary activation energy results in reaction. In any case $k_5$ is not going to be larger than $k_3$ or $k_4$ and may be much smaller. If we assume the latter to be true the ratio calculated by equation 2 becomes 0.79. Our experimental value of 1.6 is obtained if the ratio $(k_3k_4)^{1/2}/k_5 = 3.4$. The corresponding value for $k_5$ seems much too high for a reaction which involves the breaking of a bond. Therefore we believe that reaction 5 is principally a recombination of the radicals to form acetaldehyde.

The agreement cited above between the value of the methane/ethane ratio calculated from the results summarized by Blacet and Pitts and our experimental value must be considered somewhat fortuitous since the mass spectrometer analyses are not as accurate as the agreement would imply. On the other hand, the approximate constancy over the thirty-fold variation in intensity plus this agreement is strong support for the idea that the intensities we are using are so high that practically all the methyl radicals react to form ethane. If the slight increase in the ratio at low intensities is considered to be real, it corresponds to about 5% of the methyl radicals reacting with acetaldehyde according to reaction (1). On this basis it may be estimated that reaction (1) would compete with (3) in a measurable way if the light intensity were reduced to about $10^{19}$ quanta per liter per second. Our apparatus is not adaptable to such low intensities, hence its usefulness in studying the competition between (3) and other reactions of methyl radicals is limited to those cases in which the other reaction is faster than (1).

# THE DIAMAGNETIC SUSCEPTIBILITIES OF METHANE AND THE AMMONIUM ION

By K. A. VENKATACHALAM AND M. B. KABADI

*Institute of Science, Bombay, India*

Coulson's calculations for the diamagnetic susceptibility of methane,[3] based on electron pair method, have now been modified by including the ionic part of the wave function. The value $0.40 \times 10^{-18}$ e.s.u. has been used for the C–H bond moment. The value so obtained has been shown to be in better agreement with experiment, than any previously calculated value. Similar calculations have been made for the ammonium ion also, and the result obtained agrees fairly well with the experimental value.

A few attempts have been made to calculate the diamagnetic susceptibilities of molecules from purely theoretical considerations, in the case of spherically symmetrical systems such as methane and the ammonium ion, where the "temperature independent term" of Van Vleck's equation[1] can be neglected. Buckingham, Massey and Tibbs[2] and Coulson[3] have calculated the diamagnetic susceptibility of methane, while Hartmann[4] has calculated the susceptibilities of both methane and the ammonium ion. Buckingham, Massey and Tibbs have used the self consistent field method of Hartree. Coulson has employed the molecular orbital and electron pair wave functions. Hartmann has treated methane and $NH_4^+$ quantum mechanically as pseudo neon atoms using a method similar to the Slater method for atoms. Their results are given below.

| Method | Value $\chi_{mol}$ $\times 10^6$, e.m.u. | Substance |
|---|---|---|
| Self consistent field method | −33.2 | Methane |
| Molecular orbital method | −26.6 | Methane |
| Electron pair method | −27.7 | Methane |
| Pseudo neon approximation | −27.4 | Methane |
| Experimental (Bitter[5]) | −12.2 | Methane |
| Pseudo neon approximation | −17.9 | $NH_4^+$ |
| Experimental (Trew[6]) | −13.3 | $NH_4^+$ |

It is seen that none of the methods gives a result anywhere approaching the experimental value either in the case of methane or the ammonium ion. The chief reasons are that the self consistent field method gives a too diffuse charge cloud, the m.o. method allows for ionicity but neglects exchange, the e.p. method allows for exchange but neglects ionicity, while the pseudo-neon atom approximation does not preserve the well known individuality of the C–H and N–H bonds in methane and ammonium ion, respectively. In this paper an attempt has been made to modify the calculations based on the electron pair method, because the description of the chemical bond based on the electron pair treatment, resembles closely the picture of a bond, visualized as formed by the sharing of the electrons of the atoms between which the bond is formed.

A full description of a chemical bond such as the C–H bond, on the electron pair method, requires a knowledge of the relative importance of the covalent and ionic parts of the wave function. In this case we have to consider the structures $> C—H$, $> \overset{-}{C} \overset{+}{H}$ and $> \overset{+}{C} \overset{-}{H}$. Since the wave function corresponding to the structure $> \overset{+}{C} \overset{-}{H}$, has energy much greater than either the covalent or the $> \overset{-}{C} \overset{+}{H}$ wave functions,[7] we may, to a first approximation, neglect the structure $> \overset{+}{C} \overset{-}{H}$, and write for the unnormalized wave function of the bond

$$\Psi_{(C–H)} = \Psi_{cov} + \lambda \Psi_{ion}$$

where

$$\Psi_{cov} = N_c[\Psi_{(C:1)}\Psi_{(H:2)} + \Psi_{(C:2)}\Psi_{(H:1)}]$$

$$\Psi_{ion} = \Psi_{(C:1)} \Psi_{(C:2)}$$

and $\psi_{(C)}$ is the $sp^3$ hybrid wave function of carbon, viz.

$$\Psi_{(C)} = \frac{1}{2} \Psi_{(C:2s)} + \frac{\sqrt{3}}{2} \Psi_{(C:2p)}$$

$N_c$ is a normalizing constant so chosen that

$$\int \Psi^2_{cov} \, d\tau_1 \, d\tau_2 = 1$$

and 1 and 2 refer to the electrons forming the bond C–H.

Coulson[3] has neglected the ionic part of the wave function, in his calculations of the diamagnetic susceptibility of methane using the electron pair method. A knowledge of the value of $\lambda$ is required, if this is to be included. The most direct way to determine the value of $\lambda$ is to use the dipole moment of the bond.

If we denote by $x$ the coördinate of any electron in the C–H bond measured from C in the direction C → H, and if $\rho$ is the internuclear distance, the centroid of the negative charge is at a distance $\bar{x}$ from the carbon atom, where

$$\bar{x} = \frac{\int x_{(1)}\Psi^2_{(C–H)} d\tau_1 d\tau_2}{\int \Psi^2_{(C–H)} d\tau_1 d\tau_2}$$

$$= \frac{\bar{x}_{cov} + 2\lambda \bar{x}_{ci} + \lambda^2 \bar{x}_{ion}}{1 + 2\lambda S_{ci} + \lambda^2}$$

$$\bar{x}_{cov} = \int x_{(1)} \Psi^2_{cov} \, d\tau_1 \, d\tau_2$$

$$\bar{x}_{ci} = \int x_{(1)} \Psi_{cov}\Psi_{ion} d\tau_1 d\tau_2$$

$$\bar{x}_{ion} = \int x_{(1)} \Psi^2_{ion} d\tau_1 d\tau_2$$

$$S_{ci} = \int \Psi_{ion}\Psi_{cov} d\tau_1 d\tau_2$$

The centroid of the positive charge is at the geometric center of the bond, i.e., at a distance $\rho/2$ from the carbon nucleus and so the resultant moment of the bond is now

$$\mu = 2e(\bar{x} - \rho/2)$$

(1) J. H. Van Vleck, "The Theory of Electric and Magnetic Susceptibilities," Clarendon Press, Oxford, 1932, p. 275.

(2) R. A. Buckingham, H. S. W. Massey and S. R. Tibbs, *Proc. Roy. Soc. (London)*, **A178**, 119 (1941).

(3) C. A. Coulson, *Proc. Phys. Soc. (London)*, **A54**, 51 (1942).

(4) H. Hartmann, *Z. Natur.*, **IIA**, 489 (1947).

(5) F. Bitter, *Phys. Rev.*, **33**, 389 (1929).

(6) V. C. G. Trew, *Trans. Faraday Soc.*, **37**, 476 (1941).

(7) C. A. Coulson, *ibid.*, **38**, 433 (1942).

If now $\mu$ is known, $\bar{x}$ and so $\lambda$ can be calculated, provided $\bar{x}_{cov}$, etc., are known.

Calculations based on the molecular orbital method by Coulson[7] show that $\mu$ for the C–H bond is $0.40 \times 10^{-18}$ e.s.u. and that the direction of polarity is $\overset{+}{C}\overset{-}{H}$. A review of the polarity of the C–H bond by Gent[8] shows that most of the recent evidence is in favor of a polarity directed from C → H, viz., $\overset{+}{C}\overset{-}{H}$ of magnitude $0.40 \times 10^{-18}$ e.s.u. Accepting this value, we get $\bar{x} = 1.109$ ($\mu$ is positive) using $\rho = 2.06$ atomic units. The values of $\bar{x}_{cov}$, etc., can be obtained using $\rho = 2.06$ and the table of integrals supplied by Coulson.[9] They are

$\bar{x}_{cov} = 1.473$        $\bar{x}_{ci} = 0.8529$

$\bar{x}_{ion} = 0.6993$        $S_{ci} = 0.7602$

These values are slightly different from those reported by Coulson,[7] who uses for $\rho$ the value 2.0 atomic units. In this communication the value $\rho = 2.06$ atomic units has been employed. $\beta$ has been taken to be 1.1 and $\alpha = 1.625$

The value of $\lambda$ thus obtained is 0.9672.

The value of $\lambda$ is generally considered to indicate the percentage ionic character of the bond, the percentage ionic character being given by the expression

$$\% \text{ ionic character} = 100\lambda^2/(1 + \lambda^2)$$

The C–H bond thus appears to be equally as ionic as it is covalent. Such a conclusion regarding the percentage ionic character of the C–H bond does not seem to be strictly valid, as can be shown below.

If we define

$$\% \text{ ionic character} = \mu_{(C-H)}/\mu^*_{(C-H)} \times 100 \quad (1)$$

where

$$\mu_{(C-H)} = 2e(\bar{x} - \rho/2)$$

$$\mu^*_{(C-H)} = e\rho$$

equation 1 reduces to $\%$ ionic character $= 100\lambda^2/(1 + \lambda^2)$ provided

$$\int x_{(1)}\Psi_{(C:1)}\Psi_{(H:1)}d\tau_1 = 0$$

$$S = \int \Psi_{(C:1)}\Psi_{(H:1)}d\tau_1 = \int \Psi_{(C:2)}\Psi_{(H:2)}d\tau_2 = 0$$

and

$$\int x_{(1)}\Psi^2_{(C:1)}d\tau_1 = 0$$

($S$ is the overlap integral, and $\int x_{(1)}\Psi^2_{(C:1)} d\tau_1$ is the atomic dipole term.[7]) The values of these terms in the present case are 0.9854, 0.6378 and 0.6993, respectively; values which cannot be neglected in comparison with $\bar{x} = 1.109$. So, in such cases, the percentage ionic character can be interpreted only as $\mu_{(C-H)}/\mu^*_{(C-H)} \times 100$ and not as $100 \lambda^2/(1 + \lambda^2)$. Indeed, as Coulson points out, the ionic part of the wave function has here actually a covalent character in that the centroid of the negative charge is shifted by this function toward the atom using the hybrid orbital.

The wave function of the C–H bond may, therefore, be written as

$$\Psi_{(C-H)} = N'[\Psi_{cov} + 0.9672\Psi_{ion}]$$

where $N'$ is the new normalizing constant. Using this expression for $\Psi_{(C-H)}$ in the equation

(8) W. L. G. Gent, Quart. Rev., 2, 383 (1948).
(9) C. A. Coulson, Proc. Cambridge Phil. Soc., 38, 210 (1942).

$$\bar{r}_1^2 = \frac{\int r_1^2\Psi^2_{(C-H)}d\tau_1}{\int \Psi^2_{(C-H)}d\tau_1}$$

we get $\bar{r}_1^2 = 3.314$, where $\bar{r}_1^2$ is the mean square radius of any electron forming the C–H bond, from carbon.

The mean square radius of each of the two 1s electrons is 0.092 (Coulson[3]).

Substituting these values in the Van Vleck's equation for the diamagnetic susceptibility of a molecule, and equating the second term to zero, because of spherical symmetry of the system, it is seen that

$$\chi_{mol} = -21.11 \times 10^{-6} \text{ e.m.u.}$$

It may be pointed out that if the polarity of the C–H bond is assumed to be in the direction $\overset{-}{C}\overset{+}{H}$, in accordance with the electronegativity difference between C and H, and the earlier views on the C–H bond polarity, the value of $\lambda$ comes out to be 2.04, but the value of

$$\chi_{mol} = -18.66 \times 10^{-6} \text{ e.m.u.}$$

Both these values are distinct improvements over those calculated so far. Although the value calculated assuming the direction of the C–H bond polarity to be $\overset{-}{C}\overset{+}{H}$, i.e., in the direction expected from the electronegativity difference between carbon and hydrogen, agrees more closely with the experimental value than the one where the polarity is taken to be in the direction $\overset{+}{C}\overset{-}{H}$, the data reviewed by Gent[8] regarding the direction of the C–H bond polarity does not permit us to draw a conclusion in favor of $\overset{-}{C}\overset{+}{H}$.

**Diamagnetic Susceptibility of the Ammonium Ion.**—Similar calculations were carried out for $NH_4^+$ also. The hydrogen atoms in $NH_4^+$ are arranged tetrahedrally around the nitrogen atom and the N–H bond is formed by the overlapping of the $sp^3$ orbital of N and the 1s orbital of hydrogen. For purposes of the calculations it is assumed that the positive charge is situated at the nitrogen atom, so that $N^+$ with 6 electrons combines with 4H atoms, each having one electron to form the ammonium ion.

A calculation similar to that carried out by Coulson,[3] neglecting the ionic part of the wave function, and using the values $\beta = 1$, $\alpha = 2.125$ and $\rho = 1.889$ atomic units, gives

$$\chi_{mol} = -24.89 \times 10^{-18} \text{ e.m.u.}$$

When the ionic part of the wave function is introduced into the calculations, the results obtained are as follows. $N^+$ is much more electronegative than carbon, and hence the ionic part of the wave function is $\Psi_{(N:1)}\Psi_{(N:2)}$. According to Pauling,[10] the percentage ionic character of the N–H bond is twenty, the polarity being in the direction $\overset{-}{N}\overset{+}{H}$. Using these values, the value of $\lambda$ is found to be 2.77, and that of

$$\chi_{NH_4^+} = -13.4 \times 10^{-18} \text{ e.m.u.}$$

This value appears to be in fairly good agreement with those of Trew.[6,11]

(10) L. Pauling, "Nature of the Chemical Bond," 2d ed., Cornell University Press, Ithaca, N. Y., 1940, p. 72.
(11) V. C. G. Trew, Trans. Faraday Soc., 45, 217 (1949).

# PHOTOCHEMICAL PRODUCTION OF HYDROGEN PEROXIDE CATALYZED BY MERCURIC SULFIDE[1]

By L. I. GROSSWEINER

*Chemistry Division, Argonne National Laboratory, Lemont, Illinois*

*Received February 24, 1955*

Visible light irradiation of suspended red mercuric sulfide in distilled water containing oxygen induces hydrogen peroxide formation, with no apparent change occurring to the mercuric sulfide. The data obey the following rate equation: $pt = (X_0 - X) + 2X_f \log_e [(1 - X_0/X_f)/(1 - X/X_f)]$, where $X_0$ and $X$ are the initial and instantaneous $H_2O_2$ concentrations in solution, respectively, $X_f$ is proportional to the HgS surface, $p$ is proportional to the light intensity and $t$ is the irradiation time. The proposed primary products are $HO_2$ and $OH$. It is suggested that the $HO_2$ is formed *via* the capture of conduction electrons from excited HgS by adsorbed $H^+$, in the presence of dissolved oxygen, and that the OH is formed by anodic discharge of adsorbed $OH^-$. The proposed rate-controlling processes are the desorption of $HO_2$ and the decomposition of $H_2O_2$ by $HO_2$ on the surface. It is consistent with the experimental results to assume that the OH recombines to water and oxygen.

## Introduction

To gain further understanding of the mechanism of chemical reaction induced by electrons in aqueous solutions, consideration was given to the production of excited electrons *in situ* by irradiation of a photoactive material suspended in the system. A frequent product of the irradiation of aqueous systems containing dissolved oxygen is hydrogen peroxide, and it is necessary that light longer than 400 mμ be used to prevent photochemical decomposition of the latter. Further, since $\Delta F°$ for the production of hydrogen peroxide from water and oxygen is 1.1 e.v., the longest possible wave length for exothermic reaction is about 1.1 μ. In our first experiments a photoactive suspension was combined with ferrous sulfate in 0.8 N sulfuric acid, a solution which has been used as a dosimeter with some success. This imposes the additional requirement that the photoactive material be insoluble in the acid. The substance chosen was red mercuric sulfide, whose threshold for photoconduction in air is 630 mμ.[2]

A brief summary of the previously reported experiments on the ferrous-ferric sulfate system will be given here.[3] In all experiments a rapidly stirred suspension of 2.0 g. of HgS in 20.0 cc. of solution at 18° was irradiated with an AH-6 mercury lamp. It was found that: (a) irradiation of initially 100% ferrous sulfate solution caused nearly complete oxidation to ferric ion with oxygen necessary for reaction, (b) irradiation of initially 100% ferric sulfate solution caused partial reduction to ferrous ion, and oxygen hindered but did not inhibit reaction, (c) the wave length threshold for reduction was found to be 600 mμ.

The above results are simply explained if it is assumed that the irradiation produces H and OH, the former causing the reduction of ferric ion, and that the formation of $HO_2$ with oxygen present accounts for the oxidation of ferrous ion. If this were the case, one might expect the irradiation of oxygenated distilled water to yield hydrogen peroxide. A description of the studies with oxygenated distilled water forms the major part of this paper.

(1) Based on work performed under the auspices of the U. S. Atomic Energy Commission. Presented in part at the Chicago 1954 meeting of the American Physical Society.

(2) B. Gudden and R. W. Pohl, *Z. Physik*, **2**, 361 (1920).

(3) L. I. Grossweiner and Sheffield Gordon, *J. Chem. Phys.*, **22**, 1139 (1954).

## Experimental

The irradiations were carried out in a water-cooled, double-wall Pyrex vessel of about 10-cc. capacity. The light entered at the bottom through a 2-mm. optical window. The saturating gas was bubbled in through a side tube which discharged near the bottom and exited similarly near the top. The suspension was rapidly stirred with a glass rod, and a gas-tight seal for the latter maintained a uniform atmosphere above the irradiated solution. The light source was a water-cooled AH-6 mercury lamp followed by a Corning #3385 filter to eliminate ultraviolet light. Merck C.P. mercuric sulfide was used with prior washing in hot 1 N sulfuric acid. The particle size under a microscope was 1 to 3 μ. Triply-distilled water was used to make up the solutions. The irradiated solutions were analyzed by filtering the suspension on Whatman No. 2 paper and measuring the hydrogen peroxide content of the filtrate, spectrometrically, using the method developed by Ghormley.[4]

## Results

**Dark Adsorption.**—When oxygen-saturated hydrogen peroxide solutions are stirred with mercuric sulfide under the experimental conditions, the concentration in the solution decreases. Washing of the powder showed that the loss was entirely due to adsorption. This small loss, less than 10% in an hour, is a linear function of the initial concentration and increases slowly with time of contact. 1.0 N $H_2SO_4$ and 0.1 N NaOH showed no appreciable difference from distilled water.

**Hydrogen Peroxide from Distilled Water.** (a) **Dose–Yield Curves.**—The yield of hydrogen peroxide as a function of irradiation time for varying HgS concentration and light intensity is shown in Fig. 1 (circled points). The incident light intensity $I_0$ is approximately $3 \times 10^{17}$ photons per second.

(b) **Initial Yield.**—The variation of the initial rate of yield of hydrogen peroxide formation with light intensity was measured using Bausch and Lomb neutral density filters. The summarized data in Table I show that the initial yield is linear with light intensity over a 17-fold range in intensity.

(c) **Wave Length Dependence.**—The variation of the initial yield with wave length was measured with a series of Corning cut-off filters. The total light energy transmitted by the filters had been previously determined with a calibrated Eppley thermopile. The yield as a function of the "cut" of each filter used is shown in Fig. 2. The extrapolated threshold for reaction is 615 mμ.

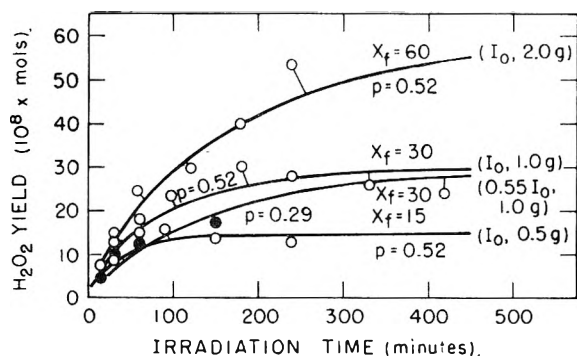(4) J. A. Ghormley, THIS JOURNAL, **56**, 587 (1952).

Fig. 1.—Comparison of data with theory for hydrogen peroxide yield from pure water; oxygen-saturated solutions at 18°, #3385 filter.

**(d)  Repeated Irradiation of Sample.**—A 1-g. sample of HgS was irradiated for successive 60-min. intervals in fresh samples of distilled water. The total accumulated yield is a linear function of the accumulated irradiation time. The linearity indicates that the limiting factor in the hydrogen peroxide yield is not a permanent chemical or physical change of the mercuric sulfide. A comparison of the optical absorption spectrum and electrical conductivity of the filtrate after blank and irradiation experiments showed no detectable concentration of ionic product due to the light. However, in view of the small $H_2O_2$ yield, about one part per million, it cannot be stated that decomposition of the HgS does not occur to this extent, although even this small amount of decomposition appears quite unlikely.

TABLE I

EFFECT OF LIGHT INTENSITY ON INITIAL YIELD OF HYDROGEN PEROXIDE[a]

| Relative transmission ($I$) | Duration of run (min.) ($t$) | $H_2O_2$ yield ($\mu$m/l.) | Yield ÷ ($I \times t$) |
|---|---|---|---|
| 1.000 | 15 | 11.0 | 0.73 |
| 0.500 | 30 | 10.2 | .68 |
| .250 | 67 | 9.6 | .57 |
| .125 | 120 | 12.0 | .80 |
| .0625 | 230 | 8.7 | .61 |
| | | | 0.68 ± 0.07 |

[a] Oxygen-saturated solutions, 0.1 g. HgS/cc., #3385 filter.

**(e)  Effect of Oxygen Pressure.**—The yield from solutions irradiated for 1 hr. under similar conditions, except that the saturating gas was helium, air and oxygen, was 3.1, 13.8 and 22.6 $\mu$m/l., respectively. The low yield with helium is due to either adsorbed oxygen on the powder which is not removed by continued washing with helium or perhaps to a mechanism not requiring oxygen. In either case, this is sufficiently small to be disregarded for our purposes. We conclude that oxygen is necessary for the major mechanism of hydrogen peroxide production from water.

**Effect of $pH$ on Hydrogen Peroxide Yield.**—A series of experiments was made on the yield of hydrogen peroxide from oxygen-saturated solutions of sulfuric acid and sodium hydroxide in triply-distilled water, and the results are shown in Table II. The yield after 60 min. increases markedly with increasing $pH$.
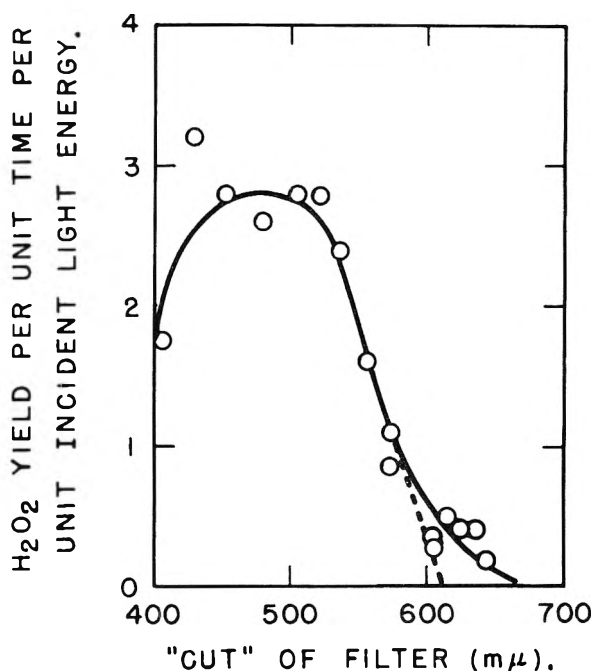


Fig. 2.—Variation of hydrogen peroxide yield from pure water with wave length of incident light; oxygen-saturated solutions at 18°, 0.1 g. HgS/cc.

**Irradiation of Hydrogen Peroxide Solutions.**—A series of hydrogen peroxide solutions was irradiated for constant time under constant conditions, and the net changes as a function of initial concentration are shown as experimental points in Fig. 3. There is a net increase in the amount of hydrogen peroxide for low initial concentrations and a net decrease for high initial concentrations, the $H_2O_2$ concentration at the crossover being approximately equal to the maximum yield for initially pure water.

TABLE II

EFFECT OF $pH$ ON HYDROGEN PEROXIDE YIELD[a]

| Solution | Yield ($\mu$m./l.) | Solution | Yield ($\mu$m./l.) |
|---|---|---|---|
| 0.8 $N$ $H_2SO_4$ | 3.4 | Triply-distilled | |
| 0.08 $N$ $H_2SO_4$ | 4.9 | $H_2O$ | 18 |
| 0.008 $N$ $H_2SO_4$ | 11.0 | 0.01 $N$ NaOH | 34.4 |
| | | 0.1 $N$ NaOH | 50.5 |

[a] Oxygen-saturated solutions, 0.1 g. HgS/cc., 60-min. runs, #3385 filter.

**Discussion**

A reasonable mechanism for the production of $H_2O_2$ in these experiments is the reaction with the solution of radicals formed on the HgS surface by irradiation. A simple kinetic scheme which leads to satisfactory results is the first-order production of $H_2O_2$ from radicals and a bimolecular back-reaction of the radicals with the $H_2O_2$ product. The corresponding rate equation is

$$(dX/dt) = k_1R - k_2RX \qquad (1)$$

where $R$ is the total number of radicals in the system per unit volume of solution and $X$ is the volume concentration of $H_2O_2$ product. We note that the rate constants $k_1$ and $k_2$ can vary with the total active surface $S$. The linearity of initial yield with light intensity (Table I) suggests that the radical
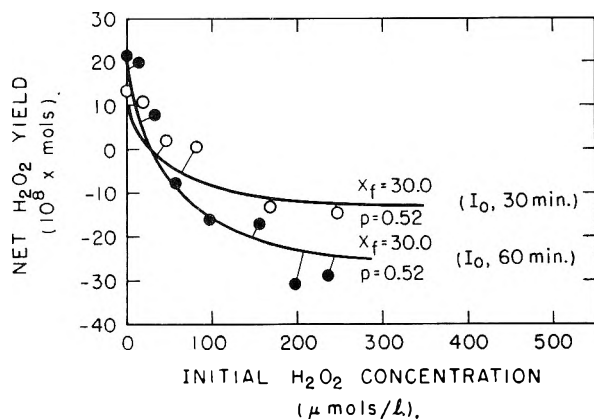
Fig. 3.—Comparison of data with theory for hydrogen peroxide yield from initial hydrogen peroxide solutions; oxygen-saturated solutions at 18°, #3385 filter, 0.1 g. HgS/cc.

concentration is in equilibrium with the incident light, so that

$$qI = k_1R + k_2RX \qquad (2)$$

where $q$ is the efficiency of radical production and $I$ is the light intensity. Integration with $k' = k_1/k_2$ gives

$$qIt = (X_0 - X) - (2/k') \log_e (1 - k'X)/(1 - k'X_0)] \qquad (3)$$

where $X_0$ is the initial product concentration.

First consider the case where $X_0 = 0$. The final product yield is equal to $X_f = (1/k')$ which is independent of light intensity. The initial rate of yield, which is designated by $p$, is numerically equal to $qI$. This gives

$$pt = -X - 2X_f \log_e (1 - X/X_f) \qquad (4)$$

Comparison to eq. 4 with the experimental data on Fig. 1 shows that the equation fits the data if $X_f$ is proportional to $S$. Using $p = 0.52$ and $X_f = $ (30.0 times the weight of HgS in grams), actually determined from one experimental curve, gives the solid lines for $I_0$. The lower intensity run uses $p = 0.55 \times 0.52 = 0.29$, based on the experimental light intensity of $0.55I_0$, and $X_f = 30$.

Now consider the case where various initial product concentrations are irradiated for constant time. Letting the net yield: $(X - X_0) = \beta$ gives

$$X_0 = X_f - \frac{\beta}{1 - \exp\left[-(^1/_2 X_f)(pt + \beta)\right]} \qquad (5)$$

where $p$ and $X_f$ are the parameters for the case where $X_0 = 0$. The solid lines in Fig. 3, plotted with the same parameters as above in eq. 5 agree satisfactorily with the data.

The assumption of $X_f$ linear with $S$, which makes these equations agree with the experimental HgS surface dependence, arises from a back-reaction term in eq. 1 of the form: const. $RX/S$. This does not correspond to a simple destruction of radicals by adsorbed product, since this would be described by: const. $(R/S)XS$, where one assumes that the amount of adsorbed product is proportional to $X$ and $S$. The required $S$-dependence of eq. 1 is consistent with photoactivated adsorption, which has been shown to occur for red HgS,[5] but in this case

(5) J. A. Hedvall and S. Nord, Z. Elektrochem., 49, 467 (1943),

one would expect an increase in the maximum yield $X_f$ with decreasing light intensity, which is not in agreement with the experiments. In fact, a process that would be qualitatively consistent with the data is an adsorption which decreases at higher light intensity, followed by destruction of radicals by adsorbed product. Although a diminished adsorption due to electrical changes occurring under irradiation is not inconceivable, the data give no information on such a process and the rate equations must be considered as empirical.

The initial yield data of Table I leads to an efficiency of $4 \times 10^3$ photons incident per $H_2O_2$ molecule. The data do not permit a unique calculation of the rate constants.

The conclusion drawn from the experimental data is that hydrogen peroxide is formed from water and oxygen. The heat of the reaction is $-1.0$ e.v., and for the minimum light energy adsorbed by HgS of 2.0 e.v., the over-all reaction is exothermic by at least 1.0 e.v. It is highly probable that the $H_2O_2$ is formed from the $HO_2$ intermediary. This latter can arise by either direct H-atom production from water or from electron capture by $O_2$ giving $O_2^-$. It appears that this latter case is less likely because: (a) the reduction of $Fe^{+++}$ proceeds in oxygen-free solutions, and the only possible explanation, excluding H-atom formation, is direct electron capture by 400 mmolar $Fe_2(SO_4)_3$ in 0.8 $N$ $H_2SO_4$; and (b) the kinetic mechanism obeyed by the data is more appropriate for direct H and OH production. Now, if this is the case, it requires 5.2 e.v. to break the H..OH bond in water so that the sum of the energies of the primary reactions must be endothermic by about 3 e.v.[6] We will describe a possible reaction scheme in which an endothermic primary reaction will not entirely inhibit the forward reaction.

The coincidence of the wave length thresholds for this reaction and photoconduction in HgS crystal suggests that the first step upon light absorption is the promotion of conduction electrons. The energy required to remove a conduction electron is the "electron affinity" of HgS crystal, about 4 e.v. (see Appendix). However, corresponding to each conduction electron there is a positively-charged site on the particle surface. The capture of an external electron at this site would return not only the electron affinity, $W$, but also the inner work-function, 2.0 e.v. It is this primary process that is less endothermic and probably occurs first. Either $H_2O$ or $OH^-$ can discharge the positive site, but the latter is more likely as: (a) it requires less energy, and (b) the observed reaction rate increases with increasing $p$H. This reaction may be written as

$$(\text{HgS})^* + OH^- (\text{aq}) \longrightarrow (\text{HgS})^- + OH (\text{ad}) \qquad (6)$$
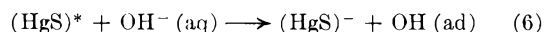
where the (HgS) signifies that a 1–3 $\mu$ HgS particle is involved and the * indicates a HgS crystal with optically-excited conduction electrons. The heat of this reaction is: $W + E_{OH} - 4.4$ e.v.; $E_{OH}$ is the adsorption energy of OH on HgS, about 0.2 e.v. (see Appendix), and the use of 4.0 e.v. for $W$ gives a value of $-0.2$ e.v. It appears that this reaction would proceed at room temperature.

(6) The thermochemical data for this paper were taken mostly from: N. Uri, Chem. Revs., 50, No. 3, 375 (1952).

However, the accumulation of negative charge on the HgS particles would rapidly inhibit further reaction by the repulsion of $OH^-$. We must postulate a corresponding electron transfer, most probably to $H^+$. This may be written as

$$(HgS)^- + H^+(aq) \longrightarrow (HgS)^0 + H(ad) \qquad (7)$$
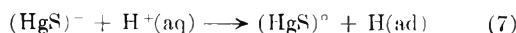
The heat of reaction is approximately $1.2 + E_H - W$ e.v., where $E_H$ is less than 0.01 e.v. and will be neglected (see Appendix). (In this calculation the full hydration energy of $H^+$ was used, 12.3 e.v., since the actual polarization energies of the HgS and water media are not known.) The use of 4.0 e.v. for $W$ gives a reaction that is endothermic by 2.8 e.v. and would scarcely proceed at room temperature. However, if we assume that the negative charges on the crystal are stabilized by adsorption of $H^+$, then the effect of these charges in inhibiti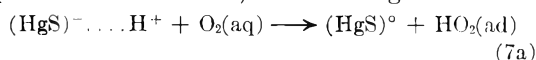ng reaction (6) will be small and the latter could proceed. Now, there is a constant concentration of dissolved oxygen in solution and when an $O_2$ molecule approaches a bound $H^+$, the following could occur

$$(HgS)^-\ldots H^+ + O_2(aq) \longrightarrow (HgS)^0 + HO_2(ad) \qquad (7a)$$

In this case the heat of reaction is $2.8 + E_{HO_2} - W$, and the use of 0.2 e.v. for $E_{HO_2}$ and 4.0 e.v. for $W$ gives $-1.0$ e.v. Again the full hydration energy of $H^+$ was used so that this is a maximum value. We suggest that eq. 6 and 7a are the primary reactions in this system. In the oxygen-free reduction of $Fe^{+++}$ it would be the latter which reacts with the bound $H^+$.

Following the formation of $HO_2$ on the surface, the subsequent reactions are the desorption and recombination near the surface to form $H_2O_2$. It is probably the former which is the rate-controlling first-order reaction in eq. 1.

We must consider the fate of the adsorbed $OH$ product from eq. 6. It most likely recombines to $H_2O$ and $O_2$ near the particle surface. This is preferred over the recombination to $H_2O_2$ because: (a) the former is more energetic by 1.2 e.v.; and (b) a net yield of $Fe^{+++}$ reduction in oxygen-free solution is not possible if $OH$ recombines to form $H_2O_2$ or reacts with $Fe^{++}$ directly.

According to the kinetic scheme, the back-reaction probably involves the surface reaction of $H_2O_2$ with the radicals, in this case $HO_2$. This may be written as

$$HO_2(ad) + H_2O_2(ad) \longrightarrow$$
$$H_2O(aq) + O_2(aq) + OH(ad) \qquad (8)$$
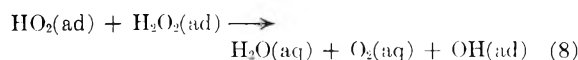
The heat of reaction is $1.9 - E_{HO_2} - E_{H_2O_2} + E_{OH}$ and neglecting $E_{H_2O}$ is equal to 1.9 e.v. Although this reaction is energetically quite favorable, its rate would be limited by the adsorption of $H_2O_2$ at a site adjacent to adsorbed $HO_2$. The decomposition of $H_2O_2$ by $HO_2$ in solution has been considered as less important, since the effective concentration of $HO_2$ near the particle surface should be considerably higher than the volume $H_2O_2$ concentration, and the more energetic $HO_2$ recombination would occur there.

**Acknowledgment.**—The author wishes to acknowledge that Sheffield Gordon first suggested to him that hydrogen peroxide is formed from distilled water when irradiated with mercuric sulfide and to thank him for helpful discussions on this research. He is indebted to Max S. Matheson for many valuable discussions on the interpretation of the results. He further wishes to thank Edwin J. Hart for furnishing the distilled water and James L. Weeks for making the thermopile measurements. (All of this Laboratory.)

## Appendix

The lattice of red HgS resembles a distorted-rock salt lattice in which the sulfur atoms are displaced alternately so as to pucker the axes.[7] For these calculations it is assumed that the binding is essentially ionic with probable strong overlap as a result of the large polarizabilities of $Hg^{++}$ and $S^=$ and the layer structure perpendicular to the axis.

If it is assumed that the Hückel equation[8] for the external field of the rock salt lattice is approximately correct for this case, when the appropriate charge and lattice distance are used, this is given by

$$E(z) \sim (8\pi e^*/d^2) \exp -(\pi\sqrt{2}z/d)$$

where $E(z)$ is the field at a distance $z$ directly above an ion, $d$ is the interionic distance and $e^*$ is the effective ionic charge. Now, the energy of the adsorbed dipole of moment $\mu$ is given by[9]

$$H = -\int_{r_0 + (L/2)}^{r_0 - (L/2)} \frac{E(z)\mu}{L} dz$$

where $L$ is the dipolar length and $r_0$ is the distance between the center of the dipole and the center of the nearest ion.

Integration gives

$$H = (8\sqrt{2}e^*e'/d) \sinh(\pi L/\sqrt{2} d) \exp -(\pi\sqrt{2}r_0/d)$$

where $e'$ is the effective dipolar charge equal to $\mu/L$. For $OH$ on HgS, it is assumed that the radical is adsorbed over a sulfur ion and that the negative end of the dipole is at the center of the $OH$ radical. The use of 1.4 Å. for the $OH$ radius and 1.8 Å. for the sulfur radius gives 2.7 Å. for $r_0$. The average interionic distance is taken as half of the distance between mercury ions or 2.43 Å., and for $e^*$ a value of only $\pm 1$ e is used to compensate for ionic shielding due to the strong overlap. Using $\mu = 1.7$ Debye and $L = 1.0$ Å. gives an adsorption energy of 0.2 e.v.

For an H-atom on HgS the polarization energy is equal to: $-E(z_0)^2\alpha/2$ where $\alpha$ is the polarizability of H, about $0.7 \times 10^{-24}$ cm.$^3$ and $z_0$ is the distance from the center of the $S^=$ to the center of the H, about 2.6 Å. This gives 0.005 e.v. which may be neglected.

Finally, it is assumed that the adsorption energy of $HO_2$ on HgS is approximately the same as that for $OH$. In view of the relatively small magnitude of these terms, this is a satisfactory assumption.

There is no experimental value available for $W$, the energy required to remove a low-energy con-

(7) P. P. Ewald and C. Hermann, "Strukturbericht," 1913–28, Vol. I, Edward Bros. Inc., Ann Arbor, Michigan, 1943, p. 87.

(8) E. Hückel, "Adsorption and Kapillarkondensation," Akad. Verlagsgesellschaft, Leipzig, 1928, p. 126.

(9) J. H. de Boer, "Advances in Colloid Science," Vol. III, Interscience Publications, Inc., New York, N. Y., 1950, p. 34.

duction electron to infinite distance. Modification of an approximational method described by Mott and Gurney[10] permits a rough estimate of this quantity. For a divalent lattice, $W$ is the order of

$$(W_\mathrm{L}/2) - (3e^2/2d)(1 - 1/n^2) + A - h\nu°$$

where $W_\mathrm{L}$ is the lattice energy of HgS, $\nu^1$ and $n$ are the minimum frequency for photoconduction and the refractive index, respectively, and $A$ is the elec-

(10) N. F. Mott and R. W. Gurney, "Electronic Processes in Ionic Crystals," Oxford University Press, New York, N. Y., 1948, pp. 58, 80.

tron affinity of S⁻.[11] The use of 36.4 e.v. for $W_\mathrm{L}$,[12] 2.0 e.v. for $h\nu^0$, $-(\geqslant 4.5)$ e.v. for $A$,[13] 2.43 Å. for $d$ and 8 for $n^2$ gives 4.0 e.v. for $W$.

(11) The second term from the left, giving the net contribution of the polarization potential of the lattice vacancy to the energy for removal of S⁻ and subsequent replacement of S⁻, uses $e$ rather than $e*/2$ since the overlap is only effective close to the normal lattice site. In addition, the refractive index squared is used rather than the low frequency dielectric constant as we consider a fast electron transfer in which the lattice positions do not relax.

(12) O. K. Rice, "Electronic Structure and Chemical Binding," McGraw-Hill Book Co., New York, N. Y., 1940, p. 242.

(13) H. O. Pritchard, Chem. Revs., 52, No. 3, 529 (1953).

# HEATS OF ADSORPTION OF POLAR MOLECULES ON CARBON SURFACES.[1]
## I. SULFUR DIOXIDE

BY R. A. BEEBE AND R. M. DELL[2]

*Department of Chemistry, Amherst College, Amherst, Mass.*

Isotherms and heats of adsorption have been measured for the polar gas sulfur dioxide at 0° on representative members of a series of carbon blacks graphitized at successively higher temperatures up to 2700°. In contrast to the behavior of the non-polar gases nitrogen and argon, which have been studied previously, it is found that removal of oxygen complexes from the carbon surface by high temperature treatment causes the amount of sulfur dioxide adsorption to be sharply reduced and the shape of the isotherm to be altered. On the untreated Spheron carbon black of high surface oxygen content, the calorimetrically measured differential heats of adsorption fall steadily with coverage from an initial value of 15 kcal./mole to values which approach the heat of vaporization (5.85 kcal./mole). Treatment at 2700° produces a comparatively uniform, graphite-like surface free from polarizing complexes. On this heat treated material, the differential heats of adsorption start at 6 kcal./mole and then rise with coverage to a maximum of 7.4 kcal./mole; this rise with coverage is attributed to lateral van der Waals forces between the adsorbed molecules. As might be expected, the heat values for Spheron (1000°) vary in a manner which is intermediate between the two extremes represented by Spheron and Spheron (2700°). From the data on the highly graphitized carbon, Spheron (2700°), it is concluded that (1) there is no sharp separation, as in the case of argon, between first and second layer formation of sulfur dioxide at 0°, and (2) lateral dipole repulsions between adsorbed polar sulfur dioxide molecules are small in comparison with van der Waals attractive forces.

## Introduction

Wide use is now being made of the physical adsorption of nitrogen at liquid air temperatures for the determination of the surface areas of finely divided non-porous solids. The volume of nitrogen required to form a single layer of adsorbed molecules may be deduced from the empirical point "B" in the adsorption isotherm or, in the case of heterogeneous surfaces only, from the equation of Brunauer, Emmett and Teller.[3] The success of this method lies, to a considerable degree, in its equal applicability to polar and non-polar solids, since the form of the isotherm, in the case of nitrogen, is relatively independent of the chemical state of the adsorbing surface. This point may be illustrated by the almost identical nature of the isotherms and of the heats of adsorption for nitrogen on a sample of carbon black (Spheron 6) having about 5% of oxygen incorporated in the surface layers and on the "devolatilized" carbon produced by heating the Spheron to 927°.[4] At this temperature some 90% of the oxygen was evolved, the physical structure of the carbon particles remaining essentially unchanged. The surface of the original,

oxygen containing, Spheron would be expected to be polar in nature. In general, the applicability of the nitrogen adsorption method to determining the surface areas of both polar and non-polar substances has been confirmed by measurements of the entropy of adsorption[5,6] which indicate monolayer coverages in accord with those obtained from the isotherm.

While the physical adsorption of nitrogen appears generally to be independent of the chemical nature of the adsorbent surface, it should be noted that this is not universally true. Stone and Tiley[7] have demonstrated that the physical adsorption of gases on metallic oxides may be markedly influenced by the presence of preabsorbed carbon monoxide. This modification of a nitrogen isotherm appears to be a specific effect, being dependent not only upon the molecular species preadsorbed, but also upon its configuration at the surface.[8] From a practical point of view, these results illustrate the importance of adopting an adequate outgassing procedure before undertaking surface area measurements.

When considering the physical adsorption of polar molecules, in contrast to nitrogen or the inert

(3) S. Brunauer, P. H. Emmett and E. Teller, J. Am. Chem. Soc., 60, 309 (1938).

(4) R. A. Beebe, J. Biscoe, W. R. Smith and C. B. Wendell, ibid., 69, 95 (1947).

(5) T. L. Hill, P. H. Emmett and L. G. Joyner, ibid., 73, 5102 (1951).

(6) L. E. Drain and J. A. Morrison, Trans. Faraday Soc., 49, 654 (1953).

(7) F. S. Stone and P. F. Tiley, Nature, 167, 654 (1951). (Similar results were obtained using nitrogen, also for other metallic oxides.)

(8) P. F. Tiley, ibid., 168, 434 (1951).

gases, we might expect rather widely different adsorption effects in dealing with surfaces of varying chemical composition and consequent varying degrees of polarity. This is indeed true, as shown by Anderson and Emmett[9] for adsorption of water and ammonia on the above-mentioned pair of carbons. When the removal of the oxygen is virtually complete, as with the pigment Graphon produced by heat treatment of carbon blacks to temperatures approaching 3000°, the adsorption of water vapor is greatly reduced and the isotherm shifts to an extreme Type III.[10] Thus it would be possible to use water vapor adsorption to estimate the degree of polarity of any given carbon surface. This method, however, is experimentally inconvenient and is further complicated by the slow chemical reaction of water with a carbon surface.[10] In the present paper it is demonstrated that sulfur dioxide may also be utilized in studying the polarity of adsorbent surfaces It meets the requirements of being a suitable polar adsorbate (dipole moment = 1.60 Debye units), while being convenient for use at 0°. A sharp change is found in comparing the sulfur dioxide isotherms of an oxygen containing surface with one from which the oxygen has been removed.

The effect of high temperature treatment of carbon blacks upon their adsorptive properties is a subject currently of general interest. A series of carbon black samples prepared by treating Spheron at successively higher temperatures up to 2700° has been described by Schaeffer, Smith and Polley,[11] who have shown by X-ray and electron microscope techniques that there is a gradual transition from a heterogeneous to a more homogeneous surface. This transition is a result of progressive graphitization of the carbon particles and an increase of three-dimensional order within the crystallites. The adsorption of the non-polar gas argon on this series of carbon blacks has been studied[12,13] and the heats of adsorption have been reported from this Laboratory. With increasing temperature of graphitization, the isotherms change progressively from normal Type II to isotherms of stepwise character. Such stepwise isotherms have been theoretically predicted for adsorption on a homogeneous surface.[14,15] The amount of adsorption at a given relative pressure is, however, essentially unchanged, as would be expected for a non-polar molecule like argon or nitrogen. Heat measurements for argon adsorption demonstrate even more clearly the increasing homogeneity of the carbon surface with increasing temperature of graphitization. With the original Spheron sample the differential heat of adsorption shows a progressive decrease as the surface is covered, this being charac-

teristic of heterogeneous surfaces. Conversely, on the sample graphitized at 2700°, the surface is much more homogeneous in adsorption potential with the result that the van der Waals attraction between adjacent adsorbed molecules is clearly demonstrated by a steady rise in the differential heat as the first monolayer is filled At the completion of a monolayer the heat drops sharply as second layer formation commences.

The experimental evidence indicates that in Spheron (2700°) we have a highly reproducible, chemically pure carbon adsorbent which has an essentially homogeneous surface of comparatively high surface area. Adsorption data on such a surface are undoubtedly more amenable to theoretical treatment than data obtained on surfaces which are chemically and geometrically more complex. Several theoretical calculations of the heat of adsorption of argon on uniform surfaces have been made[16–18] and compared with data obtained experimentally. However, attempts at similar calculations for polar molecules have been subject to an uncertainty as regards the orientation of the adsorbed molecules and thus of the coulombic forces between them Calculations for the adsorption of sulfur dioxide on conductors by Roberts[19] and on ionic solids by Crawford and Tompkins[20] are based on the assumption that the dipoles of the adsorbed molecules are oriented in a square array. Using this model, it is suggested that van der Waals attraction and coulombic repulsion between adsorbate molecules are of the same order of magnitude, preventing the heat of adsorption from varying greatly with increasing surface coverage

By experimentally measuring the heat of adsorption of a polar gas such as sulfur dioxide as a function of surface coverage on the uniform Spheron (2700°), we hoped to be able to draw inferences about the relative contributions of van der Waals attraction and dipole repulsion to the lateral interaction forces between adjacent molecules. The results suggest that dipole repulsion between adjacent molecules is of little significance compared with van der Waals attraction.

## Experimental

**Materials.**—Sulfur dioxide was obtained from the Matheson Company; the purity was stated as 99.7%. After transfer to the adsorption train it was subjected to bulb-to-bulb distillation under vacuum and the middle portion of the distillate was finally used. Oxygen was prepared from analytical grade potassium permanganate and dried over phosphorus pentoxide. The series of heat treated carbon blacks described by Schaeffer, Polley and Smith[11] was used, the samples studied being Spheron 6, Spheron (1000°), Spheron (1500°), and Spheron (2700°).[21] The specific surface areas of these four carbons, as determined by Polley, et al.,[12] by nitrogen adsorption, are 114, 91.1, 88.0 and 84.1 sq. m./g., respectively. In the present investigation, we shall be especially interested in the effect of the chemical composition of the samples on their adsorptive character-

(9) R. B. Anderson and P. H. Emmett, THIS JOURNAL, **56**, 756 (1952).

(10) C. Pierce, R. N. Smith, J. W. Wiley and H. Cordes, J. Am. Chem. Soc., **73**, 4551 (1951).

(11) W. D. Schaeffer, W. R. Smith and M. H. Polley, Ind. Eng. Chem., **45**, 172 (1953).

(12) M. H. Polley, W. D. Schaeffer and W. R. Smith, THIS JOURNAL, **57**, 469 (1953).

(13) R. A. Beebe, D. M. Young and H. Bienes, ibid., **58**, 93 (1954).

(14) G. D. Halsey, J. Am. Chem. Soc., **73**, 2693 (1951); **74**, 1082 (1952).

(15) T. L. Hill, J. Chem. Phys., **15**, 767 (1947).

(16) W. J. C. Orr, Trans. Faraday Soc., **35**, 1247 (1939); Proc. Roy. Soc. (London), A173, 349 (1939).

(17) D. M. Young, Trans. Faraday Soc., **47**, 1228 (1951).

(18) A. D. Crowell and D. M. Young, ibid., **49**, 1080 (1953).

(19) J. K. Roberts, ibid., **34**, 1342 (1938).

(20) V. A. Crawford and F. C. Tompkins, ibid., **44**, 698 (1948); **46**, 504 (1950).

(21) The temperature of heat treatment is indicated: Spheron (1500°) indicates a sample of Spheron treated for two hours at 1500°.

istics. Analysis of the carbon blacks is given in Table I.[22] Unfortunately, the oxygen data, with which we are especially concerned, are determined by difference only. However, the results of Table I for both hydrogen and oxygen content of the original Spheron are in qualitative agreement with the data of Emmett and Anderson.[9] The results illustrate well the high purity of Spheron (2700°) and the negligible sulfur content is especially reassuring in view of the investigations of Smith, Pierce and Joel which showed an appreciable sulfur content in a previously prepared sample of Graphon.[23]

TABLE I

| | Loss drying,[a] % | Hydrogen, % | Carbon, % | Ash, % | Sulfur, % | Oxygen,[b] % |
|---|---|---|---|---|---|---|
| Spheron 6 | 1.83 | 0.60 | 95.17 | 0.05 | 0.25 | 3.93 |
| | 1.71 | .59 | 95.11 | .11 | .25 | 3.94 |
| Spheron | 0.08 | .15 | 99.20 | .11 | .25 | 0.29 |
| (1000°) | .06 | .13 | 99.22 | .11 | .26 | .28 |
| Spheron | .00 | .02 | 99.70 | .08 | .09 | .11 |
| (1500°) | .00 | .02 | 99.73 | .07 | .09 | .09 |
| Spheron | .01 | .00(5) | 99.87 | .06 | .00(2) | .06(3) |
| (2700°) | .00 | .00(2) | 99.91 | .03 | .00(3) | .05(5) |

[a] Drying condition: 1 hour in stream of dry nitrogen at 150°. [b] By difference.

A single adsorption isotherm was made on a sample of graphite obtained from the same batch as used by Pierce,
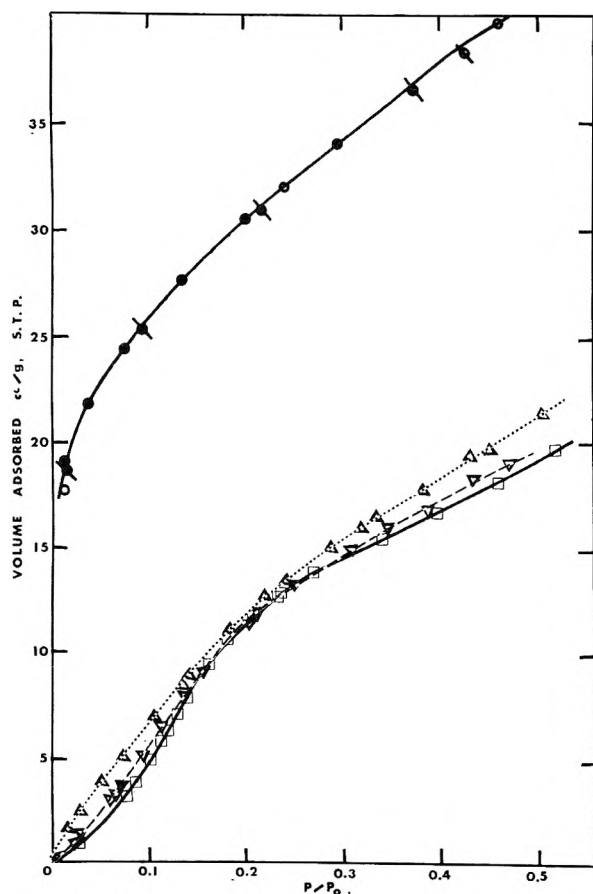


Fig. 1.—Isotherms, sulfur dioxide on carbon blacks at 0°: Spheron 6, run 1 ○, ●, run 2 ⊘, ◑; Spheron (1000°) △; Spheron (1500°) ▽, ▼; Spheron (2700°) □. Adsorption points open, desorption points blackened.

(22) M. Studebaker, "The Ultimate Analysis of Carbon Black, I." Presented before the Division of Rubber Chemistry at the Spring Meeting of the American Chemical Society, Los Angeles, California, March 1953.

(23) R. N. Smith, C. Pierce and C. D. Joel, THIS JOURNAL, 58, 298 (1954).

et al.,[10] which was reported to have an ash content of below 0.001% and to be essentially free of oxygen complex. Its surface area (nitrogen adsorption) was 4 sq. m./g.

**Apparatus and Procedure.**—The apparatus used in measuring the isotherms and in the determination of the heats of adsorption was identical with that described previously.[13] All adsorptions were carried out at 0°, crushed ice being used as a constant temperature medium. The vapor pressure ($P_0$) of sulfur dioxide at 0° is 116.5 cm.[24] After standing overnight, the thermocouple temperature was constant to better than ±0.002°, making for excellent calorimetric conditions.

Heat measurements were made using the calorimeter both isothermally and in a manner which was essentially adiabatic. The isothermal method, using helium in the outer vessel of the calorimeter, has been described.[25] In the "adiabatic" method the outer vessel was highly evacuated and cooling was quite slow. From the cooling curve, the Newton cooling coefficient was calculated and the adiabatic time-temperature curve was reconstructed. Within two or three minutes after the heat was released, the adiabatic curve reached a constant value with time. This method yielded rather more consistent and reliable results but, because of the time-consuming calculations involved, its use was restricted to the measurements on Spheron (2700°), the sample of greatest fundamental interest.

Consideration was given to correcting the measured heats for the heat of compression of the gas within the calorimeter, as given by the equations of Kington and Aston.[26] In each case the correction was less than 1%, which is well within the estimated experimental accuracy (±3%). Although this correction was not made, it is justifiable to regard the heats plotted in Figs. 4–7 as isosteric heats which are designated as $q_{st}$.

Before each run the sample was thoroughly evacuated overnight at 200–250°. The sulfur dioxide was measured in a gas buret and admitted to the adsorbent. In the case of the heat treated carbons the adsorption was rapid and equilibrium was attained in a few minutes; there was no desorption hysteresis. With the original Spheron, a continued slow uptake was observed after the initial rapid adsorption and it was necessary to allow more than an hour for equilibrium. This continuing slow uptake was too slight to introduce appreciable error into the heat measurements.

Dead space calibrations were carried out with helium, and consideration was given to correcting for the non-ideality of sulfur dioxide with respect to (1) the residual unadsorbed gas, (2) the volume measured in the buret. In estimating these corrections the virial equation was used, a mean value of −370 being taken for the second virial coefficient of sulfur dioxide at 0°. Both corrections were less than 1% in the worst case and usually far smaller; in general these were not made.

## Results

**Isotherms.**—Figure 1 shows the adsorption isotherms of sulfur dioxide at 0° on the four carbon blacks. The marked drop in adsorptive capacity of Spheron (1000°) compared with the original Spheron parallels the loss of oxygen (Table I). The question arises as to whether storage of the samples in air at room temperature causes the formation of a surface layer of oxide not removed by our standard procedure of evacuation at 200–250°. If this were so, adsorption of sulfur dioxide on all of the graphitized carbons presumably would be higher than for a pure carbon surface. To demonstrate that no oxygen not removable by evacuation at 250° was adsorbed from the air, Spheron (2700°) was placed in a platinum bucket contained in a quartz tube and evacuated for 24 hours at 950–1000°. After cooling *in vacuo*, the sulfur dioxide isotherm was repeated *in situ*. Figure 2 shows that the isotherm was identical with that for Spheron

(24) "International Critical Tables," 3, 236 (1928).

(25) R. A. Beebe, B. Millard and J. Cynarski, J. Am. Chem. Soc., 75, 839 (1953).

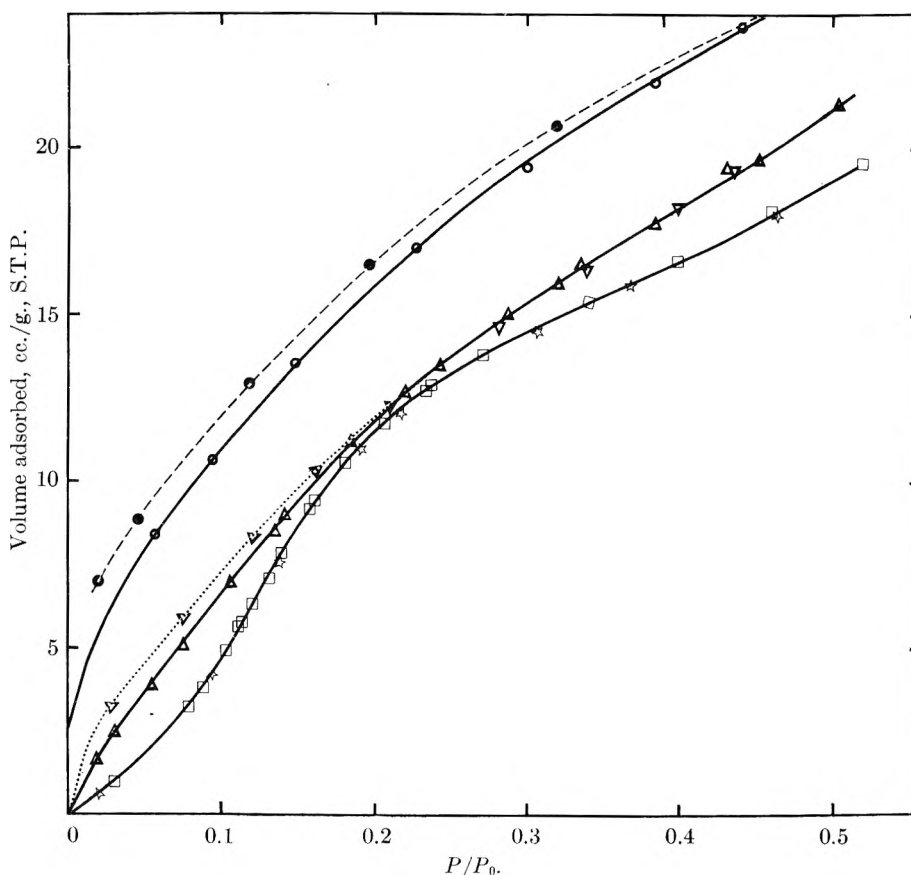(26) G. L. Kington and J. G. Aston, ibid., 73, 1929 (1951).

Fig 2.—Isotherms, sulfur dioxide on carbon blacks at 0°: Spheron (1000°) O; Spheron 6 heated to 1000° *in vacuo* ▽; Spheron (1000°) treated with oxygen at 600°, adsorption O, desorption ●; Spheron (2700°) degassed at 200° heron □; Sp (2700°) degassed at 1000° ☆.

(2700°) which had been evacuated at 200–250°. As a further test, a sample of the original Spheron was also evacuated for 24 hours at 1000°, cooled *in vacuo* and a sulfur dioxide isotherm was run. This isotherm was almost identical with that for Spheron (1000°)—see Fig. 2. This agreement must be considered excellent if we bear in mind that our experimental conditions for producing a sample by evacuation at 1000° were quite different from those obtaining in production of Spheron (1000°) in the Cabot Laboratories.[11] We conclude from these two experiments that our standard outgassing procedure is adequate to remove any oxygen taken up from the atmosphere during transfer and storage.

Spheron itself is undoubtedly highly complex, the presence of both hydrogen and oxygen giving rise to the possibility of many different surface complexes. Such a surface is perhaps of little fundamental interest and so an attempt was made to produce artificially a somewhat simpler polar surface by high temperature treatment of the devolatilized carbon black with oxygen alone. Spheron (1000°) was heated to 600° for two hours in contact with oxygen and then allowed to cool (still in oxygen) to room temperature. The volume of oxygen taken up was comparatively small, but no reliable estimate may be given as the residual gas was not analyzed for carbon monoxide and carbon dioxide. A sulfur dioxide isotherm was then measured (Fig. 2). It is at once apparent

that the adsorption of sulfur dioxide by a devolatilized carbon black is enhanced by pretreatment with oxygen.[27]

Figure 3 shows a single isotherm measured for the adsorption of sulfur dioxide on graphite. Its shape is essentially that of the isotherm on Spheron (2700°) and if the volume axis is multiplied by the ratio of the surface areas of the samples (a factor of 21) it is seen that the isotherms may be almost exactly superimposed. This experiment indicates that the graphite and the Spheron (2700°) are similar in that both have surfaces which are comparatively uniform with respect to adsorption potential.

**Heat Measurements.**—Differential heats of adsorption of sulfur dioxide as a function of surface coverage were measured for Spheron, Spheron (1000°) and Spheron (2700°). These are shown in Figs. 4, 5 and 6. The difference in the shape of the heat curves for the three samples is most striking.

In Fig. 7 the heat of adsorption of sulfur dioxide at low surface coverages on Spheron (1000°) and oxygen treated Spheron (1000°) are compared. As might have been expected from Figs. 4–6, the heat of adsorption is observed to be somewhat higher on the oxygenated surface.

(27) It is noteworthy that the adsorption and desorption branches of the isotherm for sulfur dioxide on this particular carbon black do not coincide. A similar hysteresis has been observed with ammonia on certain other carbon surfaces (see Paper II, of this series). A theory for this behavior will be presented in a later publication.
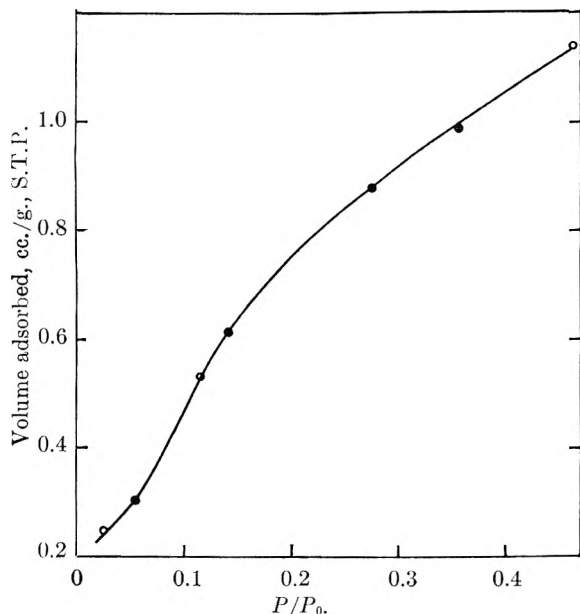
Fig. 3.—Adsorption of sulfur dioxide on graphite at 0°: adsorption ○, desorption ●.

**Entropy of Adsorption.**—Recently, Hill, Emmett and Joyner[5] have given a theoretical treatment of entropies of adsorption and have indicated how monolayer coverages may be deduced from integral entropy values. The integral entropy of adsorption $(S_s - S_g)$ may be calculated from a pair of isotherms at different temperatures by the equation[28]

$$\left(\frac{\partial \ln P}{\partial T}\right)_\phi = -(S_s - S_g)/RT \tag{1}$$

Here $\phi$ is the spreading pressure, given by the Gibbs equation

$$\phi = RT \int_0^P \Gamma \, d \ln P_{(\text{const.})} \tag{2}$$

where

$\Gamma$ = surface concn.

$\Gamma = N/A$ ($N$ = no. of mols. adsorbed on area $A$)

Such a procedure has been used in entropy calculations for the adsorption of nitrogen[5] and ethyl chloride[29] on Graphon.

Jura and Hill[30] pointed out that the integral entropy of adsorption could be computed more accurately using a calorimetric heat of immersion or heat of adsorption and a single isotherm. To date, such calculations have been made by Zettlemoyer, et al.,[31] measuring heats of immersion and Drain and Morrison[32] measuring heats of adsorption.

In the present work, the integral entropy of adsorption of sulfur dioxide on Spheron (2700°) was calculated using the equation

$$(S_s - S_g) = - Q/T - \frac{R}{V}\left[\int_0^V \ln P dV - V \ln P\right] \tag{3}$$

where $Q$ is the integral colorimetric heat. (This equation is eq. 6 of Drain and Morrison, ignoring the small correction factor for gaseous imperfection which would be within our calorimetric experimental error.)

Substituting the heat of vaporization of sulfur dioxide at 0°, $E_L = -5850$ cal.,[33] in the Gibbs–Helmholtz equation, we may calculate the entropy of vaporization $(\Delta S_L)$ at 0°.

$$\Delta S_L = \frac{E_L}{T} - R \ln P_0/P \tag{4}$$

$$= -30.87 + R \ln P$$

The net integral entropy of adsorption is then given by

$$(S_s - S_L) = (S_s - S_g) - \Delta S_L \tag{5}$$

Large scale graphs of log $P$ against $V$ for adsorption of sulfur dioxide at 0° on Spheron (2700°)
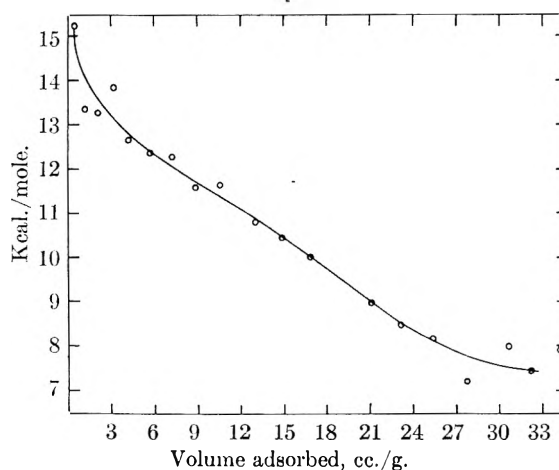


Fig. 4.—Heat of adsorption of sulfur dioxide on Spheron 6 at 0°.
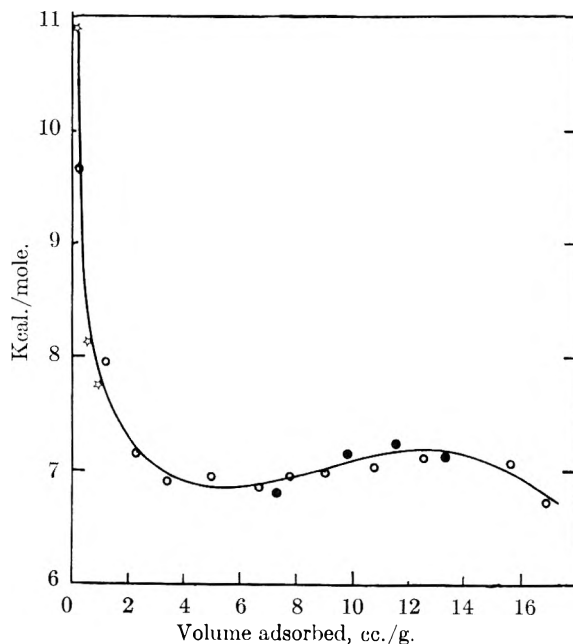


Fig. 5.—Heat of adsorption of sulfur dioxide on Spheron (1000°) at 0°: run 1, adsorption ○, desorption ●; run 2, adsorption ☆.

(28) T. L. Hill, Advances in Catalysis, 4, 247 (1952).

(29) J. Mooi, C. Pierce and R. N. Smith, THIS JOURNAL, 57, 657 (1953).

(30) G. Jura and T. L. Hill, J. Am. Chem. Soc., 74, 1598 (1952).

(31) A. C. Zettlemoyer, G. J. Young, J. J. Chessick and F. H. Healey, THIS JOURNAL, 57, 649 (1953).

(32) L. E. Drain and J. A. Morrison, Trans. Faraday Soc., 48, 840 (1952).

(33) "International Critical Tables," 5, 138 (1928).

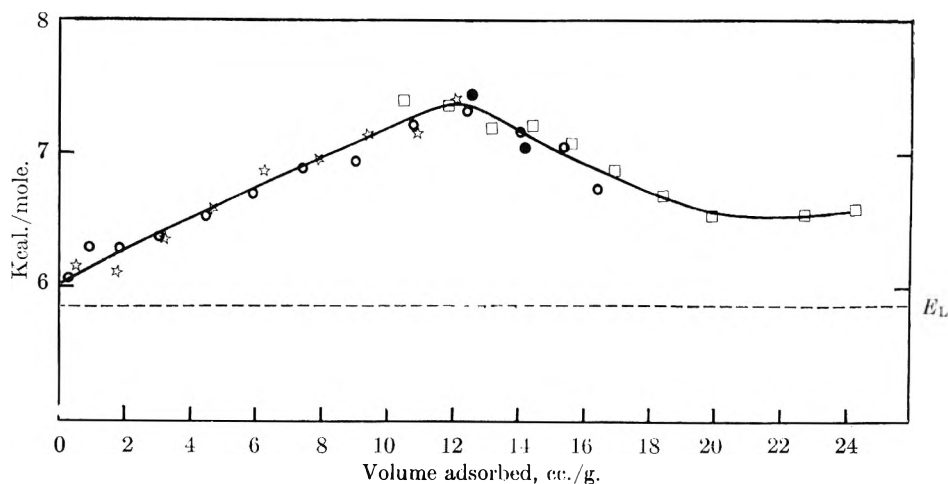Fig. 6.—Heat of adsorption of sulfur dioxide on Spheron (2700°) at 0°:  run 1 ☆;  run 2 □ ;
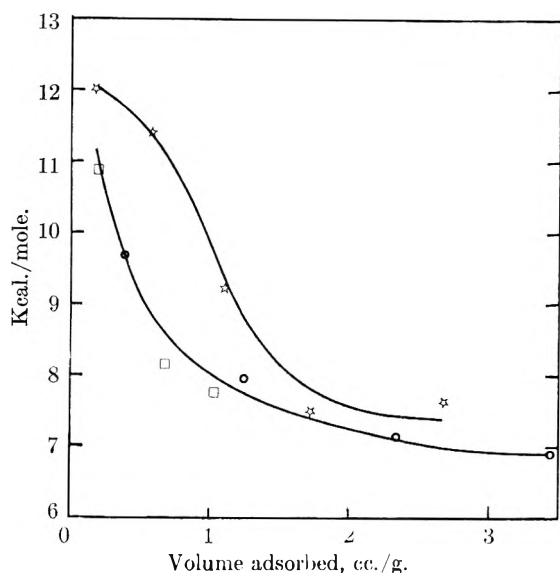run 3 adsorption ○, desorption ●.



Fig. 7.—Heat of adsorption of initial increments of sulfur dioxide on Spheron (1000°) at 0°:  run 1 □, and run 2 ○, bare surface;  run 3 ☆, surface treated with oxygen.

were numerically integrated and the net integral entropy of adsorption $(\bar{S}_s - S_L)$, calculated according to equations 3–5, is shown in Fig. 8.  The sulfur dioxide isotherm is particularly well suited to this type of calculation since there is relatively little adsorption at low pressure and, consequently, it is not necessary to take readings in the McLeod pressure range as it is for nitrogen adsorption. In making the calculation, a linear isotherm $V = kP$ was assumed below a coverage of 0.5 cc./g. This approximation is justifiable since $\int_0^{0.5} \ln P$ $dV = -0.23$, which is small compared with the total integral $\int_0^{16.5} \ln P\, dV = 44.23$.  In general, the calculation of integral entropies and of spreading pressures for adsorbates which show an isotherm convex to the pressure axis does not require adsorption data at very low pressures.

Figure 8 shows also the net differential entropies of adsorption $(\bar{S}_s - S_L)$ calculated from the differential calorimetric heats.  No attempt was made to calculate entropy values for adsorption on

Spheron as the surface is not of such fundamental interest as is that of the graphitized material and the low pressure data necessary with Type II isotherms were not available.

**Spreading Pressure.**—Harkins, Jura, et al.,[34] have calculated the decrease in surface free energy during adsorption processes.  This decrease is, by definition, equal to the spreading pressure of the adsorbed film given by the Gibbs equation 2. Calculation of the spreading pressure $\phi$ as a function of area per adsorbed molecule $\sigma$ has proved fruitful in demonstrating phase transitions both in monolayers spread on liquid surfaces and in gases adsorbed on solids.  From the magnitude of the spreading pressure, information about the physical nature of the adsorbed monolayer may be deduced.

The spreading pressure exerted by sulfur dioxide adsorbed on Spheron (2700°) was calculated according to equation 2 and is plotted in Fig. 9 as a function of $\sigma$.

### Discussion

A comparison of the isotherms shown in Fig. 1 with a similar set of isotherms for argon on the same series of carbon adsorbents[13] reveals a marked difference in the behavior of the polar sulfur dioxide and the non-polar argon adsorbates.  While heat treatment of the carbon black has little effect on argon adsorption, there is a strong effect on sulfur dioxide adsorption, the amount of sulfur dioxide adsorbed at a given relative pressure being greatly reduced.  The heat of adsorption on untreated Spheron is appreciably higher than on the heat treated carbons.  These observations illustrate the influence of a polarizing surface in enhancing the adsorption of a polar molecule.  The sustained high heat values for Spheron indicate that the influence of the polarizing surface extends into second layer adsorption ($V_m = 21.7$ cc./g. based upon the cross-sectional area $\sigma_{SO_2} = 19.4$ Å.² from liquid density measurements).

Consideration was given to the possibility that the high heat values on untreated Spheron were due to chemisorption of sulfur dioxide by surface complexes rather than to electrostatic orientation

(34)  W. D. Harkins and G. Jura, J. Chem. Phys., 12, 112 (1944); G. Jura, W. D. Harkins and E. H. Loeser, ibid., 14, 344 (1946).
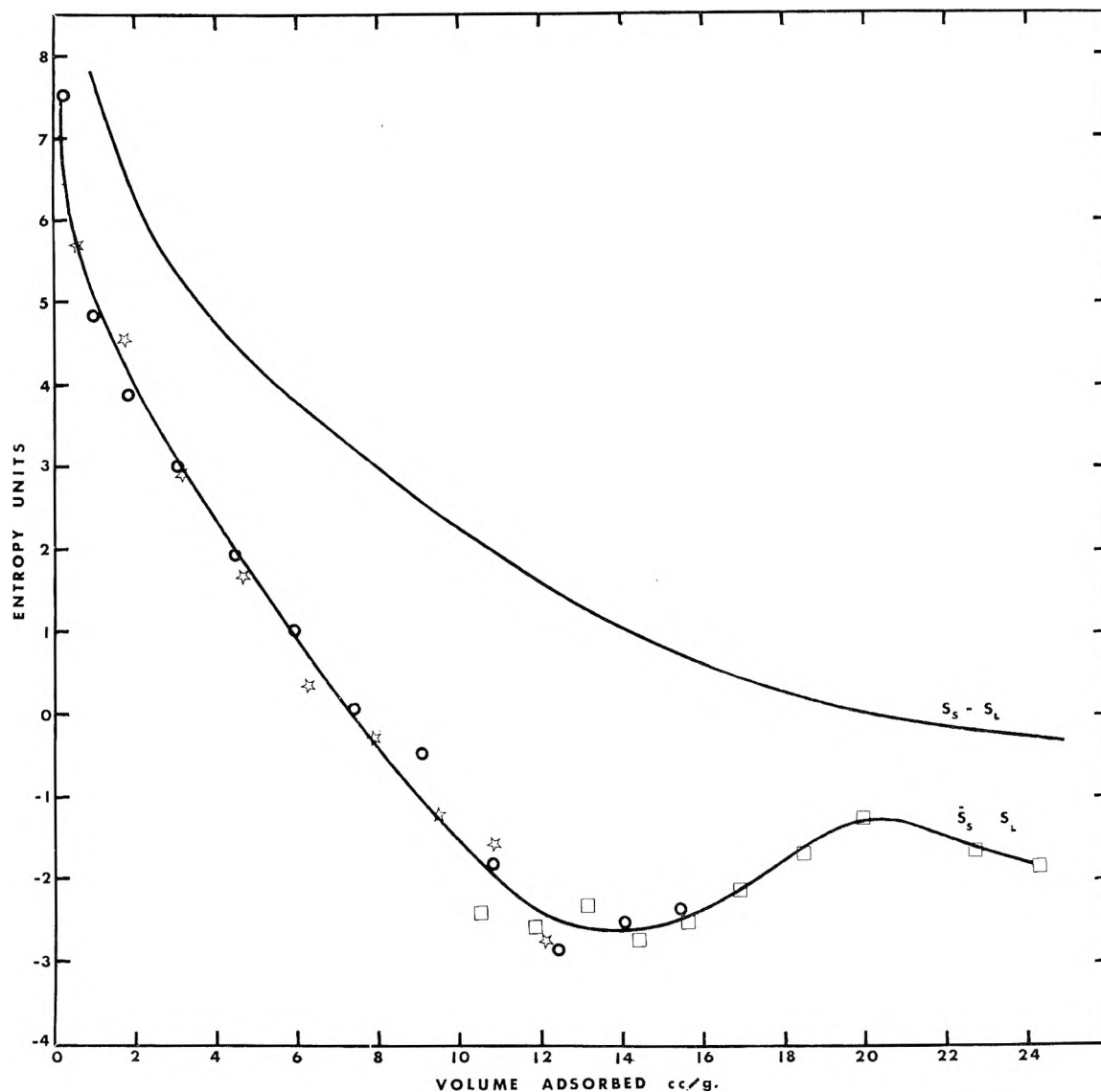
Fig. 8.—Entropy of adsorbed phase for sulfur dioxide on Spheron (2700°): net differential entropy ($\bar{S}_s - S_L$), integral entropy ($\bar{S}_s - S_L$); run 1 ☆, run 2 ○, run 3 □.

effects. Although it cannot be stated for certain that chemical reaction does not occur, it has been shown that the surface of Spheron is acidic in nature[35] and so any reaction analogous to salt formation appears to be ruled out for sulfur dioxide. Moreover, the isotherms of Crawford and Tompkins[20] for adsorption of sulfur dioxide on polar crystals of barium fluoride and calcium fluoride resemble those on Spheron in being of Type II, monolayer formation occurring at approximately the same relative pressure (about 0.1).

Heat treatment of Spheron at 1000° is known to remove most of the oxygen from the carbon, while X-ray studies show that little graphitization occurs at this temperature.[11] In comparison with the original Spheron black, the Spheron (1000°) possesses fewer sites of high adsorption potential. Such a picture is in accordance with the heat coverage curve for sulfur dioxide on Spheron (1000°). The high initial heats are indicative of a hetero-

(35) M. H. Polley, W. D. Schaeffer and W. R. Smith, *J. Am. Chem. Soc.*, **73**, 2161 (1951).

geneous surface, but, after a sharp drop, the heat reaches a value which is much lower than for Spheron. In the same manner as for argon adsorption,[13] the fall in heat with coverage due to surface heterogeneity offsets the tendency to show a rise due to van der Waals attraction between adjacent adsorbed molecules. After graphitization at 2700°, the surface is far more uniform and the effect of lateral interactions between adjacent adsorbed molecules manifests itself as an increase in heat of adsorption with coverage. Similar results were obtained for argon[13] and ethyl chloride.[29]

The increasing homogeneity of the carbon surface on graphitization is illustrated also by the changing shape of the sulfur dioxide isotherms for Spheron (1000°), Spheron (1500°) and Spheron (2700°). After heat treatment to 2700°, the sulfur dioxide isotherm is actually convex to the pressure axis at low pressures. This result will be discussed in relation to the behavior of other polar adsorbates on the same uniform surface in a future paper.

Adsorption of sulfur dioxide by non-porous

carbons has not been investigated previously. With porous charcoals, Polanyi and Welke[36] reported a two-dimensional condensation of sulfur dioxide on the surface at a few percentage coverage. Calorimetric measurements of adsorption on charcoal by Magnus and co-workers[37] provided no evidence for such a surface condensation. In the present work with non-porous carbon, Fig. 9 indicates that no first-order phase transitions occur in the pressure range with which we are dealing. Moreover, the value of $\phi\sigma$ at low coverages ($\phi\sigma = 380 \times 10^{-16}$ ergs/molecule) is almost identical with that for a perfect two-dimensional gas, indicating that the adsorbed sulfur dioxide exists as a gaseous expanded film and that condensation has not occurred at pressures lower than those measured by our technique. We conclude that two-dimensional condensation of sulfur dioxide does not occur on a uniform, non-porous carbon surface at 0°.

In Table II we have summarized the calorimetric data for the adsorption of sulfur dioxide at 0° and argon at −195° on Spheron (2700°). The first point of interest is that the initial heat of adsorption of sulfur dioxide on this uniform surface is comparable with the heat of vaporization $E_L$, whereas for argon, $q(\text{initial}) = 1.7 E_L$. Although the net heat of adsorption of sulfur dioxide is initially almost zero, the entropy of the molecules in the adsorbed film at low coverages is appreciably higher than in the liquid (Fig. 8); thus the free energy of adsorption exceeds that of liquefaction. Such a result illustrates the importance of considering free energy changes in adsorption processes and suggests that even negative net heats of adsorption might occur in certain instances. The sulfur dioxide–Spheron (2700°) system is probably the first recorded example in which the heat of adsorption is initially almost zero and increases with increasing surface coverage.
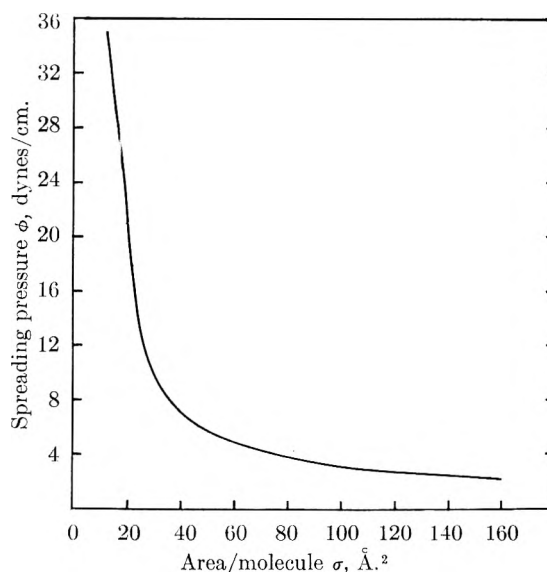


Fig. 9.—Spreading pressure of a film of sulfur dioxide adsorbed on Spheron (2700°).

suggesting that there is no clear-cut separation between first and second layer formation. An approximate value of point 'B' of 10–13 cc./g. agrees with the maximum in the heat curve. Hill, Emmett and Joyner[5] have suggested that the criterion of monolayer completion is the point of intersection of the differential and integral entropy curves. Figure 8 shows that in the present work these do not intersect and suggests that second layer formation begins around 12 cc./g., before a monolayer is completed. The heat curve beyond this point is probably composite, representing both first and second layer formation. It therefore falls more gradually than does the corresponding graph for argon adsorption, where the heat drops sharply at the monolayer value and there is a clear distinction between first and second layers.

This difference in behavior of argon and sulfur dioxide is associated with the difference in the net heat of adsorption at the maximum ($q_m - E_L$) compared with the heat of liquefaction $E_L$ (see Table II). The much lower value of the relative net heat at the maximum ($q_m - E_L)/E_L$ for sulfur dioxide compared with argon suggests a smearing out of any sharp distinction between first and second layer formation. Of course the higher thermal energy at 0° ($kT = 550$ cal.) compared with −195° ($kT = 160$ cal.) would make for greater disorder of the adsorbate, and this would lead to a greater blurring of first and second layer adsorption in the case of the sulfur dioxide.

When considering lateral interactions between adsorbed polar molecules, allowance has to be made for coulombic repulsion between dipoles as well as for van der Waals attraction. Langmuir[39] first pointed out that dipoles arranged in a parallel array exert a mutually depolarizing effect on one another, giving rise to a decrease in dipole moment as the surface becomes covered and thus reducing intermolecular coulombic repulsion. Various theoretical estimates[19,40] for sulfur dioxide and also for

### TABLE II

| Gas | 1<br>$E_L$,<br>kcal. | 2<br>$q_i$,<br>kcal. | 3<br>$q_m$,<br>kcal. | 4<br>($q_m - q_i$),<br>kcal. | 5<br>$\dfrac{q_m - E_L}{E_L}$ |
|---|---|---|---|---|---|
| Argon | 1.57 | 2.7 | 3.2 | 0.5 | 1.04 |
| Sulfur dioxide | 5.85 | 6.0 | 7.4 | 1.4 | 0.26 |

Several theoretical calculations of the heat of adsorption of gases on a uniform carbon surface (graphite) have been made, but uncertainty arises as to whether the adsorbent should be treated as a metallic conductor or as a covalent solid.[38] Crowell and Young[18] recently have calculated the heat of adsorption of argon on a bare graphite surface, but reliable calculations for polar molecules are believed not to be feasible at present.

The maximum value of the heat of adsorption of sulfur dioxide on Spheron (2700°) occurs at a surface coverage of about 12 cc./g. This is less than the monolayer coverage of 16 cc./g., based upon the value of $\sigma_{SO_2}$ for close packing. No distinct point 'B' is apparent in the isotherm (Fig. 2)

(36) M. Polanyi and K. Welke, Z. physik. Chem., **132**, 371 (1928).

(37) A. Magnus, H. Giebenhain and H. Velde, ibid., **A132**, 371 (1928).

(38) S. Brunauer, "The Adsorption of Gases and Vapors," Princeton University Press, Princeton, N. J., 1943, p. 214.

(39) I. Langmuir, J. Am. Chem. Soc., **54**, 2798 (1932).

(40) A. R. Miller, Proc. Camb. Phil. Soc., **42**, 292 (1946).

ammonia have suggested that the dipole repulsion between adsorbed molecules is of the same order of magnitude as the van der Waals attractive interaction. For a uniform surface, this results in a heat of adsorption which varies but slightly with coverage. In the present study, the heat of adsorption of sulfur dioxide on Spheron (2700°) rises steadily with coverage up to 12 cc./g. This observation leads to the conclusion that either the depolarizing

effect of the dipoles upon each other is greater than formerly estimated, or else the dipoles (and thus the sulfur dioxide molecules) are randomly oriented at the surface.

**Acknowledgment.**—The authors are much indebted to Miss H. Bienes for help with some of the experimental measurements and to Mr. J. H. Fuller for technical assistance with the construction of the apparatus.

---

# HEATS OF ADSORPTION OF POLAR MOLECULES ON CARBON SURFACES.[1]
## II. AMMONIA AND METHYLAMINE

By R. M. Dell[2] and R. A. Beebe

*Department of Chemistry. Amherst College, Amherst, Mass.*

Isotherms in the temperature range from −78 to −22° have been measured for ammonia on representative members of a series of carbon blacks graphitized at successively higher temperatures up to 2700°; and heats of adsorption for ammonia on these blacks have been calorimetrically determined at −78°. A limited number of experiments have been done with methylamine. In comparison with argon and sulfur dioxide previously studied, the ammonia presents the additional possibility of hydrogen bond formation. This may occur between the ammonia molecules and oxygen complexes on the untreated carbon surface resulting in the observed high adsorption at low relative pressures and high heat of adsorption. With the heat-treated, highly graphitized materials, however, there is relatively little attraction of the carbon surface for the ammonia molecules with the result that the isotherm is convex to the pressure axis up to about 0.5 relative pressure, going through a point of inflection to become concave to the pressure axis. The heats of adsorption of ammonia on the graphitized black, Spheron (2700°), are particularly interesting in that they are (1) virtually constant at all coverages and (2) approximately equal to the heat of vaporization of ammonia. The significance of the heats in relation to the isotherms is discussed and a model for the adsorbed film is presented in which the ammonia adsorption occurs in patches one molecule thick. It is suggested that adjacent adsorbate molecules are held together within these patches by forces of lateral interaction which are largely due to hydrogen bond formation. There is an apparent anomaly in the ammonia isotherms on Spheron (2700°) in that adsorption *increases* with temperature at a given relative pressure. This observation is discussed in relation to the heats of adsorption.

## Introduction

Recent investigations in this Laboratory have been concerned with the adsorption of gases on carbon black surfaces. In particular we have studied a series of blacks which have been graphitized at successively higher temperatures up to 2700°. The adsorbates used in these studies were argon,[3] a non-polar gas, and sulfur dioxide,[4] a typical polar adsorbate. The following two observations, which have a bearing on the present work, have come out of the research mentioned above: (1) the adsorption of sulfur dioxide, unlike that of argon, is markedly sensitive to presence of oxygen complexes on the carbon surface, (2) on the most homogeneous, highly graphitized carbon, there is strong positive lateral attraction between the adsorbed molecules whether they be argon or sulfur dioxide.

Following the studies with argon and sulfur dioxide, it is a natural step to extend the experiments to include adsorbates like water and ammonia which are capable of hydrogen bonding. Such hydrogen bonding may be expected to occur between adjacent adsorbed molecules or between adsorbed molecules and the surface if the latter contains oxygen complexes. Of the adsorbates

capable of hydrogen bond formation, methanol[5] and water[6,7] have been studied by adsorption calorimetry. The net differential heat of adsorption of methanol on Graphon has a small positive value which changes only slightly with coverage. Conversely, negative net heats of adsorption have been found for water on Graphon which is essentially the same as Spheron (2700°). Our calorimetric technique is not adaptable to the water–carbon system because in this case so little adsorption occurs before a high relative pressure has been reached. The present work has therefore been confined to ammonia and methylamine which can be handled conveniently. Particularly in the case of the system ammonia–Spheron (2700°), in support of a possible model of the adsorbed film, the heat-coverage data have provided experimental evidence which is considerably more convincing than that provided by the isotherms alone.

Evidence concerning the degree of hydrogen bonding in water adsorbed on porous silica gel and on alumina has been obtained by Freymann and Freymann[8] by means of microwave absorption. Milligan and Whitehurst[9] have measured the diamagnetic susceptibility of vapors adsorbed on

(1) This research was supported under contract by the Office of Naval Research to which our best thanks are due.

(2) Admiralty Research Laboratory. Teddington, Middlesex, England.

(3) R. A. Beebe and D. M. Young, This Journal, **58**, 93 (1954).

(4) R. A. Beebe and R. M. Dell, *ibid.*, **59**, 746 (1955).

(5) B. Millard, R. A. Beebe and J. Cynarski, *ibid.*, **58**, 468 (1954).

(6) A. C. Zettlemoyer, G. J. Young, J. J. Chessick and F. H. Healey, *ibid.*, **57**, 649 (1953).

(7) F. E. Bartell and R. M. Suggitt, *ibid.*, **58**, 36 (1954).

(8) M. Freymann and R. Freymann, *Compt. rend.*, **232**, 1096 (1951).

(9) W. O. Milligan and H. B. Whitehurst, This Journal, **56**, 1073 (1952).

silica gel. These authors conclude that, for water and propyl alcohol, hydrogen bonds are not formed between adsorbate molecules at less than monolayer coverage, but that in subsequent layers hydrogen bonding does occur.

Interpretation of data obtained by physical techniques such as microwave absorption or magnetic susceptibility, when applied to adsorption on a porous solid, is complicated by uncertainty regarding the surface area of the adsorbent and by the possibility of capillary condensation. Thus it has seemed to us to be appropriate to study the non-porous carbon blacks. In particular the Spheron (2700°) black, in addition to being non-porous, represents a non-polarizing, physically homogeneous surface. On this adsorbent, ammonia appears to be adsorbed in patches one molecule thick with hydrogen bonding between adjacent ammonia molecules in the patches.

There are on record few theoretical treatments of the adsorption of polar molecules or of molecules capable of hydrogen bonding. Calculations of the heat of adsorption of ammonia on conductors by Roberts,[10] on non-conductors by Miller[11] and on ionic crystals by Crawford and Tompkins[12] have not taken consideration of hydrogen bond formation *between adsorbed ammonia molecules.* It is our belief that such a theoretical approach as that made by the above investigators cannot at present be very fruitful when applied to the ammonia–Spheron systems because of the absence of any definite information concerning the orientations of the laterally hydrogen bonded ammonia molecules on the surface.

## Experimental

**Materials.**—Ammonia of stated purity 99.9% was supplied by the Matheson Company. The gas was admitted to an evacuated system, liquefied at $-78°$, dried over metallic sodium and subjected to two bulb to bulb distillations. The middle fraction of the distillate was collected and stored.

Methylamine was prepared by treatment of methylamine hydrochloride with calcium hydroxide. Both solid reagents were first thoroughly outgassed in a vacuum system, the hydrochloride being kept at $-78°$ together with a little frozen water. On subsequent mixing of the reactants with gentle warming, the methylamine was evolved and dried by passing over solid potassium hydroxide. The gas was condensed and redistilled several times over further potassium hydroxide to ensure drying.

Helium of 99.9% purity was also obtained from the Matheson Company. Three samples of carbon black were employed: the parent material Spheron 6, together with heat treated samples Spheron (1000°) and Spheron (2700°).[13] Treatment at 1000° removes most of the oxygen which is chemisorbed on the surface of Spheron, while heating to 2700° results in a graphitization process producing a highly uniform, graphite-like surface. The surface areas of these carbons, as measured by nitrogen adsorption, are Spheron 114 sq. m./g., Spheron (1000°) 91.1 sq. m./g., Spheron (2700°) 84.1 sq. m./g.[14] Analytical data are given in a previous publication[4] and the structure of graphitized carbon

black is discussed fully in the paper of Schaeffer, Smith and Polley.[15]

**Apparatus and Procedure.**—Adsorption isotherms of ammonia on carbon black were determined at various temperatures between $-78$ and $0°$. For measurements at $0°$ an ice-water constant temperature bath was employed, while for $-78°$ Dry Ice was used. Intermediate temperatures were obtained with baths of melting organic substances, *i.e.*, tetrachloroethylene ($-22°$), ethylene dichloride ($-36°$) and chlorobenzene ($-46°$). These were each redistilled before use. Two ammonia vapor pressure thermometers were constructed covering the range 0–1 atmosphere (below $-33°$) and 1–2 atmospheres ($-33°$ to $-18°$). As each adsorption point on an isotherm was measured, the value of $P_0$ recorded on the vapor pressure thermometer was observed and used to compute $P/P_0$. The temperature of the bath did not fluctuate by more than $\pm0.15°$ during any run, as shown below.

| Bath | Measured $P_0$, cm. | Temp., °C.[a] | M.p., °C.[b] |
|---|---|---|---|
| CCl$_2$=CCl$_2$ | 129.2–129.6 | $-22.2 \pm 0.05$ | $-22.35$ |
| CH$_2$Cl—CH$_2$Cl | 64.8–65.6 | $-36.3 \pm .1$ | $-35.3$ |
| C$_6$H$_5$Cl | 39.2–39.4 | $-45.7 \pm .0$ | $-45.1$ |
| Dry Ice | 4.05–4.15 | $-78.8 \pm .15$ | $-78.5$ |

[a] Based on vapor pressure data from "International Critical Tables." [b] The melting points were taken from the "Handbook of Chemistry and Physics," Chemical Rubber Publishing Co., 1953.

Except for the calorimeter, an all-glass vacuum system of the conventional type was employed. Increments of gas were measured in a water jacketed buret and the volume of residual unadsorbed gas calculated from deadspace calibrations made with helium. Consideration was given to correcting for the non-ideality of ammonia with respect to (1) the residual unadsorbed gas (2) the volume measured in the buret. In estimating these corrections, the virial equation was used, the second virial coefficient of ammonia being given by the data of Keyes.[16] The correction to be applied to the unadsorbed gas varied from 0.1 to 0.4% and the correction to the gas measured in the buret was approximately 0.3%. These corrections were considered to be within experimental error and therefore were not made.

Adsorption of ammonia on Spheron (2700°) was rapid and equilibrium was established almost at once; repeated runs on this adsorbent showed the measurement to be highly reproducible. In the case of the original Spheron, there was a rapid initial adsorption followed by a slow uptake which continued for several hours. After the first few minutes the rate was insufficient to introduce detectable error into the heat measurements. Similar results were found for the rate of adsorption of sulfur dioxide on these two carbons.[4] Adsorption of methylamine on Spheron (2700°) was not so rapid as that of ammonia and complete equilibrium was not attained in the first few minutes.

Calorimetric measurements were made for adsorption of ammonia at $-78°$ on all three carbon blacks and for methylamine at $0°$ on Spheron (2700°). In addition, heats were measured at $0°$ for adsorption of a few increments of ammonia on Spheron (2700°). The latter measurements could not be extended beyond a low surface coverage because of the high equilibrium pressure at $0°$.

The calorimeter design has been described previously.[17] Differential heats were measured using a single junction copper–constantan thermocouple, the voltage being amplified by a Perkin–Elmer d.c. breaker amplifier and recorded on an Esterline–Angus pen recording voltmeter. Calibration was effected by supplying electrical energy to the calorimeter through a heating coil. In the experiments on ammonia–Spheron (2700°), the calorimeter was employed "adiabatically" as described previously.[4] Operation in this fashion minimizes errors due to heat losses and gives highly reproducible results. Temperature control of a $-78°$ bath with the precision necessary for calorimetry was found to be more more difficult than for work at $0°$ or at $-195°$. However, satisfactory results were obtained

(10) J. K. Roberts, *Trans. Faraday Soc.*, **34**, 1342 (1938).

(11) A. R. Miller, *Proc. Camb. Phil. Soc.*, **42**, 292 (1946).

(12) V. A. Crawford and F. C. Tompkins, *Trans. Faraday Soc.*, **44**, 698 (1948); **46**, 504 (1950).

(13) The temperature of heat treatment is indicated: Spheron (1000°) indicates a sample of Spheron treated for two hours at 1000°. The Spheron (2700°) is essentially the same as Graphon which has been previously studied [*J. Am. Chem. Soc.*, **69**, 95 (1947)].

(14) M. H. Polley, W. D. Schaeffer and W. R. Smith, THIS JOURNAL, **57**, 469 (1953).

(15) W. D. Schaeffer, W. R. Smith and M. H. Polley, *Ind. Eng. Chem.*, **45**, 172 (1953).

(16) F. G. Keyes, *J. Am. Chem. Soc.*, **60**, 1761 (1938).

(17) R. A. Beebe, J. Biscoe, W. R. Smith and C. B. Wendell, *ibid.*, **69**, 95 (1947).

when the cold junction of the thermocouple was surrounded by alternate layers of metal conductor and insulating material. Before starting an experiment, the calorimeter was allowed to remain overnight to attain temperature equilibrium. The over-all accuracy of heat measurements obtained with this design of calorimeter is estimated to be about ±3%. In the case of ammonia adsorption at 0°, the accuracy is probably less because of the relatively large correction for unadsorbed gas. Correction of the measured heats for the heat of compression of the gas within the calorimeter was shown to be negligible, as was also true for sulfur dioxide[4,18]; this statement is especially applicable to ammonia at −78° where $P_0$ is only 4.1 cm.

## Results

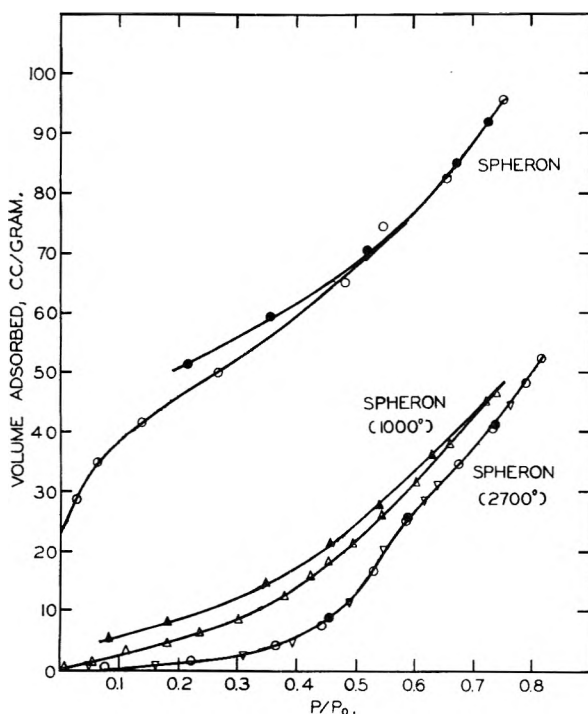Ammonia isotherms on each of the three carbon blacks studied are compared in Fig. 1 for adsorption

Fig. 1.—Isotherms, ammonia on carbon blacks at −36.3°: adsorption points open, desorption points blackened.

at −36.3° and in Fig. 2 for adsorption at −78.8°. It is observed that the parent carbon black, Spheron 6, adsorbs appreciably more ammonia than the heat treated samples and this effect is more marked for adsorption at the higher temperature. The decline in adsorptive capacity with sintering parallels qualitatively the loss in surface oxygen complex.[4] Desorption hysteresis is present for both Spheron and Spheron (1000°) at −36.3° but uptake on the comparatively uniform oxygen-free surface of Spheron (2700°) is completely reversible. No desorption measurements were made at −78.8° on account of the low equilibrium pressure; nor were desorption measurements made at −22.2 or −45.7°. Figure 3 shows isotherms for ammonia adsorption on Spheron (2700°) at four different temperatures. In each case the isotherms are reproducible. The increase with temperature of the volume adsorbed at a given relative pressure is surprising and its significance will be discussed in a later section.

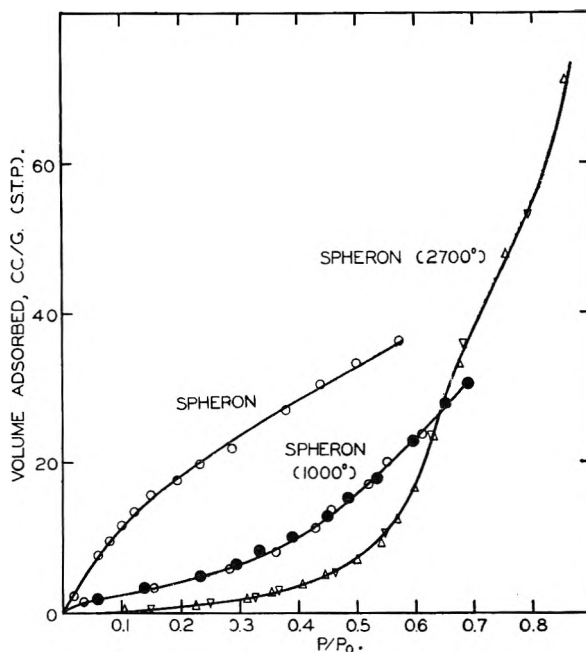(18) G. L. Kington and J. G. Aston, J. Am. Chem. Soc., 73, 1929 (1951).

Fig. 2.—Isotherms, ammonia on carbon blacks at −78.8°: adsorption points open, desorption points blackened.

In Figs. 4–6 we have plotted, as a function of coverage, the calorimetric heats of adsorption for ammonia at −78° on the three carbon blacks. Calorimetric results for ammonia–Spheron (2700°) at 0° are given in Fig. 7. In view of the negligible correction for the heat of compression as mentioned above, the calorimetric heat values in Figs. 4 and 5 and in the upper curve of Fig. 6 are identical with isosteric heats. Because of the highly uniform, graphite-like structure of the Spheron (2700°) surface and because this adsorbent was essentially free from any material other than carbon, the calorimetric data for the ammonia–Spheron (2700°) system were analyzed with special care.

The isotherm and the heat-coverage curve for adsorption of methylamine on Spheron (2700°) are shown in Figs. 8 and 9, respectively. No measurements were made of methylamine adsorption on Spheron or Spheron (1000°).

## Discussion

**I. Adsorption of Ammonia on Spheron.**— The isotherms of Figs. 1 and 2 show that the original carbon black, Spheron, is capable of adsorbing appreciably more ammonia than the heat treated material. As the degree of graphitization increases through the series Spheron, Spheron (1000°), Spheron (2700°), the shape of the ammonia isotherm changes progressively from a characteristic Type II isotherm to one that is convex to the pressure axis at low pressures. Similar though somewhat less pronounced effects are observed with sulfur dioxide.[4] In the case of the non-polar molecule argon, heat treatment of the carbon black has comparatively little effect on the amount adsorbed at a given relative pressure, although here the increasing uniformity of the surface is reflected by a minor change in the isotherm shape.[3] We have tentatively ascribed the enhanced adsorption of sulfur dioxide by Spheron, compared with that
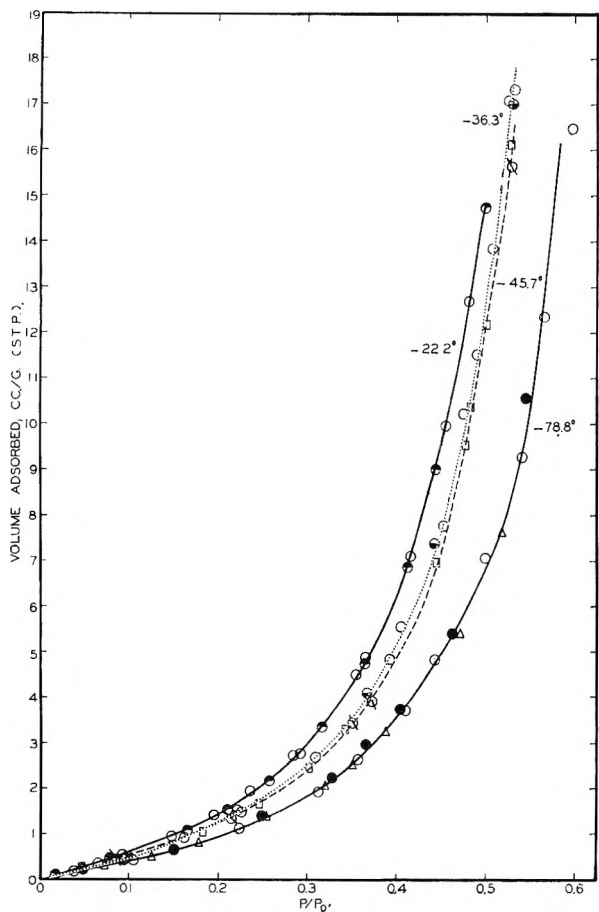
Fig. 3.—Adsorption of ammonia on Spheron (2700°): run 12 ○, run 13 ◓ at −22.2°, saturation pressure 129.5 cm.; run 5 ◕, run 9 ○ at −36.3°, saturation pressure 65.2 cm.; run 6 ◒, run 10 □ at −45.7°, saturation pressure 39.3 cm.; run 4 △, run 7 ●, run 11 ○ at −78.8°, saturation pressure 4.1 cm.

by graphitized carbon black, to orientation of the dipoles of the adsorbate by the polarizing surface, although the possibility of chemisorption on the surface oxygen is not discounted.

Comparison of the ammonia and sulfur dioxide adsorption data on Spheron reveals an important point of difference. After an initial sharp drop.
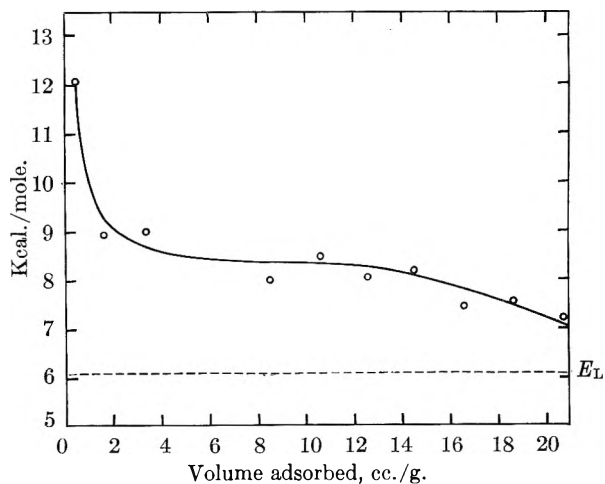


Fig. 4.—Heat of adsorption of ammonia on Spheron 6 at −78°.
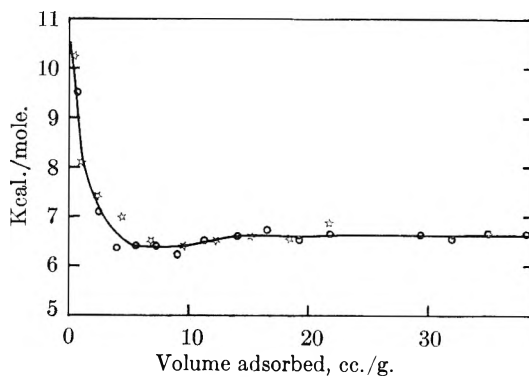


Fig. 5.—Heat of adsorption of ammonia on Spheron (1000°) at −78°.
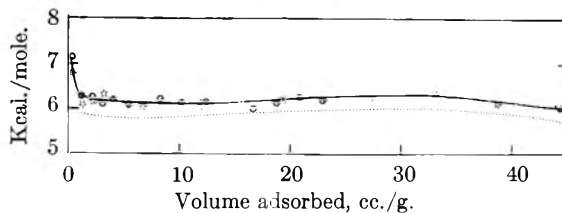


Fig. 6.—Calorimetric heat of adsorption of ammonia on Spheron (2700°) at: −78° ———; equilibrium heat . . . .
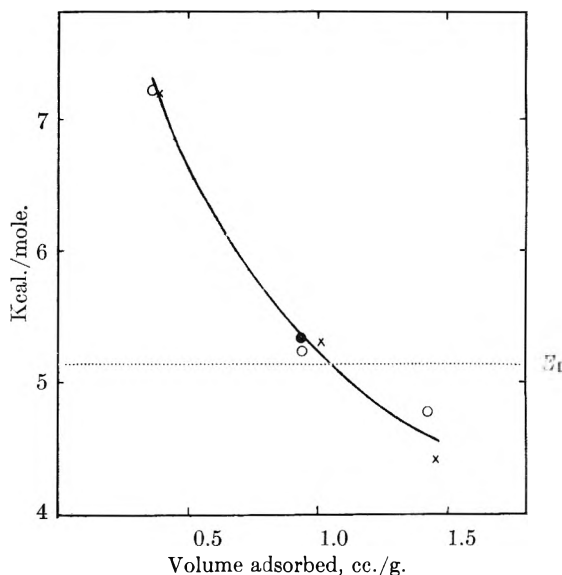


Fig. 7.—Heat of adsorption of ammonia on Spheron (2700°) at 0°.

the heat of adsorption of ammonia on Spheron remains relatively constant at 8–9 kcal. per mole up to a surface coverage of 15 cc. per g. (see Fig. 4) and remains well above the heat of vaporization. With sulfur dioxide, the heat of adsorption on Spheron falls steadily with increasing coverage and approaches the heat of vaporization. It is possible that the ammonia gas is bound to the surface oxygen by some type of chemical complex rather than by simple physical adsorption of polar molecules on a polarizing surface. It is known that the oxygen complex present on the surface of Spheron is acidic in nature and adsorption of a basic anhydride such as ammonia may well correspond to a neutralization of the surface or "salt formation." Certainly, the influence of surface oxygen complexes on porous charcoal in increasing the adsorp-

Fig. 8.—Adsorption of methylamine on Spheron (2700°) at 0°.

and Zisman[21] has shown that hydrogen bonding of adsorbate molecules to surfaces, forming complexes of the type N-H- - -F, -O-H- - -F, is a real phenomenon.

While our present results do not serve to elucidate fully the mechanism of ammonia adsorption on Spheron, largely because of the uncertain and complex composition of the surface, nevertheless the above considerations suggest that the mechanism is quite different from that responsible for sulfur dioxide.

**II. Adsorption of Ammonia on Spheron (2700°).** —At all temperatures we have studied, ammonia isotherms on Spheron (2700°) have the general form shown in Fig. 1. The isotherm is initially convex to the pressure axis at low surface coverages and then rises steeply, passing through a point of inf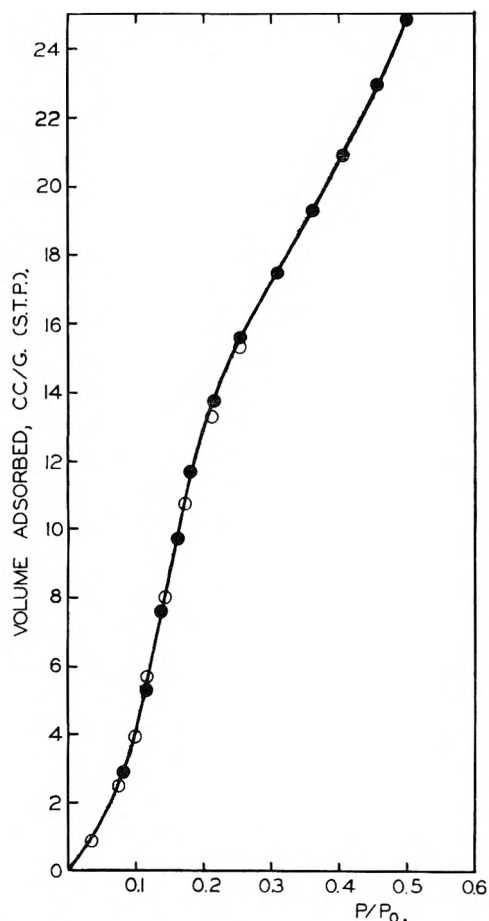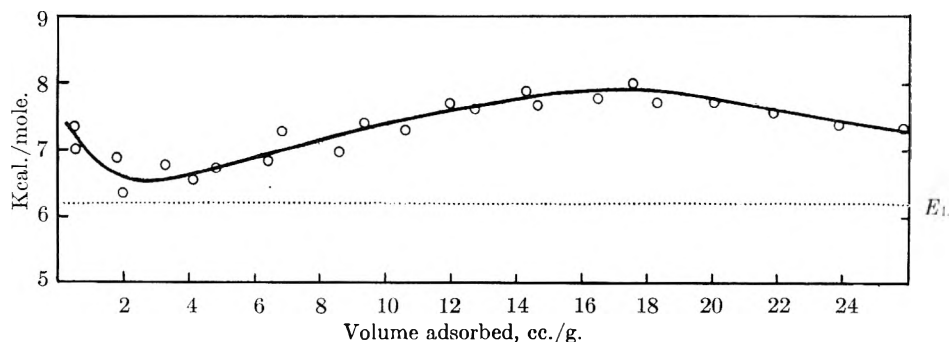lection at a relative pressure of 0.5–0.7. A qualitatively similar isotherm has been reported by Pierce and Smith[22] for the adsorption on Graphon of methanol which likewise is a hydrogen bonded substance. This shape of isotherm differs from any of the five usual types classified by Brunauer[23] and was therefore designated Type VI.

Smith and Pierce have also studied the adsorption of ammonia on graphite.[24] Here again the isotherms are of Type VI, but, because of the small surface area of graphite 4.0 sq. m./g. compared with 84 sq. m./g. for Spheron (2700°) and the correspondingly small volume of gas adsorbed, the point of inflection was overlooked at first and the isotherms reported as Type III. In a later paper, in which Type VI isotherms for methanol were reported,[22] the same authors pointed out that the ammonia isotherms as well were actually of Type VI. The above authors identified the point of



Fig. 9.—Heat of adsorption of methylamine on Spheron (2700°) at 0°.

tion of alkali from solution has been fully established.[19]

Anderson and Emmett[20] also have studied the adsorption of ammonia on carbon black and, like us, find considerably more adsorption on Spheron than on a heat treated Spheron from which most of the chemisorbed oxygen has been removed. This they attribute to solution of the ammonia in the surface oxygen complex with possible formation of hydrogen bonds. Such an explanation is not unreasonable as the unsymmetrical N-H- - -O hydrogen bond is often bound in organic compounds. Moreover, recent work by Ellison, Fox

inflection as representing the completion of a monolayer and the amount of methanol adsorbed at this point agreed well with the computed value of $V_m$ based on nitrogen surface area measurements and on an area of 16.2 sq. A. for the methanol molecule. In the present investigation of the adsorption of ammonia on Spheron (2700°), the point of inflection varies considerably with the temperature at which the isotherm was determined. The value of $V_m$, estimated from the point of inflection, is of the same order as that

(19) S. Weller and T. F. Young, J. Am. Chem. Soc., 70, 4155 (1948).

(20) R. B. Anderson and P. H. Emmett, This Journal, 56, 756 (1952).

(21) A. H. Ellison, H. W. Fox and W. A. Zisman, ibid., 57, 622 (1953).

(22) C. Pierce and R. N. Smith, ibid., 54, 354 (1950).

(23) S. Brunauer, "The Adsorption of Gases and Vapors," Princeton University Press, Princeton, N. J., 1943.

(24) R. N. Smith and C. Pierce, This Journal, 52, 1115 (1948).

expected for a close-packed monolayer based upon liquid density measurements, but more detailed considerations do not appear to be warranted.

The isosteric heats for ammonia–Spheron (2700°) shown in Fig. 6 are particularly interesting and unusual in two respects: (1) they are nearly constant at all coverages and (2) they are nearly equal to the heat of vaporization of ammonia. These observations can be explained on the basis of a model in which adsorption is initiated on relatively few active centers, and proceeds by the formation of adsorbed patches, one molecule in thickness, around these centers. Since the forces operative in holding a monolayer of ammonia to a carbon surface are by no means identical with those in the bulk liquid ammonia, it appears to be fortuitous that the heats of adsorption and of vaporization have virtually the same value.[25] However, the two systems under consideration do have the common feature that hydrogen bonding is present to a large degree in each. It is therefore of interest to form an estimate of the percentage to which hydrogen bonding contributes to the heat of vaporization and to the heat of adsorption.

It is generally accepted that hydrogen-bonding contributes heavily to the total binding energy in bulk ammonia whether solid or liquid. Using the method of Pauling[26] it is possible to estimate the contribution of van der Waals attraction and of hydrogen-bonding in solid ammonia at −78° as 2.6 and 4.8 kcal. per mole, respectively, out of a total heat of sublimation of 7.4 kcal.[27] Thus the hydrogen bond energy represents 65% of the heat of sublimation. We are not aware of a suitable method for calculating the percentage contribution of hydrogen bonding to the heat of vaporization of liquid ammonia at −78°. However, it seems probable that it would be of the same order of magnitude as in the solid state although possibly somewhat less. Thus it is reasonable to estimate that hydrogen bonding would contribute from 50 to 65% of the total binding energy in the liquid state.

(25) In comparing the heat of adsorption with the heat of vaporization, it appears to be more valid from a thermodynamic point of view to correct the isosteric heats to equilibrium heats, as defined by Hill [*J. Chem. Phys.*, **17**, 520 (1949)] at constant value of φ the spreading pressure. The equilibrium heats have been calculated for the system ammonia–Spheron (2700°) at −78° and they are shown in Fig. 6. In making this calculation the percentage error in the pressures must be small in order to avoid large errors in evaluating the spreading pressure, a quantity which is required in calculating the equilibrium heats. A similar calculation of the equilibrium heats has been made for the system sulfur dioxide–Spheron (2700°) at 0° using the experimental data given in Paper I of this series.[4] In the sulfur dioxide case, the equilibrium heats are about 0.5 kcal./mole lower than the isosteric heats at low coverage and the difference is almost 1.0 kcal./mole near the end of the monolayer. This has the effect of flattening out the maximum somewhat in the equilibrium heat curve, indicating a somewhat smaller effect due to lateral interaction than would be inferred from the isothermal heat data.

(26) L. Pauling, "Nature of the Chemical Bond," Cornell University Press, Ithaca, N. Y., 1945.

(27) The value used by Pauling for the total heat of sublimation of ammonia is believed to be in error. The heat of fusion of ammonia at −78° is 1.3 kcal./mole. Figure 10 shows that the heat of vaporization at that temperature is 6.1 kcal./mole giving a heat of sublimation of 7.4 kcal./mole. Pauling's value of 6.5 kcal./mole is based upon the heat of vaporization at the boiling point. During fusion, some of the hydrogen bonds present in the solid are broken. Further bonds are disrupted on warming the liquid to the boiling point. By using the value of 5.2 kcal. at the boiling point, Pauling does not include the latter in his calculation.
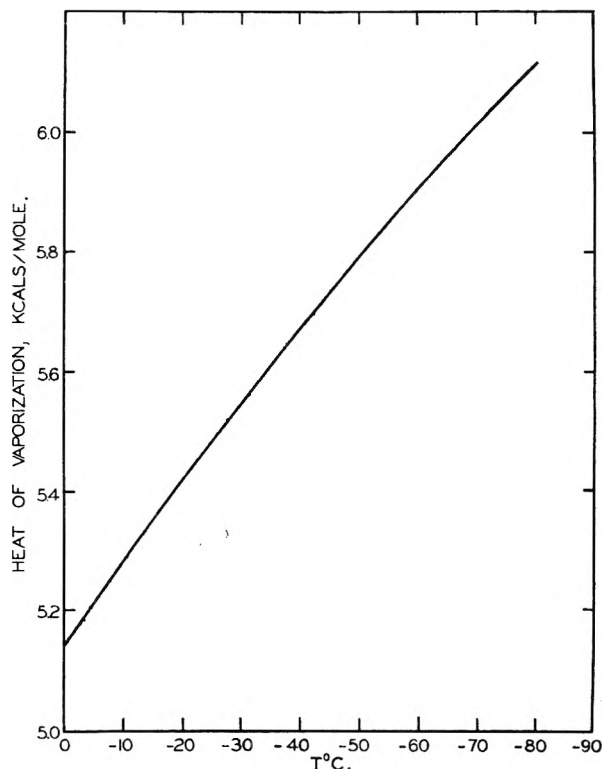


Fig. 10.—Heat of vaporization of ammonia as a function of temperature.

It seems probable to us that hydrogen bonding is likewise an important factor in the total energy of binding in the ammonia film on the carbon surface. In fact, we estimate that van der Waals attraction of the surface for ammonia molecules probably contributes no more than 50% of the heat of adsorption. This estimate is based on the following reasoning. We assume that there is virtually no oxygen on the Spheron (2700°) surface. Thus the only direct attraction between the surface and any adsorbed ammonia molecules would be due to van der Waals forces. Previous work in this laboratory has shown that the heat of adsorption of n-butane on Graphon, a carbon adsorbent which is essentially the same as Spheron (2700°), is 8–9 kcal./mole.[28] It seems justifiable to assume that the molecules of n-butane are adsorbed with their major axes lying in the plane of the adsorbing surface.[29] Thus, each −CH₂ or −CH₃ group would contribute about one fourth of the heat of adsorption or approximately 2.2 kcal./mole. It is reasonable to assume that the van der Waals attraction of the carbon surface for ammonia (molecular weight 17) would be roughly the same as that for −CH₂ (molecular weight 14), although molecular configuration would doubtless be a contributing factor. Suppose we assume a van der Waals attraction of 3.0 kcal./mole for ammonia to the carbon surface; this leaves an additional 3.0 kcal. which must be accounted for as lateral interaction between adjacent adsorbed ammonia molecules. It seems probable that lateral interaction of this magnitude must be due

(28) R. A. Beebe, M. H. Polley, W. R. Smith and C. B. Wendell, *J. Am. Chem. Soc.*, **69**, 2297 (1947).

(29) R. A. Beebe, G. L. Kington, M. H. Polley and W. R. Smith, *ibid.*, **72**, 40 (1950).

in large part to hydrogen-bonding of adjacent ammonia molecules. Moreover, since the heat of adsorption is almost 6.0 kcal./mole even at coverages as low as 2 cc./g., it would appear that the high contribution (3.0 kcal./mole) due to lateral interaction must be effective even on a relatively bare carbon surface. Such a set of conditions is satisfied by a model in which adsorption is initiated at relatively few active centers, but proceeds by the formation of patches around these centers.

The above model would differ from that which has been postulated for argon on a similar carbon surface[3] in which the surface presented to the argon a system of non-localized sites. With argon, lateral interaction becomes important only after the monolayer approaches completion.

The equilibrium entropy is readily obtained from the equilibrium heat. When regarding the system as a pseudo one-component system, i.e., adsorbate in the force field of the adsorbent, then it is this integral entropy which can be related to statistical mechanical models. As Hill, et al., point out, the corresponding differential quantities may be totally misleading.[30] "Net" entropies with coverage are plotted in Fig. 11. It may be seen, that adsorption of the first two cubic centimeters of ammonia is accompanied by a steep decrease in the equilibrium entropy curve, showing decreasing randomness of motion of the adsorbed molecule. From then on a more gradual decline toward a minimum near the completion of the first layer indicates a relatively smaller change in molecular order with coverage. As is to be expected, maximum order is to be found near the completion of the first layer.
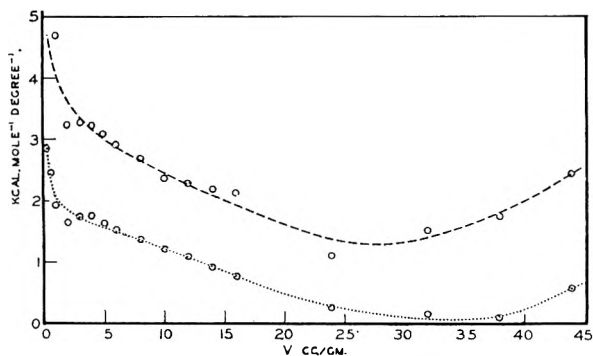


Fig. 11.—Entropy of ammonia on Spheron (2700°) at −78.8°: net equilibrium entropy ————; net differential entropy............

### III. Adsorption of Ammonia on Spheron (1000°).

—Heat treatment of Spheron at 1000° is known to remove most of the chemisorbed oxygen, while X-ray studies show that little graphitization has taken place at this temperature.[4,14,15] In these respects Spheron (1000°) stands in a position intermediate between Spheron and Spheron (2700°). This intermediate position is reflected in the isotherms of Figs. 1 and 2 and in the heat curves of Figs. 4, 5 and 6. This relative behavior of ammonia on the three blacks is very similar to that previously observed for sulfur dioxide.[4] In comparing the isotherms for the three blacks, we should

(30) T. L. Hill, P. H. Emmett and L. G. Joyner, J. Am. Chem. Soc., **73**, 5102 (1951).

remember that nitrogen surface area determinations give evidence of a decrease in specific surface area with increasing temperature of graphitization. However, the relative positions of the isotherms in Figs. 1 and 2 are not appreciably altered if the ordinates are plotted as cc. per sq. m. of surface rather than cc. per g.

It is interesting to note from Fig. 5 that most of the sites in the parent Spheron, capable of adsorbing ammonia with a heat higher than 8 kcal./mole, have been destroyed by heat treatment at 1000°. After the first 3 cc./g., any further adsorption produces heats which are only slightly greater than those observed in the most highly graphitized sample, Spheron (2700°). Since little graphitization has occurred at 1000°, the above observations confirm our previous conclusion that the high heats on the Spheron as shown in Fig. 4 are due to reaction of the ammonia with surface oxygen complex rather than to simple physical adsorption on the Spheron surface.

### IV. Adsorption of Water on Graphon.

—It is of interest to contrast the results for the adsorption of ammonia on Graphon with those for water vapor. Water, like ammonia, is a low molecular weight, hydrogen bonded substance. Yet adsorption of water vapor on the oxygen-free, non-porous carbon is virtually absent at room temperature below a relative pressure of 0.9. In fact, Graphon may be classified as a hydrophobic surface. In this respect, ammonia differs from water as is seen from Fig. 1. Simple physical adsorption of single water molecules (molecular weight 18) would not normally be expected at room temperature to any appreciable degree. Although water is strongly adsorbed at low relative pressure on many solids, the mechanism in such cases is invariably one of chemisorption, hydration of ions, capillary condensation, or hydrogen bonding to the surface. It is probable that adsorption of water on silica gel, for example, takes place by forming O-H- - -O bonds with the surface. Such adsorption of discrete molecules would explain why the magnetic susceptibility and microwave absorption technique gave no evidence of hydrogen bonding between water molecules. On a uniform, inert surface where the possibilities for the above mechanism of adsorption do not exist, water is not appreciably adsorbed, except at very high relative pressures. Droplets of water will not spread on these non-polar surfaces but form finite angles of contact. The contrast with ammonia uptake on Spheron (2700°) is marked. It appears that adsorption of water with lateral hydrogen bonding between adjacent molecules does not readily occur. The reason for this is not at once apparent, but may be associated with the relatively high energy of the O-H- - -O bond (4.5 kcal./mole) and the open tetrahedral configuration of hydrogen bonded water.[26] Ammonia, by comparison, is weakly hydrogen bonded and may have an almost close-packed structure. In order for a nucleus of adsorbed water to grow laterally in a monolayer on a uniform surface, a marked distortion of the strong O-H- - -O bonds would be necessary. With ammonia, the weaker N-H- - -N bonds may be more

readily distorted under the combined influence of the surface and the neighboring adsorbed molecules.

Recent heats of wetting measurements by Zettlemoyer, et al.,[6] for water–Graphon and by Bartell and Suggitt[7] for water–graphite have shown that the net heat of adsorption at low coverage is negative in these cases; i.e., the calorimetrically measured heat of adsorption is less than the heat of vaporization. As we have mentioned previously, it is more justifiable in comparing heats of adsorption with heats of vaporization to consider equilibrium heats of adsorption at constant spreading pressure. However, it is noteworthy that a specific adsorption type is characterized by the sign of the net heat of adsorption. Thus, as we go from a Type II isotherm as typified by nitrogen and argon on Graphon through intermediate stages (ethyl chloride,[31] methanol,[22] sulfur dioxide[4] and ammonia on Graphon) to a Type III isotherm (water–Graphon)[32] the net heats of adsorption shift from strongly positive to definitely negative values. It happens that ammonia–Graphon illustrates an intermediate stage where the net heat of adsorption is virtually zero.

**V. Adsorption of Methylamine on Spheron (2700°).**—The isotherms for adsorption of ammonia and methylamine on Spheron (2700°) and methanol on Graphon resemble each other in being of Type VI. These are the only three examples of Type VI isotherms so far reported and it will be observed that each of the adsorbates is a substance which is hydrogen bonded in the liquid state.

The heat-coverage curve for methylamine on Spheron (2700°) differs from that for ammonia in that the heat rises somewhat with coverage and passes through a maximum. In this respect, the curve is similar to that for sulfur dioxide adsorption. The maximum heat value for methylamine occurs at a coverage of about 17 cc./g. which corresponds with the rather ill-defined point $V_m$ for the isotherm (16 ± 1 cc./g.). Similarly, in the case of sulfur dioxide adsorption, the maximum heat value is found at about the same coverage as the point $V_m$. However, this coverage is somewhat less than that necessary for a close packed monolayer and entropy considerations suggest that second layer formation commences before a monolayer is completed. It is important to observe that the isotherms for both ammonia and methylamine, which are adsorbates capable of hydrogen bonding, do show a point of inflection somewhere in the region of monolayer coverage. This is strong evidence[22] that hydrogen bonding is largely confined to two dimensions between adjacent adsorbed molecules and that three dimensional bonding, resulting in droplet formation, does not occur to any appreciable extent.

On the basis of heats of adsorption and isotherm measurements alone it is not possible to draw detailed conclusions concerning the mode of adsorption of methylamine, but this adsorbate does appear to stand in a position which is intermediate

(31) J. Mooi, C. Pierce and R. N. Smith, THIS JOURNAL, **57**, 657 (1953).
(32) C. Pierce, R. N. Smith, J. W. Wiley and H. Cordes, J. Am. Chem. Soc., **73**, 4551 (1951).

between ethyl chloride[31] and ammonia when adsorbed on an oxygen-free carbon surface.

**VI. The Effect of Temperature on the Adsorption of Ammonia on Spheron (2700°).**—The isotherms shown in Fig. 3 are rather unusual in that adsorption *increases* with increasing temperature at a given relative pressure. Several examples of this phenomenon are to be found in the literature, but so far as we are aware, the examples are limited to the adsorption of either water vapor or ammonia on carbon surfaces. Coolidge[33] was the first to observe this effect in the case of water adsorption on an ash-free charcoal carefully prepared from recrystallized cane sugar. He found an increase in adsorption with temperature over the range 60 to 218° in the relative pressure region 0 to 0.3; but the isotherms at 20 to −30° were coincident. In discussing the significance of his observations Coolidge makes the following comments.

"These relations become very interesting when we consider their bearing on the energy changes involved. The "net heat of adsorption" or heat of transfer from free liquid to adsorption may be obtained by substituting the relative for the absolute pressure in the Clapeyron equation. The distance between two isotherms, measured along a line of constant concentration, evidently indicates the sign and magnitude of the net heat. More accurate values may be obtained from the slopes of the isosteres as directly determined, but the qualitative relations are more easily apprehended from the isotherms. The net heat is zero when the relative pressure is the same at different temperatures, which is true for low concentrations between −30 and 20°. Above 20° it is negative, decreasing rapidly as the temperature rises. This would seem to be the first case in which the total heat of adsorption has been found to be less than the heat of vaporization."

Pierce and Smith[34] found that the isotherms for water–Graphon were coincident at 0 and 28.6° up to 0.9 relative pressure. Following the suggestion of Coolidge, these authors conclude that their isotherm data indicate a zero net heat of adsorption. In a later paper, Pierce, et al.,[32] reported that water adsorption was considerably *increased* by raising the temperature from 28.6 to 80°. However, these investigators showed that a reaction occurs between water vapor and Graphon at all temperatures throughout the range 25 to 150°. They make the reasonable suggestion that this reaction between the water and the carbon produces a C–O complex on the surface, which is known to adsorb water better than a clean carbon surface. They therefore conclude that the large negative value of $E − E_L$ which appears to be indicated by the comparison of the 80° and the 28.6° isotherms is spurious, since the isotherms are not on the same surface.

In the system ammonia–Spheron (2700°) we have no evidence of any chemical reaction between the ammonia and the carbon surface in the temperature range studied (−78 to 0°). Certainly

(33) A. S. Coolidge, ibid., **49**, 709 (1927).
(34) C. Pierce and R. N. Smith, THIS JOURNAL, **54**, 795 (1950).

no oxygen complex is formed by reaction of the ammonia with the surface. Thus the observation that adsorption increases with temperature at constant relative pressure must be considered as evidence of a real adsorption phenomenon. Moreover, the *calorimetric* heats of adsorption at $-78°$ are, within the experimental error, equal to the heat of vaporization. If we follow Coolidge's suggestion that our isotherms over the range $-78$ to $0°$ should indicate negative net heats of adsorption as calculated by means of the Clapeyron equation, there is an apparent discrepancy between the isosteric and the calorimetric heats.

We believe the explanation of the above apparent discrepancy to be as follows. The conclusion that the net heat of adsorption is negative, if the equilibrium relative pressure decreases with increasing temperature, follows from the following mathematical expression

$$(q_{st.} - E_L) = R \frac{T_2 T_1}{T_1 - T_2} (\log P_1/P_{0_1} - \log P_2/P_{0_2}) \quad (1)$$

where $q_{st.}$ is the isosteric heat of adsorption and $P_{0_1}$ and $P_{0_2}$ are vapor pressures at temperatures $T_1$ and $T_2$, respectively. This equation is obtained by combining the integrated Clausius–Clapeyron equation for liquid/vapor equilibrium with the analogous equation for adsorption and thus involves the approximations inherent in these integrated equations, viz.: (1) $q_{st.}$ and $E_L$ are independent of temperature and (2) $PV = RT$. In a case such as the present where the net heat of adsorption is close to zero, the variations in $q_{st.}$ or in $E_L$ with temperature may well be large enough to reverse the usual order of the isotherms, giving apparent negative net heats.

In Fig. 10, the heat of vaporization of ammonia ($E_L$) is plotted as a function of temperature. Values of $E_L$ were calculated from the Clausius–Clapeyron equation in differential form

$$dP/dT = E_L/T(V_g - V_L) \quad (2)$$

using well established data for the vapor pressure and specific volumes of ammonia.[35] At the boiling point ($-33.4°$), the heat of vaporization so calculated (5.57 kcal./mole) agrees well with direct calorimetric observations of Overstreet and Giauque (5.58 kcal./mole)[36] and of Osborne and Van Dusen (5.57 kcal./mole).[37] Use of the integrated form of the Clausius–Clapeyron equation, involving the perfect gas assumption, gives a value of $E_L$ at the boiling point which is over 100 cal. too high. The variation of $E_L$ with temperature in the range in which the isotherms were measured ($-22$ to $-78°$) is as much as 660 cal. or about 11%.

It is necessary to bear in mind that, in equation 1, it is a variation with temperature in the quantity $q_{st.} - E_L$ which could produce a reversal of the usual order of the isotherms although the calorimetrically measured net heat may be virtually zero. Of course, there is no reason to believe that the quantities $q_{st.}$ and $E_L$ would have the same kind of temperature dependence and thus $q_{st.} - E_L$ may well vary appreciably with temperature. Our calculations, based on equation 1, show that a

variation of a few per cent., over the temperature range under consideration, in the quantity $q_{st.} - E_L$ would be sufficient to cause a reversal of the usual order in the isotherms such as we have observed. It seems probable that these considerations would be especially applicable to hydrogen bonding substances like water or ammonia. It is reasonable to expect a high temperature coefficient of both the heats of vaporization and of absorption because hydrogen bonds would be broken as a result of the increased thermal agitation with increasing temperature.

Because of the above considerations it is not justifiable to make use of the integrated form of the Clapeyron–Clausius equation unless the value $q_{st.} - E_L$ is independent of temperature or unless $T_1$ and $T_2$ are close together. Equation 1 is being used in effect whenever the isosteric heat is calculated from data at two temperatures only. It is noteworthy that Carman and Raal[38] have found a negative net isosteric heat for ammonia on Sterling S carbon black from adsorption data at $-33.1$ and $63.5°$. The net heat may actually be negative in this case, but we cannot be sure without more experimental data. There is of course no reason to exclude the possibility of negative net heats. They have been observed calorimetrically for the systems water–Graphon[6] and water–graphite.[7] From the work of Pierce, et al.,[34,39] it seems probable that Coolidge may have had some reaction between water vapor and his sugar charcoal to produce C–O complexes on the surface and thus account for the higher adsorption of water at higher temperature. On the other hand, there may have been very little chemical reaction with water on Coolidge's charcoal surface and his reversed order of the water isotherms with temperature may be a true adsorption phenomenon as is the case with our ammonia–Spheron (2700°) system. In the light of our above discussion of the relation between isosteric heats and the isotherms, it is evident that such a reversed order, even if real, could not be used as evidence either for or against negative net heats for Coolidge's water–carbon system.

In most laboratories it is now customary in determining isosteric heats of adsorption to plot the functions $1/T$ against $\log P$ at fixed coverages. For this purpose adsorption data are obtained for three or more different temperatures. The heats of adsorption are then read off from the slopes of these plots. This method is based on the differential form of the Clausius–Clapeyron equation. It is fair to point out that Coolidge recommended this method as giving more accurate results. The point is that the use of equation 1 (above) may give results which are so inaccurate as to be quite misleading even in a qualitative sense.

(35) "International Critical Tables," **3**, 234 (1928).

(36) R. Overstreet and W. F. Giauque, *J. Am. Chem. Soc.*, **59**, 254 (1937).

(37) N. S. Osborne and M. S. Van Dusen, *ibid.*, **40**, 14 (1918).

(38) P. C. Carman and F. A. Raal, *Trans. Faraday Soc.*, **49**, 1465 (1953).

(39) R. N. Smith, C. Pierce and C. D. Joel, THIS JOURNAL, **58**, 298 (1954).

# THE KINETICS OF FLUORINATION OF NICKEL OXIDE BY CHLORINE TRIFLUORIDE[1]

By R. Lynn Farrar, Jr., and Hilton A. Smith

*Joint Contribution from the Department of Chemistry, University of Tennessee, and Carbide and Carbon Chemicals Company, Oak Ridge, Tennessee*

*Received March 3, 1955*

A study of the kinetics of fluorination of nickel oxide powders to nickel fluoride with gaseous chlorine trifluoride has been made over the temperature range 25 to 180°, and a mechanism has been proposed by which this conversion process takes place. Pressure variations of 0.3 to 1.0 atmosphere produced a slight effect on the kinetics of conversion which could be explained by the difference in surface concentration of reactant gas at the various pressures. The activity energy was determined to be 19.6 kcal./mole when corrected for decreasing surface concentration of reactant gas at elevated temperatures. The conversion proceeded by a linear rate which meant that the fluorinated material did not form a continuous coating over the unreacted material, in spite of the fact that the molar volume of the product is larger by a factor of two than that of the nickel oxide. Evidence for this mechanism is supported by electron photomicrographs.

## Introduction

This problem was undertaken to provide an insight into the mechanism of the reaction by which very fine nickel oxide powders were converted to nickel fluoride by gaseous chlorine trifluoride. A related study has been carried out by Valensi[2] in which larger nickel powders (diameter 100 to 500 $\mu$) were oxidized at temperatures in excess of 800°. The oxide film was reported to be impervious and the kinetics obeyed the parabolic law of solid–gas reactions. Another similar study has recently been reported by Dunoyer[3] who studied the reduction of molybdenum trioxide to molybdenum dioxide with hydrogen.

## Experimental

**Nickel Oxide.**—All nickel oxide powders were prepared by decomposing basic nickel carbonate of high surface area in air at 200 to 250°. This material was jet black in color with a nitrogen surface area of 150 sq. m. per gram. Further sintering[4] under vacuum at elevated temperatures gave the desired particle sizes (from 3 to 30 sq. m. per gram) for the various experiments. The color of the oxide powders ranged from black for the high area powders (sintering temperature *ca.* 400°) through gray to light green for the low area powders (sintering temperatures *ca.* 1000°). There was an increase in nickel analysis of the powders with increasing sintering temperature. All samples showed X-ray powder patterns of the typical nickel oxide structure. One is drawn to the conclusion that there is an excess of oxygen in nickel oxide, as other workers have reported[5] and that the excess is reduced to smaller proportions as the sintering temperature is increased.

**Chlorine Trifluoride.**—The chlorine trifluoride was purified from technical grade material manufactured by the Harshaw Chemical Company. Hydrogen fluoride was removed by sorption on sodium fluoride and distillation was used to separate chlorine and chlorine oxides. Only the middle fraction was used and it analyzed, by the method of fractional melting in a calorimeter,[6] 99.8 mole % chlorine trifluoride.

**Pretreatment of the Powder.**—Very early in the course of this study it became apparent that unless the amount of chlorine trifluoride which was brought in contact with the initial nickel oxide surface was very carefully controlled, the powders would burn in the first few seconds of the reaction. The heat of this reaction is approximately 113 kcal./mole of chlorine trifluoride, and because this heat cannot be dissipated there is no control of the temperature, amount of conversion, or surface area of the powder. Therefore the initial gas was diluted with nitrogen, so that the reaction was controlled by limiting the availability of chlorine trifluoride to the surface, and also by dissipating the heat of the reaction. After 2 to 3% of the particle (1000 Å. average particle diameter) was converted, it became sufficiently stable so that 1 atmosphere of pure chlorine trifluoride did not cause the powder to burn.

**Apparatus for Kinetic Measurements.**—This solid–gas reaction differed from the usual type (such as the oxidation of metals) in that a gaseous product was evolved. Therefore it was necessary to circulate the gas in order to prevent a diffusion block by the gaseous products.

Since the variation of reaction rate with pressure was small, the chlorine trifluoride pressure was maintained sufficiently constant by frequently evacuating the system and refilling with pure reactant whenever its partial pressure was reduced to 90% of its initial value. The data obtained showed no discontinuities due to renewal of the reactant gas. The reactor was a small nickel vessel equipped with metal filter and valves. The vessel could be weighed on an analytical balance. This was loaded with about 5 g. of nickel oxide powder and placed in an all metal system. Facilities were provided in the system for introducing reactant gas, removing the gas phase, determining the pressure on the Booth–Cromer pressure transmitter[7] and recording the pressure automatically once each five minutes. The reactor, ballast volume and pump were enclosed in a box which could be thermostated at any desired temperature from 25 to 200° to better than ±0.1°. The circulating pump was similar to that described by Rosen.[8]

After the powder was pretreated as described previously, the reactor containing the sample was placed on the system and allowed to react under the desired conditions. At frequent time intervals the sample was removed, cooled, purged for 20 minutes with dry nitrogen, and weighed. By this method, the fraction converted was known to ±0.05%. Errors due to reaction with the walls of the reactor were negligible since its effective surface area was only about one per cent. of that of the sample.

## Results

The equations which are useful in discussing and handling the results are highly idealized but offer the best approximation to the true situation from the standpoint of utility and simplicity. The following assumptions are made.

1. The true area of the oxide powder is that given by the surface area method of Brunauer, Emmett and Teller (BET)[9] with nitrogen gas as the adsorbent.

(1) This document is based on work performed for the Government by Union Carbide and Carbon Corporation at Oak Ridge, Tennessee.

(2) G. Valensi, *Compt. rend.*, **202**, 309 (1936).

(3) J. M. Dunoyer, *J. chim. phys.*, **47**, 290 (1950).

(4) The term *sinter* as used here has the same meaning as that used in S. J. Gregg, "The Surface Chemistry of Solids," Reinhold Publ. Corp., New York, N. Y., 1951, p. 67.

(5) J. S. Anderson, *Ann. Rept., Chem. Soc.*, **43**, 104 (1946).

(6) J. W. Grisard, H. A. Bernhardt and G. D. Oliver, *J. Am. Chem. Soc.*, **73**, 5725 (1951).

(7) S. Cromer, "The Electronic Pressure Transmitter and Self Balancing Relay," Atomic Energy Commission, declassified March 20, 1947, (MDDC-803).

(8) F. D. Rosen, *Rev. Sci. Inst.*, **24**, 1061 (1953).

(9) S. Brunauer, P. H. Emmett and S. Teller, *J. Am. Chem. Soc.*, **60**, 309 (1938).

2. The fluoride film and the oxide powder have the same density as the corresponding bulk materials.

3. The film is uniform in thickness.

4. The particles are treated as spheres and hence

$$r = 3/Ad \qquad (1)$$

where $r$ is the radius, $A$ is the specific surface area and $d$ is the density of the solid.

Consider a cross-section of a heterogeneous spherical particle containing a core of unreacted nickel oxide and completely surrounded by a layer of reaction product, nickel fluoride. One can see that as the reaction progresses the radius of the core of nickel oxide must decrease with time and the thickness of the fluoride layer must increase with time. The following quantities may be defined on this basis:

$r_i$ = radius of initial particle of nickel oxide, obtained by eq. 1

$r_0$ = radius of unreacted oxide core at any time $t$

$r_g$ = radius of gross particle, oxide + fluoride layer, at any time $t$

$F$ = the fraction of the particle which has been converted to fluoride.

The fraction converted is obtained experimentally by the equation

$$F = \frac{S_t - S_i}{S_i \left( \frac{M_F}{M_0} - 1 \right)}$$

where

$S_i$ = weight of the initial nickel oxide sample

$S_t$ = wt. of the sample at time $t$

$M_F$ and $M_0$ = mol. wt. of fluoride and oxide, respectively

The initial volume, $v_i$, of a single average particle is

$$v_i = \frac{4}{3} \pi r_i^3$$

and after the reaction has proceeded, the volume of unreacted oxide, $v_0$, is

$$v_0 = (1 - F)v_i = \frac{4}{3} \pi r_0^3$$

then by combining these equations, one obtains $r_0$ in terms of $r_i$,

$$r_0 = r_i(1 - F)^{1/3} \qquad (3)$$

To obtain $r_g$ in terms of $r_i$, the volume of the gross particle, $v_g$, is

$$v_g = v_0 + v_F = \frac{4}{3} \pi r_g^3$$

where $v_0$ has been defined and $v_F$ is the volume of nickel fluoride in the gross particle. But

$$v_F = (v_i - v_0)\beta$$

and

$$v_g = v_i[1 - (1 - \beta)]F$$

where $\beta = (d_0 M_F)/(M_0 d_F)$, the coefficient of expansion on conversion ($d_0$ and $d_F$ are density of oxide and fluoride, respectively) and

$$r_g = r_i[1 - (1 - \beta)F]^{1/3} = r_i(1 + cF)^{1/3} \qquad (4)$$

For the nickel oxide–nickel fluoride case under consideration $\beta = 2.083$ or $c = -1.083$ and the

thickness of the uniform fluoride film, $x$, is given by the expression

$$x = r_g - r_0 = r_i[(1 + cF)^{1/3} - (1 - F)^{1/3}] \qquad (5)$$

Another useful quantity is the thickness of nickel oxide which has reacted, $x'$, a much simpler expression, which is

$$x' = r_i - r_0 = r_i[1 - (1 - F)^{1/3}] \qquad (6)$$

From these equations kinetic expressions for the correlation of the results are given below. The parabolic and linear laws have been used since they appear to be applicable to this work.

The linear law states in effect that the amount of reaction which has previously occurred is of no consequence in the rate of propagation of the reaction. The controlling factor is the amount of surface which is exposed to the reactant gas.

Accordingly

$$\frac{-dN_0}{dt} = k_1 a_0 \qquad (7)$$

where $dN/dt$ is the number of moles of oxide reacting per particle per unit time and $a_0$ the instantaneous surface area of a single average oxide particle at time $t$. Introducing the equations

$$a_0 = 4\pi r_0^2 \qquad (8)$$

and

$$N_0 = \frac{v_0}{\Omega_0} = \frac{4}{3} \pi \frac{r_0^3}{\Omega_0} \qquad (9)$$

($\Omega_0$ is the molar volume of nickel oxide) and integrating from $F = 0$ at $t = 0$ to $F = F$ at $t = t$, one obtains

$$1 - (1 - F)^{1/3} = \frac{k_1 \Omega_0}{r_i} t = f(A) \qquad (10)$$

If the linear law is obeyed, a plot of $f(A)$ vs. $t$ is a straight line and the rate of conversion of powders of different size is inversely proportional to the particle radius.

The parabolic law is given by the equation

$$\frac{dx}{dt} = \frac{k_2}{x} \qquad (11)$$

where $x$ is the film thickness, $t$ is the time and $k_2$ is the parabolic rate constant. Defining $x$, the thickness of the fluoride film, by equation 5 one obtains an equation whose integration is difficult. However, instead of the equation for $x$, one can use as an approximation the equation for the thickness of nickel oxide which has reacted, $x'$, equation 6. This thickness of oxide is almost proportional to the thickness of fluoride which has been formed. Equation 6 is differentiated and introduced into equation 11. Then integrating from $F = 0$ at $t = 0$ to $F = F$ at $t = t$, one obtains

$$1/2 + 1/2(1 - F)^{2/3} - (1 - F)^{1/3} = \frac{k_2}{r_i^2} t = f(B) \qquad (12)$$

If the parabolic law governs the reaction, a plot of $f(B)$ vs. $t$ should be a straight line and the rates of conversion of powders of different particle size should be inversely proportional to the square of the radius.

The experimental data for three runs are presented in Table I along with a summary of the conditions under which the runs were made. The time, $t$, is indicated in hours and the total fraction

<div align="center">Table I</div>

<div align="center">Summary of Data on the Conversion of Nickel Oxide to Nickel Fluoride</div>

| Run no. | 2 | 3 | 4 |
|---|---|---|---|
| Temp., °C. | 150 | 122 | 125 |
| Pressure, atm. | $1/2$ | $1/3$ | $1/3$ |
| $r_i$, Å. | 515 | 620 | 205 |
| $1/F_m$ | 0.873 | 0.806 | 0.826 |
| Linear slope, $f(A)/t$ | 0.00270 | 0.000383 | 0.00113 |
| Linear rate constant, $k_1\Omega_0$, (Å./hr.) | 1.39 | 0.24 | 0.23 |
| Parabolic slope, $f(B)/t$ | 0.00122 | 0.000136 | 0.000455 |
| Parabolic rate constant, $k_2$, (Å.²/hr.) | 323 | 52 | 19 |

<div align="center">—————————————Experimental data, $t$ in hours—————————————</div>

| $t$ | $F_T$ Run 2 | $F_R$ | $t$ | $F_T$ Run 3 | $F_R$ | $t$ | $F_T$ Run 4 | $F_R$ |
|---|---|---|---|---|---|---|---|---|
| 0 | 0.591 | 0.516 | 0.0 | 0.296 | 0.239 | 0.0 | 0.180 | 0.149 |
| 17.0 | .670 | .585 | 3.0 | .300 | .242 | 17.8 | .357 | .296 |
| 20.1 | .688 | .601 | 109.7 | .402 | .324 | 21.7 | .384 | .318 |
| 33.6 | 745 | .658 | 197.4 | .492 | .397 | 39.4 | .543 | .374 |
| 38.8 | .779 | .680 | 318.5 | .607 | .489 | 60.5 | .523 | .432 |
| 54.8 | .840 | .733 | 418.4 | .704 | .567 | 84.6 | .592 | .489 |
| 74.4 | .911 | .795 | 528.4 | .799 | .644 | 129.1 | .696 | .575 |
| 79.6 | .930 | .812 | 690.7 | .907 | .731 | 176.5 | .799 | .660 |
| 95.9 | .986 | .861 | 808.8 | .971 | .783 | 222.8 | .885 | .731 |
| 137.1 | 1.099 | .959 | 896.9 | 1.010 | .814 | 245.7 | .926 | .765 |
| 151.9 | 1.123 | .980 | 1012.1 | 1.054 | .850 | 298.9 | 1.003 | .828 |
| 178.4 | 1.134 | .990 | 1206.5 | 1.105 | .891 | 340.3 | 1.047 | .865 |
| 199.0 | 1.140 | .995 | 1463.2 | 1.163 | .937 | 385.9 | 1.088 | .899 |
| 222 | 1.145 | 1.000 | 1725.9 | 1.206 | .972 | 450.3 | 1.135 | .938 |
|  |  |  | 2217.0 | 1.240 | 999 | 500.0 | 1.161 | .958 |
|  |  |  |  |  |  | 638.7 | 1.191 | .984 |
|  |  |  |  |  |  | 783.4 | 1.206 | .997 |

conversion, $F_T$, has been calculated by equation 2. Inspection of the values of $F_T$ in this table shows that $F_T$ exceeds 1.0 before it reaches its limiting value. As will be seen later, the value $F_T$ contains a term $F_S$ which is due to adsorbed and absorbed material, as well as the term $F_R$ due to chemical reaction. This may be written

$$F_R = F_T - F_S \qquad (13)$$

The quantity $F_R$ is the term which should be used to calculate $f(A)$ and $f(B)$. The term $F_R$ due to chemical reaction, can vary from 0, when only nickel oxide is present, to 1 when the limiting value is reached and only nickel fluoride is present. As a first approximation one can say that $F_S$ is directly proportional to $F_R$, and $F_R$ is unity when $F_T$ equals its final maximum value, $F_m$, which is obtained at complete conversion of the oxide to the fluoride.

Experimental plots of $F_R$ vs. $t$ were made and values of $t$ taken at 10% intervals of conversion. Plots of $f(A)$ vs. and $f(B)$ vs. $t$ are shown in Fig. 1. The slope of the best straight line portion is tabulated in Table I and used to calculate the rate constants for the linear and parabolic mechanism.

On the basis of these plots, there is generally better agreement with the linear than the parabolic law. The parabolic plots generally have an upward curvature meaning that experimentally the conversion proceeds faster than the parabolic law would allow. The more sensitive test is shown in Table I where the rate constants have been calculated, for powders of different particle size (runs 3 and 4). The agreement between the rate constants for equivalent temperature runs is very

good for the linear law, but from the parabolic plots variation by a factor of more than 2.5 is found. One is therefore led to the conclusion that the conversion proceeds by the linear rate of attack, at least over this temperature range.
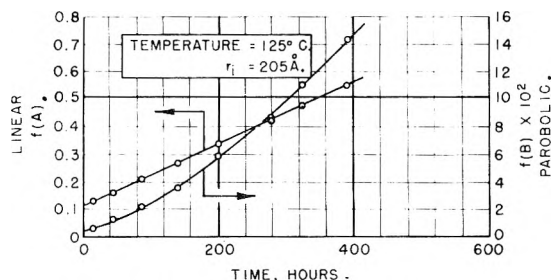


<div align="center">Fig. 1.—Typical correlation plots.</div>

The results at lower temperatures, less complete because of the considerably longer time required for conversion, and those at 180° are correlated by the linear law.

The effect of pressure with other variables constant, is illustrated in Fig. 2. The influence of pressure will also be considered with that of temperature.

The temperature variation was treated by the usual Arrhenius equation. Table II is a summary of the linear rate constants at the various temperatures, and the plot of log $k_1\Omega_0$ vs. $1/T$ is shown in Fig. 3. There is definite curvature in this figure which will be discussed later.

## Discussion of Results

**The Temperature and Pressure Effect.**—The curvature in Arrhenius plot (Fig. 3) is due to two
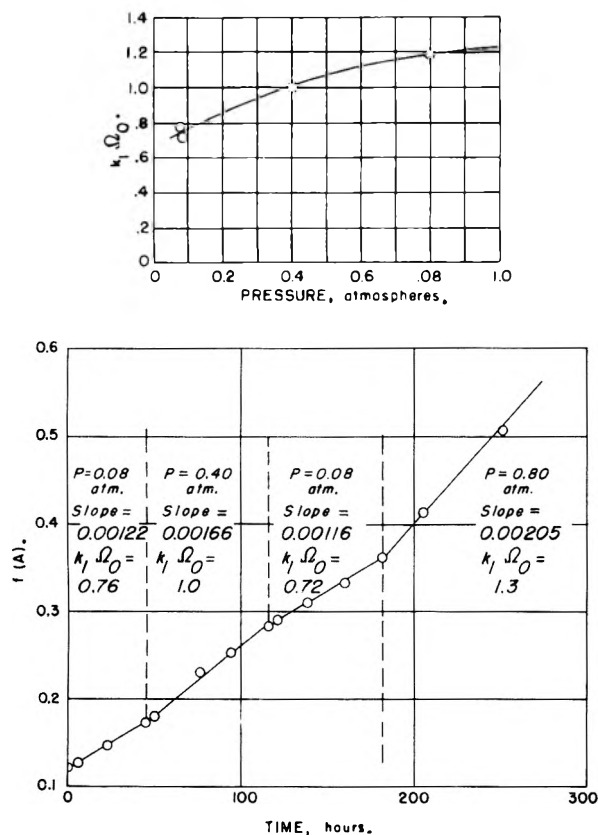
Fig. 2.—The effect of pressure, 150°.



Fig. 3.—Activation energy.

effects: (1) the variation of surface concentration with temperature and (2) a change in mechanism of attack as the initial thin film becomes thicker.

TABLE II

EFFECT OF TEMPERATURE

| Temp., °C. | $\frac{1}{T} \times 10^{-4}$ | Pressure, atm. | $k_1\Omega_0$, Å./hr. | $\gamma = \frac{G_1{}^a}{G_2}$ | $k_1\Omega_0\sigma$, Å./hr. |
|---|---|---|---|---|---|
| 26 | 33.4 | 0.90 | 0.020 | 0.74 | 0.015 |
| 26 | 33.4 | .90 | .019 | 0.74 | .014 |
| 61 | 29.9 | .85 | .024 | 1.01 | .024 |
| 65 | 29.6 | .85 | .024 | 1.01 | .024 |
| 98 | 26.9 | .85 | .068 | 1.11 | .075 |
| 100 | 26.8 | .85 | .058 | 1.11 | .064 |
| 122 | 25.3 | .30 | .24 | 1.25 | .30 |
| 125 | 25.1 | .30 | .23 | 1.25 | .29 |
| 148 | 23.8 | .08 | .76 | 1.64 | 1.2 |
| 148 | 23.8 | .40 | 1.0 | 1.35 | 1.4 |
| 148 | 23.8 | .08 | 0.72 | 1.64 | 1.2 |
| 148 | 23.8 | .80 | 1.3 | 1.30 | 1.7 |
| 150 | 23.6 | .50 | 1.4 | 1.33 | 1.8 |
| 180 | 22.1 | .50 | 2.9 | 1.59 | 4.6 |

[a] A term to correct rate constants for the variation in surface concentration. See equation 14.

At the low temperatures, 26 and 65°, the pressure was of the order of 0.8 atmosphere while at higher temperatures the pressure was lower. Adsorption experiments[10] have shown a decrease in surface concentration with increasing temperature even though the surface coverage was in all cases approximately one monolayer. At the higher temperatures the monolayer contained fewer moles

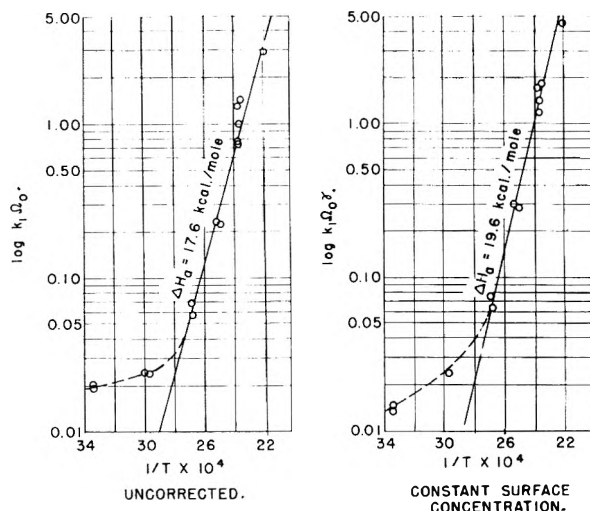(10) R. L. Farrar, Jr., and H. A. Smith, J. Am. Chem. Soc., 77, Sept. (1955).

of chlorine trifluoride per unit area of surface. An attempt has been made to correct all rate constants to some constant value of surface concentration by means of a proportionality constant, $\gamma$, where

$$\gamma = G_1/G_2 \qquad (14)$$

Here $G_1 = 20.0$ mg. $ClF_3$ per g. $NiF_2$ for a sample of surface area 30 sq.m./g. is the arbitrarily chosen value of the surface concentration to which all rate constants are corrected. $G_2$ is the surface concentration at the particular temperature and pressure of the experiments, and has been taken from adsorption experiments. Effectively, the assumption is made that at a given temperature the rate constant is directly proportional to the surface concentration. The logarithm of the new rate constant, $k_1\Omega_0\sigma$, is plotted against the reciprocal of the absolute temperature in Fig. 3. This correction tends to improve the curvature but does not remove it. The activation energy, determined on the straight line portion, is 19.6 kcal./mole.

Curvature in the low temperature portion of the plot is best explained by a change in mechanism. The last point or points on the graphs obtained with the linear rate constants do not follow the straight line. At this temperature, the rates of conversion, while already very slow and near limit of determination with the particular experimental set up, probably would continue to decrease with time giving a smaller value of the rate constant. In this range of conversion (the order of 1 to 3%) at this temperature, reaction is progressing by a parabolic mechanism with a relatively high rate of attack. The powder continues to build up a film by the parabolic mechanism until it is thick enough for cracking and recrystallization to take place, whereupon the linear mechanism takes over. This, however, as evidenced by back extrapolation of the straight line in Fig. 3 to the temperature in question, would yield a rate constant so small that it would be undetectable in this experiment.

**Electron Photomicrographs, Electron Diffraction and X-Ray Diffraction.**—Considerable information of a supporting nature has been obtained from the
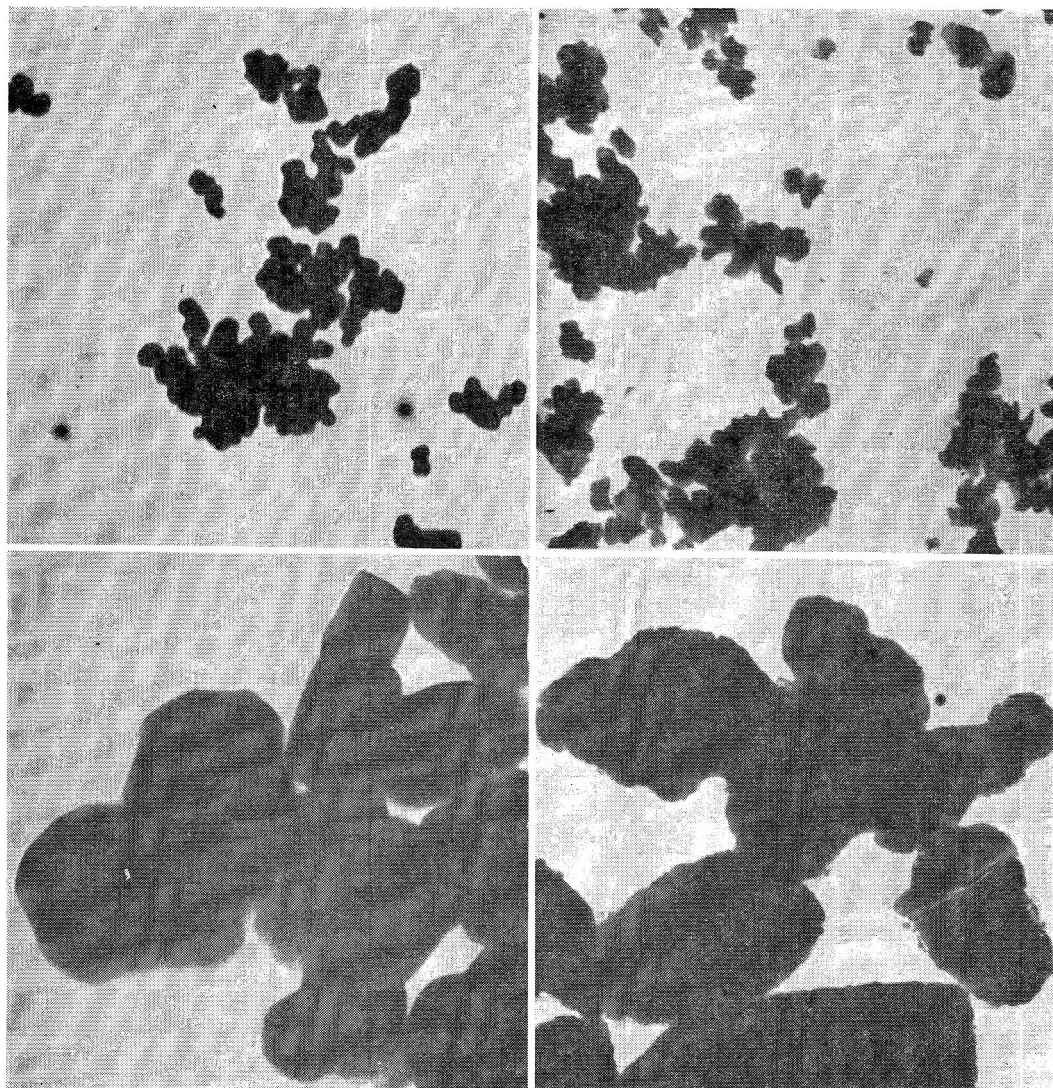
Fig. 4.—Electron photomicrographs: upper left, nickel oxide, 6.5 m.²/g. (27,000 ×); upper right, nickel fluoride from 6.5 m.²/g., nickel oxide (27,000 ×); lower left, nickel oxide, 3.7 m.²/g. (140,000 ×); lower right, nickel oxide, (3.7 m.²/g.) converted 10% to nickel fluoride (125,000 ×).

use of electron photomicrograph, and electron and X-ray diffraction patterns of the powders. Typical photomicrographs of the powders are presented for the initial and final material in Fig. 4. From this photograph at 27,000× magnification the particle size distribution of the oxide powder and the fluoride powder have been obtained, and that for the fluoride powder is presented in Fig. 5. The particle size distribution curves give the normal probability distribution curve when plotted on a logarithmic scale, and a badly skewed curve when plotted on a linear scale. This is probably due to the sintering process by which the particle size was governed. The particle size by nitrogen surface area for each of these powders is indicated for comparison. Good agreement is obtained for the oxides where no nitrogen surface area anomaly was observed, but radical disagreement is noted for the fluoride powder. This supports the contention that the oxide particles are single crystals while the fluoride particles are porous. The broadening of the lines of the X-ray and electron diffraction patterns is also in agreement with this idea.

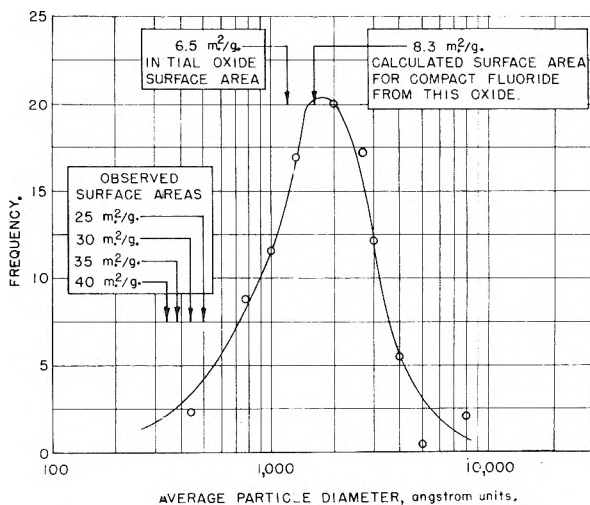The crystallite sizes in the fluoride powder are in the 50 to 100 Å. range.



Fig. 5.—Particle size distribution of NiF₂.

The high resolution photomicrographs presented in Fig. 4 show the details of some of the cracks and crevices. This constitutes definite proof of the structure of the particles which has been postulated to explain the observed experimental facts.

**Gaseous Products.**—When gaseous chlorine trifluoride reacts with nickel oxide, there are two possibilities which might reasonably be expected, namely

$$3/2NiO + ClF_3 \longrightarrow 3/2NiF_2 + 1/2Cl_2 + 3/4O_2 \quad (A)$$
$$NiO + ClF_3 \longrightarrow NiF_2 + ClF + 1/2O_2 \quad (B)$$
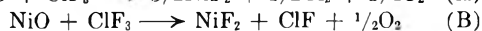
and perhaps a secondary reaction of $O_2 + Cl_2$, $O_2 + ClF$, or $O_2 + ClF_3$ to yield chlorine oxides or chlorine oxyfluorides.

A reaction attempt was made using a large sample of nickel oxide (20 g.) with chlorine trifluoride at room temperature. The system which had been filled with helium was displaced with chlorine trifluoride and all products and unreacted chlorine trifluoride passed through a trap at liquid nitrogen temperature. This material was then transferred to an analytical distillation column and the amount of material in each fraction between $-183°$ ($p = 1$ atm.) and $+11°$ was determined. The percentage results are shown in Table III.

TABLE III

CHLORINE TRIFLUORIDE–NICKEL OXIDE REACTION PRODUCTS

| Temp., °C. | Component | Mole % |
|---|---|---|
| $-183$ | $O_2$ | 1 |
| $-100$ | ClF | 1 |
| $-80$ | $CO_2$ | 4 |
| $-48$ | COClF | 4 |
| $-35$ | $Cl_2$ | 88 |
| $-6$ | $^a$ | 3 |
| | | 100 |

$^a$ The identity of this fraction is unknown but by infrared analysis it is not $Cl_2O$, $ClO_2$ or Freon-114.

The oxygen was not condensed in the cold trap since its partial pressure in the gas mixture was considerably below its vapor pressure.[11] The oxygen which was observed was probably due to physically adsorbed material The important thing to note is the $Cl_2/ClF$ ratio. These results would favor reaction (A) above. At no time have mass spectrographic analyses or infrared analyses of reaction products indicated that chlorine monofluoride was any major fraction of the products and always large amounts of chlorine have been detected.

(11) Vapor pressure of oxygen at $-195°$ is approximately 150 mm.

During the evacuation of one of the samples, which had gained about 20% more weight than simple stoichiometry would predict, the degassed material was collected at liquid nitrogen temperature. Mass spectrographic analyses showed this material to be chlorine trifluoride.

**Conclusions**

It is possible now to describe the mechanism by which chlorine trifluoride converts nickel oxide to the fluoride. It has been shown that an unreacted nickel oxide surface is extremely unstable with respect to chemical attack by the fluorinating agent, but only a very thin film of fluoride is sufficient to prevent an uncontrolled reaction from taking place. This film of fluoride increases in thickness by a diffusion process as evidenced by initial obedience to parabolic kinetics.

After the fluoride film reaches some critical thickness, a recrystallization process takes place allowing a major change in the mechanism of attack. Whereas previously the film was more or less continuous, after recrystallization a mosaic network of crystallites is formed which opens grain boundary paths allowing the adsorbed reactant gas to move closer to the unreacted oxide surface. Conversion from this point on is by linear kinetics consisting of migration of chlorine trifluoride molecules down the grain boundary paths until they enter the transition zone where chemical reaction (or the electron transfer process) takes place. The rate controlling step now is diffusion through the transition zone of relatively constant thickness rather than migration of the chlorine trifluoride molecules down the grain boundary paths. If the latter were rate controlling, the parabolic law would have been followed.

The completely converted nickel fluoride contained excess chlorine trifluoride which could be removed by evacuation. It was concluded that this material was sorbed in the inter-crystallite boundaries.

# COAGULATION OF HYDROPHOBIC SOLS *IN STATU NASCENDI*. III. THE INFLUENCE OF THE IONIC SIZE AND VALENCY OF THE COUNTERION

By B. Tezak, E. Matijevic and K. F. Schulz

*Contribution from the Laboratory of Physical Chemistry of the University of Zagreb, Croatia, Yugoslavia*

*Received March 4, 1955*

The coagulation values of different cations for negative silver bromide and silver iodide sols *in statu nascendi* have been determined. It could be shown that there exists a linear relationship between the crystallographic radii of the counterions of the same valency and the logarithms of their coagulation values. By extrapolating these straight lines to the zero value of the radius, a characteristic coagulation value has been obtained which is connected in a simple manner with the valency of the counterion by means of the equation $\log C_{coag} = -(_c d/_s d)z + \log C_{fix}$. It was possible to test this equation experimentally. The treatment used gives a very simple quantitative interpretation of the Schulze–Hardy rule excluding the influence of the size of the coagulating ions.

It is well known that the principal rule governing the electrolytic coagulation of lyophobic colloids is the Schulze–Hardy rule. It states only qualitatively that the coagulation values of the counterions strongly depend on their valency. This rule does not take into account, however, all the other factors which influence the coagulation process and the coagulation values.

We performed systematical investigations of the effects of electrolytic coagulation using silver halide sols *in statu nascendi*. In the second paper of this series the effects of the concentration of the sol and of the stabilizing ions were shown.[1] The influence of the ionic size and the valency of the counterion on the coagulation values will be presented and discussed in this paper.

If the coagulation experiments are carried out with sufficient accuracy it is possible to ascertain that different counterions of the same valency give distinct coagulation values. The differences are not very large but detectable. They depend also on the nature of the sol; in general, the larger the ion the lower is its critical coagulation concentration. In our previous publications we have given already some examples of the influence of the ionic size on the coagulation values.[2,3] Now, the results have been completed and an attempt is made at a quantitative interpretation.

## Experimental

The coagulation experiments were performed in the same way as described extensively in the first paper of this series.[4] The sols were always prepared *in statu nascendi*. The coagulation values were determined from 10-minutes concentration tyndallograms which were drawn for every investigated system. The critical time of 10 minutes was chosen on basis of kinetic analysis of time tyndallograms for silver bromide and silver iodide sols.

Figure 1 is given as an example of such concentration tyndallograms. It shows the tyndallometric curves for negative silver bromide sol coagulated by means of aluminum nitrate at different concentrations of the potential determining ion (Br⁻). In this case the coagulation values— which have been determined from the intersection point of the tangent with the axis of abscissa—decrease with increasing concentration of the stabilizing ion. However, the same effect could not be obtained with counterions of other valencies.

Figure 2 is a summarized presentation of the coagulation values for AgBr sol in dependence on the initial concentration of the potential determining ion for lithium nitrate and sulfate, magnesium nitrate and sulfate, and aluminum nitrate and sulfate at two different sol concentrations (0.0001 and 0.0005 M). The results from Fig. 1 are in-
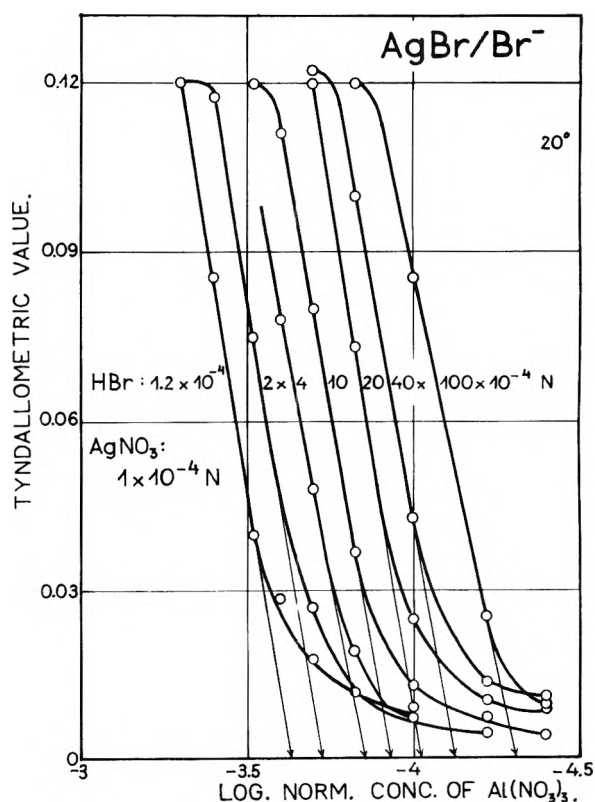


Fig. 1.—Concentration tyndallograms: the effect of the concentration of the stabilizing ion on the coagulation of the silver bromide sol *in statu nascendi* in solutions of Al(NO₃)₃, 10 minutes after mixing the reaction components. The tangents with arrows denote the coagulation values.

cluded. It should be noticed that the coagulation curves (especially such of uni- and bivalent counterions) show a linear part parallel to the abscissa. We determined similar coagulation curves for a great number of salts (nitrates and sulfates of various cations of different valencies) for silver chloride, silver bromide and silver iodide sols. Only few of these results will be presented in this paper. Figure 3 shows, *e.g.*, the coagulation curves of univalent counterions for silver iodide sol (sol concentration 0.0005 M), whereas Figs. 4 and 5 give the results for various bivalent and trivalent ions obtained on the same sol. It is evident that there exist pronounced differences in the coagulation values between ions of the same valency.

(1) B. Tezak, E. Matijević and K. Schulz, This Journal, **55**, 1567 (1951).

(2) B. Tezak, *Z. physik. Chem.*, **A191**, 270 (1942).

(3) E. Matijević and B. Tezak, *Kolloid-Z.*, **125**, 1 (1952); B. Tezak, E. Matijević, K. Schulz, M. Mirnik, J. Herak, V. B. Vouk, M. Slunjski, S. Babić, J. Kratohvil and T. Palmar, This Journal, **57**, 301 (1953).

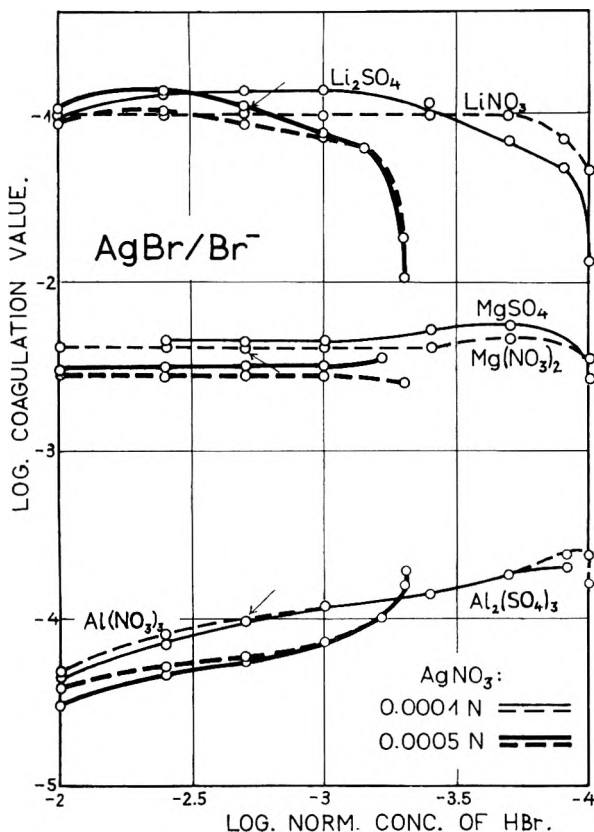(4) B. Tezak, E. Matijević and K. Schulz, *ibid.*, **55**, 1557 (1951).

Fig. 2.—Coagulation values of Li, Mg and Al nitrate and sulfate for silver bromide sol for two different sol concentrations in the presence of various amounts of the stabilizing ions. The arrows denote the values used in Fig. 6.

**Reproducibility of the Results.**—Owing to their complexity the reproducibility of colloidal phenomena is often not very good. In some cases we could establish the reasons for the low precision in determining the coagulation values; e.g., aged solutions of aluminum ion gave entirely wrong results.[5] Only with freshly prepared solutions we
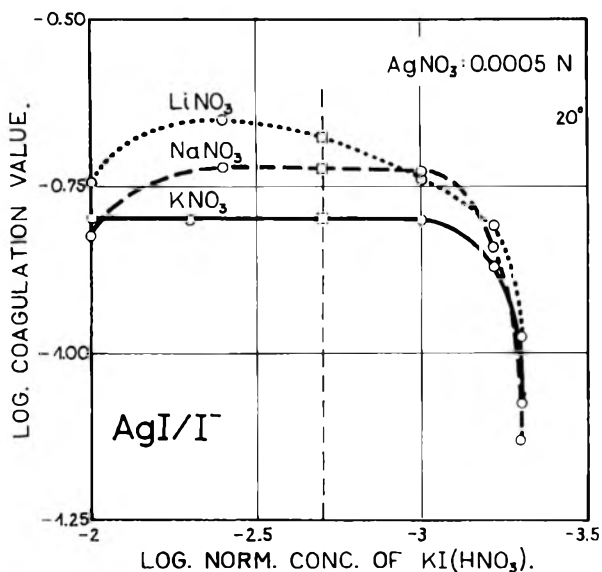


Fig. 3.—Coagulation values of different monovalent cations for silver iodide sol in statu nascendi in presence of various concentrations of the stabilizing ions. The values marked with quadrangles are further evaluated in Fig. 7.

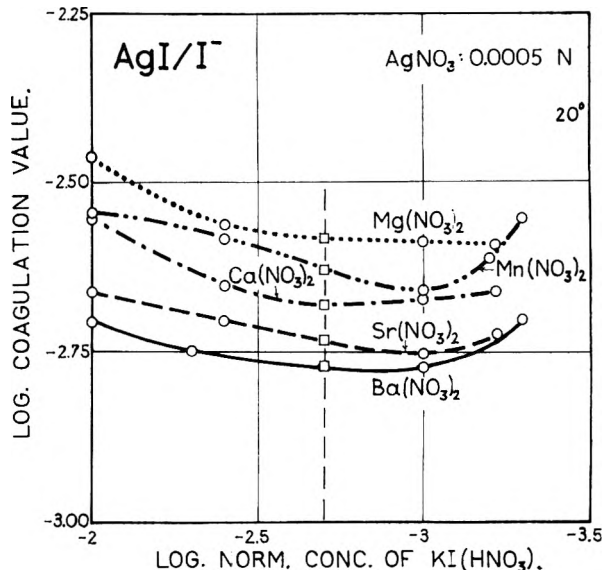(5) E. Matijević and B. Težak, This Journal, 57, 951 (1953).



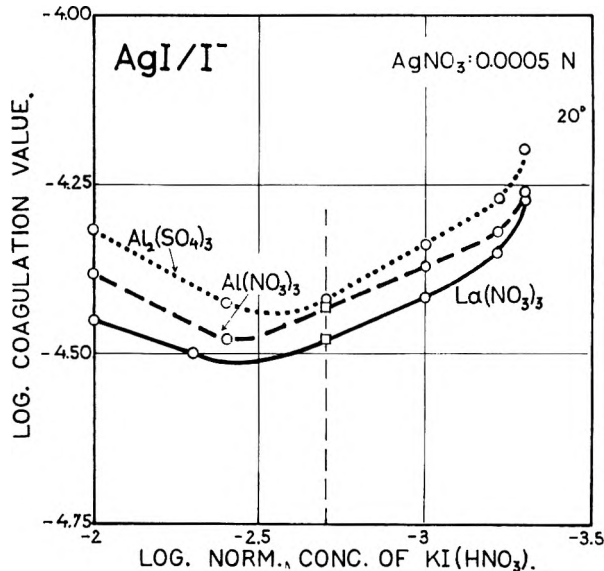Fig. 4.—The same effect as in Fig. 3 using bivalent cations.



Fig. 5.—The same effect as in Fig. 3 using trivalent cations.

could obtain correct values. We had similar experience with thorium and other complex forming ions. But we were not always successful in clearing up the inconsistencies in observed coagulation values. In the case of potassium nitrate, for instance, we obtained (for the system AgNO₃ 0.0001 N and HBr 0.0020 N) in repeated experiments (performed on different occasions within five years) the following coagulation values: 0.078, 0.072, 0.074, 0.059 and 0.060. In this example we see two distinct groups of values. When interpreting the results we used the lower values, since they seemed correct by the general trend of the coagulation curve of potassium nitrate. All attempts to find a reason for this discrepancy failed. One of the probable reasons may be the contamination of the halide component with other halides. We could show, e.g., that the addition of very low amounts of one halide ion to another silver halide system may influence considerably the coagulation values of the coagulating ion.[6] Thus the purity of the chemicals seems to be one of the most important factors for achieving good reproducibility. In all our experiments the chemicals of analytical grade (pro analysi) or at least puriss and bidistilled water were used.

Generally, it may be said that the reproducibility of the results with our experimental technique is satisfactory

(6) B. Težak, E. Matijević, K. Schulz, J. Kratohvil, R. Wolf and B. Černicki, J. Colloid Sci., Suppl. 1, 118 (1954).
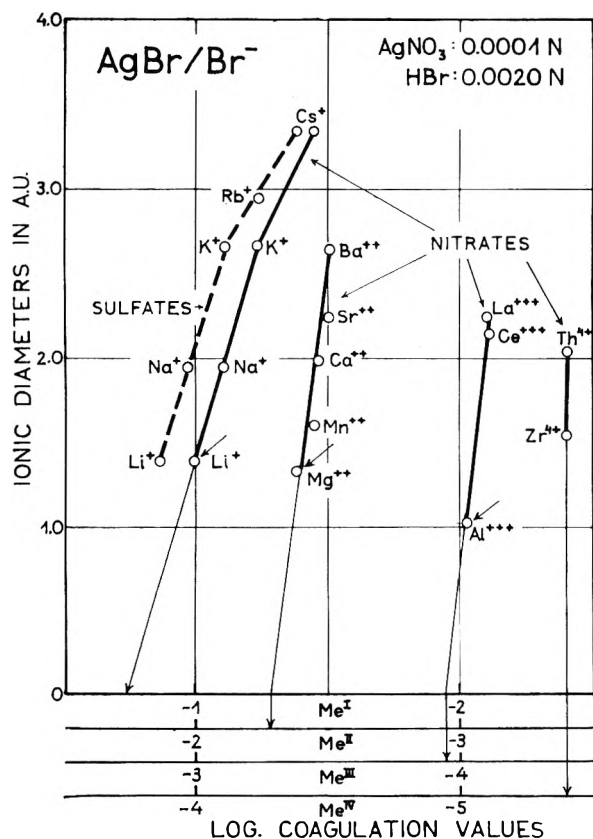
Fig. 6.—The relationship between the crystallographic radii of the coagulating cations and their coagulation values for negative silver bromide sol *in statu nascendi*. Short arrows denote the values taken from Fig. 2.



Fig. 7.—The same relationship as in Fig. 6 for silver iodide sol. Values marked with quadrangles are taken from Figs. 3, 4 and 5.

if all the factors are held completely constant and if the experiments are carried out in a systematic sequence. Higher precision could probably be obtained only with extremely pure chemicals, especially free of halide impurities, and using special precautions in the method of mixing, in cleaning the vessels, etc.

## Discussion

There were already several attempts at quantitative interpretation of the influence of the size of counterions on their coagulation values. The works of Büchner and of Ostwald should be pointed out. Büchner[7] introduced the "lyotropic numbers" ("*lyotrope Zahlen*") which are simply connected with the heat of hydration of ions and are in inverse proportion to their radii. Büchner showed that in some cases (*e.g.*, for gold sol) there exists a linear relationship between these lyotropic numbers and the corresponding coagulation values. Unfortunately this relation could not be proved generally; on the other side, the lyotropic numbers have no physical meaning.

Ostwald named the influence of ionic size on the coagulation values within a valency group the "ionic spreading" ("*Ionenspreizung*") and developed an equation on the basis of his activity coefficient theory which connects the valency and the radius of the coagulating ion with its individual activity coefficient at the critical coagulation molarity.[8] This equation contains two constants without any definite physical meaning. Ostwald's way of
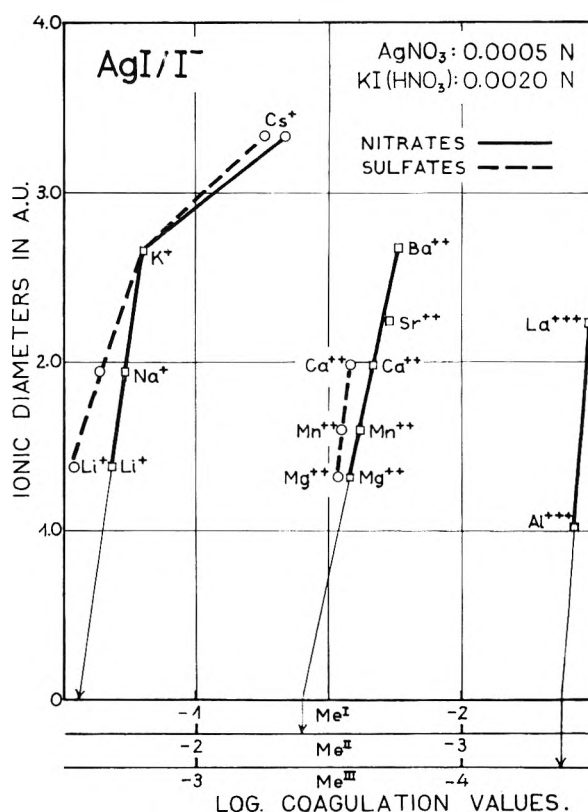
interpretation of "ionic spreading" has been criticized, as well as his theory in general.

Our approach to this problem may be shown in the following way. In an earlier paper it was established that there exists a linear relationship between the coagulation values and the crystallographic radii of univalent coagulating ions for negative silver chloride sols.[2] Figures 6 and 7 show that such linearity is obtained also in the case of silver bromide and silver iodide sols for counterions of different valencies. In Fig. 6 the coagulation values of various mono-, di-, tri- and tetravalent coagulating ions for AgBr sol are plotted against their diameters, the concentration of sol being 0.0001 $M$ and the initial concentration of the potential determining ion (Br$^-$) 0.0020 $N$. Similar linear relationships have been obtained with other sol concentrations and other concentrations of stabilizing ions.

Only in the case of univalent counterions the straight line is broken, giving two straight lines of different slopes for smaller and larger ions, respectively. This effect may be explained by different adsorbability of ions. It is very probable that larger ions (Rb$^+$, Cs$^+$) are more easily adsorbed, exerting a stronger coagulation effect than expected.

All data on the size of the radii of ions are taken from a recent paper of Ahrens.[9]

From the results presented it seems that the higher the valency the steeper is the straight line. We have to take into account the combination of

(7) E. H. Büchner, *Kolloid-Z.*, **75**, 1 (1936).

(8) Wo. Ostwald, *ibid.*, **85**, 34 (1938).

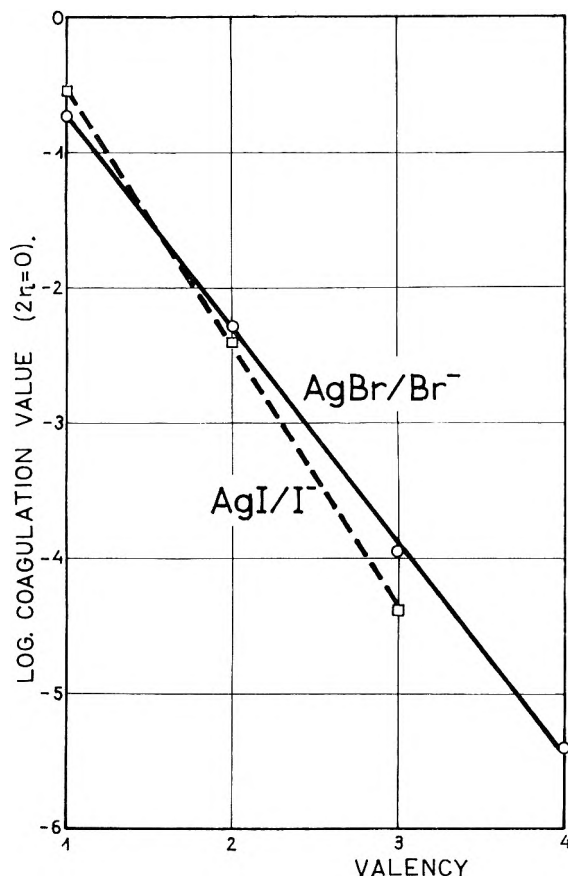(9) L. H. Ahrens, *Geochim. Cosmochim. Acta*, **2**, 155 (1952).

Fig. 8.—The relationship between the valency of the coagulating cations and their characteristic coagulation values (for $2r_i = 0$) for silver bromide and silver iodide sols *in statu nascendi*.

two influences: that of the valency, and that of the radius. Obviously, if the influence of the radius is always the same, its relative part in the coagulation value with higher valency would be lower.

Figure 7 gives similar results obtained on silver iodide sol. The sol concentration in this series of experiments was 0.0005 $M$ and the concentration of the stabilizing ion ($I^-$) the same as in Fig. 6. This figure contains also the coagulation values which have been given in Figs. 3, 4 and 5 (marked with quadrangles). It is worth while noting that the linearity is obtained also with different accompanying ions (nitrate, sulfate) although the slope of the straight lines is different.

We tried to explain these results on the basis of a theory of coagulation mechanism.[2,3,10] According to this theory the critical conditions for the coagulation are given by the correspondence of association–dissociation ionic equilibria in the bulk of the solution and analogous equilibria of the stabilizing–coagulating ion pairs in the methoric layer.[11] The theory takes into account the coulombic interaction only using the Bjerrum equation for the uni-univalent ion pair formation

$$_cd = \frac{e^2}{2DkT} \qquad (1)$$

(10) B. Težak, *Arhiv kem.*, **19**, 19 (1947); **22**, 26 (1950); E. Matijević and B. Težak, *Kolloid-Z.*, **125**, 1 (1952); B. Težak, R. Matijević, K. F. Schulz, M. Mirnik, J. Kratohvil and V. B. Vouk, *General Disc. Faraday Soc.*, Sheffield 1954 (in press).

(11) B. Težak, *Arhiv kem.*, **21**, 93 (1949).

as starting point. Here $k$ is the Boltzmann constant, $T$ the absolute temperature, $e$ the elementary charge, and $D$ the dielectric constant. For univalent point ions in water media this equation gives $_cd = 3.58$ Å.

As a consequence the following relationship between the valency, the radius of the counterion and its coagulation value may be deduced

$$z_cd + r_{i^+} = _sd(\log C_{fix} - \log C_{ccag}) \qquad (2)$$

where $r_{i+}$ denotes the radius of the coagulating ion (counterion) and $z$ its valency. $_cd$ is the critical distance, and $_sd$ is a distance which may be compared with the thickness of the ionic atmosphere. $C_{coag}$ is the critical concentration of coagulation (the coagulation value) expressed in normalities and $C_{fix}$ denotes the concentration of an uncharged species of particles which would exert the same interaction as the charged ions in the region of the critical coagulation concentration. This value is a specific quantity for the coagulating system.

As has been shown[2,3,10] the statistically representative and most simple interpretation is given by considering the elementary interaction between monovalent stabilizing ion and the counterions of different valencies (supposing that these counterions are of the same size). Thus in a plot log $C_{coag}$ against $z_cd$ in Å., the $_sd$ and $C_{fix}$ may be graphically determined as the slope of a straight line, and the intersection with the log $C_{coag}$ axis, respectively.

By extrapolating the straight lines from Figs. 6 and 7 to the zero value of the diameter we can evaluate the coagulation value characteristic for the cations of the same valency. This value is dependent on the experimental conditions but for a definite sol the differences are not large. Under this condition $(2r_i = 0)$ the equation 2 takes a much simpler form which may be written

$$\log C_{coag} = -\frac{_cd}{_sd} z + \log C_{fix} \qquad (3)$$

This equation requires a linear relationship between the characteristic coagulation value (for $2 r_i = 0$) of an ionic group and the valency. The equation 3 was tested on silver bromide and silver iodide sols *in statu nascendi*. Some examples are given in Fig. 8, where the full line represents the results with silver bromide sol for nitrates of uni-, di-, tri- and tetravalent coagulating cations. The dashed line gives the corresponding results for silver iodide. The slope of the straight lines depends on the nature of the sol. The change in the sol concentration or in the concentration of the stabilizing ion as well as the change of the accompanying ion does not influence markedly the slope of the straight lines.

In connection with the problem of the influence of the ionic size on the coagulation values the question arises how far is it justified to use crystallographic radii. In fact very little is known about the "wet-radii" of ions. The hydration numbers obtained by different methods vary very widely.[12] In our opinion only the "primary" solvation of coagulating ions could exert some effect upon their coagulation values. However, as long as the dimensions of "wet-radii" of ions are not known

(12) J. O'M. Bockris, *Quart. Revs. (London)*, **3**, 173 (1949).

with certainty, no possibility exists for an entirely quantitative explanation of the ionic size effect.

There were attempts to determine ionic radii from coagulation measurements.[13]    These results should be treated with great precaution.

(13) B. Težak and E. Matijević, *Arhiv kem.*, **19**, 29 (1947);  H. Basińska, *Roczniki Chem.*, **23**, 380 (1949).

Our results show that the equation 2 may be tested rather successfully with coagulation values obtained on silver halide sols *in statu nascendi*. It is apparent that the treatment used gives very simple quantitative interpretation of the Schulze–Hardy rule excluding the influence of the size of the coagulating ions.

---

# STRUCTURE OF THE GAS PHASE COMBUSTION REGION OF A SOLID DOUBLE BASE PROPELLANT

BY C. A. HELLER AND ALVIN S. GORDON

*Chemistry Division, U. S. Naval Ordnance Test Station, Inyokern, China Lake, California*

*Received March 7, 1955*

The temperature and composition of the gas phase combustion region of a nitrocellulose–nitroglycerine propellant have been measured.    They were measured as a function of pressure and of distance from the burning surface.    As previously known, the combustion is flameless to about 10 atmospheres, where a small flame appears and, with increasing pressure, approaches closer to the surface.    It has been possible to measure the thermal structure and composition underneath this flame.    Evidence is presented that the following zones appear in the gas phase: 1, a thin reactive zone close by the surface (Fizz zone); 2, a zone of no apparent reaction and of almost constant composition in the pressure range 0 to 350 p.s.i.g. (Induction zone); 3, the flame zone.

## Introduction

The development of the theory of solid propellant combustion has been retarded largely because of missing information concerning the nature of reactions in various zones.

It is known that the solid decomposes to $NO_2$, aldehydes and other small molecules during low temperature decomposition.    These react further to give NO, CO and $H_2$.    Finally, the NO and hydrocarbons plus CO react to give the flame.[1,2]

This study has been made to elucidate the structure and chemical compositions in the gas phase region.    The pressure range studied covered the fizz region, as well as the incipient flame.    The solid double-base propellant is similar to one previously employed in some studies by Crawford.[3]

## Experimental

The propellant used for this study contained only nitrocellulose and nitroglycerine, except for small amounts of residual moisture and perhaps traces of methanol.    Three different lots were used.    There was some variation in composition, as may be seen in analyses in Table I.

Burning rates, as shown in Fig. 1, are not very different for the three lots.

### TABLE I

#### COMPOSITION OF THREE LOTS OF PROPELLANT

| | Diameter, cm. | NC | NG | Heat of explosion (calcd.) |
|---|---|---|---|---|
| PL 673 | 0.615 | 55.0 | 45.0 | 1329 (no anal.) |
| PL 725 | 0.622 | 57.5 | 40.9 | 1304 |
| PL 748 | 0.698 | 54.51 | 44.6 | 1324 |

Burning rates were taken from motion pictures using a constant speed ($62.0 \pm 0.5$ frames per sec.) camera.    Where necessary, these rates could be corrected for burning angle.    These pictures could also be used to measure the dark zone thickness.

(1) C. E. H. Bawn, "The Decomposition and Burning of Nitric Esters," Advisory Council 10068 (Oct. 1948).

(2) R. M. H. Wyatt, "Gas Phase Reactions of the Nitrogen Oxides, A Review," E.R.D.E. Survey No. 4/S/51.

(3) B. L. Crawford, Jr., C. Huggett and J. J. McBrady, THIS JOURNAL, **54**, 854 (1950).

The uninhibited strands were burned cigarette fashion in a pressure bomb with three plexiglas viewing windows. The helium used for pressurizing was purified by passage through an activated carbon trap at $-196°$ to remove $O_2$. Ignition was effected by electrically heating the iron ignition wire.    The pressure bomb was a cylindrical block with a 4-inch internal diameter.

Gas samples were removed *via* Vycor probes into an evacuated sample flask.    Both 6-mm. i.d. probes and capillary probes were used, depending upon the zone to be sampled.    The burning surface was held at a constant level by a gold wire or quartz fiber restraint upon the propellant strand, which was pressed from below by a compressed spring.    The probe was placed a measured distance above this restraining wire.    Samples were withdrawn within 2–10 seconds; the calculated time in the hot section of the probe was always small compared to the time in the gas stream (0.1 to 1%).    The inside diameter of the small probe was varied for different samples from 20 to 250 $\mu$.
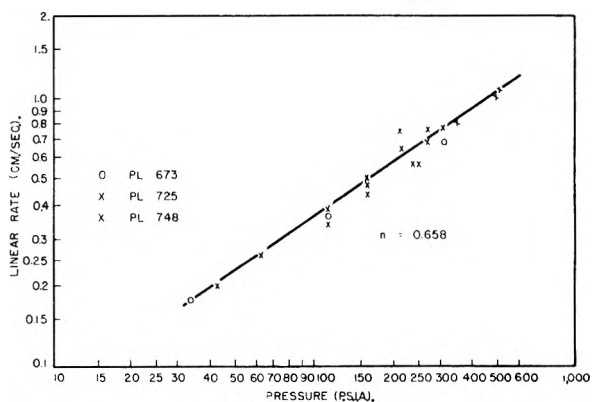


Fig. 1.—Linear burning rate (cm./sec.) *vs.* pressure (p.s.i.a.).

An infrared analysis of a $P_2O_5$ dried sample showed NO, CO, $CO_2$, $CH_4$, $C_2H_4$ and HCN.    Nitrogen dioxide and nitrous oxide were not present in detectable amounts. There were only two very small peaks unaccounted for by this analysis.

The Consolidated 21-103 Mass Spectrometer showed the above gases plus $H_2$, He, $H_2O$, $(CN)_2$ and $N_2$.    The quantitative measurement of mixtures was done by setting up a 12-square matrix and solving on the IBM 701 digital computer.    The accuracy of the analysis varied for the various components, depending upon the extent that various mass peaks overlapped.

Nitrogen and carbon monoxide have the same parent peak at mass 28 and must be distinguished by the smaller peaks at mass 12, 14 and 16. These lower peaks also have contributions from other molecules present. Thus the $CO/N_2$ ratio is of low accuracy, but the gases volatile from a liquid nitrogen trap are less complex and give about the same ratios of $CO/N_2$ as for the total sample. Methane at mass 16 has its parent peak in doubt because several oxygen containing molecules all gave mass 16 peaks. Carbon dioxide, cyanogen, nitric oxide, and total CO plus $N_2$ peak can be carefully determined. HCN is present in trace amounts and its calculated percentage varied from 0.5 to −0.3 due to errors in the matrices.

Surface temperature was obtained with Pt–Pt 10% Rh thermocouples bearing on the surface and held down by a 5-gram weight.[4] After following the surface long enough to reach a constant temperature, these thermocouples were allowed to rise into the dark zone. The temperature of the surface bearing wire was recorded by a pen and ink recorder.

The thermal wave of the burning propellant was obtained by recording the temperature–time of a very fine Pt–Pt 10% Rh thermocouple embedded in the propellant. The general features of this method have been described previously.[5]

The sizes for the surface wires were 1 or 3 mil (25 or 75 $\mu$) as dictated by the necessary strength. The embedded couples were mostly 0.3 mil (7.5 $\mu$), but 0.1 mil (2.5 $\mu$) wires were also used, and gave similar curves before breaking.

## Visual Description

**I. Foam Zone.**—A solid propellant begins to react about 0.3 to 0.05 mm. below the surface. The solid becomes a viscous liquid, and bubbles form which give the zone its name. The surface is not smooth throughout, but consists of an apparently smooth surface with craters and glowing filaments. If extinguished, the craters are just smooth holes in the translucent plastic, but the extinguished filaments are black carbonaceous material. A 40 × microscope shows that about 75–90% of the extinguished surface is smooth.

**II. Dark Zone.**—Above this surface is a large dark area filled with sparks caused by the released surface filaments. There is some radiation from the "dark" zone itself, which appears to glow faintly at the edge. Super XX film is slightly darkened by exposure to the radiation when a large lens opening is used. Table II gives the height of this zone at various pressures.

**III. Flame Zone.**—At low pressures the gas phase is only a dark zone, but as the pressure is raised a small flame spontaneously appears in the center of the gas stream about 15 mm. above the surface. The pressure necessary for the appearance of flame decreases with increasing strand diameter for a given propellant. Obstacles such as ignition wire in the gas stream can either raise or lower the minimum pressure necessary for flame, depending upon whether they act to split the gas stream or act as flame holders. As the pressure is further increased, the flame becomes wider and the dark zone becomes narrower, as first noted by Crawford, et al.[3] Decreasing the pressure reverses the process and the flame goes out at a slightly lower pressure than it appeared. The flame flickers unsteadily within a pressure range which varies with propellant compositions. Most double-base pro-

pellants appear to burn with a similar flame structure.

### TABLE II
#### Height of Dark Zone (Surface to Flame)

| Propellant lot no. | P (p.s.i.g.) | Height (mm.) | Propellant lot no. | P (p.s.i.g.) | Height (mm.) |
|---|---|---|---|---|---|
| 673 | 150 | 15.7 | 673 | 300 | 4.3 |
| 673 | 200 | 10.7 | 748 | 300 | 5.2 |
| 725 | 200 | 11.9 | 673 | 310 | 5.7 |
| 725 | 200 | 11.4 | 673 | 400 | 2.5 |
| 748 | 230 | 10.5 | 673 | 400 | 2.5 |
| 748 | 235 | 9 | 725 | 400 | 2.5 |
| 748 | 250 | 9 | 748 | 400 | 3.2 |
| 673 | 250 | 10.1 | 748 | 500 | 2.6 |
| 673 | 367 | 8.3 | 673 | 500 | 1.2 |
| 673 | 300 | 4.3 | 673 | 500 | 0.9 |

A small number of strands of pure nitrocellulose were burned. The first appearance of flame with increasing pressure was within 1 mm. of the surface. Thus the dark zone was too small for observation when the flame appeared.

## Discussion

**I. Thermocouple Measurements.**—The obstacles to accurate thermocouple measurements involve response time of the thermocouple, steepness of temperature gradient and catalysis of reactions by the wire surfaces.

Various coatings were used on the surface bearing thermocouples. There were no significant temperature differences between the various coated wires and the bare couples. This indicates that either all the surfaces were of equal catalytic value or, more probably, that none were significantly catalyzing the particular reactions involved. In some runs the presence of the wire caused a lowering of the flame height which could have been due to catalysis of the nitric oxide–hydrogen reaction. However, the effect was not uniform and may well be due to turbulence created by the wire.

The response time of the thermocouple has been calculated[4] using reasonable heat transfer coefficients. Wires of 7.5 to 12.5 $\mu$ diameter should show a lag of only 2–3 degrees in the low pressure combustion waves.

The temperature gradient results in a temperature difference from bottom to top of the thermocouple. In a linear gradient the couple should measure the mean of the lower and upper temperatures.[6] However, any non-linear gradient within the diameter of the couple would be masked. Figure 2 shows the temperature profiles, as well as the diameter of the thermocouple. At 65 p.s.i.a. and lower the over-all gradients are small. Here the steepest measured gradients are below 7°/micron. Thus the small wire (7.5 $\mu$) would mask gradient changes within 50°.

At the higher pressures the gradients measured are similar to those calculated by Olds and Shook.[7] It is apparent that any detailed structure would be masked; but if the temperature rise is smooth, the

(4) A. S. Gordon, M. H. Hunt and C. A. Heller, "Surface Temperature of Solid Propellants," NOTS TM-971 (1953), China Lake, Calif.

(5) R. Klein, M. Mentser, G. Von Elbe and B. Lewis, This Journal, **54**, 877 (1950).

(6) H. S. Carslaw and J. C. Jaeger, "Conduction of Heat in Solids," Oxford Univ. Press, New York, N. Y., 1947.

(7) Robert H. Olds and Gail B. Shook, "Mathematical Study of Thermal Processes Relating to Reaction Rates in Solid Fuels," NOTS, China Lake, Calif., TM-917 (1952).
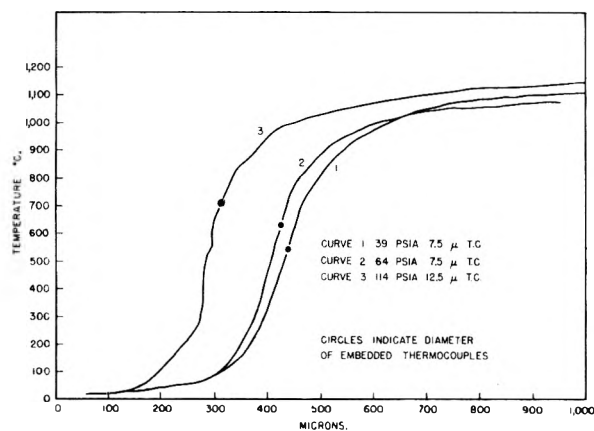
Fig. 2.—Temperature profiles Pl 748.

approximate gradient and temperature would be measured. However, a break such as is shown in curve 3 of Fig. 2 at 550° cannot be considered correct in detail.

Measurements of the 75-$\mu$ thermocouple resting on the surface are obviously taken over a much larger temperature range. Only at the lowest pressures, where the gradient is relatively small is the measured temperature close to the true surface temperature. At these low pressures the measured temperature sets an upper limit which is close to the surface temperature. As the pressure is increased the measured temperatures are increasingly above the surface.

Our couples are too large to probe the detailed thermal structure of the rapid temperature rise just above the surface. This rise terminates within a millimeter of the surface and is followed by a temperature plateau throughout the induction zone.

**II. Thermal Structure.**—As has been shown previously,[5] the temperature begins to rise slowly below the surface. A rapid rise starts just under the surface and ends above the surface. There is no apparent change in the temperature gradient at the surface. This indicates that there are no sudden changes in the reactions occurring in the foam and fizz zones as the gases leave the surface. That is, reactions such as those between $NO_2$ and aldehyde may occur in both the foam and fizz zones. One effect of increasing pressure may be to cause a more complete reaction in the foam zone, and perhaps raise the surface temperature.

As the fizz reaction ends, the temperature levels off as shown in Fig. 2. Raising the pressure increases the temperature of this plateau as shown in Fig. 4. In Fig. 4 there is a scattering of high temperatures above the indicated plateau. Where moving pictures were taken simultaneously with the temperature records, they showed flame striking back just above the thermocouple wire whenever a high temperature was recorded. We feel that this condition probably accounts for all the high temperature records where the photographs were not taken. The foam-fizz reaction apparently almost goes to completion at low pressures. At a pressure of about 150 p.s.i. the temperature of the induction seems to have reached a maximum. This corresponds roughly with the constancy of composition as shown in Fig. 3.
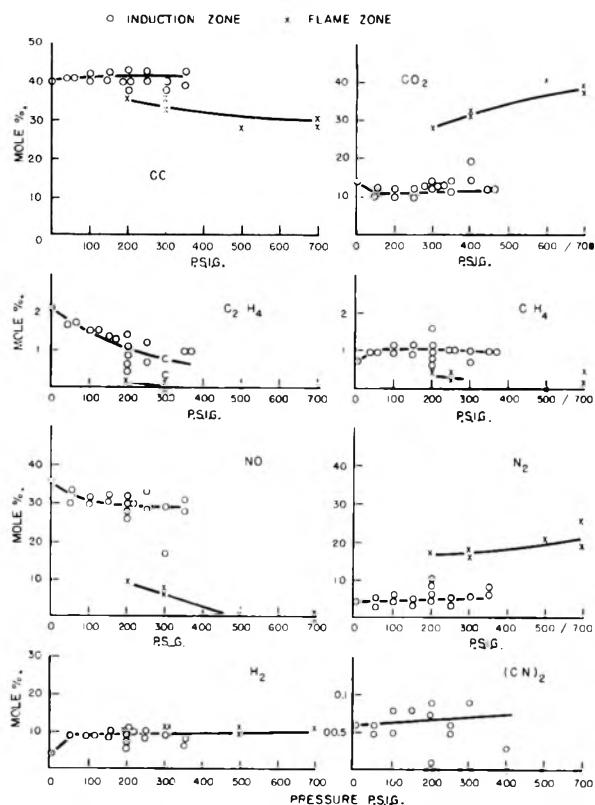


Fig. 3.—Change of composition of gas with pressure.

There is no measurable thermal gradient in the induction zone[3] prior to the appearance of a flame. When a flame appears there is a thermal gradient of about 100–500°/cm. A very minor oxidation by NO may occur prior to the spontaneous appearance of the flame. At the same distance from the surface, the composition remains unchanged within
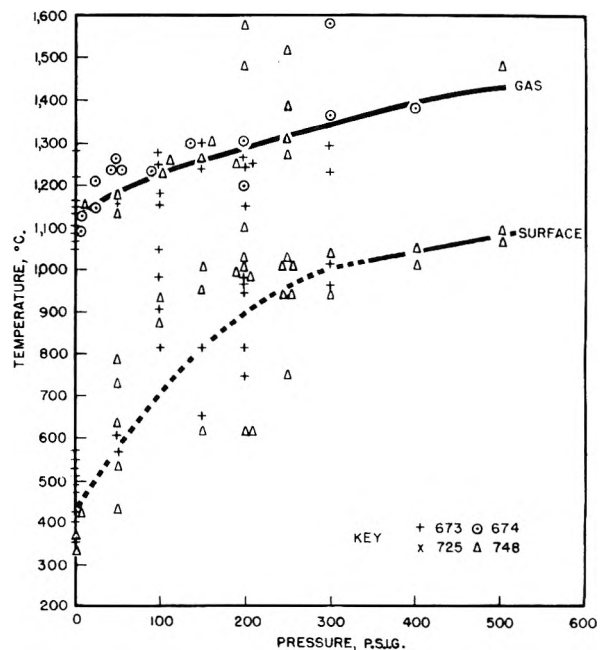


Fig. 4.—Temperatures of surface and gas at various pressures.

(8) O. K. Rice and Robert Ginell, This Journal, **54**, 885 (1950).

experimental error, whether or not there is a flame further upstream. This is so despite the fact that the temperature may have increased 300–400° because of conduction from the flame.

**III. Composition of Gases—Variation with Distance.**—Samples at various heights above the surface have the same compositions within experimental error. This is consistent with the low temperature gradient attained in this induction region indicating very slow reaction.

TABLE III

COMPOSITION OF DARK ZONE GASES AT DIFFERENT HEIGHTS

| $P_{p.s.i.g.}$ | 150 | 150 | 200 | 200 | 200 |
|---|---|---|---|---|---|
| Height (mm.) | 4 | 5 | 6 | 14 | 16 |
| Run no. | 43 | 48 | 42 | 45 | 53 |
| $H_2$ | 8.9 | 9.5 | 9.3 | 10 | 10.1 |
| He | ... | ... | ... | ... | ... |
| $CH_4$ | 0.9 | 1.1 | 0.9 | 1 | 1.1 |
| $H_2O$ | ... | ... | ... | ... | ... |
| HCN | 0 | 0.13 | −0.1 | 0.5 | 0.2 |
| $C_2H_4$ | 1.3 | 1.3 | 1.1 | 0.6 | 0.7 |
| CO | 41 | 42 | 38 | 40 | 40 |
| $N_2$ | 4.3 | 4.7 | 9 | 6 | 4.4 |
| NO | 32 | 30.9 | 30 | 28.6 | 30 |
| $CO_2$ | 11.5 | 10.9 | 12 | 13.0 | 12.9 |
| $(CN)_2$ | 0 | 0.08 | 0 | 0.09 | 0.073 |

**Variation with Pressure.**—It can be seen from Fig. 3 that there is only a slight change in composition of the dark zone gases as high as 350 p.s.i. This is in good agreement with the apparent temperature plateau with pressure for the same region. It appears, therefore, that only the rates, not the course, of the foam-fizz reactions are changed by increasing pressure. These foam-fizz reactions definitely appear to be the important reactions in controlling the linear burning rate since the onset of flame around 150 p.s.i. causes no change in the log pressure–log rate slope.

A correlation of burning rate with chemical composition has been attempted by comparing the heat of explosion of various propellants.[9] It would appear more reasonable to use the heat of the foam-fizz reaction as the basis of comparison. This value should be obtainable by calorimetric measurements at controlled pressures less than those at which the flame appears.

The compounds of CN are probably accounted for by reactions between hydrocarbon radicals and nitric oxide. Waring[10] has shown that methyl radicals produced from ketones react with nitric oxide to form hydrogen cyanide.

**IV. Reaction Leading to Flame.**—The spontaneous appearance of a flame in the gas stream containing NO, $H_2$, CO, $CH_4$ and $C_2H_4$ can be explained by two mechanisms. There can be a temperature rise due to slow reaction until ignition temperature is reached, or there can be a slow buildup of active species leading to a chain explosion.

The thermocouple measurements show a slow temperature rise above the foam-fizz zone, but this rise can be understood solely as conduction from

the flame zone. It does not occur at pressures just below those at which a flame appears. Furthermore, the NO analyses under the flame do not indicate that enough reaction is occurring to cause the temperature rise.

There is no positive evidence for active species in the induction zone from our work. Spectroscopic evidence from premixed and preheated NO–hydrocarbon flames[11] support a mechanism including a radical attack on NO.

The time $t$ in the induction zone can be calculated from the linear burning rate and the densities of propellant and gases. The fizz zone is such a small proportion of the dark zone that it can be neglected except at high pressures. Plotting log $t$ vs. log $P$ should give the order of the induction reaction for the constant temperature. The temperature does change, but the relative change of reciprocal temperature is not large over most of the induction region. The data of Table II, when calculated as residence time, gives an order of approximately 1.4 for the induction reaction. This figure cannot be taken as accurate, but this concept is more fundamental than plotting dark zone height vs. pressure. The residence times vary from 4.5 msec. at 150 p.s.i.g. to 1 msec. at 500 p.s.i.g.

The nitrocellulose mentioned above has a flame so close to the surface that any induction time must be very short. Temperature and composition studies would be necessary to explain the phenomena.

**V. Material Balance.**—A mass balance between propellant burned and gases produced cannot be obtained because only a sample of the gases is taken. However, it is possible to compare the C:H:O:N ratio of the propellant and the gases. For a 45NG–55NC (12.6% N) propellant the atomic ratio is 19.9:28:42:12. The gases must be corrected for water since this is not measured. Adding about 30% water changes the ratio in the gas to 17:28:38:12 for most of the samples. The carbon deficiency could be due to the carbonaceous ash which appears. The oxygen deficiency indicates some error in the technique, or some oxygenates as part of the carbonaceous mass. We hope to improve the experimental techniques so that percentage of water in the gases can be measured accurately.

**VI. Adiabatic Dark Zone Temperature.**—By comparing the enthalpy of the propellant and of the observed gases at various temperatures one can calculate a temperature on the basis of an adiabatic foam-fizz reaction. The temperatures obtained are in the region from 800 to 1200°—somewhat lower than those measured. However, small errors in the percentage of NO can result in large temperature errors.

**Conclusion**

At low pressures the combustion region of a double-base propellant consists of a narrow (0.3 mm.) foam-zone and a dark zone of no reaction. At a pressure of about 150 p.s.i.g. a flame appears

(9) R. E. Gibson, THIS JOURNAL., 54, 847 (1950).

(10) Dr. C. E. Waring, private communication.

(11) B. B. Fogarty and H. G. Wolfhard, Nature, 168, 1122 (1951); G. K. Adams, W. G. Parker and H. G. Wolfhard, Faraday Soc. Disc., No. 14 (1953).

and there is a wide (15 mm.) induction zone still with no measurable reaction.

The surface is at about 400–500° and causes no apparent discontinuity in the thermal wave, which becomes steeper very rapidly with pressure.

The composition of the induction zone is almost constant between 100 and 300 p.s.i.g. despite the change in linear rate and the appearance of a flame.

The flame consists of the reaction between nitric oxide and methane, ethene, carbon monoxide and $H_2$.

**Acknowledgment.**—The fine thermocouples were made and imbedded by Mr. Don Fuhlhage, and the temperature profiles recorded by Mr. Maynard H. Hunt.

# THE DECOMPOSITION OF ARSINE

By KENZI TAMARU

*Frick Chemical Laboratory, Princeton University, Princeton, N. J.*

Coherent films of arsenic by decomposition of arsine can be laid down on the surface of a reaction vessel if the glass surface is first covered by a coherent film of antimony. On such antimony and arsenic films the kinetics of the decomposition of arsine have been studied by a static method. The reaction is first order with respect to arsine and independent of hydrogen concentration. The apparent activation energy on arsenic surfaces is 23.2 kcal./mole. Arsine decomposes more easily on antimony surfaces than on arsenic surfaces. Decomposition on glass surfaces is much slower. In the decomposition of a mixture of arsine and deuteroarsine at 255° intermolecular exchange occurs and the decomposition product contains a large percentage of hydrogen deuteride. When arsine is decomposed with molecular deuterium at this temperature no hydrogen deuteride is found, indicating no exchange between hydrogen and deuterium on the arsenic surface. Analysis of the experimental data suggests the reaction $AsH_3(a) \rightarrow AsH_2(a) + H(a)$ as the rate-determining step.

Studies of the decomposition of arsine were first reported by van't Hoff in his book,[1] "Etudes de dynamique chimique" published in 1884. He and Kooj found that the decomposition on a glass surface is a first-order reaction. Stock and co-workers[2] tried without success to study the decomposition on an arsenic surface covering all the glass surface of the reaction vessel. As the vapor pressure of arsenic at the reaction temperature was appreciably high, the deposited arsenic recrystallized and sublimed, condensing in the cool parts of the system without covering the glass surface of the reaction vessel and blocking the inlet capillary tubing in four experiments.

In spite of this difficulty, the decomposition of arsine on arsenic surface remains one of the interesting catalytic reactions, since the catalyst surface is always renewed by the deposition of fresh arsenic during the reaction and the reaction system itself contains only two elements, one of which is the catalyst for the reaction. Thus we can not only get information about the reaction mechanism and the adsorption and reaction of hydrogen on the clean arsenic surface through this reaction, but also treat this most fundamental reaction from the statistical mechanical point of view.

## Experimental

**Preparation of Arsine.**—Arsine was prepared by adding chemically pure arsenic trichloride to a solution of lithium aluminum hydride[3] in ethylene glycol dimethyl ether in a nitrogen atmosphere. As the reaction is fairly violent, the solution of lithium aluminum hydride was cooled with liquid nitrogen as the arsenic trichloride was added. After the arsenic trichloride addition the liquid nitrogen was removed to allow the solution to warm up gradually. The arsine was evolved before the reaction vessel reached room temperature and was condensed in a liquid nitrogen trap. It was purified by distilling several times between solid carbon dioxide and liquid nitrogen. For the preparation of deuteroarsine, lithium aluminum deuteride of 98% purity was used instead of hydride.

**Apparatus and Procedure.**—The experiments were carried out in a static system. A pear-shaped Pyrex reaction vessel attached to a mercury manometer by means of capillary tubing was used. The volume of the vessel was 67 cc. Before the reactant was introduced into the reaction vessel a vacuum of less than $10^{-4}$ mm. was obtained by means of a mercury diffusion pump backed up by a Cenco Hy-Vac oil pump. The reaction temperature was controlled by means of vapor baths, using diphenylamine, acenaphthene, naphthalene and benzoic acid. The course of the reaction was measured by noting the pressure indicated by the manometer at suitable intervals.[4] The content of hydrogen deuteride was determined by a Nier ratio-type mass spectrometer which measures the ratio of mass 3/mass 2.

## Experimental Results

**Arsine Decomposition on a Glass Surface.**— When arsine was heated to 302° in a Pyrex glass vessel, using the diphenylamine vapor-bath, a pressure increase of 1.7% was observed in 47 hours. It decomposed as shown in Table I, when the

TABLE I

DECOMPOSITION OF ARSINE ON GLASS AT 350°

| Time, hr. | Total pressure, cm. | $P_{AsH_3}$, cm. | Time, hr. | Total pressure, cm. | $P_{AsH_3}$, cm. |
|---|---|---|---|---|---|
| 0 | 39.2 | 39.2 | 25.5 | 45.35 | 26.9 |
| 4.33 | 40.3 | 37.0 | 37.66 | 48.05 | 21.5 |
| 16 | 43.65 | 30.3 | 44.75 | 48.85 | 19.9 |

reaction temperature was raised to 350° using an electric heater. It was a first-order reaction in respect to arsine. In this case the arsenic which deposited as a reaction product did not cover the glass surface but arsenic crystals were observed in the cool capillary tubing as well as in the reaction vessel, and no marked acceleration of the reaction by arsenic was recognized. Thus, as the vapor pressure of arsenic at this temperature is appreciably high (*ca.* 2.3 mm. at 350°), it required a dif-

(1) J. H. van't Hoff, "Etudes de dynamique chimique," F. Muller and Company, Amsterdam, 1884, p. 83.

(2) A. Stock, E. Echeandia and P. R. Voigt, *Ber.*, **41**, 1319 (1908).

(3) This hydride and the corresponding deuteride were obtained from Metal Hydrides Incorporated.

(4) After the reaction the pressure increased stoichiometrically that is, up to 3/2, within the experimental error.

ferent technique to cover all the glass surface with arsenic for experiments on the decomposition of arsine.

**Arsine Decomposition on Antimony and Arsenic Surfaces.**—Arsine was found to decompose fairly fast on an antimony surface formed by decomposition of stibine. All the surface of the reaction vessel, consequently, could be covered by arsenic, depositing arsenic on the antimony surface at temperatures where its vapor pressure, or mobility, is negligibly small. The antimony film on the glass surface was prepared in the way described by Stock and co-workers[5] in their experiments on the decomposition of stibine, except that the stibine was prepared in our case by the reaction between antimony trichloride and lithium aluminum hydride as in the preparation of arsine.

The decomposition rate of arsine on the antimony surface became slower as arsenic covered the surface, and finally it reached a practically constant rate as shown in Fig. 1. This constant reaction rate was considered to be the decomposition rate of arsine on the arsenic surface, and thus the kinetics of the decomposition on the arsenic surface could be studied.
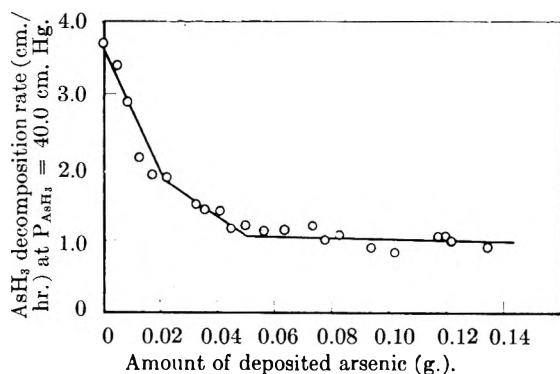


Fig. 1.—The relation between the rate of decomposition of arsine and the amount of deposited arsenic on the antimony film at 254°.

The results of the decomposition of arsine on arsenic surfaces at 278 and 218° are shown in Fig. 2 and Fig. 3, respectively, plotting the logarithm of
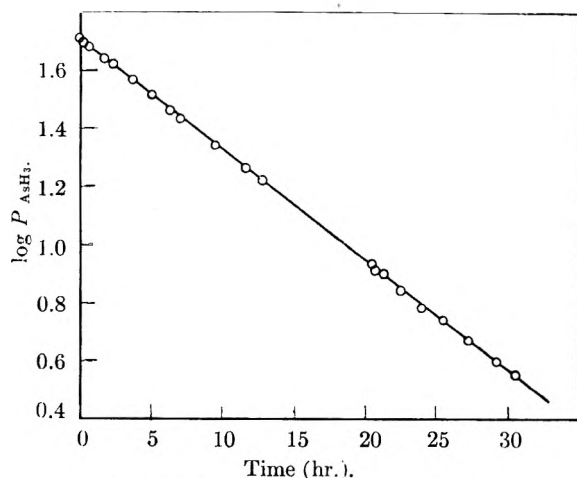


Fig. 2.—Decomposition of arsine at 278°.

(5) A. Stock, F. Gomolka and H. Heynemann, *Ber.*, **40**, 532 (1907).
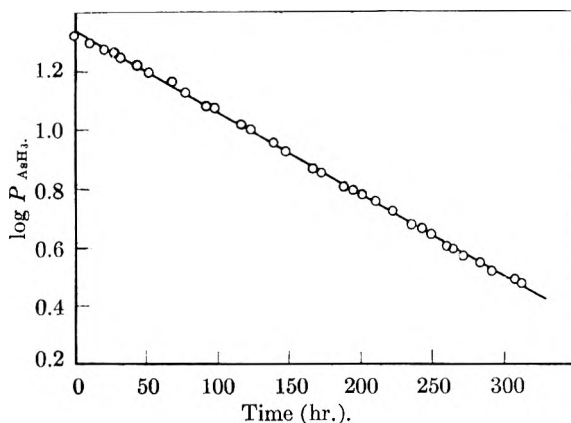


Fig. 3.—Decomposition of arsine at 218°.

the partial pressure of arsine against time. It is obvious that the reaction is first order in respect to arsine, and the velocity constants are 0.0887 and 0.0062 hr.$^{-1}$ at 278 and 218°, respectively

The dependence of the initial reaction rate upon various initial pressures of arsine at 254° is shown with circles in Fig. 4. On the other hand, when 48.3 cm. arsine was decomposed at this temperature, the rate of the reaction was plotted against the partial pressure of arsine, and is shown as triangles in Fig. 4. In this experiment the benzoic acid, used for the vapor-bath, changed its boiling point gradually. The reaction rates were corrected taking the temperature coefficient of the reaction rate into consideration. In Fig. 4 we can see that the reaction rate is independent of the partial pressure of hydrogen and is proportional to that of arsine.



Fig. 4.—Dependence of the decomposition rate of arsine upon pressure at 254°.

The temperature coefficient of the reaction is shown by the plot in Fig. 5. It obeys the Arrhenius equation, from which an apparent activation energy of 23.2 kcal./mole is obtained.

**Exchange Reactions between Arsine and Deuteroarsine and between Hydrogen and Deuterium on Arsenic Surfaces.**—When 31.7 cm. of arsine and 24.0 cm. of deuteroarsine were introduced into the reaction vessel to decompose at 255°, a large

Fig. 5.—Dependence of the decomposition rate upon temperature.

amount of hydrogen deuteride was detected in the reaction product. During the reaction the reactants were pumped out to analyze, by infrared absorption analysis, whether any exchange reaction had taken place between arsine and deuteroarsine. The infrared spectra were taken with a Perkin–Elmer, Model 21, infrared spectrometer, using a 10-cm. cell at gas pressures of about 20 cm. The results are shown in Fig. 6. In the figure (i) is t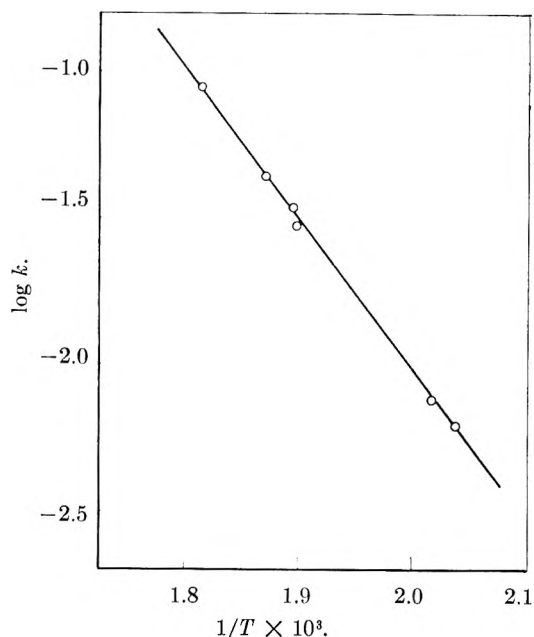he absorption spectrum for pure arsine and (ii), that for 98% pure deuteroarsine, and (iii), for the mixture of these two compounds and decomposition products after 65 and 10.5% decomposition, and (iv) was obtained putting approximately equal amounts of arsine and deuteroarsine mixtures in the compensating cell.

The infrared spectrum for the products from the reaction vessel was slightly different from that of a mixture which was not subjected to the high temperature of the reaction vessel.

31.9 cm. of arsine was allowed to decompose with 35.2 cm. of deuterium on an arsenic surface at 255° for 24 hours and the decomposition product was analyzed by means of the mass spectrometer. Practically no hydrogen deuteride was found in it. This experiment also shows that the reaction between hydrogen and deuterium on arsenic surfaces does not take place appreciably at this temperature.

**Areas of the Arsenic and Antimony Surfaces.—** The surface area of the arsenic in the reaction vessel was measured at liquid nitrogen temperature by means of krypton adsorption.[6] The result was $4.8 \times 10^3$ cm.[2], which means the roughness of the surface is approximately 50.

The area of the antimony surface before being covered by arsenic was also measured and found to be the same area as that of the arsenic surface, that is, $4.8 \times 10^3$ cm.[2].

(6) R. A. Beebe, J. B. Beckwith and J. M. Honig, *J. Am. Chem. Soc.*, **67**, 1554 (1945).

**Infrared Absorption Spectra of AsH₃ and Isotopic Molecules.—**It is shown in Fig. 6 (i) and (ii) that $AsH_3$ and $AsD_3$ have the following absorptions[7]

| $AsH_3$, cm.$^{-1}$ | 2060 | 2120 | 2185 | 906 | 1003 | |
|---|---|---|---|---|---|---|
| $AsD_3$, cm.$^{-1}$ | 1490 | 1531 | 1578 | 652 | 716 | (2120)[9] |

Howard[10] calculated the normal vibration frequencies of $AsH_3$ and tried to assign the absorption bands of $AsH_3$ to fundamental vibrations. He also calculated the fundamental frequencies in cm.$^{-1}$ of $NH_3$ and its isotopic molecules. Figure 6 must be the first observed absorption of the $AsH_xD_y$ isotopic molecules, where $x + y = 3$ and $x \neq 0$ and $y \neq 0$.
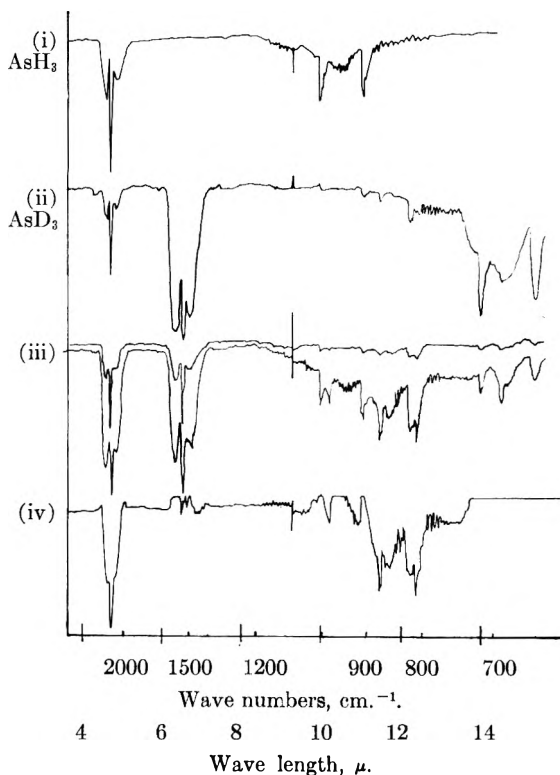


Fig. 6.—Infrared spectra of arsine and deuteroarsine: iii (upper) 65% decompn.; iii (lower) 10.5%; iv, 10.5%.

## Discussion

A first-order rate of decomposition is compatible with a diffusion-controlled process. Because of the long time intervals, up to 350 hours, in which the first-order constant is obtained, calculations of diffusion velocities through any practicable values of the stationary layer indicate that the diffusion process is so fast that it does not affect the over-all rate of reaction.

The possible consecutive processes involved in the

(7) These absorptions were reported by Lee and Wu[8] as 2122, 2185, 906 and 1005 cm.$^{-1}$ for $AsH_3$, and 1534, 660 and 714 cm.$^{-1}$ for $AsD_3$.

(8) E. Lee and C. K. Wu, *Trans. Faraday Soc.*, **35**, 1366 (1939).

(9) The absorption in the $AsD_3$ curve at 2120 cm.$^{-1}$ falls exactly in the position corresponding to the strong absorption of $AsH_3$, and according to Lee and Wu, this absorption can be considered to be due to the presence of a small amount of the light compound in the deuteride.

(10) J. B. Howard, *J. Chem. Phys.*, **3**, 208 (1935).

decomposition of an arsine molecule at an arsenic surface include

$$AsH_3(g) = AsH_3(a) \quad (1)$$
$$AsH_3(a) = AsH_2(a) + H(-As) \quad (2)$$
$$AsH_2(a) = AsH(a) + H(-As) \quad (3)$$
$$AsH(a) = As + H(a) \quad (4)$$
$$2H(a) = H_2(g) \quad (5)$$
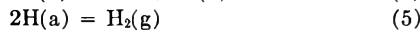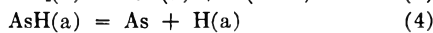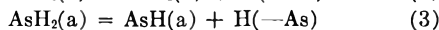
where reaction (1) is the physical adsorption and the reaction (5) is the desorption of physically adsorbed hydrogen. Theoretical considerations of the total sequences of the reactions lead to a conclusion that either reaction (1) or (2) can be compatible with the experimental results as the rate-determining step of the over-all reaction. Because the physical process of adsorption (1) is in general more rapid than the process of chemisorption (2), stage (2) or the chemisorption of arsine is actually rate determining in the experimental region studied.

The calculations suggest also that, at very low temperatures, a zero-order reaction would result, the arsenic surface being largely covered with AsH(a). The quantitative evaluation of this mechanism and that of other hydrides already studied, including $GeH_4$ and $SbH_3$, will be separately communicated.

# THE REACTION OF ACTIVE NITROGEN WITH METHYLAMINE[1]

BY G. R. FREEMAN AND C. A. WINKLER

*Contribution from the Physical Chemistry Laboratory, McGill University, Montreal, Canada*

Active nitrogen reacted with methylamine to produce hydrogen cyanide, hydrogen and a polymer, with smaller amounts of ammonia and $C_2$ hydrocarbons. The rates of methylamine destruction and hydrogen cyanide production increased with increasing temperature, while polymer formation increased with decreasing temperature. Comparison of the maximum rates of hydrogen cyanide production from methylamine and from ethylene during reaction with active nitrogen indicates that methylamine undergoes both ammonia and hydrocarbon type reactions.

The relative extents of reaction of ammonia and ethylene with active nitrogen[2] indicated that at least two reactive species are present in active nitrogen. It appeared that ammonia reacted with only one of these while ethylene (and presumably other hydrocarbons, e.g., propylene,[3a] propane,[3b] butane,[4] etc.) reacted with the other or both. Since methylamine might be expected to undergo both ammonia and hydrocarbon type reactions, it was obviously of interest to examine the reaction of active nitrogen with this compound.

## Experimental

The apparatus used was essentially the same as that described in earlier papers.[5,6]

The molecular nitrogen flow rate was $9.2 \times 10^{-5}$ mole/sec., corresponding to a pressure of 1.43 mm. in the reaction vessel.

In several experiments, the reaction vessel was surrounded by powdered Dry Ice. While the wall temperature may be assumed to have been approximately $-78°$, the temperature of the gases in the reaction vessel, as indicated by a glass encased thermocouple, was about $-5°$ during the active nitrogen–methylamine reaction.

To obtain methylamine, equal volumes of 25% methylamine solution (C.P. Fisher Scientific Co.) and 50% sodium hydroxide solution were cooled to 10°, and mixed in a flask, nitrogen was bubbled through the mixture and the gas stream passed through a condenser cooled with Dry Ice into a similarly cooled receiver containing potassium hydroxide pellets. About 10% of the recovered methylamine was removed by distillation under vacuum and discarded, and the residue distilled twice, with rejection each time of the last 20% to remove traces of water. Infrared analyses[7] of the final distillate showed that it contained 98.7% methylamine and 1.3% ammonia.

The amount of methylamine passed into the reaction vessel was estimated from the change in pressure in a storage vessel of known volume. Condensable products of the reaction were collected in a trap containing 10 ml. of standard sulfuric acid, immersed in liquid nitrogen, and their base content determined by titration to methyl red end-point of the excess acid after it had been allowed to melt in the trap. The presence of hydrogen cyanide did not affect the titration.

Ammonia was determined by infrared analysis. The condensable reaction products were collected in an evacuated bulb immersed in liquid nitrogen, then distilled into an evacuated 10 cm. absorption cell. The wave numbers of the absorption peaks used were 968 cm.$^{-1}$ for ammonia and 2930 cm.$^{-1}$ for methylamine.

The hydrogen cyanide content of the condensable products was determined by the Liebig Déniges method.[8] In some experiments, these products were also analyzed for cyanogen. To do this, condensable products were collected in a trap containing 20 ml. of 0.5 $N$ silver nitrate solution and 0.5 ml. of 6 $N$ nitric acid, immersed in liquid nitrogen. The cyanogen was flushed out of the melted solution with nitrogen (1 hr.), and the cyanogen removed from the nitrogen stream by bubbling it through potassium hydroxide

(1) Financial assistance from the National Research Council of Canada.

(2) G. R. Freeman and C. A. Winkler, THIS JOURNAL, **59**, 371 (1955).

(3) (a) G. S. Trick and C. A. Winkler, *Can. J. Chem.*, **30**, 915 (1952); (b) M. Onyszchuk, L. Breitman and C. A. Winkler, *ibid.*, **32**, 351 (1954).

(4) R. A. Back and C. A. Winkler, *ibid.*, **32**, 718 (1954).

(5) J. H. Greenblatt and C. A. Winkler, *Can. J. Res.*, **B27**, 721 (1949).

(6) H. Blades and C. A. Winkler, *Can. J. Chem.*, **29**, 1022 (1951).

(7) We are indebted to the Central Research Laboratory, Canadian Industries (1954) Ltd., McMasterville, Que., and to Ayerst McKenna and Harrison, Ltd., Montreal, Que., for the infrared analyses reported in this paper.

(8) I. M. Kolthoff and E. B. Sandell, "Textbook of Quantitative Inorganic Analysis," The Macmillan Co., New York, N. Y., 1946.

solution. The potassium hydroxide solution was then analyzed for cyanide.

The total $C_2$ fraction in the products was estimated with a Le Roy still, and its composition determined with the mass spectrometer.[9] The non-condensable products were similarly analyzed for methane and hydrogen.

## Results and Discussion

The products of the reaction between active nitrogen and methylamine were found to be hydrogen cyanide and hydrogen, with smaller amounts of ammonia and a polymer, and traces of cyanogen, methane, ethane, ethylene and acetylene. In Fig. 1 the flow rate of methylamine is plotted for
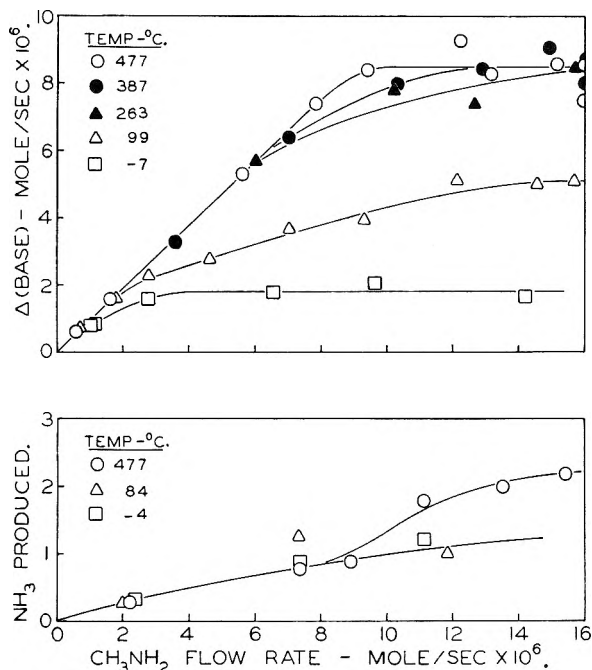


Fig. 1.—Freeman and Winkler, active nitrogen with methylamine.

different temperatures against (i) the flow rate of ammonia produced and (ii) a quantity, $\Delta$ (Base), defined as the flow rate of methylamine introduced minus the flow rate of total base found in the condensable products (i.e., residual methylamine plus ammonia produced). Obviously, (ii) plus (i) gives the rate of destruction of methylamine. The relations between the methylamine flow rate, the rate of destruction of methylamine, and the rate of production of hydrogen cyanide are shown in Fig. 2 for different temperatures. The rates of production of hydrogen, methane, cyanogen and $C_2$ hydrocarbons are shown in Table I. The $C_2$ hydrocarbons were approximately 20% ethane, 30% ethylene and 50% acetylene.

Nearly two moles of hydrogen were produced for each mole of methylamine destroyed. Methane was not produced at methylamine flow rates below about $8 \times 10^{-6}$ mole/sec., and the amount produced above that flow rate increased with increasing temperature. Cyanogen production decreased with increasing methylamine flow rate and increased with increasing temperature. The amount
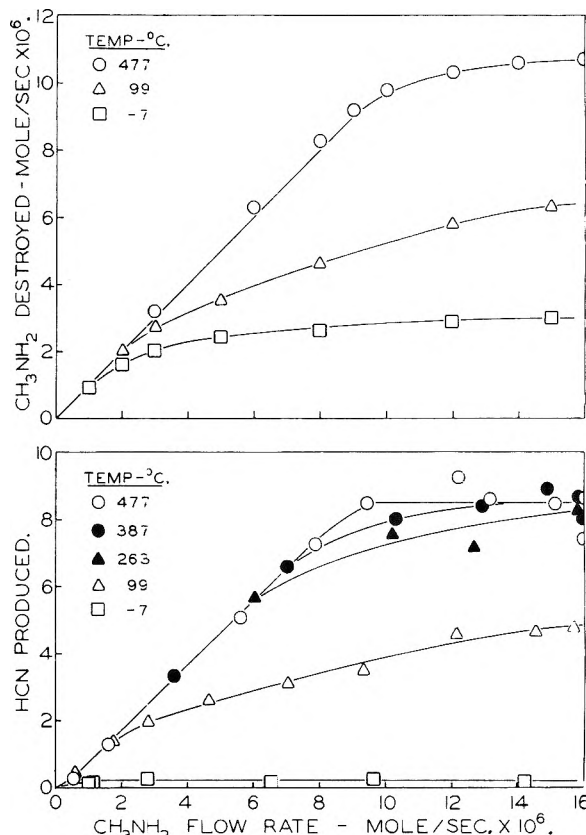
Fig. 2.—Freeman and Winkler, active nitrogen with methylamine.

of $C_2$ hydrocarbons produced at methylamine flow rates below about $8 \times 10^{-6}$ mole/sec. increased with decreasing temperature.

## TABLE I

PRODUCTION OF $H_2$, $CH_4$, $C_2N_2$ AND $C_2$ HYDROCARBONS

(All units except temperature are mole $\times 10^{-6}$/sec.)

| $T$ (°C.) | $CH_3NH_2$ flow | $H_2$ | $CH_4$ | $C_2N_2$ | $C_2$ |
|---|---|---|---|---|---|
| 468 | 7.01 | 13.7 | 0.00 | 0.010 | 0.010 |
| 480 | 10.4 | 17.7 | 0.18 | 0.003 | .092 |
| 482 | 10.4 | | | | .118 |
| 96 | 0.56 | | | .015 | |
| 74 | 1.57 | | | .010 | |
| 106 | 7.11 | | .00 | .003 | .041 |
| 101 | 7.23 | | | | .031 |
| 108 | 10.29 | 9.2 | .11 | .000 | .095 |
| 130 | 12.47 | | | .000 | |
| -6 | 0.96 | 1.88 | .00 | | |
| -2 | 1.68 | | | | .02 |
| +2 | 7.10 | 3.04 | .00 | | |
| -2 | 7.55 | | | | .65 |

The difference between the amount of methylamine destroyed and the amount of hydrogen cyanide produced at 477° corresponded closely to the amount of ammonia produced. The amount of carbon in this difference is much more than that contained in the methane, cyanogen and $C_2$ hydrocarbons. As the temperature was decreased, the amount of carbon which was measured in the products decreased progressively, and at Dry Ice temperature (gas phase temperature about $-5°$)

it corresponded to only about 10% of the total amount of methylamine destroyed. However, at this low temperature, the walls of the reaction vessel became coated with a solid white polymer which melted upon warming to room temperature. The liquid turned light yellow upon standing. During the course of several experiments in the uncleaned reaction vessel, the polymer turned into a light brown solid, which did not melt at room temperature. It was assumed that, at all temperatures, the polymer accounted for the carbon which was not measured in the products.

The active nitrogen concentration, estimated from the amount of hydrogen cyanide produced by the reaction of active nitrogen with ethylene at $360°$, was $12.3 \pm 0.4 \times 10^{-6}$ mole/sec.

If it is assumed that the component in active nitrogen which reacted with ammonia[2] would react in a similar manner with the $NH_2$ group in methylamine, and that the other component reacted with the $CH_3$ group, the experimental results may be explained by the following type of mechanism[10]

$$\Delta H^{11} \text{ (kcal.)}$$

$$CH_3NH_2 + N \longrightarrow CH_3 + N_2 + H_2 \quad -78.2 \quad (1)$$

$$CH_3NH_2 + N_3 \longrightarrow HCN + H_2 + NH_2 - (34.4 - x) \quad (2)$$

$$CH_3 + N_3 \longrightarrow [CH_3N] + N_2 \longrightarrow HCN + H_2 + N_2$$
$$-(113.4 - x) \quad (3)$$

$$NH_2 + CH_3NH_2 \longrightarrow NH_3 + CH_3NH \quad \approx -12 \quad (4a)$$
$$\longrightarrow NH_3 + CH_2NH_2 \quad \approx -12 \quad (4b)$$

$$CH_3 + CH_3NH_2 \longrightarrow CH_4 + CH_3NH \quad \approx -6 \quad (5a)$$
$$\longrightarrow CH_4 + CH_2NH_2 \quad \approx -6 \quad (5b)$$

$$CH_3NH (+ \text{ possibly } CH_2NH_2) \longrightarrow \text{polymer}$$
$$(+ \text{ possibly } H_2 + NH_3) \quad (6)$$

$$2NH_2 \longrightarrow N_2 + 2H_2 \quad -89.4 \quad (7)$$

$$2CH_3 \longrightarrow C_2H_6 \quad -83 \quad (8)$$

At high methylamine flow rates, the $N_3$ concentration would be depleted by reaction (2), thus allowing reactions (5) and (8) to compete to a certain extent with reaction (3) for methyl radicals.

Since nearly two molecules of hydrogen were produced for each molecule of methylamine destroyed, the polymer must contain a low percentage of hydrogen. The formation of some polymer at higher temperatures in the presence of excess active nitrogen indicates that polymerization occurs quite rapidly.

The photochemical (direct and mercury-sensitized) decomposition of methylamine has been investigated.[18,19,20] The products from the decomposition of one mole of methylamine were found to be one mole of hydrogen, 0.5 mole of ammonia, 0.02–0.04 mole of methane, and a polymer. The mechanism of the photochemical reaction has not been definitely established, but the fate of the $CH_3NH$ (or $CH_2NH_2$) radicals is probably similar in both the photochemical and active nitrogen reactions, since in both cases they appear to form a similar polymer with a low hydrogen content.

When the reaction vessel was surrounded by Dry Ice the value of $\Delta$(Base) was the same as the amount of ammonia destroyed by active nitrogen under similar conditions ($1.8 \times 10^{-6}$ mole/sec.[2]). However, the maximum rate of destruction of methylamine was $3.0 \times 10^{-6}$ mole/sec., with the production of only $0.2 \times 10^{-6}$ mole/sec. HCN. This can be explained if it is assumed that reaction (2) does not occur appreciably at this temperature, and that the collision complex formed in reaction (3) (*i.e.*, [$CH_3N$]) reacts with methylamine and itself to produce ammonia, hydrogen and a polymer.

(10) For the purpose of illustrating the type of mechanism, it is assumed that N and $N_3$ are the reactive species, since there is some reason to believe that excited molecules probably contribute little to the chemical activity of active nitrogen:  G. R. Freeman and C. A. Winkler, *Can. J. Chem.*, in print.

(11) These heats of reaction were calculated using the following values: $D_{N-N} = 225$ kcal.,[12] $D_{H-H} = 102.7$ kcal.,[13] $D_{H-CH_3} = 101$ kcal.,[14] $D_{CH_3-NH_2} = 79$ kcal.,[14] $D_{H-NH_2} = 107$ kcal.,[15] $\Delta H_f(HCN) = 30.1$ kcal.,[16] $\Delta H_f(CH_3) = 31$ kcal.,[14] $\Delta H_f(NH_3) = -10.9$ kcal.,[16] $\Delta H$ combustion ($CH_3NH_2$ gas) $= -262.0$ kcal.[17]. Using the appropriate values from above, it was calculated that $\Delta H_f$ ($CH_3NH_2$) $= -3.3$ kcal., $\Delta H_f$ ($NH_2$) $= 44.7$ kcal. It was assumed that $D_{H-HNCH_3} \approx D_{H-CH_2NH_2} \approx 95$ kcal.  $x = D_{N-N_2}$ in $N_3$.

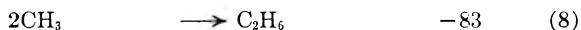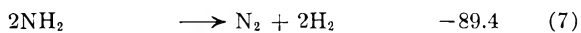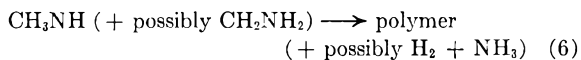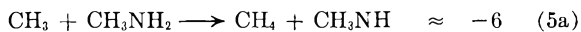(12) J. M. Hendrie, *J. Chem. Phys.*, **22**, 1503 (1954).

(13) H. Beutler, *Z. physik. Chem.*, **B29**, 315 (1935).

(14) M. Szwarc, *Chem. Revs.*, **47**, 75 (1950).

(15) J. C. Devins and M. Burton, *J. Am. Chem. Soc.*, **76**, 2618 (1954).

(16) "Handbook of Chemistry and Physics."

(17) T. L. Cottrell and J. E. Gill, *J. Chem. Soc.*, 1798 (1951).

(18) O. C. Wetmore and H. A. Taylor, *J. Chem. Phys.*, **12**, 61 (1944).

(19) C. I. Johnson and H. A. Taylor, *ibid.*, **19**, 613 (1951).

(20) J. S. Watson and B. de B. Darwent, *ibid.*, **20**, 1041 (1952).

# THE PHOTOREDUCTION OF SOME FERRIC COMPOUNDS IN AQUEOUS SOLUTION

By J. H. Baxendale and N. K. Bridge

*Department of Chemistry, University of Manchester, Manchester, England*

The quantum yields for the photoreduction of $Fe(Phen)_3^{3+}$ and $Fe(Dipy)_3^{3+}$ are found to increase with increase in the concentration of the complex ion, with increase of $pH$, with decrease of wave length of the incident light and also on the addition of an oxidizable substrate such as formic acid. Quantum yields for the reduction of $Fe(Phen)_3^{3+}$ have been measured over a range of these variables. The yellow complexes of ferric ion and dipyridyl or phenanthroline have been found to possess only little photoactivity at 365 m$\mu$. Ferric formate solutions are readily reduced by ultraviolet light and also show activity at 436 m$\mu$. It is found that the activity is due to a ferric ion–formate ion pair. A detailed investigation of the system has been made. Parker's results for the quantum yields of the reduction of ferrioxalate solutions have been confirmed at 254 and 365 m$\mu$, but slightly higher values are obtained at 436 m$\mu$. Some modifications in the technique are suggested which simplify the use of ferrioxalate as an actinometer.

The photoreduction of ferric ion when present in aqueous solution as an ion pair with anions such as hydroxide or chloride has been the subject of several recent investigations,[1] but the photoreduction of ferric complexes with non-ionic compounds has not been examined in detail. Some of these compounds absorb appreciably in the visible and it was thought that they may prove useful as actinometers in the region of the spectrum not covered by convenient chemical actinometers. We have examined the photoreduction of a number of ferric compounds with this in mind. While the work was in progress it was reported by Parker[2] that solutions of the ferrioxalate ion are more sensitive than the commonly used uranyl oxalate actinometer and hence are more convenient at the longer wave lengths. We have confirmed this in the present investigation.

## Experimental

**Materials.**—Reagents of analytical grade were used without further purification. Solutions of the ferrous tris-phenanthroline and tris-dipyridyl ions, $Fe(Phen)_3^{2+}$, $Fe(Dipy)_3^{2+}$, were prepared from the stoichiometric amounts of ferrous sulfate and base solutions. The corresponding ferric ions, $Fe(Phen)_3^{3+}$ and $Fe(Dipy)_3^{3+}$, were made from these by oxidation with lead dioxide or ceric sulfate.

**Light Sources.**—Light of wave lengths 546, 365 and 313 m$\mu$ was isolated from a 250-watt mercury vapor lamp, wave lengths 436 and 280 m$\mu$ from a 125 w. lamp and 254 m$\mu$ from a low pressure lamp. The lamps were run off rectified a.c. smoothed by conventional inductance–capacity circuits. Irradiation of the solutions usually took about 30 minutes and seldom more than an hour. During this time the lamp current was kept constant by manual adjustment of a series resistance, but this was rarely necessary after an initial warming up period.

After collimation, filter combinations were used to isolate the 546 (Wratten), 436,[3] 365,[4] 313,[4] 280[4] and 254[4] m$\mu$ lines. Intensities incident on the reaction vessels were measured by uranyl oxalate actinometry.[3]

**Procedure.**—Cylindrical reaction vessels of quartz and Pyrex, *ca.* 3 cm. long and *ca.* 2 cm. diameter, were used. The irradiated solutions could be stirred, and provision was also made for removing oxygen by a stream of pure nitrogen. Where color changes were produced directly on irradiation (*e.g.*, $Fe(Phen)_3^{3+}$ to $Fe(Phen)_3^{2+}$) the reaction was followed by transferring the reaction vessel to a colorimeter after each irradiation period. Otherwise the ferrous ion in a sample of the irradiated solution was measured colorimetrically using *o*-phenanthroline. A ferrous ion–time curve was constructed by the irradiations of several batches of the

same preparation for increasing times. When reduction was kept to a few percentage of the ferric species present, zero-order curves were invariably obtained (Fig. 2).

Side by side with the photoreaction the thermal, *i.e.*, dark reaction, was followed also on a batch of the same preparation. Quantum yields were calculated from the photochemical rates after correction for the simultaneous thermal rates. Experiments were begun usually at room temperature (16–19°) and the solution temperatures increased 2 or 3° during irradiation. In studying the effect of temperature the solutions were cooled to 5° or heated to 40° before irradiating. Except in certain cases which will be mentioned below such changes had no effect on the photoreduction rates, so that the variations of a few degrees normally encountered were of no consequence.

Absorption spectra were measured on a Beckman spectrophotometer and $pH$'s by the Cambridge glass electrode $pH$ meter.

## Results and Discussion

**Ferric Tris-phenanthroline, $Fe(Phen)_3^{3+}$.**—This ion, obtained by the oxidation of the intense red ferrous complex ion, is blue and has been reported to be reduced by light.[5] Its absorption spectrum is shown in Fig. 1. It seemed possible that some of the photoactivity might arise from the broad absorption band in the visible, and hence that the substance might be of some use as an actinometer in this region.
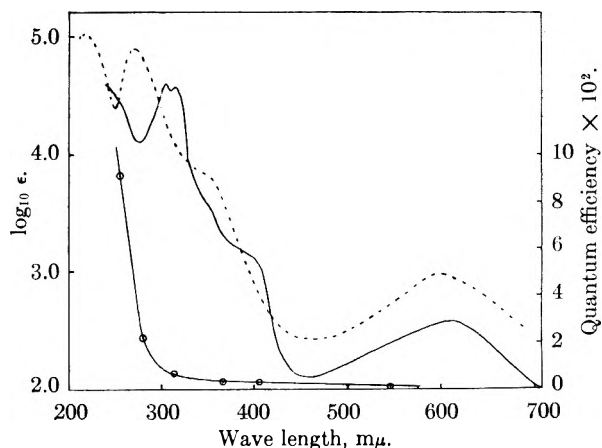


Fig. 1.—Absorption spectra of $Fe(Phen)_3^{3+}$ (----) and $Fe(Dipy)_3^{3+}$ (—) and quantum efficiencies (O) for the photoreduction of $10^{-4}$ $M$ $Fe(Phen)_3^{3+}$ in solutions 0.10 $N$ in $H_2SO_4$ and 0.50 $M$ in formic acid.

Preliminary observations with $10^{-4}$ $M$ $Fe(Phen)_3^{3+}$ in 0.1 $N$ $H_2SO_4$ using 365 m$\mu$ light showed that the rate of photoreduction was not very re-

(1) N. Uri, *Chem. Revs.*, **50**, 413 (1952).

(2) C. A. Parker, *Proc. Roy. Soc. (London)*, **A220**, 104 (1953).

(3) E. J. Bowen, "The Chemical Aspects of Light," Oxford University Press, New York, N. Y., 1946.

(4) M. Kasha, *J. Optical Soc. Am.*, **38**, 929 (1948).

(5) F. Blau, *Monatsh.*, **19**, 647 (1898).

producible with different preparations of the ferric complex. Traces of reducing impurities in the solutions were suspected and to remove the uncertainty, and at the same time possibly increase quantum yields, the effect of adding oxidizable materials was examined. Ethyl alcohol, hydrogen peroxide and oxalic acid all increased the yield but had the disadvantage of giving high dark reduction rates. Formic acid was much less objectionable in this respect and had the desired effects of giving increased and reproducible quantum yields. All subsequent experiments were done in the presence of formic acid.

Typical rate curves from which quantum yields are obtained are given in Fig. 2. The dependence

Fig. 2.—Rates of photoreduction of $10^{-4}$ $M$ Fe(Phen)$_3$$^{3+}$ by 365 m$\mu$ light in 0.10 $N$ H$_2$SO$_4$ with various concentrations of formic acid present: A, 0.947 $M$; B, 0.714 $M$; C, 0.474 $M$; D, 0.237 $M$. Dark reduction rate approximately 0.06 × $10^{-8}$ mole per minute.

of the quantum yield on the formic acid and Fe(Phen)$_3$$^{3+}$ concentrations, and on $p$H was examined at 365 m$\mu$. In 0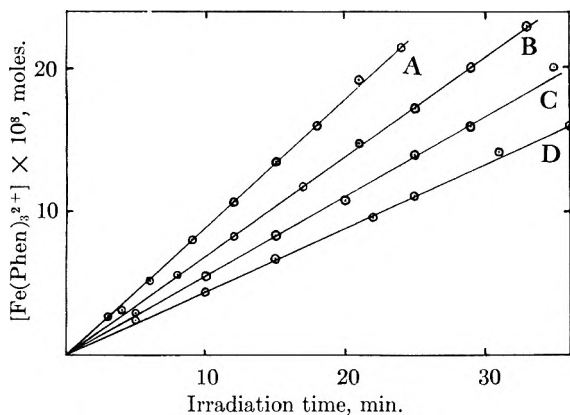.1 $N$ H$_2$SO$_4$ the yields increase linearly with both formic acid and Fe(Phen)$_3$$^{3+}$ as shown in Fig. 3. The range of $p$H available is limited since above $p$H 3 Fe(Phen)$_3$$^{3+}$ dissociates at an appreciable rate at room temperature. The effect of $p$H on the yield is appreciable as is shown in Table I, particularly in the presence of formic acid. No effect on the quantum yield at 365 m$\mu$ was observed by (a) decreasing the temperature to 5°, (b) decreasing the light intensity tenfold and (c) adding Fe(Phen)$_3$$^{2+}$ to the extent which is usually produced in a run. Figure 1 shows that the quantum yield increases as the wave length decreases and that the photo-activity is limited to the ultraviolet for all practical purposes.

Possible photodissociation of Fe(Phen)$_3$$^{3+}$ to Fe$^{3+}$ and phenanthroline was looked for by taking the photoreduction to 50% of the Fe(Phen)$_3$$^{3+}$ present and then reducing the remainder with hydroquinone. Within experimental error all the original Fe(Phen)$_3$$^{3+}$ is recovered as Fe(Phen)$_3$$^{2+}$, showing that there is no photodissociation.

In spite of the much smaller quantum efficiency for the photoreduction of Fe(Phen)$_3$$^{3+}$ compared with the uranyl oxalate system, the former constitutes a more sensitive actinometer because of the smaller changes which can be measured. Thus an exposure of 30 minutes was sufficient to measure
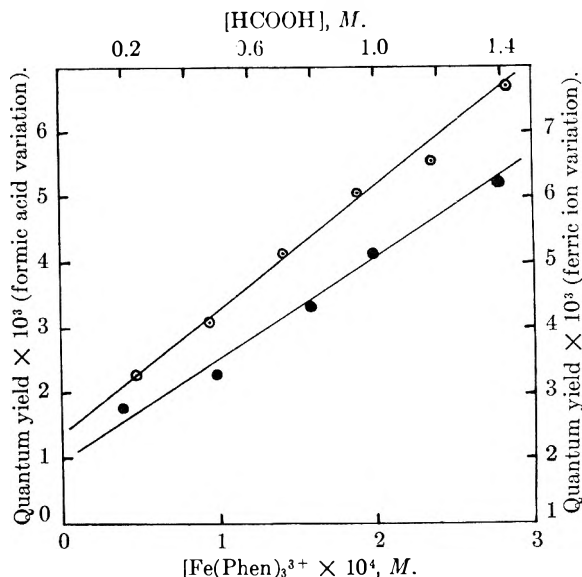
Fig. 3.—Variation of the quantum yield for the reduction of Fe(Phen)$_3$$^{3+}$ in 365 m$\mu$ light with: ⊙, formic acid concentration, at constant Fe(Phen)$_3$$^{3+}$ = $10^{-4}$ $M$; ●, Fe(Phen)$_3$$^{3+}$ concentration, at constant formic acid = 0.47 $M$.

the output of a 250-w. lamp at 365 m$\mu$, whereas with uranyl oxalate 18 hours were required. However, there are objections to Fe(Phen)$_3$$^{3+}$ as an actinometer. The instability of the solution makes it necessary to prepare them just before use, the sensitivity to $p$H requires carefully made up buffers, and additional observations are required to correct for the dark reaction.

It is of interest to compare the photoreduction of this complex ion with that which occurs in complexes of the ion pair type, Fe$^{3+}$OH$^-$, Fe$^{3+}$Cl$^-$, etc.[1] In the latter it is supposed that reduction occurs by an electron transfer resulting from the light absorption

$$\text{Fe}^{3+}\text{OH}^- \xrightarrow{h\nu} \text{Fe}^{2+}\cdot\text{OH}$$
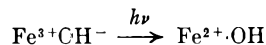
The net quantum yield is governed by the relative efficiencies of the reactions of HO· with Fe$^{2+}$ and with an added oxidizable substrate. It is unlikely that ion pair formation is of any importance in the photoreduction of Fe(Phen)$_3$$^{3+}$ in view of the size of the cation, but one could consider the phenanthroline ligand as analogous to the anion. However, electron transfer from the ligand and ultimate separation of a ligand radical seems improbable in view of the observed absence of photo-dissociation. We prefer to explain the observations simply in terms of the reactions of an excited complex ion with a normal complex ion (C$^{3+}$) and formic acid (RH)

$$\text{C}^{3+} \underset{k_d}{\overset{h\nu}{\rightleftarrows}} (\text{C}^{3+})^* \tag{1}$$

$$(\text{C}^{3+})^* + \text{C}^{3+} \xrightarrow{k_c} \left.\vphantom{\begin{matrix}a\\b\end{matrix}}\right\} \text{C}^{2+} + \text{products} \tag{2}$$

$$(\text{C}^{3+})^* + \text{RH} \xrightarrow{k_a} \tag{3}$$

The low quantum yields observed are accounted for by the predominance of deactivation process ($k_d$), so that

$$k_d \gg k_a(\text{RH}) \text{ or } k_c(\text{C}^{3+})$$

In these conditions the quantum yield is given by

$$\phi = k_8(\text{RH})/k_d + k_c(\text{C}^{3+})/k_d$$

The results of Fig. 3 conform to this expression with $k_c/k_d = 16$ and $k_8/k_d = 3.8 \times 10^{-3}$ mole.$^{-1}$ l.

In reaction (2) above, oxidation of the complex to give a quadrivalent iron complex seems unlikely, and the process probably involves oxidation of the phenanthroline ligand to give ultimate hydroxylation without dissociating from the complex. The oxidation of formic acid by reaction (3) is very dependent on pH as is shown by the results in Table I. These observations would be consistent with reaction (3) occurring with the formate ion as well as, or instead of, the undissociated acid. The contribution of the latter is in fact found to be negligible since when the quantum yields are extrapolated to high acidity the value obtained is that due to the complex only. However, the pH dependence shown in Table I cannot be accounted for quantitatively in terms of the reaction of the formate ion only, and it would appear that another pH dependent factor is present. This is also evident from the pH dependence of the photoreduction in the absence of formic acid shown in Table I. It is possible that this is concerned with the ability of the complex ion to act as a base to give the ion $\text{HFe}(\text{Phen})_3^{4+}$, which shows a difference in reactivity. Such ions have been invoked to account for certain aspects of the kinetics of dissociation of complexes of this type.[6]

TABLE I

PHOTOREDUCTION OF $10^{-4}$ $M$ Fe(Phen)$_3^{3+}$ AT 365 m$\mu$

(i) No formic acid present; (ii) formic acid 1.42 $M$.

| (i) pH | 1.0 $N$ | | | |
|---|---|---|---|---|
| | H$_2$SO$_4$ | 1.23 | 2.10 | 3.05 |
| Quantum yield $\times 10^2$ | 0.14 | 0.16 | 0.29 | 0.60 |
| (ii) pH | 1.0 $N$ | 0.10 $N$ | | |
| | H$_2$SO$_4$ | H$_2$SO$_4$ | 2.44 | 2.66 |
| Quantum yield $\times 10^2$ | 0.27 | 0.67 | 4.04 | 6.26 |

**Ferric Tris-dipyridyl, Fe(Dipy)$_3^{3+}$.**—The absorption spectrum of this ion is given in Fig. 1. It is very similar in photochemical behavior to the phenanthroline compound. The same methods were used to follow the photoreduction but the compound was not examined in detail because of the lower stability of both ferrous and ferric forms to low and high pH's, respectively.

Using $10^{-4}$ $M$ Fe(Dipy)$_3^{3+}$ with 0.47 $N$ formic acid and 0.01 $N$ sulfuric acid the quantum yields at 365 and 546 m$\mu$ were found to be 0.0078 (0.005) and 0.006 (0.001), respectively, the values in parentheses being the corresponding figures for Fe(Phen)$_3^{3+}$. It was found that, as for Fe(Phen)$_3^{3+}$, the yields increased with both formic acid and complex ion concentrations.

**The Yellow Ferric Ion Dipyridyl Complex.**—The addition of ferric ion to $\alpha,\alpha'$-dipyridyl solutions gives a labile yellow-brown complex.[5] This is very different from the ion Fe(Dipy)$_3^{3+}$ described above. The latter can only be prepared by oxidation of Fe(Dipy)$_3^{2+}$, it is blue, and is much more stable to acid than the yellow compound.

(6) T. S. Lee, I. M. Kolthoff and D. L. Leussing, *J. Am. Chem. Soc.*, **70** 3596 (1948); J. H. Baxendale and P. George, *Trans. Faraday Soc.*, **46**, 736 (1950).

From a photometric study of ferric ion + dipyridyl solutions[7] we have found that, if the formula of the yellow complex is represented by Fe(Dipy)$_n^{3+}$, then $n$ increases to about 2.5 as the concentration of dipyridyl is increased to saturation.

In preliminary experiments we observed that these yellow solutions gave Fe(Dipy)$_3^{2+}$ when exposed to 365 m$\mu$ light. However, a more detailed study showed that the quantum efficiency for this reduction is not very high. Table II gives the effect of increasing the dipyridyl concentration in a formate buffer containing $3 \times 10^{-4}$ $M$ ferric ion. The quantum yield decreases appreciably, although at the same time more of the yellow complex is formed, as is evident from the increasing intensity of color. These observations show that the complex has a lower photoactivity than the ferric solution has in the absence of dipyridyl. As will be shown below, in the latter conditions a ferric ion–formate ion pair is the photoactive species. When the results of Table II are extrapolated to high dipyridyl concentration they give a quantum efficiency of *ca.* 0.03 for the photoreduction of the yellow complex.

TABLE II

PHOTOREDUCTION OF THE YELLOW FERRIC-DIPYRIDYL COMPLEX AT 365 m$\mu$

[Fe$_3^+$] = $2.94 \times 10^{-4}$ $M$, total formic acid + formate = 0.46 $M$, pH 3.70.

| [Dipy] $\times 10^3$, $M$ | 0.14 | 0.32 | 1.28 | 3.20 |
|---|---|---|---|---|
| Quantum yield | .26 | .20 | 0.081 | 0.035 |

**The Yellow Ferric Ion Phenanthroline Complex.**—This is exactly analogous to the dipyridyl complex. Its photoactivity is even less than the latter. Thus with $3 \times 10^{-4}$ $M$ ferric ion, and $10^{-3}$ $M$ phenanthroline in 0.46 $M$ formate–formic acid buffer at pH 3.7, the reduction quantum yield with 365 m$\mu$ light was found to be *ca.* 0.007.

**Ferric Formate.**—We have shown[7] by a spectroscopic study of solutions containing ferric sulfate (1 to 10 $\times 10^{-3}$ $M$) and formic acid (0.1 to 1.0 $M$) at pH 3.6 that a 1:1 compound is formed according to the equilibrium

$$\text{Fe}^{3+} + \text{HCOOH} \overset{K}{\rightleftharpoons} \text{Fe}^{3+}\text{HCOO}^- + \text{H}^+$$

where $K = 8.5 \times 10^{-4}$ at 20°.

We find that the ferric ion in these solutions is reduced to ferrous by exposure to ultraviolet radiation. The photoreduction by 365 m$\mu$ has been studied in a variety of conditions by estimating the ferrous ion with *o*-phenanthroline. There is negligible reduction in the dark.

At constant ferric ion concentration $3 \times 10^{-3}$ $M$ and pH 3.6, increasing the total formic acid present (as free acid plus formate) increases the quantum yield and changes the optical density of the solution at 365 m$\mu$, as shown in Fig. 4. These observations are consistent with the presence of an increasing amount of the ferric formate complex which is photochemically more active than the ferric ion, but which is not as strongly absorbing. The observations in Fig. 4 are quantitatively consistent with this as can be seen from the following analysis.

(7) J. H. Baxendale and N. K. Bridge, unpublished work.

Fig. 4.—Variation with formic acid concentration of the optical density ($\times$) and quantum yield ($\bigcirc$) for the reduction of $13.5 \times 10^{-3}$ $M$ ferric ion in 365 m$\mu$ light at pH 3.6.

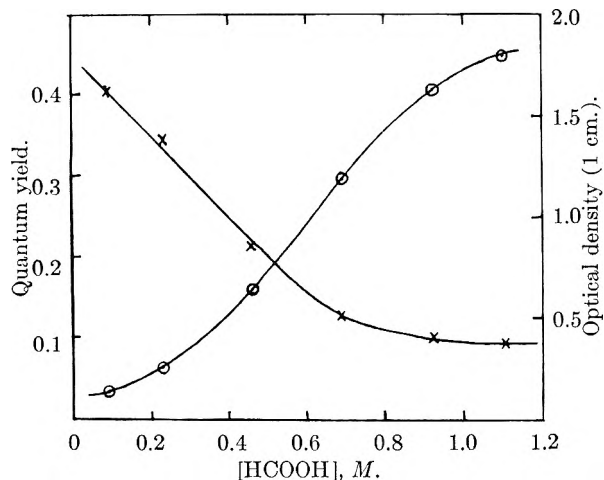Let $\epsilon_c$, $C_c$ and $\phi_c$ be the molar extinction coefficient, concentration and quantum efficiency of the complex, let $\epsilon_f$, $C_f$ and $\phi_f$ be the same quantities for the ferric ion and let $D$ be the optical density of 1 cm. of the solution.

Assuming the complex and ferric ion to be the only photoactive species present, the net quantum efficiency $\phi$ is given by

$$\phi = (\epsilon_c C_c \phi_c + \epsilon_f C_f \phi_f)/D$$

Putting $C_c$ and $C_f$ in terms of the total ferric ion concentration $a$, formic acid [RH], and the above equilibrium constant $K$, we obtain

$$\phi D(1 + K[RH]) = aK\epsilon_c\phi_c[RH] + a\epsilon_f\phi_f$$

As shown in Fig. 5 where $\phi D(1 + K[RH])$ is plotted against [RH] the observations are consistent with this equation. Since the line passes through the origin $\phi_f$ is zero, i.e., the contribution to the reduction by the ferric ion not in the formate complex is negligible. From Fig. 5 the value of $\phi_c\epsilon_c$ obtained from the slope of the line is 63. Unfortunately, as will be indicated below, the value of $\epsilon_c$ is made uncertain by the presence of another absorbing species. However, the optical density of these solutions, if due entirely to the complex, would give $\epsilon_c$ *ca.* 100 so that $\phi_c > 0.6$.
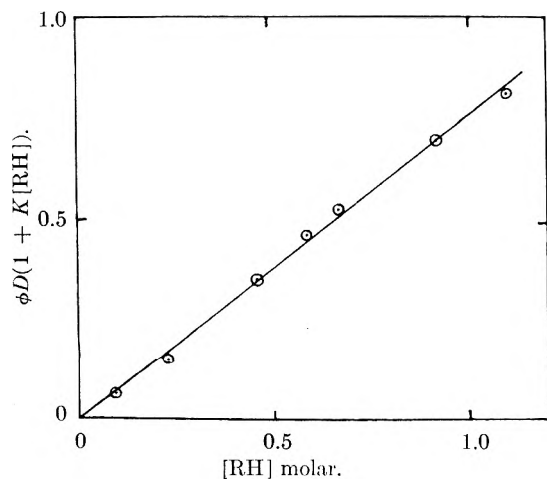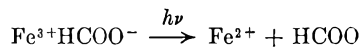


[RH] molar.

Fig. 5.

The reduction process is presumably similar to that postulated for other ion pairs, *viz.*

$$Fe^{3+}HCOO^- \xrightarrow{h\nu} Fe^{2+} + HCOO$$

Since zero-order reduction rates are obtained in our conditions, the reverse oxidation of $Fe^{2+}$ by the formate radical must be negligible and the most probable fate of the radical is further oxidation by $Fe^{3+}$

$$Fe^{3+} + HCOO\cdot \longrightarrow Fe^{2+} + H^+ + CO_2$$

The variations of optical density and quantum yield with pH are shown in Fig. 6. Both the increase in yield from a.most zero and the decrease in optical density are consistent with increasing complex formation with pH, as expected if the complex is an ion pair as written in the above equilibrium. However, this would not account for the decrease in yield and increase in density beyond pH 2.8 and it seems likely that less active complexes containing a higher ratio of formate to ferric ion are formed in these conditions.



Fig. 6.—Variation with pH of the quantum yield ($\bigcirc$-$\bigcirc$) and optical density ($\times$) at 365 m$\mu$ of solutions containing $3.5 \times 10^{-3}$ $M$ ferric ion and 0.46 $M$ formic acid + formate.

An oddity in the reduction by 365 m$\mu$ light is that at constant formate concentration the quantum yield decreases with increase of ferric ion, as shown in Table III. This behavior is not consistent with the assumption that the formate complex *only* is responsible for the photoreduction yield, for with the large excess of formic acid over $Fe^{3+}$ used here, the fraction of $Fe^{3+}$ present as complex will be independent of the concentration of $Fe^{3+}$. An indication that other species are involved is given by the variation in optical density with ferric ion concentration shown in Fig. 7. If $Fe^{3+}$ and the complex are the only absorbing species, the optical density should be linear with ferric ion concentration since formic acid is in large excess. At 330 m$\mu$ and below this is seen to be the case but significant deviations from linearity occur above this wave length. These deviations cannot be accounted for by the simultaneous existence of other complexes of the type $Fe^{3+}(HCOO^-)_n$ but require the new species to contain more than one ferric ion. Such polynuclear ferric ion complexes have been invoked in other $Fe^{3+}$ systems.[8] The amount of ferric ion bound in this way in the conditions used here cannot be very great since deviations from

(8) T. H. Siddall and W. C. Vosburgh, *J. Am. Chem. Soc.*, **73**, 4270 (1951).

Fig. 7.—Optical densities at different wave lengths of 0.50 $M$ formic acid + formate solutions at $p$H 3.7 containing varying amounts of ferric ion: A, 280 m$\mu$; B, 310 m$\mu$; C, 320 m$\mu$; D, 330 m$\mu$; E, 340 m$\mu$; F, 350 m$\mu$; G, 365 m$\mu$.

linearity in Fig. 7 would then occur at all wave lengths. The bigger effect at the lower wave lengths presumably arises because of the larger absorption coefficient of the polynuclear species in this region compared with the other species present.

### TABLE III

PHOTOREDUCTION OF FERRIC FORMATE AT 365 m$\mu$

Total formic acid + formate = 0.46 $M$, $p$H 3.6.

| $[Fe^{3+}] \times 10^3, M$ | 0.15 | 0.50 | 1.01 | 3.07 | 5.11 | 10.2 |
|---|---|---|---|---|---|---|
| Quantum yield | .34 | .34 | 0.32 | 0.20 | 0.12 | 0.065 |

The decrease in quantum yield with ferric ion shown in Table III can now be explained by a decrease in the fraction of light absorbed by the monoformate complex caused by the increasing absorption of the much less photo-active poly-nuclear compound.

The variation of quantum yield with wave length was examined, using $2 \times 10^{-3}$ $M$ ferric sulfate in 0.5 $M$ formic acid neutralized to $p$H 3.7. The results, together with the absorption spectrum, are shown in Fig. 8. Much higher yields are obtained than with the dipyridyl or phenanthroline complexes. Appreciable activity is observed in the blue and the general sensitivity below 450 m$\mu$ is such that it constitutes a far more convenient actinometer than uranyl oxalate.

**Ferrioxalate Ion, FeOx$_3^{3-}$.**—Parker[2] has recently shown that a solution of the ferrioxalate ion is a very useful actinometer, and because of its similarity to the ferric formate system described above, we have repeated some of Parker's observations with a few modifications in the technique.

The ferrioxalate ion, like the ferric formate complex, is in very rapid equilibrium with ferric and oxalate ions, so that the preparation and ultimate solution of solid potassium ferrioxalate, as was done by Parker, seems unnecessary. A mixture of solutions of ferric alum and potassium oxalate of the right concentrations is more convenient to make and should lead to the same solution of the complex ion as that obtained by dissolving the solid salt. To confirm this we ran parallel photoreduction experiments on solutions made up in the two ways.

The solutions used throughout contained 0.005



Fig. 8.—Absorption coefficients (—) and quantum yields (○), for the photoreduction of $2.0 \times 10^{-3}$ $M$ ferric ion in 0.5 $M$ formic acid + formate at $p$H 3.7.

### TABLE IV

PHOTOREDUCTION OF FERRIOXALATE SOLUTIONS

Solution I: 0.005 $M$ K$_3$FeOx$_3$, 0.10 $N$ H$_2$SO$_4$; solution II: 0.005 $M$ ferric alum, 0.015 $M$ K$_2$Ox, 0.10 $N$, H$_2$SO$_4$. Irradiations at 365 and 254 m$\mu$ were done at 17–19° and those at 436 m$\mu$ at 25°. At 365 and 254 m$\mu$ there was complete absorption of the incident light and at 436 m$\mu$ 90% was absorbed. All exposure times are in minutes, amounts of ferrous ion in moles $\times 10^6$ and incident light intensities in einsteins per minute.

436 m$\mu$, incident intensity = 6.17 $\times 10^{-7}$

| | Time | 2 | 5 | 8 | 10 | |
|---|---|---|---|---|---|---|
| I | Fe$^{2+}$ | 1.20 | 2.91 | 4.80 | 5.92 | |
| | Quantum yield | 1.09 | 1.05 | 1.08 | 1.07 | |
| | | | | | Mean = 1.07 | |

| | Time | 2 | 5 | 7 | 10 | |
|---|---|---|---|---|---|---|
| II | Fe$^{2+}$ | 1.12 | 2.85 | 3.90 | 5.65 | |
| | Quantum yield | 1.02 | 1.05 | 1.01 | 1.03 | |
| | | | | | Mean = 1.03 | |

| | Time | 2 | 4.5 | 7.5 | 11 | |
|---|---|---|---|---|---|---|
| II | Fe$^{2+}$ | 1.10 | 2.55 | 4.26 | 6.37 | |
| | Quantum yield | 1.00 | 1.03 | 1.03 | 1.06 | |
| | | | | | Mean = 1.03 | |

365 m$\mu$, incident intensity = 6.32 $\times 10^{-7}$

| | Time | 0.5 | 1.0 | 2.0 | 2.5 | 3.0 |
|---|---|---|---|---|---|---|
| I | Fe$^{2+}$ | 0.38 | 0.76 | 1.51 | 1.95 | 2.20 |
| | Quantum yield | 1.20 | 1.20 | 1.19 | 1.24 | 1.16 |
| | | | | | Mean = 1.20 | |

| | Time | 0.5 | 1.0 | 1.5 | 2.0 | 2.5 | 3.0 |
|---|---|---|---|---|---|---|---|
| II | Fe$^{2+}$ | 0.38 | 0.78 | 1.20 | 1.52 | 1.92 | 2.30 |
| | Quantum yield | 1.21 | 1.23 | 1.27 | 1.20 | 1.22 | 1.21 |
| | | | | | | Mean = 1.22 | |

| | Time | 0.5 | 1.17 | 1.5 | 2.0 | 2.6 |
|---|---|---|---|---|---|---|
| II | Fe$^{2+}$ | 0.37 | 0.88 | 1.12 | 1.48 | 2.02 |
| | Quantum yield | 1.17 | 1.19 | 1.18 | 1.17 | 1.20 |
| | | | | | Mean = 1.18 | |

254 m$\mu$, incident intensity = 1.29 $\times 10^{-7}$

| | Time | 2 | 4 | 5 | 8 | 10 | 15 |
|---|---|---|---|---|---|---|---|
| I | Fe$^{2+}$ | 0.35 | 0.62 | 0.78 | 1.32 | 1.63 | 2.43 |
| | Quantum yield | 1.35 | 1.20 | 1.21 | 1.25 | 1.26 | 1.25 |
| | | | | | | Mean = 1.25 | |

| | Time | 5 | 10 | 15 | | | |
|---|---|---|---|---|---|---|---|
| II | Fe$^{2+}$ | 0.78 | 1.58 | 2.32 | | | |
| | Quantum yield | 1.21 | 1.22 | 1.19 | | | |
| | | | | Mean = 1.21 | | | |

| | Time | 4 | 8 | 12 | 16 | | |
|---|---|---|---|---|---|---|---|
| II | Fe$^{2+}$ | 0.62 | 1.28 | 1.86 | 2.42 | | |
| | Quantum yield | 1.20 | 1.24 | 1.20 | 1.17 | | |
| | | | | | Mean = 1.20 | | |

$M$ ferrioxalate (assuming all the ferric ion is present as this) and 0.1 $N$ sulfuric acid. The absorption spectrum of the ferric alum + potassium oxalate mixture was found to be identical with that of the potassium ferrioxalate solution and both agreed very well with the spectrum reported by Parker.

Using the method of estimation of ferrous ion by o-phenanthroline described by Parker, we found the color formation rather slow. It is speeded up considerably by the addition of ammonium fluoride, presumably due to the removal of the interfering ferric ion. Hence for analysis we have taken 10 cc. of the photolyzed solution, and added 3 cc. of $M$ sodium acetate, 3 cc. of 0.1% o-phenanthroline and 1 cc. of 2 $M$ ammonium fluoride, which is the same procedure as in the ferric formate experiments. The optical densities of these solutions reach their maximum very rapidly and remain constant for at least several hours. The solutions were stirred during irradiation but Parker has shown that this is unnecessary for low conversions. No rigorous temperature control was used except

when using 436 m$\mu$ light. Here the light absorption was not complete and, since temperature fluctuation might cause variation in the equilibrium amount of ferrioxalate ion present, irradiations were done in a thermostat at $25 \pm 0.1°$.

The observations are given in Table IV. It will be seen that there is little if any difference between solutions made up from solid $K_3FeOx_3$ and those made by mixing ferric alum and potassium oxalate solutions. The summary of the results given in Table V shows that there is good agreement with Parker's figures at 254 and 365 m$\mu$, but at 436 m$\mu$ our value is some 6% greater.

TABLE V

VARIATION OF QUANTUM YIELD WITH WAVE LENGTH

| Wave length, m$\mu$ | Parker | Present work |
|---|---|---|
| 436 | 0.98[a] | 1.04 |
| 365 | 1.18 | 1.20 |
| 254 | 1.23 | 1.22 |

[a] Dr. Parker informs us that his more recent and accurate measurements give 1.1 at this wave length.

# THE ELECTROSTATIC FREE ENERGY OF GLOBULAR PROTEIN IONS IN AQUEOUS SALT SOLUTION

BY CHARLES TANFORD

*Contribution from the Department of Chemistry, State University of Iowa, Iowa City, Iowa*

New equations are derived for the electrostatic free energy of globular protein ions in aqueous salt solution. The equations show that a considerable decrease in free energy occurs if salt ions are allowed to penetrate into the interior of the protein ion. If some of the fixed charges of the protein ion are also located in the interior, a decrease in free energy occurs at high ionic strength, but there is an increase at low ionic strength. The equations can be tested by comparison with experimental data obtained from the effect of charge on hydrogen ion dissociation. Such tests show that the equations are applicable to expanded protein ions, such as serum albumin in acid solution, but not to normal, sparingly solvated protein ions. The solvation in such ions appears to consist of tightly-bound water molecules, so that no penetration of salt ions is possible.

In the calculation of the electrostatic free energy of globular (*i.e.*, non-fibrous) protein ions in aqueous salt solutions it has heretofore been customary to assume that these macro-ions are spheres with their charge uniformly distributed over their surface, and that these spheres are impenetrable by salt ions of the solvent. One then obtains for the electrostatic free energy, per mole of ions[1,2]

$$F°_{elec} = \frac{N\epsilon^2 Z^2}{2DR} \left(1 - \frac{\kappa R}{1 + \kappa a_i}\right) \quad (1)$$

where $N$ is Avogadro's number, $\epsilon$ the protonic charge, $D$ the dielectric constant of water, $\kappa$ the Debye-Hückel constant proportional to the square root of the ionic strength, $Z$ the *net* charge on the protein ion, $R$ its radius, and $a_i$ the closest distance of approach of salt ions dissolved in the water. The distance $a_i$ is greater than $R$ by the average radius of such salt ions. Its presence in equation 1 arises from the assumption of impenetrability of the protein sphere.

It has been discovered recently that serum albumin in acid solution undergoes reversible expan-

sion.[3-6] Viscosity studies[5] indicate that the radius of a sphere equivalent to the protein ion may be doubled, so that the volume may increase almost tenfold. When this occurs more than 90% of the effective ionic sphere must consist of solvent, and the "impenetrable sphere" model of a protein ion becomes unacceptable. This model must also be invalid for serum albumin and many other proteins in solutions of urea or of guanidine salts, for under such conditions expansion is also observed.[7]

The principal purpose of the present paper is to present a new model for a solvated protein ion and new equations for the electrostatic free energy, which are likely to be applicable to such highly solvated ions.

For normal, sparingly hydrated protein ions the assumption of impenetrability is a reasonable one. Although such protein ions are known to contain water (frequently estimated to be of the order of 20

(1) K. Linderstrom-Lang, *Compt. rend. trav. lab., Carlsberg*, **15**, No. 7 (1924).

(2) G. Scatchard, *Ann. N. Y. Acad. Sci.*, **51**, 660 (1949).

(3) G. Scatchard, *American Scientist*, **40**, 61 (1952).

(4) C. Tanford, *Proc. Iowa Acad. Sci.*, **59**, 206 (1952); also in T. Shedlovsky, ed., "Electrochemistry in Biology and Medicine," John Wiley and Sons, New York, N. Y., 1955.

(5) J. T. Yang and J. F. Foster, *J. Am. Chem. Soc.*, **76**, 1588 (1954).

(6) H. Gutfreund and J. M. Sturtevant, *ibid.*, **75**, 5447 (1953).

(7) W. Kauzmann, *et al.*, *ibid.*, **75**, 5139, 5152, 5154, 5157, 5167 (1953).

weight per cent.),[8,9] much of this water may be firmly attached to polar or charged groups, and would thus contain no dissolved salt ions. It is customarily taken into account in the use of equation 1 by an appropriate increase in values of $R$ beyond those estimated on the basis of unsolvated ions. For the majority of proteins to which equation 1 has been applied in this way, the calculated values of $F^0_{elec}$ have been considerably higher than experimental values, a fact which may be ascribed to deviation from spherical shape, or perhaps to the discrete charge distribution which actually exists in protein ions instead of the continuous distribution assumed by the model. However, a second object of this paper will be to examine the alternative explanation for this discrepancy, that it is due to ion penetration.

**Solution of the Poisson–Boltzmann Equation.—** We shall begin by continuing to represent the protein ion (Fig. 1) by a sphere of radius $R$, with a net charge $q$ evenly distributed over its surface, postponing for later consideration the possibility that some of the protein charge may be within the sphere rather than on the surface. The space within this sphere occupied by protein substance and any tightly bound water is designated as $4/3 \pi R_0^3$, so that the space occupied by free solvent, and thus available to salt ions, is $4/3 \pi (R^3 - R_0^3)$.

Let the sphere have a core of radius $R_1$ (which cannot be greater than $R_0$) occupied entirely by protein substance and tightly bound water. The remaining volume, $4/3 \pi (R^3 - R_1^3)$, will contain both protein substance (with its tightly bound water) and free solvent. The fraction of this volume occupied by free solvent and thus available to salt ions we shall call $\alpha^2$, i.e.

$$\alpha^2 = (R^3 - R_0^3)/(R^3 - R_1^3) \qquad (2)$$

It is open to question whether or not salt ions are excluded from some of the volume occupied by free solvent. If the portion of the protein substance bordering on the volume occupied by free solvent consists of polar groups (e.g., alcohol side chains), then the centers of the ions may well be able to penetrate to the very edge of the volume. In any case, an excluded volume can be taken into account very simply by increasing $R_0$ by, say, 2.5 Å., since for the purpose of electrostatic effects any space occupied by water, but inaccessible to salt ions, is equivalent to space occupied by tightly bound water.

In view of the prevailing spherical symmetry, Poisson's equation takes on the form

$$\nabla^2 \psi = \frac{1}{r} \frac{d^2(r\psi)}{dr^2} = -4\pi\rho/D \qquad (3)$$

where $D$ is the dielectric constant of the medium containing the charges, $r$ is the radial distance from the center of the protein ion, and $\psi$ and $\rho$ are, respectively, the potential and charge density at any value of $r$. For the sake of simplicity in the derivation we shall assume that all dissolved salts are 1:1 electrolytes. We shall also make the customary Debye–Hückel assumption, that terms in $(\epsilon\psi/$
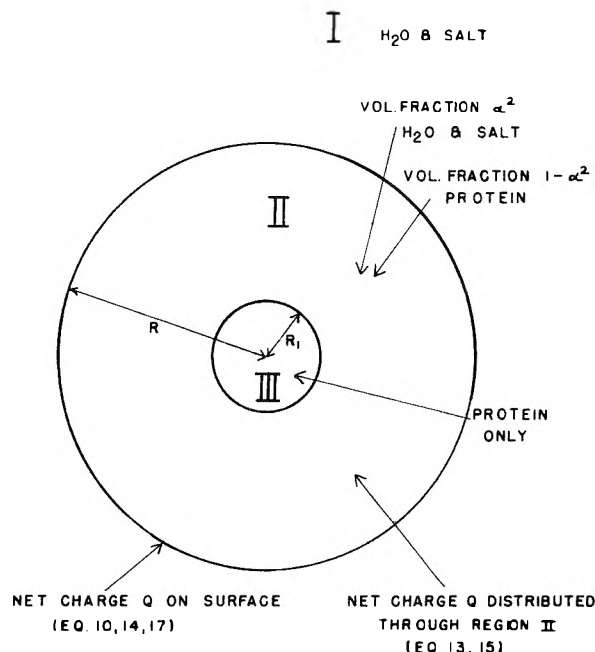
(8) J. T. Edsall in H. Neurath and K. Bailey, ed., "The Proteins," Vol. IB, Academic Press, Inc., New York, N. Y., 1953, p. 549.

(9) J. H. Wang, *J. Am. Chem. Soc.*, **76**, 4755 (1954).

Fig. 1.—Model for expanded protein ion. Space filled by protein includes tightly-bound water.

$kT)^3$ are negligible compared to terms in $\epsilon\psi/kT$. Since the charge density on protein ions is lower than that on ordinary salt ions, this assumption should be valid to the same extent as in ordinary electrolyte solutions, i.e., up to salt concentrations of about 0.1 molar.[10]

In region I of Fig. 1 the solution to equation 3 is exactly the same as in the vicinity of ordinary salt ions.[12] A net charge density arises entirely from unequal distribution of positive and negative salt ions, and its value is computed with the aid of the Boltzmann distribution law. With the Debye–Hückel assumption previously mentioned one obtains $\rho = -2n\epsilon^2\psi/kT$, where $n$ is the electrolyte concentration, in molecules per cc., in the bulk of the solution, $\epsilon$ is the protonic charge, $k$ is Boltzmann's constant and $T$ is the absolute temperature. One thus obtains the Poisson–Boltzmann equation

$$\nabla^2 \psi = \kappa^2 \psi \qquad (4)$$

where

$$\kappa^2 = 8\pi n\epsilon^2/DkT \qquad (5)$$

The solution to equation 4, with the condition that $\psi$ vanishes as $r$ becomes infinite, is

$$\psi = C_1 e^{-\kappa r}/r \qquad (6)$$

In region II of Fig. 1 a net charge density can arise also only as a result of unequal distribution of salt ions, and, as before, in that part of the volume of region II occupied by solvent, $\rho = -2n\epsilon^2 \psi/kT$.

(10) Another assumption made throughout this paper is that the protein ions do not interact with each other. This is probably never true at extremely low ionic strength, where protein–protein interaction becomes important even for protein molecules with a net charge of zero, as shown, for example, by the theory of Kirkwood and Shumaker (ref. 11). In the region of ionic strength 0.01 to 0.15, however, interaction between the protein ions may be expected to be unimportant at working concentrations of the order of 0.1 to 1%. Under these conditions one does not, for instance, normally observe an effect of protein concentration upon hydrogen ion equilibria.

(11) J. G. Kirkwood and J. B. Shumaker, *Proc. Natl. Acad. Sci., U. S.*, **38**, 863 (1952).

(12) See, for example, D. A. MacInnes, "The Principles of Electrochemistry," Reinhold Publ. Corp., New York, N. Y., 1939, Ch. 7.

However, only a fraction $\alpha^2$ of the total volume is occupied by solvent, so that the average charge density throughout the region becomes $\rho = -2n \cdot \epsilon^2 \alpha^2 \psi / kT$, and the Poisson–Boltzmann equation becomes

$$\nabla^2 \psi = \alpha^2 \kappa^2 \psi \tag{7}$$

with the solution

$$\psi = C_2 e^{-\alpha \kappa r}/r + C_3 e^{\alpha \kappa r}/r \tag{8}$$

Provided that $\alpha^2$ is reasonably large, say 0.75 or greater, the dielectric constant, and therefore $\kappa$, will be essentially the same in regions II and I.

Region III of Fig. 1 is devoid of charge. It is therefore a region of constant potential, with $d\psi/dr = 0$.

To evaluate the constants $C_1$, $C_2$ and $C_3$ one utilizes the conditions that $d\psi/dr$ in region II must become zero at the boundary with region III, i.e., where $r = R_1$, that $\psi$ must be continuous where $r = R$, and that the total charge due to salt ions must exactly balance the charge on the protein ion. The latter condition is given as

$$\int_{R_1}^{R} 4\pi r^2 \rho \, dr + \int_{R}^{\infty} 4\pi r^2 \rho \, dr = -q \tag{9}$$

We are interested here in the potential at $r = R$ only. With the conditions here enumerated it becomes

$$\psi = \frac{q}{D\kappa R^2} \frac{\dfrac{1 + \alpha \kappa R_1}{1 - \alpha \kappa R_1} e^{2\alpha \kappa (R - R_1)} - 1}{(1 + \alpha) \dfrac{1 + \alpha \kappa R_1}{1 - \alpha \kappa R_1} e^{2\alpha \kappa (R - R_1)} - (1 - \alpha)} \tag{10}$$

We consider next the possibility that the fixed charges of the protein ion may be distributed uniformly throughout the region II, rather than confined to its surface, following the method used by Hermans and Overbeek[13] in evaluating the electrostatic free energy of a randomly-coiled polyelectrolyte. There must then be added to the charge density in region II the term $3q/4\pi(R^3 - R_1^3)$ so that the Poisson–Boltzmann equation for this region becomes

$$\nabla^2 \psi = \alpha^2 \kappa^2 \psi - 3q/D(R^3 - R_1^3) \tag{11}$$

with the solution

$$\psi = C_4 e^{-\alpha \kappa r}/r + C_5 e^{\alpha \kappa r}/r + 3q/\alpha^2 \kappa^2 D(R^3 - R_1^3) \tag{12}$$

The potential in regions I and III is the same as before; also, the same boundary conditions apply, except that the charge due to the protein charges is of course, not counted on the left-hand side of equation 9. With these conditions one may solve for $C_4$ and $C_5$ and obtain

$$\psi = \frac{3q(1 + \kappa R)}{\kappa^3 D(R^3 - R_0^3)} \left\{ \frac{\kappa}{1 + \kappa R} - \right.$$
$$\left. \frac{\dfrac{1 + \alpha \kappa R_1}{1 - \alpha \kappa R_1} e^{\alpha \kappa (r + R - 2R_1)} - e^{\alpha \kappa (R - r)}}{r \left[ (1 + \alpha) \dfrac{1 + \alpha \kappa R_1}{1 - \alpha \kappa R_1} e^{2\alpha \kappa (R - R_1)} - (1 - \alpha) \right]} \right\} \tag{13}$$

**The Electrostatic Free Energy.**—The electrostatic free energy of a protein ion with net charge of $Z\epsilon$, where $Z$ may be positive or negative, is the work done in raising the charge $q$, at constant

(13) J. J. Hermans and J. Th. G. Overbeek, *Rec. trav. chim. Pays-Bas*, **67**, 761 (1948).

ionic strength, by infinitesimal steps from zero to $Z\epsilon$. If the charge lies entirely on the surface of the protein ion, then, using equation 10

$$F^\circ_{elec} = N \int_0^{Z\epsilon} \psi dq =$$
$$\frac{NZ^2\epsilon^2}{2D\kappa R^2} \frac{\dfrac{1 + \alpha \kappa R_1}{1 - \alpha \kappa R_1} e^{2\alpha \kappa (R - R_1)} - 1}{(1 + \alpha) \dfrac{1 + \alpha \kappa R_1}{1 - \alpha \kappa R_1} e^{2\alpha \kappa (R - R_1)} - (1 - \alpha)} \tag{14}$$

Avogadro's number has been introduced so that equation 14 may apply to one mole of protein ions. The work done is a contribution to the *standard* free energy $(F^\circ)$ because it is independent of concentration.

If the charge $q$ is distributed over the entire region II, then, for each increment $dq$ in total charge, there is an increment of $4\pi r^2 dq dr / \frac{4}{3} \pi (R^3 - R_1^3)$ in a spherical layer of thickness $dr$. Thus

$$F^\circ_{elec} = \frac{N}{R^3 - R_1^3} \int_{q=0}^{Z\epsilon} \int_{r=R_1}^{R} 3r^2 \psi \, dq dr$$

which, by use of equation 13, becomes

$$F^\circ_{elec} = \frac{9NZ^2\epsilon^2}{2\kappa^2 D(R^3 - R_0^3)} \left\{ \frac{1}{3} + \frac{1 + \kappa R}{\kappa^3(R^3 - R_0^3)} \times \right.$$
$$\left. \frac{(1 - \alpha \kappa R) \dfrac{1 + \alpha \kappa R_1}{1 - \alpha \kappa R_1} e^{2\alpha \kappa (R - R_1)} - (1 + \alpha \kappa R)}{(1 + \alpha) \dfrac{1 + \alpha \kappa R_1}{1 - \alpha \kappa R_1} e^{2\alpha \kappa (R - R_1)} - (1 - \alpha)} \right\} \tag{15}$$

With $R_1 = 0$ and $\alpha^2 = 1$, conditions applicable to a very loosely-coiled ion, equation 15 reduces to

$$F^\circ_{elec} = \frac{3NZ^2\epsilon^2}{2DR} \left\{ \frac{1}{\kappa^2 R^2} - \frac{3}{2\kappa^5 R^5} [\kappa^2 R^2 - 1 + (1 + \kappa R)^2 e^{-2\kappa R}] \right\}$$

which, as it should be, is identical with the equation given by Hermans and Overbeek.[13] If $R_1 = R = R_0$ we return to the impenetrable sphere model, without, however, a radius of exclusion. Under these conditions both equation 14 and 15 reduce, as they should, to equation 1 with $a_i = R$

$$F^\circ_{elec} = \frac{N\epsilon^2 Z^2}{2DR(1 + \kappa R)} \tag{16}$$

**Expanded Protein Ions.**—Equations 14 and 15 have been used to calculate the electrostatic free energy of an expanded protein ion. We have chosen $R_0 = 25$ Å., corresponding to a molecular weight near 50,000, and have used two values of $R$: 35 and 50 Å. The results are summarized in Table I.

It can be seen that the three different models of an expanded protein ion inherent in equations 1, 14 and 15 differ most markedly in the effect of ionic strength upon the electrostatic free energy, this effect being greatest for equation 15 and smallest for equation 1. This can provide the basis for distinguishing experimentally between the three models (see below).

It can also be seen from Table I that values of $F^\circ_{elec}$ depend relatively little on the choice of $R_1$, i.e., it seems to be unimportant whether the incorporated solvent lies in an external layer with $\alpha^2$ close to unity, or whether it penetrates further into the sphere with a reduced value of $\alpha^2$. This can

TABLE I

VALUES OF $F^\circ_{elec}/Z^2$ FOR EXPANDED ION WITH $R_0 = 25$ Å.

| $R$ | Ionic strength | Eq. 1 | $R_1 = 0$ | 10 Å. | 20 Å. | 25 Å. | $R_1 = 0$ | 10 Å. | 20 Å. | 25 Å. |
|---|---|---|---|---|---|---|---|---|---|---|
| | | | | Eq. 14 | | | | Eq. 15 | | |
| 35 Å. | 0.001[a] | 44.6 | 43.4 | 43.4 | 43.4 | 43.4 | 54.9 | 54.2 | 51.1 | 48.8 |
| | .01 | 29.3 | 25.0 | 25.0 | 25.0 | 24.9 | 33.6 | 33.2 | 30.9 | 29.1 |
| | .05 | 19.0 | 12.9 | 12.9 | 12.7 | 12.6 | 16.9 | 16.7 | 15.7 | 14.7 |
| | .15 | 13.8 | 7.55 | 7.51 | 7.29 | 7.06 | 8.43 | 8.22 | 8.01 | 7.61 |
| 50 Å. | 0.001[a] | 28.1 | 26.5 | 26.5 | 26.5 | 26.5 | 43.1 | 42.5 | 41.8 | 40.7 |
| | .01 | 16.8 | 12.7 | 12.7 | 12.7 | 12.6 | 16.6 | 16.5 | 16.1 | 15.7 |
| | .05 | 10.3 | 5.95 | 5.94 | 5.87 | 5.80 | 6.37 | 6.36 | 6.27 | 6.17 |
| | .15 | 7.26 | 3.44 | 3.43 | 3.38 | 3.33 | 2.69 | 2.69 | 2.67 | 2.65 |

[a] *Cf.* footnote 10, regarding the possibility that protein–protein interaction may be important at an ionic strength as low as 0.001.

hold true, of course, only for expanded protein where $\alpha^2$ is relatively large even with $R_1 = 0$, otherwise deeper penetration involves a decrease in the dielectric constant of the medium containing the charges. The lack of dependence on $R_1$ is especially pronounced in the case of equation 14, and permits simplification of this equation by placing $R_1 = R_0$, and hence $\alpha^2 = 1$, so that

$$F^\circ_{elec} = \frac{NZ^2\epsilon^2}{4D\kappa R^2}\left[1 - \frac{1 - \kappa R_0}{1 + \kappa R_0} e^{-2\kappa(R - R_0)}\right] \quad (17)$$

Equations 15 and 17 are also quite insensitive to uncertainties in $R_0$ arising from questions regarding the amount of tightly bound water and whether or not to allow for a radius of exclusion. For example, increasing $R_0$ from 25 to 27.5 Å. in equation 17 increases $F^\circ_{elec}$ for an over-all radius of 35 Å. by less than 0.5% at ionic strength 0.001 and by 4% at ionic strength 0.15. Where $R$ is 50 Å. the increase in $F^\circ_{elec}$ is less than 0.1% at all ionic strengths. These results are in marked contrast to those obtained for sparingly hydrated protein ions, where the amount of tightly bound water and exact knowledge of the excluded volume are of great importance.

The equations here presented may be applied to an actual example: the dissociation of hydrogen ions from the carboxyl groups of serum albumin. This process occurs in the acid $p$H range where the protein is in an expanded form. The reaction may be described by the equation[2,4]

$$pH - \log\frac{x}{1 - x} = pK_{int} - 0.868Zw \quad (18)$$

where $x$ is the degree of dissociation at any $p$H, $pK_{int}$ is the negative logarithm of the *intrinsic* dissociation constant (*i.e.*, the dissociation constant of carboxyl groups attached to an *uncharged* protein molecule), $Z$ is the charge on the protein at any $p$H and $w$ is a factor such that $2NkTwZ$ is the increase in electrostatic free energy per mole of protein ions per unit increase in charge. Thus $2NkTwZ$ is $(\partial F^\circ_{elec}/\partial Z)$. Since each of the equations for $F^\circ_{elec}$ is proportional to $Z^2$, the partial derivative becomes $2F^\circ_{elec}/Z$, and, hence

$$w = \frac{F^\circ_{elec}}{Z^2NkT} \quad (19)$$

By use of equation 18, $w$ may be evaluated from experimental data, and we see by equation 19 that this is essentially an evaluation of the electrostatic free energy.

In the case of serum albumin $w$ is found experi-

mentally to decrease with decreasing $p$H, as a result of the expansion of the protein ion.[4] The experimental values, together with equations 19 and 1, 15 or 17 may then be used to estimate $R$ as a function of $p$H. One may obtain a value of $R_0$ for use in such computations by assuming that the inaccessible volume is given by the product of molecular weight $(65,000)$[14] and partial specific volume $(0.734)$.[15] This leads to $R_0 = 26.65$ Å. As was previously indicated, it is not important whether this value is exactly right. In using equation 15 it is necessary to choose a value of $R_1$: we have chosen $R_1 = 22.5$ Å. which is sufficiently large to make $\alpha^2$ greater than 0.75 for all values of $R$ pertinent to the problem.

The experimental values[4] of $w$ at ionic strength 0.15, together with corresponding calculated $R$ values, are shown in Table II. In the last column of this table are given radii calculated by a quite different method, from the viscosity data of Yang and Foster,[5] using the relation derivable from Einstein's law for the viscosity increment due to suspensions of spheres[16]

TABLE II

RADIUS OF EQUIVALENT SPHERE FOR SERUM ALBUMIN, 25°, $\mu = 0.150$

| $p$H | $w$ | Eq. 15 | Eq. 17 | Eq. 1 | Radius from viscosity, Å. |
|---|---|---|---|---|---|
| | | Radius, Å. | | | |
| 3.94 | 0.0117 | 37.1 | 35.6 | 51.3 | 34.2 |
| 3.52 | .0105 | 38.3 | 37.2 | 54.5 | 37.2 |
| 3.22 | .00912 | 40.1 | 39.6 | 58.8 | 39.8 |
| 2.67 | .00780 | 42.1 | 42.5 | 63.7 | 43.8 |

$$100[\eta] = \left(\frac{2.5N}{M}\right)\frac{4}{3}\pi R^3 \quad (20)$$

where $[\eta]$ is the weight intrinsic viscosity based on concentrations in grams/100 cc., and $M$ is the molecular weight. Clearly, equations 15 and 17 both give radii in remarkably good agreement with those calculated from viscosity, whereas the radii calculated by equation 1 are, as expected, far too large.

Neither the viscosity measurements nor the titrations used in the calculations of Table II were sufficiently precise so that a choice can be made between equations 15 and 17. Thus we cannot decide whether the fixed charges on the protein ion

(14) J. M. Creeth, *Biochem. J.*, **51**, 10 (1952).

(15) M. O. Dayhoff, G. E. Perlmann and D. A. MacInnes, *J. Am. Chem. Soc.*, **74**, 2515 (1952).

(16) A. Einstein, *Ann. Physik*, **19**, 289 (1906); **34**, 591 (1911).

are concentrated at the surface or embedded within the ion. Similar data at low ionic strength, however, would enable one to make such a decision, for, as Table I shows, the difference between the two models becomes greater at low ionic strength. The necessary experimental studies at low ionic strength are in progress in this Laboratory.

**Sparingly Hydrated Protein Ions.**—It was pointed out in the Introduction that the assumption of impenetrability inherent in equation 1 is reasonable for normal, sparingly hydrated protein ions. Yet electrostatic free energies calculated by its means are often larger than experimental values obtained by equation 19.

This discrepancy cannot be explained by assuming that the solvent incorporated in the protein is free solvent containing salt ions, for this would alter the calculated $F^{\circ}_{elec}$ values appreciably only at high ionic strength, and not at low ionic strength, as is already apparent for a moderately expanded protein ion (Table I, $R = 35$ Å.). Experimentally, the discrepancy is equally great at low and high ionic strength.

It is possible to consider, however, an alternative model with spherical symmetry. We may suppose that the usual small amount of water of the order of 0.2 gram per gram of protein is tightly bound to the protein substance, but that the charged side chains project outward from the protein sphere, to a distance of, say, 2 Å. This is equivalent to greatly increasing the hydration of the protein ion for the purpose of electrostatic free energy computation, while leaving unchanged the hydrodynamic hydration, for the solvent between the projecting charges might be expected to drain freely. A protein ion of this kind would be expected to deviate in individual hydrodynamic properties from those calculated for a sphere of equal volume (not including the free-draining solvent) in the same direction as an ellipsoid, i.e., the model proposed is not invalidated by the fact that individual hydrodynamic properties of proteins may be interpreted in terms of equivalent ellipsoids.[17]

In using this model as the basis for a free energy calculation one would locate the charges as evenly distributed over a surface of radius $R$. Tightly bound water is included when estimating $R_0$. If the ions in the solvent are unable to penetrate at all into the sphere of radius $R_0$, their centers would be excluded approximately the distance $R$, so that equation 16 would apply. If one wishes to allow the centers of ions to penetrate to the surface at $R_0$, equation 17 would apply. Both equations succeed in reducing $F^{\circ}_{elec}$ or $w$ at both low and high ionic strength. However, they cause too great a reduction at high ionic strength. This is illustrated in the case of ribonuclease, for which fairly reliable values for $w$ have recently been obtained,[18] in Table III. In calculating $w$ for this protein we have based values of $R_0$ and $R$ on a molecular weight of 13,900,[19] a partial specific

volume of 0.71,[20] and 0.2 gram of hydration per gram of protein. One then obtains $R_0 = 17.1$ Å., and we have used $R = 19$ Å. (In using equation 1, $R = 17.1$ Å.)

TABLE III

VALUES OF $w$ FOR RIBONUCLEASE

| Ionic strength | Eq. 1 | Projecting charges Eq. 16 | Eq. 17 | Obsd. |
|---|---|---|---|---|
| 0.01 | 0.137 | 0.116 | 0.113 | 0.112 |
| .03 | .113 | .090 | .086 | .093 |
| .15 | .079 | .055 | .048 | .061 |

Thus it must be concluded that the ionic strength dependence does not permit one to account for the deviations from equation 1 by the model of projecting charge. This same conclusion applies to β-lactoglobulin[21] and to ovalbumin. In the case of ovalbumin, this procedure has in effect already been tried. Cannan and co-workers[22] evaluated $w$ for this protein by using a value of $R$ larger than would be obtained on the basis of just 0.2 gram of hydration per gram of dry protein,[23] and then employed equation 16. They found that the ionic strength dependence could not be accounted for in this way. It was accounted for by equation 1, however, although the calculated values were consistently too large.

One final possibility may be disposed of: that the charges project outward at low ionic strength, but not at high ionic strength. The only conceivable driving force for such a change would lie in the greater electrostatic free energy of the ion at low ionic strength. The effect of charge on $F^{\circ}_{elec}$ is, however, so much greater than that of ionic strength that a similar change in location of charges would then occur with a change in $Z$, leading to changes in $w$ and also in hydrodynamic properties with $Z$. These are not observed.

One must conclude that a non-spherical shape is responsible for the deviations from equation 1, or else that they are due to the fact that the charge on a protein ion is not, in fact, evenly distributed, but present in the form of discrete charges. Scatchard[2] has indicated that this would manifest itself principally by an apparent value of $R$ in equation 1, different from that based on the size of the ion.

### Discussion

This paper illustrates again the remarkable resistance to deformation of many protein ions. The values of $w$ for serum albumin in Table II fall to less than one third the value for isoionic albumin. Since the net charge under these conditions is well over 50, this corresponds to a gain in electrostatic free energy of 35,000 calories per mole or more. The expansion required to achieve this gain is not very great, so that it is quite remarkable that only serum albumin of proteins examined so far has a sufficiently adaptable structure to allow it to take place. It is of interest that the suggestion that

(17) See, in this connection, H. A. Scheraga and L. Mandelkern, J. Am. Chem. Soc., 75, 179 (1953); C. Tanford and J. G. Buzzell, ibid., 76, 3356 (1954).

(18) C. Tanford and J. D. Hauenstein, in preparation.

(19) C. H. W. Hirs, W. H. Stein and S. Moore, J. Biol. Chem., 211, 941 (1954).

(20) A. Rothen, J. Gen. Physiol., 24, 203 (1940).

(21) R. K. Cannan, A. H. Palmer and A. C. Kibrick, J. Biol. Chem., 142, 803 (1942).

(22) R. K. Cannan, A. C. Kibrick and B. H. Palmer, Ann. N. Y. Acad. Sci., 41, 243 (1941).

(23) An experimental value close to 0.2 gram is given by Wang (Ref. 9).

the structure of serum albumin is more easily adaptable to small changes in configuration than other proteins, was already made several years ago by Karush to account for its ability to combine with a variety of small molecules and ions[24] and that the same phenomenon is observed upon the addition of urea to serum albumin solutions.[7]

No such adaptability exists, at least acid to the isoionic point, for β-lactoglobulin, ovalbumin or ribonuclease. These proteins, it would seem, cannot adapt themselves even to the extent of allowing their charged groups to project outward from the surface of the ion.

It is also remarkable that the charge on these protein ions is located so close to their surface. In no protein, with the possible exception of

lysozyme,[25] has there so far been observed the increase in electrostatic free energy, especially at low ionic strength, which would result from a penetration of the fixed charges to even 2 or 3 Å. below the surface. Nor have there been observed, except for phenolic groups, the changes in ionization constant which would result, as predicted by Schellman,[26] if ionizable groups were in an environment of relatively low dielectric constant.

(24) F. Karush, *J. Am. Chem. Soc.*, **72**, 2705 (1950).

(25) C. Tanford and M. L. Wagner, *ibid.*, **76**, 3331 (1954).
(26) J. A. Schellman, THIS JOURNAL, **57**, 472 (1953).

# HOMOGENEOUS CATALYTIC ACTIVATION OF MOLECULAR HYDROGEN BY CUPRIC PERCHLORATE

BY E. PETERS[1] AND J. HALPERN

*Metal Chemistry Laboratory, Department of Mining and Metallurgy, University of British Columbia, Vancouver, Canada*

In aqueous solutions containing cupric perchlorate, molecular hydrogen was found to react homogeneously with oxidants such as dichromate, *i.e.*, $Cr_2O_7^- + 3H_2 + 8H^+ \rightarrow 2Cr^{+++} + 7H_2O$. The kinetics are represented by $-d[H_2]/dt = k[Cu^{++}] \cdot [H_2]$. The bimolecular rate constant is given by: $k = 1.0 \times 10^{13} \exp. [-26,600/RT]$ l. mole$^{-1}$ min.$^{-1}$. The $Cu^{++}$ ion, acting as a catalyst, apparently activates the $H_2$ molecule by forming a complex with it in the rate-determining step of the reaction.

## Introduction

Earlier it was demonstrated that, in aqueous solution, cupric acetate interacts with molecular hydrogen so that the latter is activated and rendered capable of undergoing homogeneous reaction at relatively low temperatures.[2-4] Thus it was found that cupric acetate itself can be reduced homogeneously by hydrogen to cuprous salts,[3] and that it can function as a catalyst for the homogeneous hydrogenation of dissolved oxidants such as dichromate.[4] Kinetic evidence was presented for the formation of a complex, involving one $Cu(OAc)_2$ molecule and one $H_2$ molecule, as the rate-controlling step of these reactions. The hydrogen apparently becomes activated in this step so that it reacts rapidly with reducible substrates in the solution.

Cupric acetate is weakly ionized in aqueous solution[5] and, in the studies referred to above, it was demonstrated that the observed catalytic activity was due almost wholly to undissociated $Cu(OAc)_2$ molecules, which constituted the predominant cupric species. The object of the present investigation was to determine the corresponding catalytic activity of the simple $Cu^{++}$ ion. This was achieved by examining the kinetics of the hydrogenation of dichromate and other oxidants in aqueous perchlo-

ric acid solutions containing cupric perchlorate. In this medium, complexing of $Cu^{++}$ is believed to be negligible.

## Experimental

All chemicals used were of reagent grade. $Ce(HSO_4)_4$, $Cu(ClO_4)_2$, and other perchlorate salts were obtained from G. F. Smith Chemical Co. $HClO_4$, $Na_2Cr_2O_7$, $KIO_3$ and other reagents were supplied by Nichols Chemical Co. The solutions employed in the kinetic studies were prepared by diluting standardized stock solutions. $H_2$ and $N_2$ gases were supplied by Canadian Liquid Air Co.

The experiments were conducted in a stainless steel autoclave, described in an earlier paper.[3] Three liters of solution was placed in the autoclave which was then sealed, flushed with $N_2$, and heated to the desired reaction temperature, maintained to within ±0.3° by means of a Leeds and Northrup Micromax recording controller. During the experiment, a constant partial pressure of $H_2$ was maintained above the solution, which was stirred with a 3-inch impeller, rotating at 900 r.p.m., to ensure saturation. Samples of the solution were withdrawn periodically, and the concentration of unreacted oxidant measured, to determine the reduction rate.

$Cr_2O_7^-$ was determined with a Beckman DU spectrophotometer using the 3500 Å. peak; the results obtained in this way always agreed with those based on standard volumetric determinations. $IO_3^-$ and $Ce^{++++}$ were measured volumetrically. A known amount of $FeSO_4$ was added to the sample and the excess was back-titrated with standard $Ce(SO_4)_2$ solution. The $Cu^{++}$ content of the solutions was determined electrolytically.

In each experiment, prior to introduction of the $H_2$, the solution was allowed to remain in the autoclave at the reaction temperature under $N_2$, for a period of time comparable with the duration of the subsequent run. The rate at which the oxidant was consumed under these conditions, presumably due to corrosion of the stainless steel reaction vessel, was determined and subtracted from the subse-

(1) Holder of a National Research Council of Canada Studentship, 1954-1955.
(2) J. Halpern and R. G. Dakers, *J. Chem. Phys.*, **22**, 1272 (1954).
(3) R. G. Dakers and J. Halpern, *Can. J. Chem.*, **32**, 969 (1954).
(4) E. Peters and J. Halpern, *ibid.*, **33**, 356 (1955).
(5) K. J. Pedersen, *Kgl. Danske Videnskab. Selskab Mat.-fys. Medd.*, **22**, No. 12 (1945).

quently measured rate of consumption in the presence of $H_2$ to obtain the rate of reaction with $H_2$. This correction was always small, usually less than 5% of the latter rate.

## Results and Discussion

Some typical rate plots for the reduction of $Cr_2O_7^=$ by $H_2$ in the presence of $Cu(ClO_4)_2$ are shown in Fig. 1. At constant temperature and $H_2$ pressure,
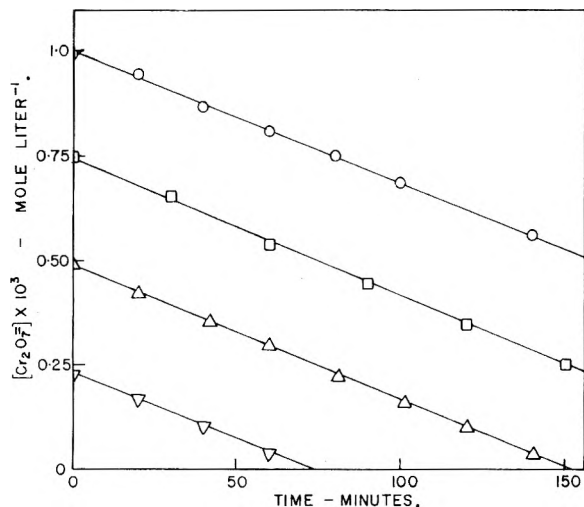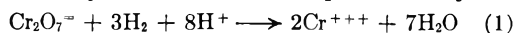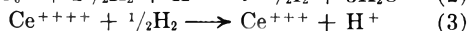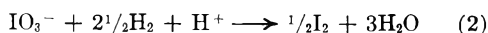


Fig. 1.—Typical rate plots for the reduction of $Cr_2O_7^=$; 0.10 $M$ $Cu(ClO_4)_2$; 110°; 20 atm. $H_2$.

the concentration of $Cr_2O_7^=$ is seen to decrease linearly with time, corresponding to zero-order kinetic behavior. The slopes of the zero-order plots are independent of the initial $Cr_2O_7^=$ concentration. The stoichiometry of the reaction is represented by

$$Cr_2O_7^= + 3H_2 + 8H^+ \longrightarrow 2Cr^{+++} + 7H_2O \quad (1)$$

Other oxidants, including $IO_3^-$ and $Ce^{++++}$ were also found to react with $H_2$ in the presence of $Cu(ClO_4)_2$ as

$$IO_3^- + 2^1/_2H_2 + H^+ \longrightarrow {}^1/_2I_2 + 3H_2O \quad (2)$$
$$Ce^{++++} + {}^1/_2H_2 \longrightarrow Ce^{+++} + H^+ \quad (3)$$

or, in general

$$Ox + nH_2 + qH^+ \longrightarrow rRed + sH_2O \quad (4)$$

In each case the kinetics of reduction were of zero order with respect to Ox. No change in the concentration of $Cu^{++}$ could be detected during the reactions, suggesting that $Cu^{++}$ acts as a true catalyst.

The reaction rates were estimated from the slopes of rate plots such as those shown in Fig. 1, after introducing corrections for the contributions due to corrosion. Duplicate rate measurements generally reproduced to within ±5% in the case of $Cr_2O_7^=$ and $IO_3^-$ and to within ±10% with $Ce^{++++}$. The rates for the different oxidants can best be compared by expressing them in terms of the equivalent rates of consumption of $H_2$, calculated from the stoichiometric relation of equation 4, i.e.

$$-\frac{d[H_2]}{dt} = -n\frac{d[Ox]}{dt} = k_0 \quad (5)$$

Equivalent rate plots for the reaction of $H_2$ with various oxidants i.e., $Cr_2O_7^=$, $IO_3^-$ and $Ce^{++++}$ are shown in Fig. 2. At constant $Cu^{++}$ concentration the slopes of these plots, and hence the values of



Fig. 2.—Comparison of reaction rates of various oxidants; 110°; 20 atm. $H_2$.

$k_0$, are seen to be essentially independent of the nature of the oxidant, within the limits of the experimental uncertainties involved in their comparison. This observation, coupled with the zero-order reaction kinetics, strongly suggest that the oxidant species does not participate in the rate-determining step, and that this step is the same for all the oxidants.

Further indication of this is provided by Fig. 3, in which the rates are plotted as functions of the $Cu^{++}$ concentration, and the points for $Cr_2O_7^=$, $IO_3^-$ and $Ce^{++++}$ are all seen to lie on a single straight line. The fact that $k_0$ is directly proportional to $[Cu^{++}]$ is consistent with the latter's suggested catalytic role.



Fig. 3.—Dependence of rate on $Cu^{++}$ concentration; 110°; 20 atm. $H_2$.

The reaction of $Cr_2O_7^=$ proved to be the most convenient one on experimental grounds, and to yield the most precise measurements of the rate of activation of $H_2$. It was therefore selected to elucidate the remaining kinetic variables. Figures 4 and 5 depict the effect of $H_2$ on the rate of this reaction. In the range from 0 to 25 atm., $k_0$ is seen to be directly proportional to the $H_2$ partial pressure, $P_{H_2}$. The small residual rate of disappearance of $Cr_2O_7^=$ in the absence of $H_2$, evident in Fig. 4, is
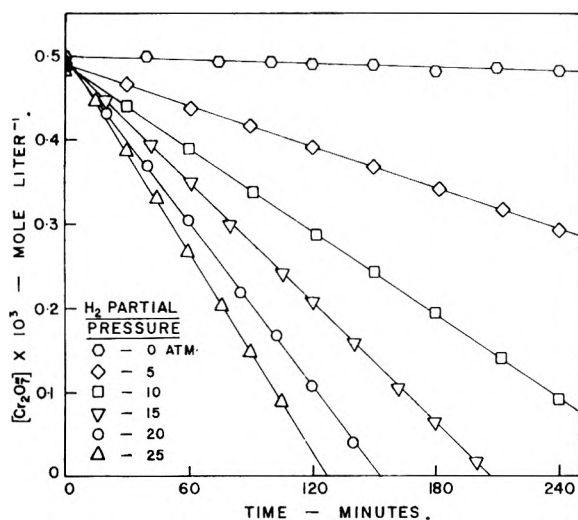
Fig. 4.—Reduction of $Cr_2O_7^-$ at different $H_2$ partial pressures; 0.10 $M$ $Cu(ClO_4)_2$; 110°.
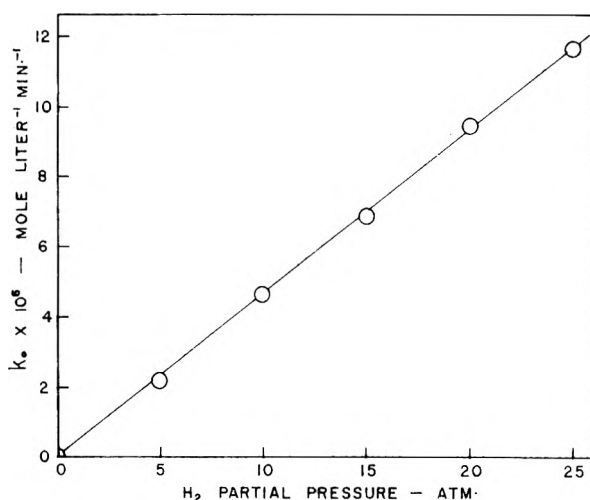


Fig. 5.—Dependence of rate on $P_{H_2}$; 0.10 $M$ $Cu(ClO_4)_2$; 110°.

believed to arise from the corrosion reaction discussed earlier. The contribution due to this was subtracted from the slopes of the other rate plots to evaluate $k_0$. The correction was small and the error from this source is believed to be negligible.

The rate of reaction can thus be represented by

$$-\frac{d\,[H_2]}{dt} = k_0 = k'\,[Cu^{++}]\,P_{H_2}$$
$$= k\,[Cu^{++}][H_2] \qquad (6)$$

where $[H_2]$ is the concentration of molecular hydrogen in solution, since the system obeys Henry's law[6] in the pressure range under consideration. $k'$ and $k$ are related by Henry's constant, $\alpha$, denoting the solubility of $H_2$, i.e.

$$k' = \alpha k \qquad (7)$$

At 100°, the experimental value of $k'$ for the $Cu^{++}$-catalyzed reaction between $H_2$ and $Cr_2O_7^-$ is $1.9 \times 10^{-6}$ atm.$^{-1}$ min.$^{-1}$. This value is about 120 times lower than for the corresponding Cu(OAc)$_2$-catalyzed reaction.[4]

(6) A. Seidell, "Solubilities of Inorganic and Metal Organic Compounds," 3rd ed., Vol. I, D. Van Nostrand Co., Inc., New York, N. Y., 1940, pp. 553–560.

Rate measurements were made at seven different temperatures ranging from 80 to 140° and the resulting Arrhenius plot is shown in Fig. 6. The slope corresponds to an apparent activation energy of $26.6 \pm 0.8$ kcal. This value is about 2 kcal. higher than that reported earlier for Cu(OAc)$_2$, consistent with the latter's greater catalytic activity.[3,4]



Fig. 6.—Arrhenius plot for the $Cu^{++}$-catalyzed reaction between $H_2$ and $Cr_2O_7^-$.

The rate constants for the $Cu^{++}$-catalyzed reaction are thus given by

$$k' = 7.3 \times 10^9 \exp\left[-\frac{26,600}{RT}\right] \text{ atm.}^{-1}\text{ min.}^{-1} \quad (8)$$

and

$$k = 1.0 \times 10^{13} \exp\left[-\frac{26,600}{RT}\right] \text{ l. mole}^{-1}\text{ min.}^{-1} \quad (9)$$

In calculating the latter expression for $k$, it was assumed that the solutions (which contained 0.1 $M$ Cu(ClO$_4$)$_2$, 0.01 $M$ HClO$_4$ and 0.0005 $M$ Cr$_2$O$_7^=$) were sufficiently dilute, so that $\alpha$ had the same value as for pure water, i.e., $7.14 \times 10^{-4}$ mole l.$^{-1}$ atm.$^{-1}$, and that this value was independent of temperature in the region under consideration. The available data provide some support for these assumptions[6] and it is not likely that a significant error is introduced through them.

The Arrhenius frequency factor in equation 9, i.e., $1.0 \times 10^{13}$ l. mole$^{-1}$ min.$^{-1}$ and the corresponding activation entropy, $\Delta Sc^{\ddagger}$, of $-9.6$ e.u. at 100°, are normal for a simple bimolecular reaction in solution[7] and agree, within experimental error, with the values reported earlier[3,4] for the corresponding activation of $H_2$ by Cu(OAc)$_2$.

In Table I are listed the rates of Cr$_2$O$_7^=$ reduction in several solutions of differing composition. The rate of reaction is seen to be essentially independent of the NaClO$_4$ concentration from 0 to 1.0 $M$ and of the HClO$_4$ concentration from 0.004 to 0.025 $M$. At higher HClO$_4$ concentrations a slight decrease in the rate was noted, which may be due to the competing reduction of HClO$_4$ itself.

(7) E. A. Moelwyn-Hughes, "The Kinetics of Reactions in Solution," 2nd ed., Oxford Univ. Press, London, 1947, pp. 68–77; G. K. Rollefson, THIS JOURNAL, 56, 976 (1952).

The results suggest that at the $HClO_4$ concentration used in most of the experiments, i.e., 0.010 M, complications from this source were negligible. Additions of 0.38 M $Ca(ClO_4)_2$ or $Zn(ClO_4)_2$ were without effect while 0.25 M $Al(ClO_4)_3$ depressed the rate slightly. The general ionic strength effect, if any, is apparently small, consistent with the fact that one of the reactants, i.e., $H_2$, is uncharged. The absence of a specific perchlorate salt effect supports the conclusion that the catalytic activity, observed in this system, is due to the uncomplexed $Cu^{++}$ ion.

## Table I

RATES OF REACTION BETWEEN $Cr_2O_7^=$ AND $H_2$ IN DIFFERENT SOLUTIONS

$Cu(ClO_4) = 0.1 m$; $Na_2Cr_2O_7 = 0.0005 m$; $T = 110°C$.; $P_{H_2} = 20$ atm.

| Expt. no. | $HClO_4$, $M$ | Added salt, $M$ | $k_0 \times 10^6$, mole l.$^{-1}$ min.$^{-1}$ | $k' \times 10^6$, atm.$^{-1}$ min.$^{-1}$ |
|---|---|---|---|---|
| T-11 | 0.004 | ... | 9.27 | 4.64 |
| T-9 | .013 | ... | 9.27 | 4.64 |
| T-8 | .017 | ... | 9.48 | 4.74 |
| T-7 | .025 | ... | 9.18 | 4.59 |
| T-6 | .050 | ... | 8.52 | 4.26 |
| T-5 | .10 | ... | 7.65 | 3.83 |
| T-10 | .010 | 0.00 $NaClO_4$ | 9.30 | 4.65 |
| T-13 | .010 | 0.25 $NaClO_4$ | 9.33 | 4.67 |
| T-14 | .010 | 0.50 $NaClO_4$ | 9.00 | 4.50 |
| T-15 | .010 | 0.75 $NaClO_4$ | 9.18 | 4.59 |
| T-12 | .010 | 1.00 $NaClO_4$ | 8.88 | 4.44 |
| T-16 | .010 | 0.38 $Ca(ClO_4)_2$ | 9.00 | 4.50 |
| T-17 | .010 | 0.38 $Zn(ClO_4)_2$ | 9.18 | 4.59 |
| T-18 | .010 | 0.25 $Al(ClO_4)_3$ | 8.31 | 4.16 |
| W-1[a] | .010 | ... | 9.36 | 4.68 |
| W-2[b] | .010 | ... | 9.18 | 4.59 |
| W-3[c] | .010 | ... | 8.94 | 4.47 |

[a] Baffle added to increase stirring efficiency. [b] Stirrer velocity reduced from 900 to 600 r.p.m. [c] 30 g. of stainless steel powder added.

Direct evidence for the homogeneous character of the reaction is provided by the results of an experiment (W-3, Table I) in which 30 g. of stainless steel powder, of similar composition to the autoclave itself, was added. Although the area of this powder was at least twice that of the autoclave surface normally exposed to the solution, no increase in the reaction rate could be detected.

Varying the stirring efficiency, either by reducing the impeller velocity to 600 r.p.m. from its normal value of 900 r.p.m. (expt. W-2) or by introducing a baffle into the autoclave (expt. W-1) also had no effect on the rate. This indicates, as do other features of the kinetics, that under the conditions of these experiments the reaction was not limited by the rate of solution of hydrogen.

## Conclusions

The kinetic results suggest that the rate-determining step of these reactions is a homogeneous bimolecular process involving one $H_2$ molecule and one $Cu^{++}$ ion. The $H_2$ must become activated in this step so that its subsequent reaction with the reducible substrate is fast. The hydrogenation of $Cr_2O_7^=$ may thus be represented by the following sequence of steps

$$3H_2 + 3Cu^{++} \xrightarrow[\text{slow}]{k} 3[Cu-H_2]^{++} \qquad (10)$$

Followed by

$$3[Cu-H_2]^{++} + Cr_2O_7^= + 8H^+ \xrightarrow[\text{fast}]{}$$
$$2Cr^{+++} + 7H_2O + 3Cu^{++} \qquad (11)$$

The $Cu^{++}$ is regenerated and thus functions as a true catalyst.

This sequence is similar to that suggested earlier[2] for the $Cu(OAc)_2$-catalyzed reaction between $H_2$ and $Cr_2O_7^=$, except that in the present system the activating cupric species is considered to be the simple $Cu^{++}$ ion. Among the factors supporting this interpretation are (a) the view, now generally admitted, that ions such as $Cu^{++}$ are uncomplexed in perchlorate media, (b) the bimolecular kinetics and normal frequency factor of the reaction, and (c) the absence of an appreciable pH dependence and of salt effects due to dichromate or perchlorate. The mechanism of the activation process and the nature of the complex formed in the rate-determining step have been discussed in a recent paper.[8] However the available kinetic data alone do not permit their detailed resolution.

Only a few other examples of the homogeneous catalytic activation of molecular hydrogen in solution have been reported. In addition to $Cu(OAc)_2$ several other metal compounds including $Cu_2$-$(OAc)_2$,[9] $Hg(OAc)_2$[10] and $Co_2(CO)_8$.[11] have been found to possess such activity under certain conditions. However, this appears to be the first time that the ability to activate $H_2$ homogeneously has been demonstrated for a simple metal ion.

(8) J. Halpern and E. Peters, J. Chem. Phys., **23**, 605 (1955).

(9) M. Calvin, Trans. Faraday Soc., **34**, 1181 (1938); J. Am. Chem. Soc., **61**, 2230 (1939); S. Weller and G. A. Mills, ibid., **75**, 769 (1953).

(10) J. Halpern, G. J. Korinek and E. Peters, Research, London, **7**, S61 (1954).

(11) I. Wender, M. Orchin and H. H. Storch, J. Am. Chem. Soc., **72**, 4842 (1950); M. Orchin in "Advances in Catalysis," Vol. V, Academic Press, Inc., New York, N. Y., 1953, p. 385.
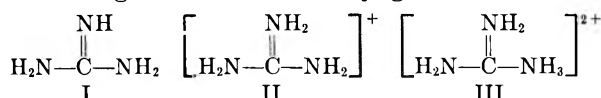
# NOTES

## THE IONIZATION CONSTANTS OF GUANIDINE AND ALKYL GUANIDINES

By A. J. Owen

*25 Thaxted Way, Waltham, Abbey, Essex, England*
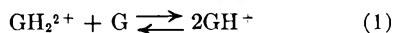*Received November 30, 1954*

The usefulness of the simple molecular orbital theory, neglecting overlap, has been demonstrated for urea and thiourea.[1] In the present work calculations have been made of the guanidine molecule I, the singly charged cation II, and the doubly charged cation III, and the results applied to a theoretical interpretation of the ionization constants of guanidine and the alkyl guanidines.

$$\underset{\text{I}}{\overset{\overset{\displaystyle NH}{\|}}{H_2N-C-NH_2}} \qquad \left[\underset{\text{II}}{\overset{\overset{\displaystyle NH_2}{\|}}{H_2N-C-NH_2}}\right]^+ \qquad \left[\underset{\text{III}}{\overset{\overset{\displaystyle NH_2}{\|}}{H_2N-C-NH_3}}\right]^{2+}$$

Using the parameters $\alpha_{=N-} = \alpha + 0.5\ \beta_{cc}$; $\alpha_{-N-} = \alpha + \beta_{CC}$; $\alpha_{C(-N)} = \alpha + 0.3\ \beta_{CC}$; $\beta_{CN} = \beta_{CC}$; ($\alpha_r$ is the coulombic term for atom r; $\beta_{rs}$ is the resonance integral between atomic orbitals $\phi_r$ and $\phi_s$); the mobile bond order for the carbon–nitrogen bond in the guanidinium ion is 0.5660, and corresponds to a bond distance of 1.34 Å., close to the experimental values of 1.33[2] and 1.34 Å.[3] Calculation of the resonance energies of I, II, III, leads to values of 1.18$\beta$, 1.41$\beta$, and 0.79$\beta$, respectively. Hyperconjugation of the $-\overset{+}{N}H_3$ group with the rest of the molecule has been neglected as its contribution is likely to be small.[4-5]

The difference between the first and second ionization constants of guanidine $\Delta pK_1'' = pK_a'' - pK_a'$ $\sim 24.6$.[6-8] If the process

$$GH_2{}^{2+} + G \rightleftarrows 2GH^+ \qquad (1)$$

is considered, $\Delta w$, the reversible work expended in the transfer of a proton from one ionizing group to another, can be expressed as contributions from three separate effects. $\Delta w_1$ is regarded as purely electrostatic in origin; $\Delta w_2$ is due to resonance energy changes; and $\Delta w_3$ is the contribution due to the intrinsic structure of the ionizing group.

In a thoretical interpretation of $\Delta pK_1''$ for guanidine, Williams and Hardy[8] considered $\Delta w_1$ only by applying the Kirkwood and Westheimer theory[9] to process (1), but used an improbable carbon–nitrogen bond distance of 1.18 Å.[10] and obtained $\Delta pK_1''$ $\sim 19.5$. If, however, the bond distance of 1.34 Å. is used (other data as Williams and Hardy), $\Delta pK_1''$

(1) A. J. Owen, Thesis, Wales, 1952.
(2) L. Kellner, *Proc. Roy. Soc. (London)*, **A177**, 456 (1941).
(3) J. Drenth, W. Drenth, A. Vos and E. H. Wiebenga, *Acta Cryst.*, **6**, 424 (1953).
(4) V. A. Crawford, *J. Chem. Soc.*, 2061 (1953).
(5) H. C. Longuet-Higgins, *J. Chem. Phys.*, **18**, 275 (1950).
(6) S. J. Angyal and W. K. Warburton, *J. Chem. Soc.*, 2492 (1951).
(7) W. F. Hall and M. R. Sprinkle, *J. Am. Chem. Soc.*, **54**, 3469 (1932).
(8) G. Williams and M. Hardy, *J. Chem. Soc.*, 2560 (1953).
(9) J. G. Kirkwood and F. H. Westheimer, *J. Chem. Phys.*, **6**, 506 (1938); **7**, 437 (1939).
(10) W. Theilacker, *Z. Krist.*, **90**, 51, 256 (1938).

$\sim 13.7$ is obtained. If the nitrogen–hydrogen bond distance is taken into account $\Delta pK_1''$ $\sim 11.7$. These values are only approximately half the observed figure.

The difference in resonance energy for process (1) is 0.85$\beta$, or 17 kcal./mole if $\beta$ is taken as 20 kcal./mole, and leads to $\Delta pK_1''$ $\sim 12.7$. This effect is mainly due to the difference in resonance energy between the singly charged cation II and the doubly charged cation III, (*cf.* Gillespie and Leisten[11]). The difference in resonance energy between guanidine I and the singly charged guanidinium cation II, 0.23$\beta$ (4.6 kcal./mole), is somewhat lower than the value of 6 to 8 kcal./mole estimated by Pauling,[12] but closer agreement would be obtained if the change $\delta\alpha$ in the coulomb integral between $=$NH and $-$NH$_2$ was greater than 0.5$\beta$.[13] It is significant that if the effects of hyperconjugation are small,[4,5] N,N'-dialkylguanidines would have the same resonance energy changes as guanidine, and should therefore be strong bases and not weak ones as suggested by Pauling.[12] Recent experimental work[6,14] shows this to be so, $pK_a''$ for both guanidine and N,N'-dimethylguanidine being 13.6.

The contribution $\Delta w_3$ due to the intrinsic structure of the ionizing group is likely to be small, as $pK_a''$ for alkyl amines is between 10.7 and 11.1 and for dialkyl amines and piperidine, between 10.7 and 11.2.

Thus the difference $\Delta pK_1''$ in the ionization constants of guanidine is due to two factors, both of similar magnitude, one due to electrostatic effects, and the other to resonance energy changes. The sum of these two effects gives a value of $\Delta pK_1''$ between 24.4 and 26.4, close to the experimental value of 24.6.

The author thanks Professor Gwyn Williams, Dr. K. W. Sykes and Dr. T. M. Walters for helpful discussion.

(11) R. J. Gillespie and J. A. Leisten, *Quart. Revs.*, **7**, 40 (1954).
(12) L. Pauling, "Nature of the Chemical Bond," Cornell Univ. Press, Ithaca, N. Y., Second Ed., 1948, p. 213.
(13) The author is indebted to one of the referees for pointing out the importance of the change in the value of $\alpha$ between $=$NH and $-$NH$_2$.
(14) R. Neivelt, E. C. Mayo, J. H. Tiers, D. H. Smith and G. W. Wheland, *J. Am. Chem. Soc.*, **73**, 3475 (1951).

## BRÖNSTED'S WORK PRINCIPLE AND GIBBS' TREATMENT OF ELECTROMOTIVE FORCE

By Duncan MacRae

*Route 3, Bel Air, Maryland*
*Received March 14, 1955*

In 1940, MacDougall[1] commented on a paper by Brønsted[2] as follows: "...It must be left to his readers to decided for themselves whether or not his proposed 'work principle' and his derivation of

(1) F. H. MacDougall, This Journal, **44**, 713 (1940).
(2) J. N. Brønsted, *ibid.*, **44**, 699 (1940).

a number of important physico-chemical relations represent a thermodynamic method which is superior in any way to what I suppose he would call the traditional or classical method."

Since then, there have been at least seven papers[3] which, on the whole, clarify and support Brønsted's formulation of thermodynamics. One of these[3c] strongly supports one of Brønsted's criticisms of traditional thermodynamics and another[3d] shows that Brønsted's postulates are completely equivalent to the classical laws and calls his methods elegant and concise. None of these authors, however, including Brønsted himself, mentions the fact that Gibbs[4] discussion of the "Modifications of the Conditions of Equilibrium by Electromotive Force" is a very good example of what Brønsted, many years later, called the "work principle."

The "work principle" is exceedingly simple. It is very nearly the same as the "principle of work" used in the discussion of machines, even in high-school textbooks of physics[5]; or the "energy principle" in a current textbook of "College Physics."[6] For example, if the turbine and generator of a hydroelectric plant are considered as a single machine in which losses due to friction and other causes may be neglected, the input of work is equal to the output, or

$$(P_{g1} - P_{g2})\delta K_g + (P_{e1} - P_{e2})\delta K_e = 0$$

in which $\delta K_g$ is the weight of water which flowed from the height $P_{g1}$ to the height $P_{g2}$ and $\delta K_e$ is the quantity of electricity which flowed from the electric potential $P_{e1}$ to the electric potential $P_{e2}$. If, on the other hand, a thermodynamic system includes the reservoir, tail race, turbine, generator and power lines of a hydroelectric plant, the work principle says that the loss in gravitational work is equal to the gain in electric work. This may be expressed by the same equation.

Without naming any specific principle, Gibbs[4] obtained a similar result

$$(P_{e1} - P_{e2})\delta K_e + (P_{c1} - P_{c2})\delta K_c + (P_{g1} - P_{g2})\delta K_g = 0$$

in which "The first term represents the increment of the potential energy of electricity, the second the increment of the intrinsic energy of the ponderable matter, and the third the increment of the energy due to gravitation" when a quantity of electricity $\delta K_e$ passes from one electrode of a galvanic cell to another under equilibrium conditions. Gibbs, of course, defined his "intrinsic potentials" in terms of mass. So, $\delta K_c$ was equal to $\delta K_g$; but $\delta K_c$ can be expressed in moles and $P_{c1} - P_{c2}$ can be the difference in what we now call chemical potentials. In that case, if we neglect the effect of gravity, the last equation above becomes

(3) (a) B. Leaf, *J. Chem. Phys.*, **12**, 89 (1944); (b) D. MacRae' *J. Chem. Educ.*, **23**, 366 (1946); (c) H. H. Steinour, *ibid.*, **25**, 15 (1948); (d) V. K. La Mer, O. Foss and H. Reiss, *Ann. N. Y. Acad. Sci.*, **51**, 605 (1949); *Acta Chem. Scand.*, **3**, 1238 (1949); (e) T. Rosenberg, *ibid.*, **3**, 1215 (1949); (f) P. Colmant, *ibid.*, **3**, 1220 (1949); (g) H. Holtan, Jr., *J. Chem. Phys.*, **19**, 519 (1951).

(4) J. W. Gibbs, "Collected Works I," Longmans, Green, and Co., New York, N. Y., 1931, pp. 331–333.

(5) N. H. Black and H. N. Davis, "New Practical Physics," The Macmillan Co., New York, N. Y., 1933, p. 39.

(6) Sears-Zemansky, "College Physics," 2nd Ed., Addison-Wesley Pub. Co., Cambridge, Mass., 1953, pp. 460–1.

$$(P_{e1} - P_{e2})\delta K_e + (P_{c1} - P_{c2})\delta K_c = 0$$

the well known relation between the electromotive force of a cell and the chemical potentials of the ion involved.

These examples show that the work principle, far from competing with the methods of traditional thermodynamics, is itself one of them; and that at least one derivation of a principle of physical chemistry with the aid of the work principle is simpler than that usually given in the textbooks. Since the work principle is not in conflict with the usual methods of physics or thermodynamics, such derivations can be inserted in any course in physical chemistry or thermodynamics without any modification whatsoever in the rest of the course except, perhaps, to admit that it is sometimes permissible to distinguish between the different kinds of energy in a thermodynamic system.

---

## INTRINSIC VISCOSITY AND KINEMATIC VISCOSITY

By Charles Tanford

*Contribution from the Department of Chemistry, State University of Iowa, Iowa City, Iowa*

The quantity of most interest in the viscometry of macromolecular solutions is the intrinsic viscosity, $[\eta]$, defined as the limiting value, at zero concentration, of the relative viscosity increment, *i.e.*

$$[\eta] = \frac{1}{\eta_0} \mathop{L}_{c \to 0} \frac{\eta - \eta_0}{c} = \frac{1}{\eta_0} \mathop{L}_{c \to 0} \frac{d\eta}{dc} \qquad (1)$$

where $\eta$ is the viscosity of a macromolecular solution of concentration $c$ (customarily expressed in grams per 100 ml. of solution), and $\eta_0$ is the viscosity of solvent.

Most frequently used for viscosity measurement are capillary viscometers. The flow time of a liquid in such a viscometer is, however, a measure, not of viscosity, but of kinematic viscosity, $\nu$. For a given viscometer $\nu = f(t) = At - B/t$, where $A$ and $B$ are constants determined by calibration with liquids of known viscosity. The true viscosity is related to kinematic viscosity through the density, $\rho$, *i.e.*, $\eta = \rho\nu$, so that, in terms of capillary flow times

$$[\eta] = \frac{1}{\rho_0\nu_0} \mathop{L}_{c \to 0} \frac{d(\rho\nu)}{dc} = \frac{1}{\rho_0 f_0(t)} \mathop{L}_{c \to 0} \frac{d(\rho f(t))}{dc} \qquad (2)$$

where the subscript zero refers to measurements with solvent. To obtain intrinsic viscosities by equation 2 thus requires accurate measurement of both flow time and density as a function of concentration. Since accurate density measurements are laborious, it would be simpler to measure the quantity $[\nu]$

$$[\nu] = \frac{1}{\nu_0} \mathop{L}_{c \to 0} \frac{d\nu}{dc} = \frac{1}{f_0(t)} \mathop{L}_{c \to 0} \frac{df(t)}{dc} \qquad (3)$$

It is sometimes suggested[1] that the difference between $\rho$ and $\rho_0$ be ignored in the relation between $\eta$ and $\nu$, so that $\eta = \rho_t\nu$. If this is done, then, by equation 2, $[\eta] = [\nu]$. The purpose of this paper is to show that this equality will, in general, be incor-

(1) *E.g.*, P. J. Flory, "Principles of Polymer Chemistry," Cornell University Press, Ithaca, N. Y., 1953, p. 309.

rect (though the error is likely to be inappreciable for most solutions of linear polymer), but that a simple relation between $[\eta]$ and $[\nu]$ can be derived which does permit the evaluation of intrinsic viscosity without accurate density measurements.

Differentiating $\eta = \rho\nu$ and expanding $\rho$ and $\nu$ in terms of Taylor series, we have

$$\frac{d\eta}{dc} = \left(\rho_0 + \frac{d\rho}{dc}c + \ldots\right)\frac{d\nu}{dc} + \left(\nu_0 + \frac{d\nu}{dc}c + \ldots\right)\frac{d\rho}{dc}$$

so that, at the limit of $c = 0$, by equations 1 and 3

$$[\eta] = [\nu] + \frac{1}{\rho_0}\mathop{L}_{c\to 0}\frac{d\rho}{dc} \qquad (4)$$

To evaluate $d\rho/dc$, let a solution contain $g_1$ grams of solvent and $g_2$ grams of macromolecular solute. Let $\bar{v}_1$ and $\bar{v}_2$ be the corresponding partial specific volumes, so that the total volume is $V = g_1\bar{v}_1 + g_2\bar{v}_2$. The relation between $c$ and $g_2$ is then, $c = 100(g_2/V)$, the volume being measured in ml., so that

$$\mathop{L}_{c\to 0}\left(\frac{\partial c}{\partial g_2}\right)_{g_1} = \frac{100\,(V - g_2\bar{v}_2)}{V^2} = \frac{100 g_1\bar{v}_1}{(g_1\bar{v}_1 + g_2\bar{v}_2)^2} \qquad (5)$$

where the partial specific volumes are the limiting values at zero concentration.

The density may also be related to $g_1$ and $g_2$, *i.e.*, $\rho = (g_1 + g_2)/V$, so that

$$\mathop{L}_{c\to 0}\left(\frac{\partial\rho}{\partial g_2}\right)_{g_1} = \frac{V - (g_1 + g_2)\bar{v}_2}{V^2} = \frac{g_1(\bar{v}_1 - \bar{v}_2)}{(g_1\bar{v}_1 + g_2\bar{v}_2)^2} \qquad (6)$$

Since the relation between $\rho$ and $c$ must be independent of $g_1$, we obtain, from equations 5 and 6

$$\mathop{L}_{c\to 0}\frac{d\rho}{dc} = \mathop{L}_{c\to 0}\left(\frac{\partial\rho}{\partial c}\right)_{g_1} = \frac{\bar{v}_1 - \bar{v}_2}{100\bar{v}_1} = \frac{1 - \bar{v}_2\rho_0}{100} \qquad (7)$$

the last equality arising from the fact that the limiting value of $\bar{v}_1$ at $c = 0$ is merely the reciprocal of solvent density. Combining with equation 4 then gives

$$[\eta] = [\nu] + \frac{1 - \bar{v}_2\rho_0}{100\rho_0} \qquad (8)$$

The last term in equation 8 may be negligible for many polymer solutions, especially when the intrinsic viscosity is large. For polyisobutylene in benzene, for example, at 20°, $\bar{v}_2$ is 1.063 ml./g. and $\rho_0$ is 0.879[2] so that this term becomes 0.000747. In other polymer solutions it may be as high as 0.003, which would not be negligible for viscosity measurements at relatively low degrees of polymerization.

The last term in equation 8 is especially important for aqueous solutions of proteins, where its value is of the order of 0.0025. Since the intrinsic viscosity of such solutions is often between 0.03 and 0.04, this term may thus amount to nearly 10% of the intrinsic viscosity. It is, however, easily evaluated, since the partial specific volume need not be known with high precision.

As an experimental test of the validity of equation 8, we may examine data for serum albumin recently obtained in this laboratory by J. G. Buzzell. The upper line of Fig. 1 shows an extrapolation according to equation 2, both density and flow time being determined at each concentration. The lower
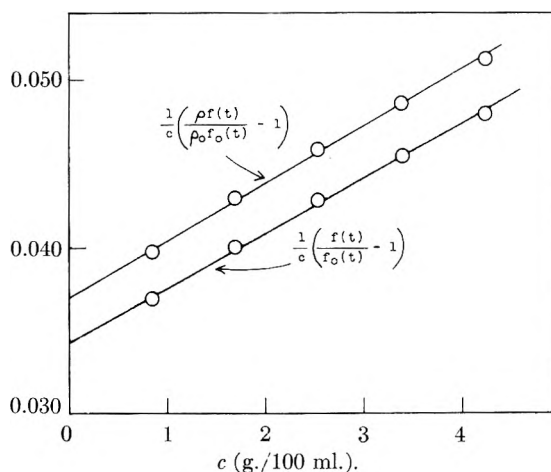
(2) W. R. Krigbaum and P. J. Flory, *J. Am. Chem. Soc.*, **75**, 5254 (1953).



Fig. 1.—Viscosity data for isoionic bovine serum albumin in 0.01 $M$ KCl at 25°. (Straight lines determined by least squares.)

curve shows extrapolation of the same data according to equation 3, using flow times only. The intercepts, determined by the method of least squares, are, respectively, $[\eta] = 0.03704$ and $[\nu] = 0.03436$, the difference between these being 0.00268. The difference calculated by equation 8, using $\bar{v}_2 = 0.734$[3] and a measured $\rho_0$ of 0.9975, is also 0.00268. Since the reproducibility of the data does not justify use of the last significant figure given for $[\eta]$, it would clearly have sufficed to know $\bar{v}_2$ within an accuracy of ±0.01, in order to obtain an accurate value of $[\eta]$ from flow times only.

(3) M. O. Dayhoff, G. E. Perlmann and D. A. MacInnes, *ibid.*, **74**, 2515 (1952).

---

# A SIMPLE KINETIC METHOD FOR SOME SECOND-ORDER REACTIONS

By Marvin C. Tobin

*General Research Organization, Olin Mathieson Chemical Corporation, New Haven, Connecticut*

The determination of rate constants and the general treatment of kinetic data are most simple if some function of a concentration variable is expressible as a linear function of time. This note indicates that the integrated kinetic expressions for four complex reactions involving second-order steps[1] may be recast to give such a function.

The usefulness of this formulation goes beyond these four limited cases, since it has been found that the expressions derived are very useful as empirical equations.[2] They may sometimes be used to reduce fragmentary data when the experimental curves are sigmoid in shape.
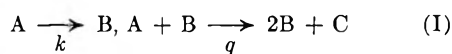
The analysis is carried out in detail for the sim-

(1) S. Glasstone, "Textbook of Physical Chemistry," D. Van Nostrand Co., Inc., New York, N. Y., 1945, pp. 1061, 1071.

(2) J. P. Fowler and M. C. Tobin, THIS JOURNAL, **58**, 382 (1954).

ple autocatalytic sequence, and is indicated for the others.

$$A \xrightarrow{k} B, \quad A + B \xrightarrow{q} 2B + C \qquad (I)$$

The rate of loss of A may be expressed as

$$dx/dt = k(a - x) + qx(a - x) \qquad (1)$$

where

$a$ = initial concn. of A

$x$ = amount of A used to time $t$

Equation 1 may readily be integrated to the useful form

$$\ln\left(\frac{(k/q) + x}{a - x}\right) = q\,[(k/q) + a]t + \ln(k/aq) \qquad (2)$$

which may be written as

$$\log((b + x)/(a - x)) = dt + c \qquad (3)$$

It may be shown by setting the derivative of (1) equal to zero, that

$$b = a - 2x_m \qquad (4)$$

where $x_m$ is the value of $x$ when $dx/dt$ reaches its maximum value.

With $b$ thus known, a plot of $\log((b + x)/(a - x))$ *versus* $t$ may be used to obtain $d$ and $c$. $d$ has the dimensions of a first-order rate constant and may be treated as such in the Arrhenius equation.

Two other quantities of interest are the maximum slope

$$(dx/dt)_m = q(a + b)^2/4 \qquad (5)$$

and the time at which the maximum slope is reached

$$t_m = -c/d \qquad (6)$$

An analogous treatment holds for the following three cases, for which only integrated expressions are given. Equations 3–6 are valid for these if the proper values of $c$, $d$ and $b$ are used.

$$A \underset{q}{\overset{k}{\rightleftarrows}} B + C \qquad (II)$$

$$\ln\left(\frac{(ax_e)/(a - x_e) + x)}{x_e - x}\right) = \left(\frac{2a - x_e}{x_e}\right) kt + \ln\left(\frac{a}{a - x_e}\right) \qquad (7)$$

where

$x$ = concn. of B or C

$x_e$ = equilibrium concn. of B or C

$a$ = initial concn. of A

$$A + B \underset{q}{\overset{k}{\rightleftarrows}} C + D, \quad A_0 = B_0 \qquad (III)$$

$$\ln\left(\frac{(ax_e/(a - ax_e)) + x)}{x_e - x}\right) = \left(\frac{2a(a - x_e)}{x_e}\right) kt + \ln\left(\frac{a}{a - ax_e}\right) \qquad (8)$$

$a$, $x_e$ and $x$ as in II.

$$A^2 \xrightarrow{k} B, \quad A + B \xrightarrow{q} 2B + C \qquad (IV)$$

$$\ln\left(\frac{(ka/Q) + x}{a - x}\right) = Q\left(\frac{ka}{Q} + a\right)t + \ln\left(\frac{k}{Q}\right) \qquad (9)$$

Here

$Q = q - k$

$a$ = initial concn. of a

$x$ = amount of a used to time $t$

It should be mentioned that all the expressions given are integrals of the equation

$$dx/dt = (l + mx)(a - x) \qquad (10)$$
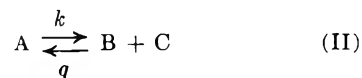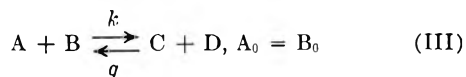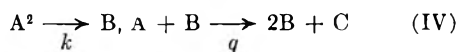
The method of this note may be used to treat any equation whose kinetics are expressible in this form.

*Follow*

*the*

*newest*

*field...* **NON-METALLICS**

HUGHES RESEARCH AND DEVELOP-
MENT LABORATORIES HAVE SEVERAL
OPENINGS FOR CHEMICAL AND
OTHER ENGINEERS IN DEVELOPMENT
LEADING TO PRODUCTION OF NEW
APPLICATIONS FOR NON-METALLIC
MATERIALS.

**ENGINEERS
AND
PHYSICISTS**

Hughes Laboratories are engaged in
a highly advanced research, development
and production program involving wide
use of non-metallic materials in missile
and radar components. The need is for
men with experience in these materials to
investigate the electrical, physical, and
heat-resistant properties of plastics and
other non-metallics.

**ENGINEERS
OR APPLIED
PHYSICISTS**

These men are required to plan, coordi-
nate, and conduct special laboratory and
field test programs on missile components.
Experience is required in materials devel-
opment, laboratory instrumentation, and
design of test fixtures.

**RESEARCH
CHEMIST**

The Plastics Department has need for an
individual with a Ph.D. Degree, or equiva-
lent experience in organic or physical
chemistry, to investigate the basic proper-
ties of plastics. Work involves research into
the properties of flow, mechanisms of cure,
vapor transmission, and electrical and
physical characteristics of plastics.

*Scientific
and
Engineering
Staff*    **HUGHES** RESEARCH & DEVELOPMENT LABORATORIES

*Culver City,
Los Angeles County, California*